Doctoral Dissertation

博士論文

Universality of open systems: non-Hermiticity, topology, and localization

(非平衡開放系の普遍性：非エルミート性・トポロジー・局在)

A Dissertation Submitted for the Degree of Doctor of Philosophy

December 2021

令和 3 年 12 月博士（理学）申請

Department of Physics, Graduate School of Science,
The University of Tokyo

東京大学 大学院理学系研究科 物理学専攻

Kohei Kawabata

川畑 幸平

Abstract

In physics, we describe and predict various phenomena on the basis of fundamental concepts such as symmetry and topology, which further leads to the universal understanding about nature. Despite the great success, the conventional physics mainly focused on closed systems at thermal equilibrium or open systems near thermal equilibrium, and a universal understanding of open systems far from equilibrium has yet to be developed. In this thesis, we develop a general theory of open systems effectively described by non-Hermitian Hamiltonians and explore new nonequilibrium phenomena that arise from the interplay between non-Hermiticity, topology, and localization. First, we show that the non-Hermitian skin effect, which is the anomalous localization due to non-Hermiticity, originates from intrinsic non-Hermitian topology. Such a topological origin not merely explains the universal feature of the known skin effect, but also leads to new types of the skin effects—symmetry-protected skin effects. As prime examples, we investigate reciprocal skin effects and higher-order skin effects that originate from symmetry-protected non-Hermitian topology. Furthermore, we develop a field-theoretical description of the intrinsic non-Hermitian topological phases. Because of the dissipative and nonequilibrium nature of non-Hermiticity, our theory is formulated solely in terms of spatial degrees of freedom, which contrasts with the conventional theory for closed systems defined in spacetime. Our theory provides a universal understanding of non-Hermitian topological phenomena, including the unidirectional transport in one dimension and the chiral magnetic skin effect in three dimensions. In addition, we show that the non-Hermitian skin effect is a signature of an anomaly from the field-theoretical perspective. The universality of our theory manifests itself as applicability even in the presence of disorder. We develop a scaling theory of localization in non-Hermitian disordered systems. We find that non-Hermiticity introduces a new scale and breaks down the one-parameter scaling, which is the central assumption of the conventional scaling theory of localization. Instead, we identify the origin of unconventional non-Hermitian delocalization as the two-parameter scaling. We also classify the universality classes of non-Hermitian disordered systems according to symmetry. Our work establishes the new universality of open systems.

Publications

1. Kohei Kawabata, Ryohei Kobayashi, Ning Wu, and Hosho Katsura,
Exact zero modes in twisted Kitaev chains,
Phys. Rev. B **95** (2017) 195140.

2. Kohei Kawabata, Yuto Ashida, and Masahito Ueda,
Information Retrieval and Criticality in Parity-Time-Symmetric Systems,
Phys. Rev. Lett. **119** (2017) 190401.

3. Kohei Kawabata, Yuto Ashida, Hosho Katsura, and Masahito Ueda,
Parity-time-symmetric topological superconductor,
Phys. Rev. B **98** (2018) 085116 [selected for Editors' Suggestion].

4. Zongping Gong, Yuto Ashida, Kohei Kawabata, Kazuaki Takasan, Sho Higashikawa, and Masahito Ueda,
Topological Phases of Non-Hermitian Systems,
Phys. Rev. X **8** (2018) 031079 [featured in Viewpoint (Physics **11** (2018) 96) and highlighted in Special Feature (Physics **14** (2021) 158) of Physics].

5. Kohei Kawabata, Ken Shiozaki, and Masahito Ueda,
Anomalous helical edge states in a non-Hermitian Chern insulator,
Phys. Rev. B **98** (2018) 165148.

6. Kohei Kawabata, Sho Higashikawa, Zongping Gong, Yuto Ashida, and Masahito Ueda,
Topological unification of time-reversal and particle-hole symmetries in non-Hermitian physics,
Nat. Commun. **10** (2019) 297 [selected for Editors' Highlight].

7. Tao Liu, Yu-Ran Zhang, Qing Ai, Zongping Gong, Kohei Kawabata, Masahito Ueda, and Franco Nori,
Second-Order Topological Phases in Non-Hermitian Systems,
Phys. Rev. Lett. **122** (2019) 076801.

8. Kohei Kawabata, Takumi Bessho, and Masatoshi Sato,
Classification of Exceptional Points and Non-Hermitian Topological Semimetals,
Phys. Rev. Lett. **123** (2019) 066405.

9. Ryusuke Hamazaki, Kohei Kawabata, and Masahito Ueda,
Non-Hermitian Many-Body Localization,
Phys. Rev. Lett. **123** (2019) 090603.

10. Kohei Kawabata, Ken Shiozaki, Masahito Ueda, and Masatoshi Sato,
Symmetry and Topology in Non-Hermitian Physics,
Phys. Rev. X **9** (2019) 041015 [highlighted in Special Feature (Physics **14** (2021) 158) of Physics].

11. Lei Xiao, Kunkun Wang, Xiang Zhan, Zhihao Bian, Kohei Kawabata, Masahito Ueda, Wei Yi, and Peng Xue,
Observation of Critical Phenomena in Parity-Time-Symmetric Quantum Dynamics,
Phys. Rev. Lett. **123** (2019) 230401.

12. Nobuyuki Okuma, Kohei Kawabata, Ken Shiozaki, and Masatoshi Sato,
Topological Origin of Non-Hermitian Skin Effects,
Phys. Rev. Lett. **124** (2020) 086801.

13. Takumi Bessho, Kohei Kawabata, and Masatoshi Sato,
Topological Classification of Non-Hermitian Gapless Phases: Exceptional Points and Bulk Fermi Arcs,
JPS Conf. Proc. **30** (2020) 011098.

14. Kohei Kawabata, Nobuyuki Okuma, and Masatoshi Sato,
Non-Bloch band theory of non-Hermitian Hamiltonians in the symplectic class,
Phys. Rev. B **101** (2020) 195147.

15. Ryusuke Hamazaki, Kohei Kawabata, Naoto Kura, and Masahito Ueda,
Universality classes of non-Hermitian random matrices,
Phys. Rev. Research **2** (2020) 023286.

16. Raj Cosmic, Kohei Kawabata, Yuto Ashida, Hiroki Ikegami, Shunsuke Furukawa, Pranay Patil, Jacob M. Taylor, and Yasunobu Nakamura,
Probing XY phase transitions in a Josephson junction array with tunable frustration,
Phys. Rev. B **102** (2020) 094509.

17. Kohei Kawabata and Masatoshi Sato,
Real spectra in non-Hermitian topological insulators,
Phys. Rev. Research **2** (2020) 033391.

18. Kohei Kawabata, Masatoshi Sato, and Ken Shiozaki,
Higher-order non-Hermitian skin effect,
Phys. Rev. B **102** (2020) 205118 [selected for Editors' Suggestion].

19. Norifumi Matsumoto, Kohei Kawabata, Yuto Ashida, Shunsuke Furukawa, and Masahito Ueda,
Continuous Phase Transition without Gap Closing in Non-Hermitian Quantum Many-Body Systems,
Phys. Rev. Lett. **125** (2020) 260601.

20. Kohei Kawabata and Shinsei Ryu,
Nonunitary Scaling Theory of Non-Hermitian Localization,
Phys. Rev. Lett. **126** (2021) 166801.

21. Kohei Kawabata, Ken Shiozaki, and Shinsei Ryu,
Topological Field Theory of Non-Hermitian Systems,
Phys. Rev. Lett. **126** (2021) 216405 [selected for Editors' Suggestion].

22. Xunlong Luo, Zhenyu Xiao, Kohei Kawabata, Tomi Ohtsuki, and Ryuichi Shindou,
Unifying the Anderson Transitions in Hermitian and Non-Hermitian Systems,
preprint at arXiv:2105.02514.

23. Kohei Kawabata and Masahito Ueda,
Nonlinear Landauer Formula: Nonlinear Response Theory of Disordered and Topological Materials,
preprint at arXiv:2110.08304.

The papers most relevant to this thesis are Refs. 12, 14, 18, 20, and 21.

- Chapter 3 is based on Ref. 12.
- Chapter 4 is based on Refs. 12, 14, and 18.
- Chapter 5 is based on Ref. 21.
- Chapter 6 is based on Ref. 20.

Contents

Chapter 1

Introduction

1.1 Background

In physics, we describe and predict various phenomena and develop the universal understanding about nature. The development of physics accompanies the development of fundamental concepts. In mechanics, we conceive the ideas of force and energy, which give a unified understanding about the motion of a falling apple and a planet. In electromagnetism, we introduce the concepts of electric and magnetic fields, by which we identify the origin of light. In thermodynamics, we formulate the ideas of temperature, heat, and entropy, which underlie the industrial revolution. The universality of theoretical concepts is a key to the success of physics. If a theory were not based on a general and universal formulation, it could not describe actual natural phenomena, which inevitably include complicated disorder and imperfection that cannot be taken into account for theoretical modeling.

In modern physics, one of the important fundamental concepts is symmetry. Symmetry is invariance of a system under a certain transformation. Translation invariance of time and space is closely related to the conservation of time and momentum, respectively [LL60]. Spontaneous breaking of symmetry lies at the heart of classifying phases of matter such as magnets and superconductors, as well as characterizing the structure of the universe [NJL61b, NJL61a]. The critical phenomena accompanying spontaneous symmetry breaking do not depend on specific details of systems but depend solely on symmetry and dimensions, forming the universality classes of phase transitions [Gol92, Car96]. Furthermore, the gauge symmetry, which is artificial symmetry that keeps the theory invariant and controls the degrees of freedom, constitutes the standard model of particle physics [Wei95]. In addition to continuous symmetry, discrete symmetry also plays a fundamental role. In particular, time-reversal invariance is important for chaos and integrability of quantum many-body systems [Wig59, Dys62]. Similarly, time-reversal symmetry, together with particle-hole symmetry and chiral symmetry [AZ97], characterizes the universality classes of Anderson localization in disordered electron systems, not depending on details of the systems.

Another crucial concept in contemporary physics is topology. Mathematically, topology is concerned with geometrical properties invariant under continuous deformations. Topology characterizes phases and order of matter that are captured solely by global properties. Such topological phases cannot be described by the paradigm of spontaneous symmetry breaking since it is based only on local order parameters. The prototype of topological phases is found in the quantum Hall effect [KDP80]. In a two-dimensional electron system with a strong magnetic field at low temperature, the Hall conductivity is quantized to be multiples of a physical constant. The quantized Hall conductivity originates from the topological invariant, Chern

number, of the ground-state wave function, which remains invariant as long as an energy gap is open [TKNdN82]. Thanks to the topological protection, the quantization of the Hall conductivity is immune to local perturbations including disorder and many-body interaction, which is even applied to the calibration of electrical resistance. Topological phases are ubiquitous in nature and found in insulators [Hal88, KM05b, KM05a, BHZ06, KWB+07] and superconductors [RG00, Kit01]. In the field-theoretical perspective, topological phases are formulated on the basis of the gauge principle. In particular, the bulk-boundary correspondence, which is the central principle of topological phases, is understood by an inflow of quantum anomaly: a topological field theory is gauge dependent at the boundary, and this gauge noninvariance must be compensated by the anomaly at the boundary.

Despite the great success, the conventional physics mainly focused on closed systems at thermal equilibrium. In open systems far from equilibrium, by contrast, we need to reconsider the fundamentals of physics. While closed systems are described by Hermitian Hamiltonians, open systems are no longer described by Hermitian Hamiltonians. Rather, non-Hermiticity is a new concept that constitutes the nature of open systems. Recent years have witnessed the new rich physics of non-Hermitian Hamiltonians that effectively describe open classical and quantum systems [EGMK+18, BBK21]. Non-Hermiticity induces a new type of spontaneous symmetry breaking that accompanies an exceptional point [BB98]. Non-Hermiticity also enables a localization transition even in one-dimensional disordered systems [HN96, HN97]. Moreover, non-Hermiticity gives rise to new topological phases that have no analogs in Hermitian systems [RL09, ESHK11, HH11, Sch13, MPS15, Lee16, LBH+17, XWD17, SZF18, KFar, GAK+18, KHG+19, YW18, KEBB18, LT19, KSUS19, KBS19, YM19]. Non-Hermitian physics finds practical applications such as unidirectional invisibility [Mos09, LRE+11, RBM+12, FXF+13, POL+14], enhanced sensitivity [Wie14, LZO+16, HHW+17, COZ+17, LC18, ZSH+19], and topological lasing [SJGG+17, PWH+18, BNV+17, ZMT+18, HBL+18, BWH+18, ZQW+19]. Still, a general theory of open systems far from equilibrium, including non-Hermitian physics, has yet to be established. It is unclear how non-Hermiticity changes the fundamental concepts in physics including symmetry and topology. Such a general theory should be helpful in systematically predicting new physical phenomena that can be observed in experiments. The nonequilibrium physics of open systems awaits further theoretical and experimental advances.

1.2 Summary

In this thesis, we develop a general theory of open systems that describes the interplay between non-Hermiticity, topology, and localization. On the basis of the universality of our theory, we also predict a variety of new nonequilibrium phenomena in open systems.

This thesis is organized as follows. While all the chapters are closely related, each chapter is written so that it can be read independently.

- In Chap. 2, we review the recent development of non-Hermitian physics. First, we begin with reviewing the basic mathematics of non-Hermitian matrices, especially their unique properties such as biorthogonality of eigenstates and exceptional points. Next, we review how non-Hermiticity appears in nature. Non-Hermiticity is ubiquitous and plays a leading role in open classical and quantum systems. Furthermore, we review symmetry in non-Hermitian physics [KSUS19]. We demonstrate that non-Hermiticity changes the nature of symmetry by ramifying and unifying [KHG+19] symmetry, culminating in the 38-fold internal-symmetry classification instead of the 10-fold classification for Hermitian systems.

Finally, we review topological phases of non-Hermitian systems [KSUS19]. The rich non-Hermitian topology originates from the two types of complex-energy gaps—point gap and line gap. These two types of complex-energy gaps enable topological classification of non-Hermitian systems, as well as exceptional points [KBS19]. We provide the periodic tables of Hermitian and non-Hermitian topological phases in Appendix A.

- In Chap. 3, we discuss the non-Hermitian skin effect, which is a unique feature of non-Hermitian systems and plays a crucial role in non-Hermitian topology [Lee16, YW18, KEBB18]. The skin effect is the anomalous localization and the extreme sensitivity to boundary conditions due to non-Hermiticity. We illustrate this with a prototypical non-Hermitian model with nonreciprocal hopping [HN96,HN97]. Remarkably, the Bloch band theory no longer describes the bulk of non-Hermitian systems with open boundaries if the skin effect occurs. To elucidate such a non-Bloch band feature, recent works [YW18, YM19] have developed a non-Bloch band theory that is applicable to non-Hermitian systems with arbitrary boundary conditions, which we also review. After these reviews, we reveal that the skin effect actually originates from intrinsic non-Hermitian topology and identify the skin effect as an intrinsic non-Hermitian topological phenomenon in terms of band theory and spectral theory [OKSS20]. This work provides a universal understanding about the bulk-boundary correspondence and the skin effect in non-Hermitian systems.

- In Chap. 4, we reveal new types of non-Hermitian topological phenomena—symmetry-protected skin effects. As a prime example, we discover the reciprocity-protected skin effect that originates from $\mathbb{Z}_2$ non-Hermitian topology [OKSS20]. We also demonstrate that this $\mathbb{Z}_2$ skin effect invalidates the standard non-Bloch band theory; instead, we develop a modified non-Bloch band theory in the symplectic class in a general manner [KOS20]. We provide the details about this nonstandard non-Bloch band theory in Appendix B. Furthermore, we classify possible other symmetry-protected skin effects for the 38-fold internal symmetry class in arbitrary dimensions [OKSS20]. As another prime example of symmetry-protected skin effects, we discover higher-order counterparts of the non-Hermitian skin effect [KSS20]. We show that the higher-order skin effect accompanies the new boundary physics that has no analogs in Hermitian higher-order topological phases and non-Hermitian first-order topological phases. We provide the details about the corner skin effect in Appendix C.

- In Chap. 5, we develop a field-theoretical description of the intrinsic non-Hermitian topological phases [KSR21]. Because of the dissipative and nonequilibrium nature of non-Hermiticity, our theory is formulated solely in terms of spatial degrees of freedom, which contrasts with the conventional theory defined in spacetime. Our theory provides a universal understanding of non-Hermitian topological phenomena such as the unidirectional transport in one dimension and the chiral magnetic skin effect in three dimensions. Furthermore, it systematically predicts new physics; we illustrate this by revealing transport phenomena and skin effects in two dimensions induced by a perpendicular spatial texture. From the field-theoretical perspective, the non-Hermitian skin effect is a signature of an anomaly. This work establishes a new connection between nonequilibrium physics and high-energy physics.

- In Chap. 6, we develop a scaling theory of localization in non-Hermitian systems [KR21]. While disorder inevitably leads to Anderson localization in Hermitian systems in one dimension, non-Hermiticity can destroy Anderson localization and lead to delocalization even in one dimension [HN96, HN97]. We reveal that non-Hermiticity introduces a new

scale and breaks down the one-parameter scaling, which is the central assumption of the conventional scaling theory of localization. Instead, we identify the origin of unconventional non-Hermitian delocalization as the two-parameter scaling. Furthermore, we establish the threefold universality of non-Hermitian localization based on reciprocity; reciprocity forbids delocalization without internal degrees of freedom, while symplectic reciprocity results in a new type of symmetry-protected delocalization. This work elucidates the new universality of open disordered systems. We provide several detailed discussions on non-Hermitian disordered systems in Appendix D.

Chapter 2

Non-Hermitian physics

Hermiticity of Hamiltonians is a common assumption in quantum mechanics. It ensures real spectra and unitarity of the dynamics. However, even non-Hermitian Hamiltonians can have real spectra in the presence of parity-time ($\mathcal{PT}$) symmetry [BB98, BBJ02, Ben07]. Such non-Hermitian Hamiltonians can be physically realized in open classical and quantum systems by appropriately controlling external coupling to the environment, such as gain and loss. Soon after the early theoretical proposals in classical optics [MEGCM08, EGMCM07, MMEGC08], a signature of a non-Hermitian Hamiltonian with $\mathcal{PT}$ symmetry was indeed observed in experiments [GSD+09, RMEG+10]. A number of theoretical and experimental developments followed to understand the unique and universal features of non-Hermitian systems [KYZ16, FEGG17, EGMK+18, MA19, ORNY19]. Away from open systems far from thermal equilibrium, non-Hermiticity is ubiquitous in nature. Non-Hermiticity appears also in electron systems at equilibrium as a result of finite lifetimes of quasiparticles [KFar, ZZ18, PIF19, SF18, YPK18, YPKH19, BB19, MR19, KYK19, NQI+20]. Effective non-Hermitian matrices are relevant also to the depinning transition of superconductors in a tilted magnetic field [HN96, HN97] and the dielectric breakdown of Mott insulators [FK98, OA10]. Non-Hermitian matrices exhibit unconventional characteristics in comparison with Hermitian matrices: eigenstates can be nonorthogonal [Bro14] and a complex spectrum can possess exceptional points [Kat66, Ber04, Hei12]. These mathematical properties lead to a number of unique phenomena and functionalities without Hermitian counterparts in theory [MEGCM08, EGMCM07, MMEGC08, KGM08, Mos09, Lon09, CGCS10, Lon10, CGS11, LRE+11, Wie14, JOL+14, ZRS+14, LZO+16] and experiments [GSD+09, RMEG+10, SLZ+11, RBM+12, BBPS13, FXF+13, POL+14, POR+14, FWM+14, HMH+14, FSA15, GEB+15, DMB+16, XMJH16, POL+16, MZS+16, HHW+17, COZ+17, AYF17, LPH+19] of open classical systems, as well as theory [BBJM07, GKN08, GS08, BG12, LC14, LRM14, AFU17, KAU17, QNO+18, LC18, ZSH+19, NKU18, DHM19, YNA+19] and experiments [ZZS+16, PCS+16, LHL+19, XWZ+19, WLG+19, NAJM19, OLH+21] of open quantum systems.

Meanwhile, the past decades have witnessed the dramatic development of topological phases of matter [HK10, QZ11, CTSR16]. One of the early examples of topological phases was found in the integer quantum Hall effect [KDP80, TKNdN82, Hal88]. Beyond this prototype, topological phases were shown to be much more ubiquitous [KM05b, KM05a, BHZ06, KWB+07]. Notably, while the topological phase in the quantum Hall effect disappears in the presence of time-reversal invariance, the $\mathbb{Z}_2$ topological phase that accompanies the quantum spin Hall effect [KM05b, KM05a, BHZ06, KWB+07] is protected by time-reversal invariance. These competing effects of symmetry enrich the properties of topological phases. More generally, the most fundamental symmetry for topological insulators and superconductors is internal symmetry known as the Altland-Zirnbauer symmetry in the random-matrix theory [AZ97]. On the

basis of the Altland-Zirnbauer symmetry, together with K-theory [Kar78], the periodic table of topological insulators and superconductors was developed [SRFL08, Kit09, RSFL10, CTSR16], which serves as a general and comprehensive theoretical framework of topological phases. This periodic table is generally applicable to the topological phases in insulators [SSH79, KDP80, TKNdN82, Koh85, Hal88, KM05b, KM05a, FK06, MB07, Roy09, FKM07, BHZ06, FK07, KWB+07] and superconductors [RG00, Iva01, Kit01, FK08, QHRZ09, STF09, SLTDS10, LSDS10, ORvO10, AOR+11, NSS+08, Ali12, SA17]. The universality of topology even leads to applications to synthetic materials such as photonic systems [LJS14, OPA+19] and cold atoms [GBZ16, CDS19]. Further development includes topological phases of gapless systems [NN83, Hcv05, Sat06, Mur07, WTVS11, BB11, BHB11, YZT+12, LWY+15, XBA+15, LWF+15, AMV18] and crystalline insulators [Fu11, HPB11, SMJZ13, CYR13, MF13, SS14, SSG16, WACB16, KdBvW+17, PVW17, BEC+17, WPV18, PWV18, ZJS+19, TPVW19, VEF+19, OPW20] including higher-order topological phases [BBH17a, BBH17b, LPT+17, SFF17, FF19, SCV+18, Kha18].

Recent studies have found the remarkable interplay of the aforementioned two research fields, non-Hermitian physics and topological physics [OTO+20, BBK21]. While topological phases were mainly investigated for Hermitian systems at thermal equilibrium, much research in recent years has focused on the topological characterization of non-Hermitian systems both in theory [RL09, SHEK12, ESHK11, HH11, LH13, PN13, Sch13, SJCPA16, LGV15, MPS15, Lee16, RLLar, MKKO20, LBH+17, XWD17, MH17, Xio18, SZF18, KFar, Lie18a, ZZ18, TN18, MABVFT18, CXYF18, KAKU18, CB18, PIF19, SF18, YJL+18, GAK+18, KHG+19, YW18, YSW18b, YPK18, KEBB18, PHG18, KSU18, MPBC18, CZ18, Lie18b, YH19, WRZ19, LT19, JS19, BCKB19, OY19, LZA+19, ZLLZ19, YPKH19, LLG19, CSBB19, KD19, EKB19, KSUS19, ZL19, HBR19, ZRLC+19, CC20, HPG19, ZRR21, RZS19, BKS20, KBS19, YM19, LZ19, BB19, MR19, OS19, SYW19a, SYW19b, KYK19, Lon19b, GWWK20, LAZV19, YKH19, RHS19, Sch20, IT19, HRB19, CYWR20, ZF20, WBN20, NQI+20, ZYF20, OKSS20, MLLG20, Lon20, XZGC21, LM21, WSBcvF20, YSHC21, KB20, WGK20, YZFH20, LLY20, MKA+20, YMH20, SIV20, YM20, LHY+20, YY20, LLMG20, YJS21, KOS20, TK20, BB20, MC20, KS20, XLH+21, SBGI20, LZYC20, SS20, BS21, YMB21, ZR21, DSS+21, MHar, OTY20, KSS20, FHW21, Leiar, KSR21, OS21, YM21, ZYFar, SZH21, LMLG21, OTY21, VDNS21, SO21, PMRar, YH21, SP21, LZZar, BFvdBM21, KP21] and experiment [PBK+15, ZRP+15, ZHI+15, WKP+17, XZB+17, SJGG+17, PWH+18, BNV+17, ZMT+18, ZPY+18, HBL+18, BWH+18, CHC+19, ZQW+19, BLLC19, HHI+20, GBvWC20, XDW+20, HHS+20, WKH+20, YHU+ar, WKLS21, WDY+21, ZOH+21, PTG+20, HZZ+21, ZTJ+21, WDWF21]. Certain topological phases of Hermitian systems survive even in the presence of non-Hermiticity [RL09, SHEK12, ESHK11], including non-Hermitian extensions of the Su-Schrieffer-Heeger model [SHEK12, ESHK11, Sch13, Lee16, YW18, KD19, WKP+17, SJGG+17, PWH+18], the Chern insulator [SZF18, YSW18b, KEBB18, KSU18, HBL+18, BWH+18], and the quantum spin Hall insulator [KHG+19]. On the other hand, non-Hermiticity induces new types of nonequilibrium topological phases without Hermitian analogs. In fact, non-Hermitian topological phases arise generally in odd spatial dimensions [GAK+18, KSUS19] while no topological phases appear in these dimensions for Hermitian systems without symmetry. These unique topological phases arise from the complex-valued nature of spectra, which enables two types of complex-energy gaps—point and line gaps [KSUS19]. On the basis of these two types of complex-energy gaps, topological classification of non-Hermitian systems was established for the 38-fold symmetry class [KSUS19]. Furthermore, non-Hermiticity changes the properties of topological boundary modes. For example, non-Hermiticity makes the edge modes amplified and enables novel lasers topologically protected against disorder and defects [SJGG+17, PWH+18, BNV+17, ZMT+18, HBL+18, BWH+18, ZQW+19]. The bulk-boundary correspondence, which is a central principle of topological phases, can also break down in non-Hermitian systems. This breakdown

arises from the extreme sensitivity of non-Hermitian systems to boundary conditions, which is called the non-Hermitian skin effect [Lee16, YW18, KEBB18]. Spectra and wave functions of non-Hermitian systems under the open boundary conditions can be strikingly different from those under the periodic boundary conditions, only the latter of which are predicted by the Bloch band theory. To elucidate such a non-Bloch feature of non-Hermitian systems, recent works have developed a non-Bloch band theory that works even under arbitrary boundary conditions [YW18, YM19].

In this chapter, we review the recent development of non-Hermitian physics. In Sec. 2.1, we discuss the mathematics of non-Hermitian matrices. Even in the absence of Hermiticity, $\mathcal{PT}$ symmetry can give rise to entirely real spectra [BB98]. Non-Hermitian matrices exhibit unique features that have no counterparts in Hermitian matrices, such as nonorthogonal eigenstates and exceptional points. In Sec. 2.2, we review non-Hermitian physics in the classical regime. Non-Hermitian Hamiltonians appear in a variety of open classical systems and lead to new phenomena and functionalities unique to non-Hermitian systems. In Sec. 2.3, we review non-Hermitian physics in the quantum regime. Non-Hermitian Hamiltonians effectively describe open quantum systems, as well as finite-lifetime quasiparticles in solids. In Sec. 2.4, we review symmetry of non-Hermitian Hamiltonians [KSUS19]. Non-Hermiticity changes the nature of symmetry by ramifying and unifying symmetry in a fundamental manner. Consequently, the 10-fold symmetry classification for Hermitian systems [AZ97] is replaced by the 38-fold symmetry classification for non-Hermitian systems [KSUS19]. In Sec. 2.5, we review topology of non-Hermitian systems [KSUS19]. The rich non-Hermitian topology originates from the complex-valued nature of the spectrum, which enables two types of complex-energy gaps: point gap and line gap. These two types of complex-energy gaps enable the general classification of non-Hermitian topological phases and lead to universal nonequilibrium topological phenomena intrinsic to open systems.

2.1 Mathematics

2.1.1 Real spectra in non-Hermitian Hamiltonians having $\mathcal{PT}$ symmetry

While Hermitian Hamiltonians always have real spectra, non-Hermitian Hamiltonians generally have complex spectra. However, Hermiticity is not necessary for the entirely real spectra; spectra can be real even in non-Hermitian Hamiltonians. A non-Hermitian Hamiltonian in one dimension

$$\hat{H} = \hat{p}^2 - (\mathrm{i}\hat{x})^N \quad (N \in \mathbb{R}) \tag{2.1}$$

was shown to have entirely real spectra for some N [BB98, Ben07]. This model reduces to the harmonic oscillator

$$\hat{H} = \hat{p}^2 + \hat{x}^2 \quad \text{for} \quad N = 2, \tag{2.2}$$

whose energy levels are

$$E_n = 2n + 1 \quad (n = 0, 1, 2, \cdots). \tag{2.3}$$

Also for $N \geq 2$, the spectrum is entirely real and positive. For $1 < N < 2$, although some number of eigenenergy remain real, an infinite number of the eigenenergy are no longer real and form complex-conjugate pairs. For $N \leq 1.42207$, the eigenenergy is real only for the ground state. As N approaches 1 from the above, the ground-state energy diverges, and no real eigenenergy appears for $N \leq 1$. The entirely real spectrum of this non-Hermitian model was rigorously proved in Refs. [DDT01a, DDT01b].

In Ref. [BB98], it was pointed out that the numerically confirmed real spectra are due to parity-time ($\mathcal{PT}$) symmetry. Here, space inversion (parity transformation) $\hat{\mathcal{P}}$ is defined by

$$\hat{\mathcal{P}}\hat{x}\hat{\mathcal{P}} = -\hat{x}, \quad \hat{\mathcal{P}}\hat{p}\hat{\mathcal{P}} = -\hat{p}, \quad \hat{\mathcal{P}}z\hat{\mathcal{P}} = z \tag{2.4}$$

for $z \in \mathbb{C}$, and time reversal $\hat{\mathcal{T}}$ is defined by

$$\hat{\mathcal{T}}\hat{x}\hat{\mathcal{T}} = \hat{x}, \quad \hat{\mathcal{T}}\hat{p}\hat{\mathcal{T}} = -\hat{p}, \quad \hat{\mathcal{T}}z\hat{\mathcal{T}} = z^*. \tag{2.5}$$

While space inversion does not accompany complex conjugation and hence is unitary symmetry, time reversal accompanies complex conjugation and hence is anti-unitary symmetry. Although the non-Hermitian model defined by Eq. (2.1) respects neither parity nor time-reversal symmetry, it respects the combined $\mathcal{PT}$ symmetry:

$$(\hat{\mathcal{P}}\hat{\mathcal{T}})\,\hat{H}\,(\hat{\mathcal{P}}\hat{\mathcal{T}})^{-1} = \hat{H}. \tag{2.6}$$

In addition to the specific model in Eq. (2.1), generic non-Hermitian Hamiltonians can have entirely real spectra in the presence of $\mathcal{PT}$ symmetry. To see this property, we consider eigenenergy $E \in \mathbb{C}$ and the corresponding right eigenstate $|\varphi\rangle$:

$$\hat{H}\,|\varphi\rangle = E\,|\varphi\rangle\,. \tag{2.7}$$

Then, because of $\mathcal{PT}$ symmetry, we have

$$\hat{H}\,(\hat{\mathcal{P}}\hat{\mathcal{T}}\,|\varphi\rangle) = \hat{\mathcal{P}}\hat{\mathcal{T}}\,(\hat{H}\,|\varphi\rangle) = \hat{\mathcal{P}}\hat{\mathcal{T}}\,(E\,|\varphi\rangle) = E^*\,(\hat{\mathcal{P}}\hat{\mathcal{T}}\,|\varphi\rangle), \tag{2.8}$$

which implies that $\hat{\mathcal{P}}\hat{\mathcal{T}}\,|\varphi\rangle$ is also an eigenstate of the Hamiltonian $\hat{H}$ with its eigenenergy E^*. Here, antiunitary of $\mathcal{PT}$ symmetry is used [i.e., $(\hat{\mathcal{P}}\hat{\mathcal{T}})\,E\,(\hat{\mathcal{P}}\hat{\mathcal{T}})^{-1} = E^*$]. Thus, if $\mathcal{PT}$ symmetry is not spontaneously broken, i.e., the eigenstate $|\varphi\rangle$ itself respects $\mathcal{PT}$ symmetry

$$\hat{\mathcal{P}}\hat{\mathcal{T}}\,|\varphi\rangle \propto |\varphi\rangle\,, \tag{2.9}$$

we have $E = E^*$, which leads to $E \in \mathbb{R}$. Importantly, an eigenstate itself does not necessarily respect $\mathcal{PT}$ symmetry even if the Hamiltonian respects $\mathcal{PT}$ symmetry because the $\mathcal{PT}$-symmetry operator is not unitary but antiunitary. As a result, $\mathcal{PT}$ symmetry can be spontaneously broken. If $\mathcal{PT}$ symmetry is spontaneously broken, i.e., if the eigenstate $|\varphi\rangle$ itself does not respect $\mathcal{PT}$ symmetry, we only have complex-conjugate pairs of eigenenergy. For the model in Eq. (2.1), all the eigenstates themselves respect $\mathcal{PT}$ symmetry for $N \geq 2$, while some eigenstates do not respect $\mathcal{PT}$ symmetry for $N < 2$. It is also notable that unbroken $\mathcal{PT}$ symmetry is sufficient for real spectra but not necessary; a necessary and sufficient condition for real spectra in non-Hermitian Hamiltonians is known to be pseudo-Hermiticity (see also Sec. 2.4.3 for details about pseudo-Hermiticity) [Mos02a, Mos02b, Mos02c].

The discovery that $\mathcal{PT}$ symmetry can lead to real spectra even in non-Hermitian Hamiltonians generated considerable interest in the physics and mathematics of non-Hermitian Hamiltonians. One of the important initial aims was to replace Hermiticity, which is a mathematical condition whose physical content is obscure, with another fundamental physical condition as the requirement of quantum mechanics. Notably, Hermiticity ensures not only real spectra but also unitarity of the dynamics; real spectra do not necessarily lead to unitarity. Hence, it is nontrivial whether a consistent physical theory can be built on non-Hermitian Hamiltonians solely with real spectra. Such a quantum theory with non-Hermitian Hamiltonians having unbroken $\mathcal{PT}$ symmetry was demonstrated to be well defined in a consistent manner [BBJ02]. This work

introduced unnoticed charge-conjugation symmetry $\mathcal{C}$ inherent in all $\mathcal{PT}$-symmetric Hamiltonians and constructed a positive-definite metric structure using $\mathcal{CPT}$ conjugation. It should be noted that this complex extension of quantum mechanics is equivalent to and indistinguishable from conventional quantum mechanics in terms of physics since the $\mathcal{CPT}$ metric is not physically observable [Mos03, Bro16]. Nevertheless, intriguing physical phenomena of non-Hermitian Hamiltonians are observable in different setups—open systems far from equilibrium.

2.1.2 Biorthogonal formalism

Here, we review basic mathematical properties of non-Hermitian Hamiltonians, which are also useful in understanding the physics of non-Hermitian Hamiltonians. One of the crucial properties of non-Hermitian Hamiltonians is that orthogonality of eigenstates is replaced by biorthogonality that defines the relation between the Hilbert space and its dual space [Bro14]. To see the biorthogonal formalism, we consider a generic non-Hermitian Hamiltonian $\hat{H}$. Let E_n be its complex eigenenergy and $|\varphi_n\rangle$ ($\langle\chi_n|$) be the corresponding right (left) eigenstate:

$$\hat{H}\,|\varphi_n\rangle = E_n\,|\varphi_n\rangle\,, \quad \langle\chi_n|\,\hat{H} = E_n\,\langle\chi_n|\,. \tag{2.10}$$

Here, we assume that the spectrum is not degenerate. For Hermitian Hamiltonians, the right and left eigenstates are always equivalent to each other: $|\varphi_n\rangle = |\chi_n\rangle \coloneqq (\langle\chi_n|)^\dagger$. For generic non-Hermitian Hamiltonians, however, this is not true. Moreover, the right eigenstates are not necessarily orthogonal with each other, and the same property applies to the left eigenstates:

$$\langle\varphi_m|\varphi_n\rangle \neq \delta_{mn}\,\langle\varphi_n|\varphi_n\rangle\,, \quad \langle\chi_m|\chi_n\rangle \neq \delta_{mn}\,\langle\chi_n|\chi_n\rangle\,. \tag{2.11}$$

Nevertheless, the right and left eigenstates are biorthogonal:

Biorthogonality

If the spectrum is not degenerate, we have

$$\langle\chi_m|\varphi_n\rangle = \delta_{mn}\,\langle\chi_n|\varphi_n\rangle\,. \tag{2.12}$$

To prove biorthogonality, from the right eigenequation $\hat{H}\,|\varphi_n\rangle = E_n\,|\varphi_n\rangle$, we have

$$\langle\chi_m|\hat{H}|\varphi_n\rangle = E_n\,\langle\chi_m|\varphi_n\rangle\,. \tag{2.13}$$

Meanwhile, from the left eigenequation $\langle\chi_m|\,\hat{H} = E_m\,\langle\chi_m|$, we have

$$\langle\chi_m|\hat{H}|\varphi_n\rangle = E_m\,\langle\chi_m|\varphi_n\rangle\,. \tag{2.14}$$

Then, these equations lead to

$$(E_m - E_n)\,\langle\chi_m|\varphi_n\rangle = 0, \tag{2.15}$$

by which we have $\langle\chi_m|\varphi_n\rangle = 0$ for $m \neq n$ since the spectrum is not degenerate by assumption.

We also show that the eigenstates $\{|\varphi_n\rangle\}$ are linearly independent and complete although they are not necessarily orthogonal:

Completeness

For a non-Hermitian Hamiltonian without degeneracy, a full set of the eigenstates $\{|\varphi_n\rangle\}$ is linearly independent and complete.

To prove linear independence, we consider a set of numbers $\{c_n\}$ that satisfies

$$\sum_n c_n |\varphi_n\rangle = 0. \tag{2.16}$$

Because of biorthogonality $\langle\chi_m|\varphi_n\rangle = \delta_{mn} \langle\chi_n|\varphi_n\rangle$, we have

$$c_n \langle\chi_n|\varphi_n\rangle = 0 \tag{2.17}$$

for all n. We note $\langle\chi_n|\varphi_n\rangle \neq 0$ for a Hamiltonian without degeneracy. Hence, we have $c_n = 0$, i.e., linear independence of the set of the eigenstates $\{|\varphi_n\rangle\}$. Since the number of these linearly independent eigenstates is equal to the dimension of the Hilbert space, this set is also complete.

Moreover, we have the following completeness condition:

Completeness condition

If eigenstates are complete, we have

$$\sum_n \frac{|\varphi_n\rangle \langle\chi_n|}{\langle\chi_n|\varphi_n\rangle} = \hat{I} \tag{2.18}$$

with the identity operator $\hat{I}$.

To prove this condition, we show

$$\langle\psi| \left(\sum_n \frac{|\varphi_n\rangle \langle\chi_n|}{\langle\chi_n|\varphi_n\rangle} \right) |\psi\rangle = \langle\psi|\psi\rangle \tag{2.19}$$

for an arbitrary state $|\psi\rangle$. Because of the completeness of the eigenstates, we can expand it as

$$|\psi\rangle = \sum_n c_n |\varphi_n\rangle, \quad c_n \coloneqq \frac{\langle\chi_n|\psi\rangle}{\langle\chi_n|\varphi_n\rangle}. \tag{2.20}$$

Then, we have

$$\langle\psi| \left(\sum_m \frac{|\varphi_m\rangle \langle\chi_m|}{\langle\chi_m|\varphi_m\rangle} \right) |\psi\rangle = \sum_{lmn} c_l^* \frac{\langle\varphi_l|\varphi_m\rangle \langle\chi_m|\varphi_n\rangle}{\langle\chi_m|\varphi_m\rangle} c_n = \sum_{ln} c_l^* \langle\varphi_l|\varphi_n\rangle c_n = \langle\psi|\psi\rangle. \tag{2.21}$$

2.1.3 Exceptional point

We have so far assumed that non-Hermitian Hamiltonians have no degeneracy. By contrast, non-Hermitian Hamiltonians can possess unique level degeneracy called exceptional points [Kat66, Ber04, Hei12]. At exceptional points, eigenstates coalesce with each other and are incomplete. Since Hermiticity ensures completeness of eigenstates even in the presence of level degeneracy, exceptional points cannot appear in Hermitian systems and are hence unique to non-Hermitian systems.

To understand properties of exceptional points, we consider a simple non-Hermitian Hamiltonian with two levels:

$$\hat{H} = \hat{\sigma}_x + \mathrm{i}\gamma\hat{\sigma}_z = \begin{pmatrix} \mathrm{i}\gamma & 1 \\ 1 & -\mathrm{i}\gamma \end{pmatrix}, \tag{2.22}$$

where $\hat{\sigma}_i$'s are Pauli matrices, and $\gamma \geq 0$ controls the degree of non-Hermiticity. As discussed in Sec. 2.2, this two-level system has been experimentally realized in various open systems. The energy spectrum is obtained as

$$E_\pm = \pm\sqrt{1-\gamma^2}. \tag{2.23}$$

For $\gamma \leq 1$, the spectrum is entirely real; for $\gamma > 1$, the eigenenergy appears in a complex-conjugate pair. The entirely real spectrum is due to $\mathcal{PT}$ symmetry; in fact, the Hamiltonian respects it for

$$\hat{\mathcal{P}}\hat{\mathcal{T}} \coloneqq \hat{\sigma}_x\mathcal{K} \tag{2.24}$$

with complex conjugation $\mathcal{K}$. The corresponding eigenstates are obtained as

$$|\varphi_\pm\rangle \propto \begin{pmatrix} 1 \\ -\mathrm{i}\gamma \pm \sqrt{1-\gamma^2} \end{pmatrix}, \quad |\chi_\pm\rangle \propto \begin{pmatrix} 1 \\ \mathrm{i}\gamma \pm \sqrt{1-\gamma^2} \end{pmatrix}. \tag{2.25}$$

Therefore, the eigenstates indeed respect $\mathcal{PT}$ symmetry for $\gamma < 1$, but they do not for $\gamma > 1$, which is consistent with the discussions in Sec. 2.1.1.

The two levels coalesce at $\gamma = 1$. In addition to the eigenenergy, the eigenstates coincide with each other for $\gamma = 1$:

$$|\varphi_+\rangle = |\varphi_-\rangle \propto \begin{pmatrix} 1 \\ -\mathrm{i} \end{pmatrix}, \quad |\chi_+\rangle = |\chi_-\rangle \propto \begin{pmatrix} 1 \\ \mathrm{i} \end{pmatrix}. \tag{2.26}$$

These eigenstates satisfy self-orthogonality

$$\langle\chi_\pm|\varphi_\pm\rangle = 0. \tag{2.27}$$

The Hamiltonian is not diagonalizable and becomes defective at $\gamma = 1$:

$$\hat{H} = \hat{\sigma}_x + \mathrm{i}\hat{\sigma}_z = \begin{pmatrix} \mathrm{i} & 1 \\ 1 & -\mathrm{i} \end{pmatrix}. \tag{2.28}$$

Notably, such a deficit of an eigenspace is impossible in Hermitian systems.

Exceptional points appear in nature and give rise to unique phenomena and functionalities that have no Hermitian counterparts, as discussed below. In addition, exceptional points possess unique topological structures, as demonstrated in Sec. 2.5.4. It should also be noted that spontaneous symmetry breaking induced by non-Hermiticity plays a fundamental role in statistical mechanics [YL52, LY52, Fis78, ID89].

2.2 Classical physics

2.2.1 Open classical systems

The past two decades have witnessed new rich physics of non-Hermitian Hamiltonians in a variety of open classical systems. In a couple of early theoretical works [MEGCM08,EGMCM07, MMEGC08], it was proposed that non-Hermitian Hamiltonians can be experimentally realized in classical optics instead of quantum mechanics. This theoretical proposal is based on the relationship between the classical optical equation and the Schrödinger equation. In particular, the paraxial propagation of light in photonic lattices is described by [Jac62]

$$\mathrm{i}\frac{\partial}{\partial z}\psi\left(x,y;z\right)=-\frac{1}{2k_0}\left(\frac{\partial^2}{\partial x^2}+\frac{\partial^2}{\partial y^2}\right)\psi\left(x,y;z\right)+\frac{k_0\Delta n\left(x,y;z\right)}{n_0}\psi\left(x,y;z\right), \tag{2.29}$$

where light propagates in the z direction; $\psi\left(x,y;z\right)$ is the electric field envelope function defined by $E\left(x,y;z\right)=\psi\left(x,y;z\right)e^{\mathrm{i}(k_0z-\omega t)}$ with the electric field $E\left(x,y;z\right)$, and $n_0+\Delta n\left(x,y;z\right)$ is the refractive index. This paraxial equation of light has the same form as the Schrödinger equation in two dimensions

$$\mathrm{i}\frac{\partial}{\partial t}\psi\left(x,y;t\right)=-\frac{\hbar^2}{2m}\left(\frac{\partial^2}{\partial x^2}+\frac{\partial^2}{\partial y^2}\right)\psi\left(x,y;t\right)+V\left(x,y;t\right)\psi\left(x,y;t\right), \tag{2.30}$$

where a quantum particle in two dimensions (x,y) evolves in time t, and $\psi\left(x,y;t\right)$ denotes its wave function. Thus, the propagation of light in the array of waveguides in the z direction is formally equivalent to the temporal evolution (i.e., evolution in the t direction) of a quantum particle in a two-dimensional lattice. Notably, we can make the refractive index $n_0+\Delta n\left(x,y;z\right)$ complex-valued. Here, the real part describes the index profile of the lattice, and the imaginary part represents the gain-loss distribution. To respect $\mathcal{PT}$ symmetry in Eq. (2.29), the complex refractive index should satisfy

$$\mathrm{Re}\left[\Delta n\left(x,y;z\right)\right]=\mathrm{Re}\left[\Delta n\left(-x,-y;z\right)\right], \tag{2.31}$$
$$\mathrm{Im}\left[\Delta n\left(x,y;z\right)\right]=-\mathrm{Im}\left[\Delta n\left(-x,-y;z\right)\right], \tag{2.32}$$

which can be achieved by a judicious design that involves a combination of optical gain and loss and the process of index guiding.

In addition to the above experimental proposal, Refs. [MEGCM08,EGMCM07,MMEGC08] studied the optical beam dynamics in complex $\mathcal{PT}$ arrays and found its unique characteristic that originates from nonorthogonality of the associated Bloch eigenmodes. In particular, the following $\mathcal{PT}$-symmetric periodic potential in one dimension was studied:

$$V\left(x\right)=4\left[\cos^2\left(x\right)+\mathrm{i}V_0\sin\left(2x\right)\right], \tag{2.33}$$

which indeed respects $\mathcal{PT}$ symmetry $V\left(x\right)=V^*\left(-x\right)$. The band structure is entirely real for $V_0<0.5$ and complex for $V_0>0.5$. The $\mathcal{PT}$-transition point $V_0=0.5$ serves as an exceptional point, at which some bands begin to coalesce with each other. Such unique complex band structures do not appear in the absence of gain or loss.

Consistent with the general discussions in Sec. 2.1.2, the eigenmodes of this non-Hermitian Hamiltonian are nonorthogonal:

$$\int_{-\infty}^{\infty}\varphi_m^*\left(k,x\right)\varphi_n\left(k',x\right)dx\neq\delta_{mn}\delta\left(k-k'\right), \tag{2.34}$$

where $\varphi_n(k,x)$ is a right eigenmode with Bloch momentum k. As a direct consequence of this nonorthogonality, unusual phenomena occur in this complex $\mathcal{PT}$-symmetric potential. In the $\mathcal{PT}$-symmetric array, the beam splits in two, and birefringence occurs. This asymmetry can be intuitively understood in terms of the presence of a chiral energy flow due to the $\mathcal{PT}$-symmetric structure involving balanced gain and loss. Moreover, the power oscillates during propagation due to the nonorthogonality between eigenmodes. This power oscillation can occur even though the spectrum is entirely real.

Soon after the theoretical proposal [MEGCM08,EGMCM07,MMEGC08], the non-Hermitian Hamiltonian in Eq. (2.22) was experimentally realized [GSD+09, RMEG+10]. These first experiments observed spontaneous $\mathcal{PT}$-symmetry breaking that accompanies an exceptional point and power oscillation due to nonorthogonality of eigenstates. After the first experimental observations, the unique properties of non-Hermitian systems were extensively studied both in theory and experiment. Several unconventional phenomena and functionalities were revealed, such as power oscillations [MEGCM08, EGMCM07, MMEGC08, RBM+12], unidirectional invisibility [Mos09, LRE+11, RBM+12, FXF+13, POL+14], high-performance lasers [CGCS10,Lon10,CGS11,JOL+14,POR+14,FWM+14,HMH+14,MZS+16], exceptional-point encirclement [GEB+15,DMB+16,XMJH16], and enhanced sensitivity [Wie14, LZO+16, HHW+17, COZ+17, LC18, ZSH+19], which we review in the rest of this section.

2.2.2 Unidirectional invisibility

$\mathcal{PT}$-symmetric periodic potentials can act as unidirectional invisible media near the $\mathcal{PT}$-symmetry-breaking point that accompanies an exceptional point [Mos09, LRE+11]. For example, we consider the $\mathcal{PT}$-symmetric periodic structure whose refractive index is given as

$$n(z) = \begin{cases} n_0 + n_1 \cos(2\beta z) + \mathrm{i} n_2 \sin(2\beta z) & (|z| \le L/2)\,; \\ n_0 & (|z| \ge L/2)\,. \end{cases} \tag{2.35}$$

This potential is Hermitian for $n_2 = 0$ and possesses an exceptional point at $n_1 = n_2$. We solve the scattering problem, whose solution is obtained as the following matrix:

$$\begin{pmatrix} E_f^+ \\ E_b^+ \end{pmatrix} = \begin{pmatrix} M_{11} & M_{12} \\ M_{21} & M_{22} \end{pmatrix} \begin{pmatrix} E_f^- \\ E_b^- \end{pmatrix}, \tag{2.36}$$

where E_f and E_b are the amplitudes of the forward and backward propagating waves, respectively. Here, the transmission and reflection amplitudes for the left and right incidence waves are obtained as

$$t_{\mathrm{L}} = t_R = \frac{1}{M_{22}}; \quad r_{\mathrm{L}} = -\frac{M_{21}}{M_{22}}, \quad r_{\mathrm{R}} = \frac{M_{12}}{M_{22}}. \tag{2.37}$$

For the $\mathcal{PT}$-symmetric potential described by Eq. (2.35) with zero detuning $k = \beta$, the scattering problem is straightforwardly solved as

$$t_{\mathrm{L}} = t_{\mathrm{R}} = \frac{1}{\cos^2(\lambda L)}; \quad r_{\mathrm{L}} = \frac{(n_1 - n_2)^2 k^2/4n_0^2}{|\lambda|^2 |\cot^2(\lambda L)|}, \quad r_{\mathrm{R}} = \frac{(n_1 + n_2)^2 k^2/4n_0^2}{|\lambda|^2 |\cot^2(\lambda L)|}, \tag{2.38}$$

where λ is defined as

$$\lambda := \sqrt{-\frac{k^2(n_1^2 - n_2^2)}{4n_0^2}}. \tag{2.39}$$

In the Hermitian case with $n_2 = 0$, we have $r_\mathrm{L} = r_\mathrm{R}$. In the non-Hermitian case with $n_2 \neq 0$, by contrast, the asymmetry in the left and right reflection coefficients arises. At the exceptional point with $n_1 = n_2$, this asymmetry is most pronounced:

$$t_\mathrm{L} = t_\mathrm{R} = 1; \quad r_\mathrm{L} = 0, \quad r_\mathrm{R} = 1. \tag{2.40}$$

Therefore, the wave entering the sample from the left is entirely unaffected while the wave entering the same sample from the right experiences perfect reflection. Such unidirectional invisibility was experimentally observed in various classical systems [RBM+12, FXF+13, POL+14] and may find applications in designing novel metamaterials.

2.2.3 Exceptional-point encirclement

An important property of exceptional points is the geometry of the self-intersecting Riemann sheets on which the complex eigenvalues unfold [Hei12]. This mathematical property directly leads to unconventional phenomena in physics. In particular, the system does not return to its initial state upon encirclement but to a different state on another Riemann sheet, requiring a second encirclement to return to the initial state. In addition, nonadiabatic transitions give rise to chiral behavior through which the direction of encirclement solely determines the final state of the system in a fully dynamical picture.

Such encirclement around an exceptional point was observed in experiments [GEB+15, DMB+16, XMJH16]. For example, the dynamical encirclement of an exceptional point was mapped onto the spatial propagation in a two-mode waveguide that features suitably engineered boundary modulations and internal losses [DMB+16]. Since the polarity of the encirclement is dictated solely by the propagation direction, the chiral behavior manifests itself in unique transmission characteristics: the waveguide transmits predominantly into one mode depending on the direction of propagation. In another optomechanical experiment [XMJH16], a mechanical membrane was placed inside an optical resonator, and an external laser was used to implement the above chiral transfer.

2.2.4 Enhanced sensitivity

Exceptional points can qualitatively enhance the sensitivity of a sensor [Wie14]. To see this enhancement, we consider the 2×2 Hamiltonian

$$H = \begin{pmatrix} 0 & A \\ B & 0 \end{pmatrix} + \varepsilon \begin{pmatrix} 0 & 1 \\ 1 & 0 \end{pmatrix} = \begin{pmatrix} 0 & A+\varepsilon \\ B+\varepsilon & 0 \end{pmatrix}, \tag{2.41}$$

where $A, B \geq 0$ are intrinsic parameters of the sensor and $\varepsilon \geq 0$ controls an external perturbation. The sensor is Hermitian for $A = B$, but non-Hermitian for the asymmetric coupling $A \neq B$. The splitting of the eigenenergy is readily obtained as

$$\Delta E\left(\varepsilon\right) = 2\sqrt{\left(A+\varepsilon\right)\left(B+\varepsilon\right)}, \tag{2.42}$$

which is measured as a function of ε to detect the target. For the Hermitian sensor with $A = B$, it linearly increases with respect to the perturbation:

$$\Delta E\left(\varepsilon\right) - \Delta E\left(0\right) = 2\varepsilon. \tag{2.43}$$

For the non-Hermitian sensor with $A, B \neq 0$, on the other hand, it is obtained as

$$\Delta E\left(\varepsilon\right) - \Delta E\left(0\right) \simeq \frac{A+B}{\sqrt{AB}}\varepsilon \quad \left(\varepsilon \ll A, B\right), \tag{2.44}$$

which also increases linearly with respect to ε. However, at the exceptional point with $B = 0$, this splitting is given as

$$\Delta E(\varepsilon) - \Delta E(0) = \sqrt{(A+\varepsilon)\,\varepsilon} \simeq \sqrt{A\,\varepsilon}, \quad (\varepsilon \ll A), \tag{2.45}$$

which is proportional to $\varepsilon^{1/2}$ and qualitatively enhanced compared with the Hermitian sensor.

This enhancement of sensitivity due to exceptional points was experimentally observed in optical systems [HHW+17, COZ+17]. In one experiment [COZ+17], two nanoscale scatterers were used to tune a whispering-gallery-mode micro-toroid cavity, where light propagates along a surface in a controlled manner. Subsequently, a target nanoscale object perturbs the system from its exceptional point, leading to the aforementioned square-root singularity. In another experiment [HHW+17], a $\mathcal{PT}$-symmetric photonic laser molecule was realized in a coupled cavity arrangement with balanced gain and loss. Notably, this system is a three-level system, and even the $\varepsilon^{1/3}$ singularity was experimentally observed. The effect of quantum noise was also discussed theoretically [LC18, ZSH+19].

2.3 Quantum physics

2.3.1 Open quantum systems

Beyond the classical regime, non-Hermitian Hamiltonians can effectively describe open quantum systems. In an early work [Gam28], complex-valued energy was introduced to describe the alpha decay, in which a particle can escape from the nucleus by quantum tunneling. In such an effective description, the real and imaginary parts of complex energy were shown to respectively describe energy levels and widths of the nuclear resonance. Subsequently, complex-valued potentials were introduced to describe the scattering between neutrons and nuclei [FPW54, Fes58, Fes62], in which the imaginary part of the potentials arises from the neutron absorption and the formation of compound nuclei. While non-Hermiticity was introduced phenomenologically in these early works, this approach can be rigorously justified in terms of the scattering theory [Rot09, Moi11]. Other theories can also provide formal and rigorous justification for the use of non-Hermiticity to effectively describe open quantum systems, such as the quantum jump method [DZR92, DCM92, MCD93, Car93, PK98, Dal05].

To capture the essence of such an effective non-Hermitian description of open quantum systems, let us consider a simple quantum two-level particle that is subject to a probabilistic decay [LC14]. Here, we assume that the decay of the particle can be tracked by an ancillary detector, which plays a role of the environment. The whole system, the particle and the ancilla, is initially prepared as

$$|\psi(t)\rangle = (\alpha\,|\downarrow\rangle + \beta\,|\uparrow\rangle)\,|0\rangle, \tag{2.46}$$

where $|\downarrow\rangle$ and $|\uparrow\rangle$ describe the two levels of the particle, and $|0\rangle$ describes the initial state of the ancilla. In a short time interval dt, the particle decays with the probability $p \coloneqq \gamma\,|\beta|^2\,dt \ll 1$. The wave function then evolves to

$$|\psi(t+dt)\rangle = \alpha\,|\downarrow\rangle\,|0\rangle + \beta\left(1 - \frac{\gamma dt}{2}\right)|\uparrow\rangle\,|0\rangle + \sqrt{p}\,|a\rangle\,|1\rangle, \tag{2.47}$$

where $|a\rangle$ is an eigenstate with no particle, and $|1\rangle$ is a state of the ancilla corresponding to the measurement outcome of the particle decay. At this point, the ancilla detects the presence or absence of the particle. When the particle decays and the ancilla detects the particle, $|1\rangle$ is projected out as

$$|\psi_\circ(t+dt)\rangle = |a\rangle\,|1\rangle. \tag{2.48}$$

On the other hand, when the particle does not decay and the ancilla detects no particle, $|0\rangle$ is projected out as

$$|\psi_\times(t+dt)\rangle = \alpha\left(1+\frac{\gamma|\beta|^2\,dt}{2}\right)|\downarrow\rangle|0\rangle + \beta\left(1-\frac{\gamma|\alpha|^2\,dt}{2}\right)|\uparrow\rangle|0\rangle\,. \tag{2.49}$$

Therefore, the conditional dynamics in the absence of the particle decay is described by

$$|\psi_\times(t+dt)\rangle = \frac{e^{-\mathrm{i}\hat{H}_{\mathrm{eff}}dt}|\psi(t)\rangle}{\|e^{-\mathrm{i}\hat{H}_{\mathrm{eff}}dt}|\psi(t)\rangle\|}, \tag{2.50}$$

where $\hat{H}_{\mathrm{eff}}$ is the effective non-Hermitian Hamiltonian defined as

$$\hat{H}_{\mathrm{eff}} \coloneqq -\frac{\mathrm{i}\gamma}{4}(\hat{\sigma}_z+\hat{I}). \tag{2.51}$$

It should be noted that quantum operations with gain or loss of energy and particles entail a probabilistic process and cannot be performed in a deterministic manner, which is to be contrasted with classical operations. Consequently, the continuous measurement of a particle—precise control of the environment—is essential for the effective description by the non-Hermitian Hamiltonian. Although we here focus on a specific two-level system, such a discussion can be generalized to arbitrary dissipative quantum dynamics [Car93, PK98, Dal05].

Unique features of non-Hermitian quantum systems were theoretically studied in a number of recent works [BBJM07, GKN08, GS08, BG12, LC14, LRM14, AFU17, KAU17, QNO+18, LC18, ZSH+19, NKU18, DHM19, YNA+19]. For example, phase transitions [LC14, AFU17, NKU18, DHM19], entanglement [LRM14, KAU17], and sensing [LC18, ZSH+19] in non-Hermitian quantum systems were investigated. Furthermore, the spectral transitions and exceptional points, which are clear signatures of non-Hermitian systems, were experimentally observed in several open quantum systems [ZZS+16, PCS+16, LHL+19, XZB+17, XWZ+19, WLG+19, NAJM19, OLH+21], including cold atoms [LHL+19, OLH+21], single photons [XZB+17, XWZ+19], single spins in a nitrogen-vacancy center [WLG+19], and superconducting qubits [NAJM19].

2.3.2 Lifetime of quasiparticles

Away from the nonequilibrium setups, non-Hermiticity effectively describes the lifetimes of quasiparticles in solids at thermal equilibrium [KFar]. According to the band theory [AM76], quasiparticles in noninteracting periodic crystals have infinite lifetimes. By contrast, many-body interaction and disorder, as well as coupling to external leads, give rise to scattering of the quasiparticles and make their lifetimes finite [AGD63, Dat95, AS06]. Here, the finite lifetimes of quasiparticles are described by the imaginary parts of their energy, and the effective Hamiltonian of the finite-lifetime quasiparticles lacks Hermiticity.

More formally, the effective non-Hermitian Hamiltonian $H(\boldsymbol{k},\omega)$ for quasiparticles is defined by the retarded Green function $G^R(\omega)$:

$$G^R(\omega) = [\omega - H(\boldsymbol{k},\omega)]^{-1}, \quad H(\boldsymbol{k},\omega) \coloneqq H_0(\boldsymbol{k}) + \Sigma(\boldsymbol{k},\omega), \tag{2.52}$$

where $H_0(\boldsymbol{k})$ is a single-particle Hamiltonian in a periodic potential, and $\Sigma(\boldsymbol{k},\omega)$ is the self-energy that includes the effects of, for example, electron-electron scattering, electron-phonon scattering, and electron-impurity scattering. Importantly, the self-energy $\Sigma(\boldsymbol{k},\omega)$ is non-Hermitian for finite-lifetime quasiparticles even if the original Bloch Hamiltonian $H_0(\boldsymbol{k})$ is

Hermitian. The quasiparticle Hamiltonian $H(\boldsymbol{k},\omega)$ provides a natural generalization of the noninteracting Bloch Hamiltonian $H_0(\boldsymbol{k})$.

In recent years, the physical consequences of non-Hermiticity in the self-energy were extensively studied [KFar, ZZ18, PIF19, SF18, YPK18, YPKH19, BB19, MR19, KYK19, NQI+20]. As a prime example, non-Hermiticity in the self-energy is shown to deform a Fermi surface and give rise to a Fermi arc in the bulk that bridges two exceptional points [KFar]. The emergence of the bulk Fermi arc is understood, for example, by the following non-Hermitian Dirac model:

$$H(\boldsymbol{k}) = k_x\sigma_x + (k_y + \mathrm{i}\gamma)\,\sigma_y, \tag{2.53}$$

with Pauli matrices σ_x and σ_y and the degree $\gamma \in \mathbb{R}$ of non-Hermiticity. This continuum model describes a single valley degree of freedom of graphene in the absence of non-Hermiticity [CNGP+09, DSAHR11]; the non-Hermiticity γ effectively describes the lifetimes of quasiparticles. The spectrum of this Dirac model is

$$E(\boldsymbol{k}) = \pm\sqrt{k_x^2 + (k_y + \mathrm{i}\gamma)^2} = \pm\sqrt{\boldsymbol{k}^2 - \gamma^2 + 2\mathrm{i}\gamma k_y}. \tag{2.54}$$

Now, we set the Fermi energy to zero (i.e., $\mathrm{Re}\,E = 0$) and investigate the Fermi surface. In the absence of non-Hermiticity (i.e., $\gamma = 0$), the two bands touch with each other at zero energy, and hence the Fermi surface reduces to a point:

$$k_x = k_y = 0. \tag{2.55}$$

In the presence of non-Hermiticity (i.e., $\gamma \neq 0$), by contrast, the Fermi surface described by $\mathrm{Re}\,E = 0$ is determined as

$$|k_x| \leq |\gamma|\,, \quad k_y = 0, \tag{2.56}$$

which forms an arc in momentum space. Notably, Fermi surfaces in the bulk are always closed in Hermitian systems. Thus, the bulk Fermi arc is forbidden in Hermitian systems and hence unique to non-Hermitian systems. The emergence of the bulk Fermi arc due to non-Hermiticity was theoretically proposed to induce quantum oscillations even in insulators [SF18].

It should be noted that the effective non-Hermitian description of finite-lifetime quasiparticles is not necessarily independent of open quantum systems discussed in Sec. 2.3.1; a relationship of the effective non-Hermitian description between open quantum systems and strongly correlated electron systems has been demonstrated in a recent work [MP20].

2.3.3 Vortex pinning and dielectric breakdown

Non-Hermitian Hamiltonians can have different origins. For example, depinning of flux lines from extended defects in type-II superconductors subject to a tilted external magnetic field was shown to be effectively described by a non-Hermitian Hamiltonian [HN96, HN97]. The depinning transition of the flux lines is well described by the classical partition function

$$Z = \int \mathcal{D}\boldsymbol{x}\; e^{-E[\boldsymbol{x}(\tau)]/k_\mathrm{B}T}, \tag{2.57}$$

where k_B is the Boltzmann constant, T is temperature, and $\boldsymbol{x} \in \mathbb{R}^d$ describes the flux lines. The energy $E[\boldsymbol{x}(\tau)]$ of the flux lines phenomenologically reads

$$E[\boldsymbol{x}(\tau)] = \int \left[\frac{m}{2}\left(\frac{d\boldsymbol{x}}{d\tau}\right)^2 - \boldsymbol{g}\cdot\frac{d\boldsymbol{x}}{d\tau} + V(\boldsymbol{x})\right] d\tau, \tag{2.58}$$

where m is the effective mass, $\boldsymbol{g} \in \mathbb{R}^d$ is the degree of the tilted external magnetic field, and V is the potential energy. The classical-quantum correspondence [Suz76, Kog79] lets us transform this classical problem into another quantum problem. In Refs. [HN96, HN97], the above classical system was shown to be equivalent to the quantum Hamiltonian

$$\hat{H} = \frac{(\hat{\boldsymbol{p}} + \mathrm{i}\boldsymbol{g})^2}{2m} + V(\hat{\boldsymbol{x}}). \tag{2.59}$$

Here, $\boldsymbol{g}$ acts like an imaginary vector potential and makes the Hamiltonian non-Hermitian. It was further demonstrated that the imaginary vector potential $\boldsymbol{g}$ enables delocalization even in disordered one-dimensional systems, although such delocalization is forbidden in disordered one-dimensional systems with Hermiticity. This continuum model and its lattice counterpart, which were first introduced by Hatano and Nelson [HN96, HN97], are prototypical models that exhibit topological phases intrinsic to non-Hermitian systems, as extensively discussed later in this thesis.

In a related context, it was proposed that the imaginary gauge potential describes the dielectric breakdown of a Mott insulator [FK98]. There, the imaginary vector potential was demonstrated to destroy the Mott-insulating phase and lead to a new type of quantum phase transition. This discovery shows a unique role of non-Hermiticity in quantum many-body physics. The connection between the imaginary vector potential and the dielectric breakdown was rigorously justified in a subsequent work [OA10].

It is also notable that the equivalence between non-Hermitian systems in flat spaces and Hermitian systems in curved spaces has been proposed for specific models in a recent work [LZZar]. This equivalence implies that non-Hermiticity can be engineered by controlling the geometry of the underlying space.

2.4 Symmetry

Symmetry plays a significant role in modern physics. In non-Hermitian physics, $\mathcal{PT}$ symmetry is relevant to real spectra and exceptional points, as discussed in Sec. 2.1.1. Here, we review general classification of internal symmetry for Hermitian and non-Hermitian systems. In Sec. 2.4.1, we review the 10-fold symmetry classification of Hermitian systems (Table 2.1), which was first provided by Altland and Zirnbauer [AZ97]. In Sec. 2.4.2, we show that non-Hermiticity changes the nature of symmetry by ramifying and unifying symmetry in a fundamental manner. In Sec. 2.4.3, we review the symmetry classification of non-Hermitian systems (Table 2.2) [KSUS19]. As a consequence of the symmetry ramification and unification, the symmetry classification of non-Hermitian systems is 38 fold instead of 10 fold. This 38-fold symmetry classification is a fundamental theoretical framework of non-Hermitian physics and describes, for example, non-Hermitian topological phases and non-Hermitian random matrices.

2.4.1 Altland-Zirnbauer symmetry

We summarize the tenfold internal-symmetry class for noninteracting fermionic systems (Table 2.1) [AZ97, EM08, Bee15, CTSR16]. We consider a generic noninteracting fermionic system described by the Hermitian Hamiltonian

$$\hat{H} = \sum_{m,n} \hat{c}_m^\dagger H_{m,n} \hat{c}_n. \tag{2.60}$$

Table 2.1: Tenfold Altland-Zirnbauer (AZ) symmetry class [AZ97]. The symmetry class is specified by the presence or absence of time-reversal symmetry (TRS), particle-hole symmetry (PHS), and chiral symmetry (CS). The entries ± 1 indicate the signs of TRS and PHS. The entries 0 indicate the absence of the symmetry.

AZ class	TRS	PHS	CS
A	0	0	0
AIII	0	0	1
AI	+1	0	0
BDI	+1	+1	1
D	0	+1	0
DIII	−1	+1	1
AII	−1	0	0
CII	−1	−1	1
C	0	−1	0
CI	+1	−1	1

Here, $\hat{c}_n$ ($\hat{c}_n^\dagger$) annihilates (creates) a fermion on site n, satisfying the canonical anticommutation relations $\{\hat{c}_m, \hat{c}_n^\dagger\} = \delta_{m,n}$. The indices n describe the lattice sites, as well as possible internal degrees of freedom such as the spin degree of freedom. The Hermitian matrix $H = (H_{m,n})_{m,n}$ is the single-particle Hamiltonian. While we discuss normal fermionic systems in Eq. (2.60) in the following, the discussion can be straightforwardly generalized to Bogoliubov-de Gennes Hamiltonians for superconductors by using the Nambu spinors instead of the complex fermion operators.

We begin with unitary symmetry that does not mix fermion annihilation and creation operators. We introduce a symmetry transformation by

$$\hat{c}_m \to \hat{c}'_m \coloneqq \hat{\mathcal{U}} \hat{c}_m \hat{\mathcal{U}}^{-1} = \sum_n \mathcal{U}_{m,n} \hat{c}_n. \tag{2.61}$$

Here, $\hat{\mathcal{U}}$ is a unitary operator that acts on the fermionic Fock space, while $\mathcal{U} = (\mathcal{U}_{m,n})_{m,n}$ is a unitary matrix instead of a second-quantized operator. Because of unitarity of $\hat{\mathcal{U}}$, the canonical anticommutation relations are preserved under the symmetry transformation:

$$\left\{\hat{c}_m, \hat{c}_n^\dagger\right\} = \hat{\mathcal{U}} \left\{\hat{c}_m, \hat{c}_n^\dagger\right\} \hat{\mathcal{U}}^{-1}. \tag{2.62}$$

Symmetry of the system is described by the invariance of the Hamiltonian $\hat{H}$ under the symmetry operation $\hat{\mathcal{U}}$:

$$\hat{\mathcal{U}} \hat{H} \hat{\mathcal{U}}^{-1} = \hat{H}, \tag{2.63}$$

which is equivalent to

$$\mathcal{U}^{-1} H \mathcal{U} = H \tag{2.64}$$

for the single-particle Hamiltonian H. The unitary operation $\hat{\mathcal{U}}$ is internal when it acts only on the internal degrees of freedom and does not act on the spatial degrees of freedom. Such internal symmetry is relevant to disordered electron systems and characterizes the universality classes of Anderson localization and topological phases. We note that the tenfold symmetry classification [AZ97] does not include the unitary symmetry that commutes with single-particle Hamiltonians. This is because the Hamiltonian is block diagonalized in a trivial manner in the presence of such unitary symmetry.

Time-reversal symmetry Time-reversal symmetry is described by the antiunitary operation defined by

$$\hat{\mathcal{T}}\hat{c}_m\hat{\mathcal{T}}^{-1} = \sum_n \mathcal{T}_{m,n}\hat{c}_n \tag{2.65}$$

and

$$\forall\, z \in \mathbb{C} \quad \hat{\mathcal{T}} z \hat{\mathcal{T}}^{-1} = z^*. \tag{2.66}$$

Here, $\hat{\mathcal{T}}$ is an antiunitary operator that acts on the fermionic Fock space, while $\mathcal{T} = (\mathcal{T}_{m,n})_{m,n}$ is a unitary matrix. A system respects time-reversal invariance if the Hamiltonian $\hat{H}$ satisfies

$$\hat{\mathcal{T}}\hat{H}\hat{\mathcal{T}}^{-1} = \hat{H}. \tag{2.67}$$

If this relation is satisfied, we have

$$\hat{\mathcal{T}}\hat{O}\left(t\right)\hat{\mathcal{T}}^{-1} = \hat{O}\left(-t\right), \tag{2.68}$$

where $\hat{O}\left(t\right) = e^{\mathrm{i}\hat{H}t}\hat{O}e^{-\mathrm{i}\hat{H}t}$ is the time-evolved operator of a fermionic operator $\hat{O}$. In terms of the single-particle Hamiltonian H, time-reversal invariance is equivalent to

$$\mathcal{T}^{-1}H^*\mathcal{T} = H. \tag{2.69}$$

In the presence of translation invariance, time-reversal symmetry imposes

$$\mathcal{T}H^*\left(\boldsymbol{k}\right)\mathcal{T}^{-1} = H\left(-\boldsymbol{k}\right) \tag{2.70}$$

on the Bloch Hamiltonian $H\left(-\boldsymbol{k}\right)$ in momentum space. Because of antiunitarity of time-reversal symmetry, the symmetry operator and matrix are required to satisfy

$$\hat{\mathcal{T}}^2 = \left(\pm 1\right)^{\hat{N}}, \quad \mathcal{T}^*\mathcal{T} = \pm 1 \tag{2.71}$$

with the number operator $\hat{N} \coloneqq \sum_n \hat{c}_n^\dagger \hat{c}_n$. The signs in these equations correspond to the signs of time-reversal symmetry in Table 2.1. For $\hat{\mathcal{T}}^2 = -1$, time-reversal symmetry leads to the Kramers degeneracy. Generally, while time-reversal symmetry with $\mathcal{T}^*\mathcal{T} = +1$ enhances Anderson localization [GLK79, AKLL80], time-reversal symmetry with $\mathcal{T}^*\mathcal{T} = -1$ suppresses Anderson localization [HLN80]. Similarly, while time-reversal symmetry with $\mathcal{T}^*\mathcal{T} = +1$ leads to the absence of topological phases in two dimensions, time-reversal symmetry with $\mathcal{T}^*\mathcal{T} = -1$ gives rise to the $\mathbb{Z}_2$ topological phases that host the quantum spin Hall effect [KM05b, KM05a].

Particle-hole symmetry Particle-hole symmetry (or equivalently, charge-conjugation symmetry) is described by the unitary operation defined by

$$\hat{\mathcal{C}}\hat{c}_m\hat{\mathcal{C}}^{-1} = \sum_n \mathcal{C}_{m,n}^*\hat{c}_n^\dagger, \tag{2.72}$$

where $\hat{\mathcal{C}}$ and $\mathcal{C} = (\mathcal{C}_{m,n})_{m,n}$ are unitary operators and matrices, respectively. In contrast to time-reversal symmetry, this operation mixes fermion annihilation and creation operators. It describes the transformation between particles and holes, and flips the sign of the electron charge with respect to the charge neutral point:

$$\hat{\mathcal{C}}\hat{Q}\hat{\mathcal{C}}^{-1} = -\hat{Q} \tag{2.73}$$

with $\hat{Q} \coloneqq \hat{N} - N/2$. The Hamiltonian is particle-hole symmetric if it satisfies

$$\hat{\mathcal{C}}\hat{H}\hat{\mathcal{C}}^{-1} = \hat{H}, \tag{2.74}$$

which leads to $\operatorname{tr} H = 0$ and

$$\mathcal{C}^{-1}H^{T}\mathcal{C} = -H \tag{2.75}$$

in real space and

$$\mathcal{C}H^{T}(\boldsymbol{k})\mathcal{C}^{-1} = -H(-\boldsymbol{k}) \tag{2.76}$$

in momentum space. Particle-hole symmetry acts as unitary symmetry on the fermionic Fock space but acts as antiunitary symmetry on the single-particle Hilbert space. Similarly to time-reversal symmetry, the symmetry operator and matrix are required to satisfy

$$\hat{\mathcal{C}}^{2} = (\pm 1)^{\hat{N}}, \quad \mathcal{C}^{*}\mathcal{C} = \pm 1. \tag{2.77}$$

In the presence of particle-hole symmetry, eigenenergy appears in opposite-sign pairs $(E, -E)$; zero-energy modes are subject to a special constraint. Similarly to time-reversal symmetry, particle-hole symmetry changes the universality classes of Anderson localization and topological phases. For $\mathcal{C}^{*}\mathcal{C} = +1$, for example, zero modes remain to be delocalized even in one-dimensional disordered systems [BFGM00], while such delocalization is forbidden in one-dimensional disordered systems without symmetry protection. Furthermore, particle-hole symmetry plays a crucial role in topological superconductors [Ali12, SA17].

Chiral symmetry Finally, chiral symmetry (or equivalently, sublattice symmetry) is defined by the antiunitary operation defined by

$$\hat{\Gamma}\hat{c}_{m}\hat{\Gamma}^{-1} = \sum_{n} \Gamma_{m,n}\hat{c}_{n}^{\dagger}, \tag{2.78}$$

where $\hat{\Gamma}$ is an antiunitary operator on the fermionic Fock space, and $\Gamma = (\Gamma_{m,n})_{m,n}$ is a unitary matrix on the single-particle Hilbert space. The system respects chiral symmetry if the Hamiltonian satisfies

$$\hat{\Gamma}\hat{H}\hat{\Gamma}^{-1} = \hat{H}, \tag{2.79}$$

which leads to $\operatorname{tr} H = 0$ and

$$\Gamma^{-1}H\Gamma = -H \tag{2.80}$$

in real space and

$$\Gamma H(\boldsymbol{k})\Gamma^{-1} = -H(\boldsymbol{k}) \tag{2.81}$$

in momentum space. The symmetry matrix Γ can be chosen to be Hermitian and satisfy $\Gamma^{2} = 1$ without loss of generality. In the simultaneous presence of time-reversal symmetry and particle-hole symmetry, chiral symmetry appears as a combination of the two symmetry. Even in the absence of time-reversal symmetry and particle-hole symmetry, chiral symmetry can be respected, for example, in bipartite hopping models. Similarly to particle-hole symmetry, chiral symmetry imposes a special constraint on zero modes, which results in delocalization even in one-dimensional disordered systems [Dys53, BMSA98]. Chiral symmetry can also protect topological phases in one dimension and lead to pairs of zero modes at boundaries, for example, in a model of polyacetylene [SSH79].

2.4.2 Symmetry ramification and unification

Non-Hermiticity changes the nature of symmetry [KSUS19]. In fact, non-Hermiticity ramifies and unifies symmetry in a fundamental manner. First, to see the symmetry ramification, let us consider particle-hole symmetry as an example. For Hermitian systems, particle-hole symmetry is defined by Eq. (2.75). Thus, particle-hole symmetry can be generalized by the same equation for non-Hermitian systems. However, we can generalize particle-hole symmetry in another way. The key property is that transposition coincides with complex conjugation for Hermitian systems by definition:

$$H^* = H^T. \tag{2.82}$$

As a result, for Hermitian systems, Eq. (2.75) is equivalent to the following equation defined with complex conjugation:

$$\mathcal{C}^{-1} H^* \mathcal{C} = -H. \tag{2.83}$$

Importantly, Eqs. (2.75) and (2.83) are not equivalent for non-Hermitian systems. Thus, non-Hermiticity ramifies particle-hole symmetry. Since non-Hermitian Bogoliubov-de Gennes Hamiltonians for superconductors and superfluids satisfy Eq. (2.75) as shown below, the symmetry in Eq. (2.75) [Eq. (2.83)] is denoted by PHS (PHS†) for non-Hermitian systems.

Such symmetry ramification occurs also for all the other symmetry. Another crucial example is chiral symmetry and sublattice symmetry, which are equivalent to each other and defined by Eq. (2.80) for Hermitian systems. Equation (2.80) can be directly generalized to non-Hermitian systems, but again, chiral symmetry can be generalized in a different manner. For Hermitian systems, Eq. (2.80) is equivalent to

$$\Gamma^{-1} H^\dagger \Gamma = -H, \tag{2.84}$$

because of $H = H^\dagger$. Importantly, Eqs. (2.80) and (2.84) are not equivalent to each other for non-Hermitian systems although they are equivalent in the presence of Hermiticity. Since the physical chiral symmetry, which is the combined symmetry of time-reversal symmetry and particle-hole symmetry, is described by Eq. (2.84) as shown below, the symmetry in Eq. (2.84) [Eq. (2.80)] is denoted by CS (CS†) for non-Hermitian systems. Here, CS† is also denoted by SLS because bipartite lattice systems realize this symmetry even in the presence of non-Hermiticity.

Non-Hermiticity not only ramifies but also unifies symmetry [KHG+19]. To see this symmetry unification, we consider the following antiunitary symmetry:

$$\mathcal{T}^{-1} H^* \mathcal{T} = H, \quad \mathcal{C}^{-1} H^* \mathcal{C} = -H, \tag{2.85}$$

where $\mathcal{T}$ and $\mathcal{C}$ are unitary matrices. As discussed above, $\mathcal{T}$ describes time-reversal symmetry (TRS), while $\mathcal{C}$ describes the Hermitian conjugate of particle-hole symmetry (i.e., PHS†), which are clearly distinct from each other for Hermitian systems. However, when a non-Hermitian system H respects TRS, another non-Hermitian system iH respects PHS†. Thus, a set of all non-Hermitian systems having TRS coincides with another set of all non-Hermitian systems having PHS†; non-Hermiticity unifies TRS and PHS†.

As a consequence of the symmetry ramification and unification, the 10-fold symmetry classification for Hermitian systems (Table 2.1) [AZ97] is replaced by the 38-fold symmetry classification for non-Hermitian systems (Table 2.2) [KSUS19], as demonstrated in the following.

Table 2.2: AZ and AZ† symmetry classes for non-Hermitian Hamiltonians [KSUS19]. Time-reversal symmetry (TRS) and particle-hole symmetry (PHS) are defined by $\mathcal{T}H^*(\boldsymbol{k})\mathcal{T}^{-1} = H(-\boldsymbol{k})$ with $\mathcal{T}\mathcal{T}^* = \pm 1$ and $\mathcal{C}H^T(\boldsymbol{k})\mathcal{C}^{-1} = -H(-\boldsymbol{k})$ with $\mathcal{C}\mathcal{C}^* = \pm 1$, respectively. As a combination of TRS and PHS, chiral symmetry (CS) is defined by $\Gamma H^\dagger(\boldsymbol{k})\Gamma^{-1} = -H(\boldsymbol{k})$ with $\Gamma^2 = 1$. The 10-fold AZ symmetry class is divided into the 2-fold complex class that only involves CS and the 8-fold real class where TRS and PHS are relevant. Moreover, TRS† and PHS† are respectively defined by $\mathcal{T}H^T(\boldsymbol{k})\mathcal{T}^{-1} = H(-\boldsymbol{k})$ with $\mathcal{T}\mathcal{T}^* = \pm 1$ and $\mathcal{C}H^*(\boldsymbol{k})\mathcal{C}^{-1} = -H(-\boldsymbol{k})$ with $\mathcal{C}\mathcal{C}^* = \pm 1$, which constitute the AZ† symmetry class. Class AI (AII) in the real AZ symmetry class and class D† (C†) in the real AZ† symmetry class are equivalent.

Symmetry class		TRS	PHS	TRS†	PHS†	CS
Complex AZ	A	0	0	0	0	0
	AIII	0	0	0	0	1
Real AZ	AI	+1	0	0	0	0
	BDI	+1	+1	0	0	1
	D	0	+1	0	0	0
	DIII	−1	+1	0	0	1
	AII	−1	0	0	0	0
	CII	−1	−1	0	0	1
	C	0	−1	0	0	0
	CI	+1	−1	0	0	1
Real AZ†	AI†	0	0	+1	0	0
	BDI†	0	0	+1	+1	1
	D†	0	0	0	+1	0
	DIII†	0	0	−1	+1	1
	AII†	0	0	−1	0	0
	CII†	0	0	−1	−1	1
	C†	0	0	0	−1	0
	CI†	0	0	+1	−1	1

2.4.3 38-fold symmetry

AZ symmetry We consider a generic noninteracting fermionic system described by the following second-quantized non-Hermitian Hamiltonian

$$\hat{H} = \sum_{m,n} \hat{c}_m^\dagger H_{m,n} \hat{c}_n, \tag{2.86}$$

where the matrix H is a single-particle non-Hermitian Hamiltonian. In contrast to the previous discussions, we do not impose Hermiticity on $\hat{H}$ or H. Time reversal is described by an antiunitary operator $\hat{\mathcal{T}}$ that acts on the fermion operators in the same manner as the Hermitian case:

$$\hat{\mathcal{T}}\hat{c}_m\hat{\mathcal{T}}^{-1} = \sum_n \mathcal{T}_{m,n}\hat{c}_n, \quad \hat{\mathcal{T}}z\hat{\mathcal{T}}^{-1} = z^* \quad (\forall\, z \in \mathbb{C}), \tag{2.87}$$

where $\mathcal{T}$ is a unitary matrix ($\mathcal{T}\mathcal{T}^\dagger = \mathcal{T}^\dagger\mathcal{T} = 1$). This operation serves as time reversal also in non-Hermitian systems. Time-reversal invariance of the second-quantized Hamiltonian leads to

$$\mathcal{T}^{-1}H^*\mathcal{T} = H, \quad \mathcal{T}\mathcal{T}^* = \pm 1 \tag{2.88}$$

in real space, and

$$\mathcal{T}H^*(\boldsymbol{k})\mathcal{T}^{-1} = H(-\boldsymbol{k}), \quad \mathcal{T}\mathcal{T}^* = \pm 1 \tag{2.89}$$

in momentum space. This action on a single-particle non-Hermitian Hamiltonian by TRS is the same as that on a Hermitian one [AZ97]. As discussed in Sec. 2.1.1, TRS is relevant to the reality of spectra and the stability of non-Hermitian systems.

Similarly to the Hermitian case, PHS is described by a unitary operator $\hat{\mathcal{C}}$ that acts on the fermion operators as

$$\hat{\mathcal{C}}\hat{c}_m\hat{\mathcal{C}}^{-1} = \sum_n \mathcal{C}^*_{m,n}\hat{c}^\dagger_n, \tag{2.90}$$

where $\mathcal{C}$ is a unitary matrix ($\mathcal{C}\mathcal{C}^\dagger = \mathcal{C}^\dagger\mathcal{C} = 1$). The presence of PHS for the second-quantized Hamiltonian $\hat{\mathcal{C}}\hat{H}\hat{\mathcal{C}}^{-1} = \hat{H}$ leads to

$$\mathcal{C}^{-1}H^T\mathcal{C} = -H, \quad \mathcal{C}\mathcal{C}^* = \pm 1 \tag{2.91}$$

in real space, and

$$\mathcal{C}H^T(\boldsymbol{k})\mathcal{C}^{-1} = -H(-\boldsymbol{k}), \quad \mathcal{C}\mathcal{C}^* = \pm 1 \tag{2.92}$$

in momentum space. As also pointed out in Sec. 2.4.2, in the presence of Hermiticity ($\hat{H}^\dagger = \hat{H}$), this PHS condition is equivalent to $\mathcal{C}H^*(\boldsymbol{k})\mathcal{C}^{-1} = -H(-\boldsymbol{k})$ [AZ97]. For non-Hermitian Hamiltonians, however, complex conjugation and transposition do not coincide with each other, and thus PHS is defined in terms of transposition instead of complex conjugation.

As a combination of TRS and PHS, CS is defined by an antiunitary operator $\hat{\Gamma} \coloneqq \hat{\mathcal{T}}\hat{\mathcal{C}}$. The invariance of the Hamiltonian $\hat{H}$ under $\hat{\Gamma}$ imposes the following condition on a single-particle Hamiltonian:

$$\Gamma^{-1}H^\dagger\Gamma = -H, \quad \Gamma^2 = 1 \tag{2.93}$$

in real space, and

$$\Gamma H^\dagger(\boldsymbol{k})\Gamma^{-1} = -H(\boldsymbol{k}), \quad \Gamma^2 = 1 \tag{2.94}$$

in momentum space. This CS condition is equivalent to $\Gamma H(\boldsymbol{k})\Gamma^{-1} = -H(\boldsymbol{k})$ in the presence of Hermiticity ($\hat{H}^\dagger = \hat{H}$) [AZ97], but it is not for non-Hermitian Hamiltonians. For example, graphene [SHEK12, ESHK11] and the Su-Schrieffer-Heeger model [Sch13, WKP+17, Lie18a, PWH+18] with balanced gain and loss respect CS.

The three symmetry $\mathcal{T}$, $\mathcal{C}$, and Γ constitute a natural and physical extension of the Altland-Zirnbauer symmetry class for non-Hermitian Hamiltonians (Table 2.2), which respectively act on a non-Hermitian Hamiltonian as Eqs. (2.89), (2.92), and (2.94). The 10-fold symmetry class is divided into the 2-fold complex class that only involves CS and the 8-fold real class where TRS and PHS are relevant.

AZ† symmetry In contrast to the Hermitian case, other internal symmetry arises. As a result of the difference between complex conjugation and transposition for non-Hermitian Hamiltonians (i.e., $H^* \neq H^T$), a variant of TRS appears, which is defined with transposition by

$$\mathcal{T}H^T(\boldsymbol{k})\mathcal{T}^{-1} = H(-\boldsymbol{k}), \quad \mathcal{T}\mathcal{T}^* = \pm 1, \tag{2.95}$$

where $\mathcal{T}$ is a unitary matrix ($\mathcal{T}\mathcal{T}^\dagger = \mathcal{T}^\dagger\mathcal{T} = 1$). Similarly, a variant of PHS can be defined with complex conjugation by

$$\mathcal{C}H^*(\boldsymbol{k})\mathcal{C}^{-1} = -H(-\boldsymbol{k}), \quad \mathcal{C}\mathcal{C}^* = \pm 1, \tag{2.96}$$

where $\mathcal{C}$ is a unitary matrix ($\mathcal{C}\mathcal{C}^\dagger = \mathcal{C}^\dagger\mathcal{C} = 1$). In the following, the symmetry described by Eq. (2.95) is denoted by TRS†, and the symmetry described by Eq. (2.96) is denoted by PHS†. This is because TRS† (PHS†) is defined by Hermitian conjugation of TRS (PHS). For Hermitian Hamiltonians ($H = H^\dagger$), TRS and PHS respectively coincide with TRS† and PHS†; however, this is not the case in the presence of non-Hermiticity. This Hermitian-conjugate counterpart of the Altland-Zirnbauer symmetry also appears naturally in non-Hermitian systems. For example, onsite dissipation often breaks Hermiticity and TRS at the same time, but their combination can be retained as TRS†. Furthermore, effective non-Hermitian Hamiltonians in the scattering theory support the symmetry. It is also notable that TRS† describes reciprocity of non-Hermitian Hamiltonians and plays an important role in the skin effects and the anomalous delocalization, as discussed later in this thesis.

TRS† and PHS† in addition to CS also constitute the 10-fold symmetry class, which we call the AZ† symmetry class (Table 2.2). This AZ† symmetry class is again divided into the 2-fold complex class that only involves CS and the 8-fold real class where TRS† and PHS† are relevant. Here, each complex AZ† class coincides with the corresponding complex AZ class. Moreover, class AI in the real AZ class and class D† in the real AZ† class are equivalent because of the topological unification of TRS and PHS† [KHG+19]: when a non-Hermitian Hamiltonian H respects TRS, another non-Hermitian Hamiltonian iH respects PHS†. Similarly, class AII in the real AZ class and class C† in the real AZ† class are equivalent.

Sublattice symmetry Another important internal symmetry is SLS, which is defined in momentum space by

$$\mathcal{S}H\left(\boldsymbol{k}\right)\mathcal{S}^{-1} = -H\left(\boldsymbol{k}\right), \quad \mathcal{S}^2 = 1, \tag{2.97}$$

where $\mathcal{S}$ is a unitary matrix ($\mathcal{S}\mathcal{S}^\dagger = \mathcal{S}^\dagger\mathcal{S} = 1$). For example, SLS appears in a bipartite lattice where particle hopping only connects sites on different sublattices, such as the Su-Schrieffer-Heeger model [SSH79] with asymmetric hopping [Lee16, Lie18a, MABVFT18, YJL+18, YW18, KEBB18]. SLS coincides with CS defined by Eq. (2.94) in the presence of Hermiticity ($H = H^\dagger$) [AZ97], but this is not the case for non-Hermitian Hamiltonians.

SLS can be considered as additional symmetry to the AZ symmetry (see Tables XI and XII in Appendix A of Ref. [KSUS19] for details). There are 3 symmetry classes for the complex AZ class with SLS and 19 symmetry classes for the real AZ class with SLS.

Pseudo-Hermiticity As pointed out in Sec. 2.1.1, pseudo-Hermiticity serves as another key internal symmetry [Mos02a, Mos02b, Mos02c], which is defined by

$$\eta H^\dagger\left(\boldsymbol{k}\right)\eta^{-1} = H\left(\boldsymbol{k}\right), \quad \eta^2 = 1, \tag{2.98}$$

with a unitary and Hermitian matrix η ($\eta\eta^\dagger = \eta^\dagger\eta = 1$ and $\eta^\dagger = \eta$). Here, pseudo-Hermiticity is a generalization of Hermiticity, in that it is trivially satisfied with $\eta = 1$ in the presence of Hermiticity. In addition, it has a similar role to $\mathcal{PT}$ symmetry [BB98, BBJ02, Ben07] because positivity of η is equivalent to the real spectrum of a non-Hermitian Hamiltonian [Mos02a, Mos02b, Mos02c]. Pseudo-Hermiticity can also be considered as additional symmetry to the AZ or AZ† symmetry class. Moreover, the AZ or AZ† class with pseudo-Hermiticity is equivalent to the AZ or AZ† class with SLS (see Table XIV in Appendix B of Ref. [KSUS19] for details).

38-fold classification The symmetry discussed above constitutes all the internal symmetry in non-Hermitian physics, which generalizes and extends the AZ symmetry classification [AZ97]

for Hermitian Hamiltonians to that for non-Hermitian Hamiltonians. This symmetry classification is 38 fold: the 10 AZ symmetry classes with the additional 6 AZ† symmetry classes, as well as the 22 AZ symmetry classes with SLS. This 38-fold symmetry classification is generally applicable to a number of non-Hermitian systems.

The 38-fold classification [KSUS19] is basically equivalent to the Bernard-LeClair symmetry classification that describes non-Hermitian random matrices [BL02, Mag08, SHEK12, ESHK11, Lie18b, BCKB19]. The Bernard-LeClair symmetry classification initially overlooked five symmetry classes, which were corrected and completed by the 38-fold symmetry classification in Ref. [KSUS19] (see Sec. II F of Ref. [KSUS19] for details). The physical insight into these symmetry classes was also elucidated in Ref. [KSUS19].

2.5 Topology

Topology plays a central role in contemporary physics. In particular, topology describes a variety of phases of matter that cannot be described by spontaneous symmetry breaking [HK10, QZ11, CTSR16]. Topological phases are ubiquitous in insulators and superconductors, as well as semimetals, all of which are classified according to symmetry [CTSR16]. A signature of topology manifests itself as the bulk-boundary correspondence: nontrivial bulk topology results in the emergence of anomalous boundary states. Certain topological phases and their anomalous boundary modes are protected by symmetry.

Here, we review topological phases of Hermitian and non-Hermitian systems. In Sec. 2.5.1, we review topological phases and their classification of Hermitian insulators and superconductors. In Sec. 2.5.2, we introduce two types of complex-energy gaps, point and line gaps, which are key to understanding non-Hermitian topology. In Sec. 2.5.3, we review the topological classification of non-Hermitian systems on the basis of the two types of complex-energy gaps and the 38-fold internal symmetry (see also Sec. 2.4 for details about symmetry in non-Hermitian physics). In Sec. 2.5.4, we demonstrate that the interplay of the two types of complex-energy gaps characterizes unique topological structures of exceptional points.

2.5.1 Topological classification of Hermitian systems

In one dimension, chiral symmetry or particle-hole symmetry gives rise to topological phases although no topological phases appear in the absence of symmetry. Such symmetry-protected topological phases in one dimension are characterized by the quantized polarization of the bulk [Van18]. In the presence of boundaries, zero modes appear at the two ends [SSH79]. In superconductors, the zero modes obey the statistics of Majorana fermions [Kit01], which may be applied to topological quantum computation [NSS+08]. In two dimensions, topological phases can appear even in the absence of symmetry. In fact, the ground-state wave function is characterized by the Chern number [TKNdN82, Koh85, Hal88], which induces the quantum Hall effect. Although an energy gap is open in the bulk, chiral gapless modes accompany this topological phase in the presence of boundaries. Moreover, while the topological phase of the Chern insulator does not rely on any symmetry, time-reversal symmetry

$$\mathcal{T}^{-1}H^*\mathcal{T} = H, \quad \mathcal{T}\mathcal{T}^* = -1 \tag{2.99}$$

leads to a new type of topological phases characterized by a $\mathbb{Z}_2$ topological invariant [KM05b, KM05a]. This type of time-reversal symmetry is respected in spinful fermionic systems. In the presence of such time-reversal symmetry, the quantum Hall response vanishes, but the quantum

spin Hall response arises. Furthermore, anomalous helical edge modes appear in the presence of boundaries, which are subject to the Kramers degeneracy.

As seen in the above prime examples, symmetry plays an important role also in topological phases of matter. The interplay of symmetry and topology is two fold:

- Symmetry imposes constraints and reduces topological phases. For example, the topological phases in the Chern insulator break down in the presence of time-reversal symmetry.
- Symmetry protects and enriches topological phases. For example, the $\mathbb{Z}_2$ topological phase in the quantum spin Hall insulator is protected by time-reversal symmetry.

These competing effects enrich topological phases.

Topological insulators and superconductors in the band theory are generally classified into a periodic table (see Table A.1 in Appendix A.1) [SRFL08, Kit09, RSFL10]. Most fundamentally, topological insulators and superconductors are classified according to the Altland-Zirnbauer symmetry (Table 2.1) [AZ97], which is reviewed in Sec. 2.4.1. On the basis of the internal symmetry, Hermitian topological insulators and superconductors are classified in a general manner (see Appendix A.1 for its derivation).

2.5.2 Complex-energy gaps

In the topological classification of Hermitian insulators and superconductors, two Hermitian Hamiltonians are defined to be topologically equivalent if and only if they are continuously deformed into each other while retaining symmetry and an energy gap. In the non-Hermitian case, on the other hand, it is nontrivial how to define an energy gap since the spectrum is complex for a generic non-Hermitian Hamiltonian.

Here, we recall that an energy gap means the presence of an energy region where no states are present. In the Hermitian case, such a vacant region in the spectrum should be contractible to a zero-dimensional point $E = E_{\mathrm{F}}$ called the Fermi energy since the spectrum is entirely real and forms a one-dimensional parameter space. Thus, it is naturally and uniquely defined to have an energy gap if and only if its energy bands do not cross the Fermi energy $E = E_{\mathrm{F}}$ [Fig. 2.1 (a)]. In the non-Hermitian case, by contrast, a forbidden energy range where no states exist is not necessarily contractible to a zero-dimensional point since the complex spectrum of a generic non-Hermitian Hamiltonian forms a two-dimensional parameter space. As a result, such a forbidden energy region can be either a zero-dimensional point or a one-dimensional line, and accordingly the definition of the complex-energy gap in a non-Hermitian Hamiltonian is not unique. We can define a zero-dimensional point gap if and only if complex-energy bands do not cross a reference point $E = E_{\mathrm{P}}$ in the complex-energy plane [Fig. 2.1 (b)]. Independently, we can also define a one-dimensional line gap if and only if complex-energy bands do not cross a reference line in the complex-energy plane [Fig. 2.1 (c)]. The precise definitions of these complex-energy gaps are provided later in this section.

Importantly, the two definitions are independent of each other, and which one should be adopted depends on the individual physical situations that we are interested in. For example, the Anderson transition in a one-dimensional non-Hermitian system can be captured by topology in terms of a point gap [HN96, HN97, SN98, GAK+18]. On the other hand, topologically protected boundary states experimentally observed in non-Hermitian optical and photonic systems [PBK+15, WKP+17, XZB+17, SJGG+17, PWH+18, BNV+17, ZMT+18, BWH+18] can be understood by a line gap. The two definitions of the complex-energy gaps are thus complementary to each other. Moreover, the topological classification drastically changes according to the definition of the complex-energy gaps, as discussed in detail in Sec. 2.5.3. In the absence

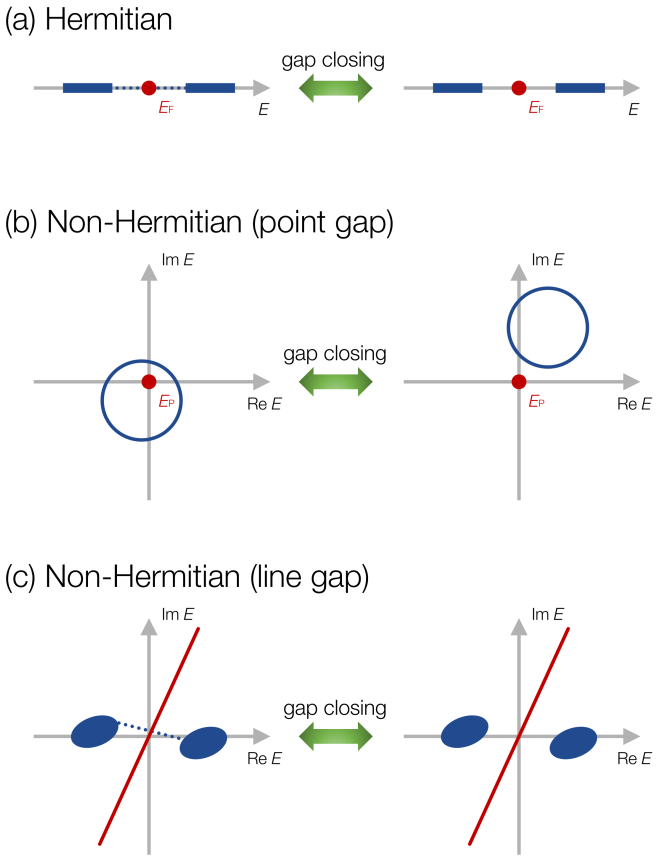

Figure 2.1: Definition of energy gaps for Hermitian and non-Hermitian Hamiltonians. (a) Energy gap for a Hermitian Hamiltonian. A Hermitian Hamiltonian is defined to be gapped if and only if its energy bands do not cross the Fermi energy E_{F} (red dot), and gap closing associated with a topological phase transition occurs between the trivial and topological phases. (b) Point gap for a non-Hermitian Hamiltonian. A non-Hermitian Hamiltonian is defined to have a point gap if and only if its complex-energy bands do not cross a reference point $E = E_{\mathrm{P}}$ in the complex-energy plane (red dot). (c) Line gap for a non-Hermitian Hamiltonian. A non-Hermitian Hamiltonian is defined to have a line gap if and only if its complex-energy bands do not cross a reference line in the complex-energy plane (red line). Reproduced from Fig. 1 of Ref. [KSUS19]. Copyright 2019 by the American Physical Society.

of symmetry, for example, a topological phase characterized by a point gap is present only in odd spatial dimensions, while a topological phase characterized by a line gap is present only in even spatial dimensions (see class A of Table A.3 in Appendix A.2).

Point gap Although a complex-energy point $E = E_{\mathrm{P}}$ that serves as an obstacle in the complex-energy plane is arbitrary in the absence of symmetry, it is subject to restrictions in the presence of symmetry. For example, it should be taken as $\mathrm{Im}\, E_{\mathrm{P}} = 0$ in the presence of time-reversal symmetry since eigenenergy comes in complex-conjugate pairs (E, E^*); it should be taken as $E_{\mathrm{P}} = 0$ in the presence of sublattice symmetry since eigenenergy comes in opposite-sign pairs $(E, -E)$. Thus, it is convenient to choose E_{P} to be zero energy, which leads to the precise definition of the point gap as follows:

Point gap

A non-Hermitian Hamiltonian $H(\boldsymbol{k})$ is defined to have a point gap if and only if it is invertible, i.e.,

$$\forall\, \boldsymbol{k} \quad \det H(\boldsymbol{k}) \neq 0, \tag{2.100}$$

and all the eigenenergy is nonzero, i.e.,

$$\forall\, \boldsymbol{k} \quad E(\boldsymbol{k}) \neq 0. \tag{2.101}$$

Under this definition, a gapless system possesses a zero-energy state for some $\boldsymbol{k}$. A point gap helps understand the Anderson transition in non-Hermitian one-dimensional systems [HN96, HN97, SN98, GAK+18] that occurs as a result of the competition between disorder and non-Hermiticity. Since one-dimensional Hermitian systems always show the Anderson localization [AALR79, ATAF80], the delocalization is unique to non-Hermitian systems. Here, a topological invariant can be assigned to a generic non-Hermitian system in one dimension. In the Hatano-Nelson model [i.e., Eq. (2.59)], wave functions are delocalized (localized) and the system is metallic (insulating) if the winding number is nonzero (zero) [GAK+18]. Moreover, in a non-Hermitian quasicrystal (Aubry-André-Harper model [AA80]), localization (delocalization) of wave functions corresponds to the nontrivial (trivial) topology [Lon19a]. Topology in terms of a point gap also characterizes exceptional points, as discussed in Sec. 2.5.4.

Line gap In the absence of symmetry, a complex-energy line that serves as an obstacle in the complex-energy plane is arbitrary. In the presence of symmetry, by contrast, such a line is subject to restrictions. In particular, it should be either the imaginary axis ($\operatorname{Re} E = 0$) or the real axis ($\operatorname{Im} E = 0$) when symmetry imposes a real structure on the complex spectrum. For example, the real axis should be considered when complex-conjugate pairs (E, E^*) appear in the spectrum because of time-reversal symmetry; the imaginary axis should be considered when pairs $(E, -E^*)$ appear because of chiral symmetry. In contrast to the point gap, there are no restrictions due to sublattice symmetry since sublattice symmetry does not give the complex spectrum real structures [eigenenergy just comes in $(E, -E)$ pairs]. Thus, it is convenient to choose the line that determines the complex gap as the imaginary axis (real gap) or the real axis (imaginary gap), which leads to the precise definition of the line gap in the following:

Line gap

A non-Hermitian Hamiltonian $H(\boldsymbol{k})$ is defined to have a line gap in the real (imaginary) part of its complex spectrum [real (imaginary) gap] if and only if it is invertible, i.e.,

$$\forall\, \boldsymbol{k} \quad \det H(\boldsymbol{k}) \neq 0, \tag{2.102}$$

and the real (imaginary) part of all the eigenenergy is nonzero, i.e.,

$$\forall\, \boldsymbol{k} \quad \operatorname{Re} E(\boldsymbol{k}) \neq 0 \quad (\operatorname{Im} E(\boldsymbol{k}) \neq 0). \tag{2.103}$$

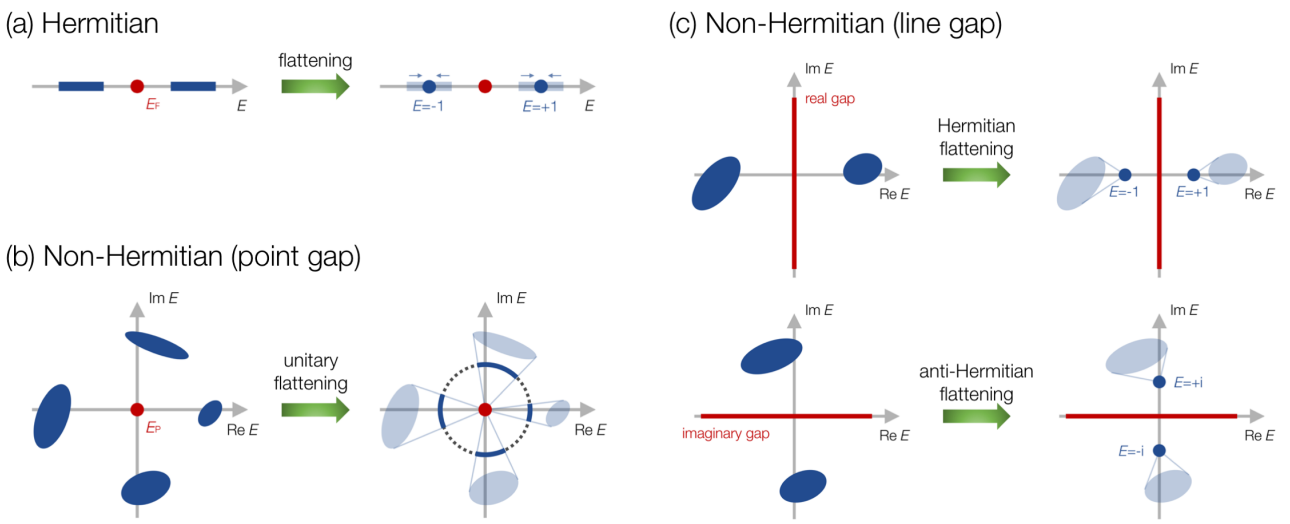

Figure 2.2: Flattening procedures of Hermitian and non-Hermitian Hamiltonians. (a) Flattening of a Hermitian Hamiltonian with an energy gap. A Hermitian Hamiltonian can be flattened to another Hermitian Hamiltonian with $H^2 = 1$ without closing the energy gap. (b) Unitary flattening of a non-Hermitian Hamiltonian with a point gap. A non-Hermitian Hamiltonian can be flattened to a unitary Hamiltonian with $H^\dagger H = 1$ without closing the point gap. (c) Hermitian flattening of a non-Hermitian Hamiltonian with a line gap. A non-Hermitian Hamiltonian can be flattened to a Hermitian (an anti-Hermitian) Hamiltonian with $H^2 = +1$ ($H^2 = -1$) in the presence of a real (an imaginary) gap. Reproduced from Fig. 2 of Ref. [KSUS19]. Copyright 2019 by the American Physical Society.

Under this definition of a real (imaginary) gap, a gapless system includes eigenenergy with $\mathrm{Re}\, E(\boldsymbol{k}) = 0$ ($\mathrm{Im}\, E(\boldsymbol{k}) = 0$) for some $\boldsymbol{k}$. Line gaps were employed explicitly in Refs. [SHEK12, ESHK11, SZF18, KHG+19] and implicitly in many other works. They characterize topologically protected boundary states, which were also observed in experiments [PBK+15, WKP+17, XZB+17, SJGG+17, PWH+18, BNV+17, ZMT+18, BWH+18]. Notably, topologically protected boundary states in Hermitian systems are immune to non-Hermiticity as long as a real gap is open and relevant symmetry is respected, which is generally ensured by the nontrivial non-Hermitian topology in terms of line gaps. Furthermore, the presence of an imaginary gap has a significant influence on the open quantum dynamics [KHG+19] although it has no counterpart in closed systems.

2.5.3 Topological classification of non-Hermitian systems

We provide the topological classification of non-Hermitian systems according to all the 38 symmetry classes discussed in Sec. 2.4.3 and the two types of the complex-energy gaps discussed in Sec. 2.5.2. Here, non-Hermitian Hamiltonians $H_0(\boldsymbol{k})$ and $H_1(\boldsymbol{k})$ are defined to be topologically equivalent if and only if there exists a continuous family of non-Hermitian Hamiltonians $H_\lambda(\boldsymbol{k})$ ($0 \leq \lambda \leq 1$) that interpolates between them, i.e.,

$$H_{\lambda=0}(\boldsymbol{k}) = H_0(\boldsymbol{k}), \quad H_{\lambda=1}(\boldsymbol{k}) = H_1(\boldsymbol{k}) \tag{2.104}$$

with certain symmetry and a complex-energy gap for all $\lambda \in [0, 1]$. Our strategy is to reduce this non-Hermitian problem to the established topological classification of Hermitian Hamiltonians

in the AZ symmetry class without [SRFL08, Kit09, RSFL10] and with [SS14] additional symmetry. In particular, we demonstrate that a non-Hermitian Hamiltonian can be continuously deformed into a unitary matrix in the presence of a point gap [Fig. 2.2 (b)] and a Hermitian or an anti-Hermitian matrix in the presence of a line gap [Fig. 2.2 (c)]. The results are listed in the periodic tables in Appendix A.2.

Unitary flattening for point gaps In the presence of a point gap, a non-Hermitian Hamiltonian can be flattened into a unitary matrix without point-gap closing. This property is guaranteed by the following theorem (see Appendix C in Ref. [KSUS19] for a proof):

Unitary flattening for point gaps

If a non-Hermitian Hamiltonian $H(\boldsymbol{k})$ has a point gap, it can be continuously deformed into a unitary matrix $U(\boldsymbol{k})$ while keeping the point gap and its symmetry [Fig. 2.2 (b)].

This theorem reduces the topological classification of a non-Hermitian Hamiltonian to the classification of a unitary matrix. Furthermore, with the flattened unitary matrix $U(\boldsymbol{k})$, we have a flattened Hermitian matrix

$$\tilde{H}(\boldsymbol{k}) \coloneqq \begin{pmatrix} 0 & U(\boldsymbol{k}) \\ U^\dagger(\boldsymbol{k}) & 0 \end{pmatrix}, \quad \tilde{H}^2(\boldsymbol{k}) = 1. \tag{2.105}$$

Symmetry of the original non-Hermitian Hamiltonian $H(\boldsymbol{k})$ discussed in Sec. 2.4.3 imposes the constraints also on the extended Hermitian Hamiltonian $\tilde{H}(\boldsymbol{k})$. In addition to these constraints, $\tilde{H}(\boldsymbol{k})$ respects additional chiral symmetry (sublattice symmetry):

$$\Sigma\tilde{H}(\boldsymbol{k})\Sigma^{-1} = -\tilde{H}(\boldsymbol{k}), \quad \Sigma \coloneqq \begin{pmatrix} 1 & 0 \\ 0 & -1 \end{pmatrix}. \tag{2.106}$$

Since there exists a one-to-one correspondence between a unitary matrix $U(\boldsymbol{k})$ and an extended Hermitian matrix $\tilde{H}(\boldsymbol{k})$ that satisfies Eq. (2.106) [RH17, GAK+18], topology of $H(\boldsymbol{k})$ can also be captured by the extended Hermitian Hamiltonian $\tilde{H}(\boldsymbol{k})$. Therefore, the topological classification of a non-Hermitian Hamiltonian $H(\boldsymbol{k})$ with a point gap and symmetry reduces to that of a Hermitian Hamiltonian that respects the original symmetry and the additional chiral symmetry in Eq. (2.106), which reduces to the topological classification of Hermitian systems [SRFL08, Kit09, RSFL10, SS14]. In this manner, the periodic tables under point gaps are obtained as Tables A.3-A.9 in Appendix A.2.

Hermitian flattening for line gaps In contrast to the unitary flattening for point gaps, the flattening procedure changes for line gaps. A non-Hermitian Hamiltonian can be flattened into a Hermitian matrix in the presence of a real gap and an anti-Hermitian matrix in the presence of an imaginary gap. This property is guaranteed by the following theorem (see Appendix D in Ref. [KSUS19] for a proof):

Hermitian flattening for line gaps

If a non-Hermitian Hamiltonian $H(\boldsymbol{k})$ has a line gap in the real (imaginary) part of its complex spectrum [real (imaginary) gap], it can be continuously deformed into a Hermitian (an anti-Hermitian) matrix while keeping the line gap and its symmetry [Fig. 2.2 (c)].

This theorem also reduces the topological classification of a non-Hermitian Hamiltonian to that of a Hermitian matrix [SRFL08, Kit09, RSFL10, SS14]. Here, we note that topology of an anti-Hermitian Hamiltonian $H(\boldsymbol{k})$ [i.e, $H^\dagger(\boldsymbol{k}) = -H(\boldsymbol{k})$] under an imaginary gap is equivalent to that of a Hermitian Hamiltonian $\mathrm{i}H(\boldsymbol{k})$ under a real gap [KHG+19]. The periodic tables under line gaps are also obtained as Tables A.3-A.9 in Appendix A.2.

In summary, the rich non-Hermitian topology is attributed to the complex-valued nature of the spectrum, which enables the aforementioned two types of complex-energy gaps: line gap and point gap. Since a non-Hermitian Hamiltonian with a line gap is continuously deformed to a Hermitian Hamiltonian without closing the line gap, topology for a line gap describes the robustness of conventional topological phases against non-Hermitian perturbations, which is relevant to topological lasers [SJGG+17, PWH+18, BNV+17, ZMT+18, HBL+18, BWH+18, ZQW+19], for example. On the other hand, a non-Hermitian Hamiltonian with a point gap is allowed to be deformed to a unitary one. Thus, point-gapped topological phases cannot always be continuously deformed into any Hermitian counterparts; topology for a point gap can be intrinsic to non-Hermitian systems in contrast to a line gap. Consequently, point gaps describe unique non-Hermitian topological phenomena, as extensively explored in this thesis.

2.5.4 Non-Hermitian topology of exceptional points

The two types of complex-energy gaps are also relevant to exceptional points and enable their topological classification [KBS19].

Non-Hermitian gapless structures As discussed in Sec. 2.5.2, in the presence of a point (line) gap, complex-energy bands do not cross a reference point (line) in the complex-energy plane [Fig. 2.3 (a, b)]. If symmetry exists, both complex-energy gaps should be invariant under the symmetry. Without loss of generality, the reference point is supposed to be placed on the reference line. Then, a line gap is always closed when a point gap is closed. However, the converse is not necessarily true; a point gap can be open even when a line gap is closed.

This nature of complex-energy gaps enables two distinct types of non-Hermitian gapless structures. We encircle a gapless region (point, line, surface, and so on) in momentum space by a $(p-1)$-dimensional sphere S^{p-1} $(p \geq 1)$, where S^0, S^1, and S^2 denote a pair of points, a circle, and a surface, respectively. The system has a complex-energy gap on S^{p-1}, but two different situations may happen:

(i) Both point and line gaps are open [Fig. 2.3 (c)].

(ii) Only a point gap is open [Fig. 2.3 (d)].

In the former case [i.e., (i)], the non-Hermitian Hamiltonian on S^{p-1} can be continuously deformed into a Hermitian (or an anti-Hermitian) Hamiltonian [KSUS19]. Thus, in a manner

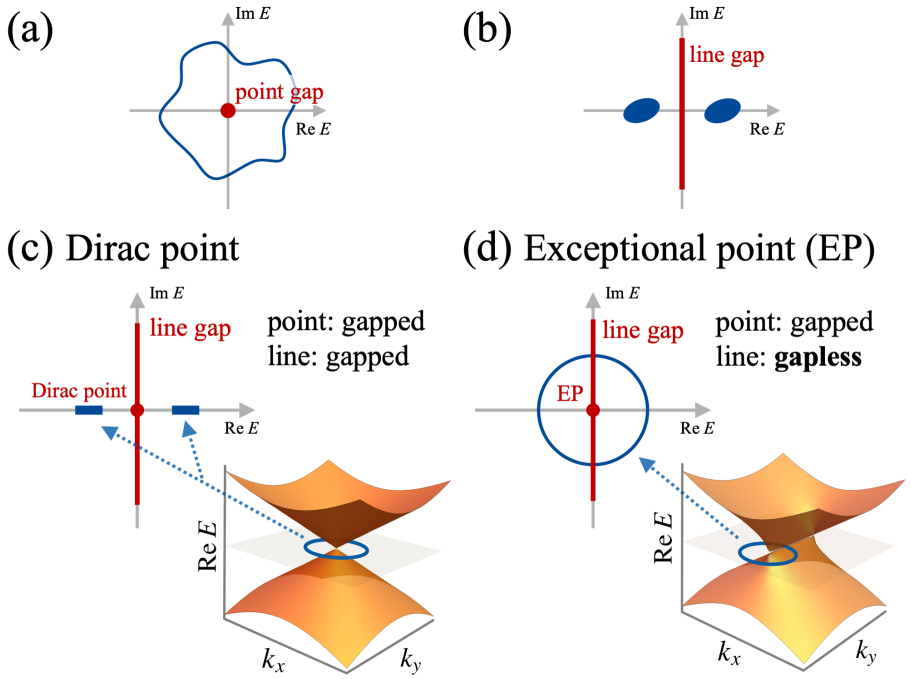

Figure 2.3: Non-Hermitian gapless structures. Complex spectra (blue regions) in non-Hermitian systems may host two types of energy gaps: (a) point gap and (b) line gap. A point (line) gap is open when the complex spectrum does not cross a reference point (line) in the complex-energy plane. (c) Hermitian gapless point (Dirac point). On a region (blue circle) around it, both point and line gaps are open. (d) Exceptional point. On a region (blue circle) around it, a point gap is open but a line gap is closed. Reproduced from Fig. 1 of Ref. [KBS19]. Copyright 2019 by the American Physical Society.

analogous to the Chern number for the Weyl point [AMV18], the gapless region hosts a topological charge essentially identical to that in the Hermitian case. In the latter case [i.e., (ii)], by contrast, we need to assign a different topological charge to the gapless region on the basis of the point gap on S^{p-1}. It should be noted that the latter is intrinsic to non-Hermitian systems and impossible in Hermitian ones, since there is no distinction between point and line gaps for Hermitian Hamiltonians.

Importantly, exceptional points realize the latter unique gapless structure as shown in Fig. 2.3 (d) and are characterized by topological charges for point gaps. A distinctive property of an exceptional point is the swapping of eigenenergy and eigenstates upon its encirclement, as mentioned in Sec. 2.2.3. For illustration, let us consider a two-dimensional system with no symmetry that has an exceptional point $\boldsymbol{k} = \boldsymbol{k}_{\mathrm{EP}}$ at which two complex bands $E_{\pm}(\boldsymbol{k})$ coalesce. A representative model is given as

$$H(\boldsymbol{k}) = k_x \sigma_x + (k_y + \mathrm{i}\gamma)\,\sigma_y \tag{2.107}$$

with Pauli matrices $\sigma_{x,y}$ and the degree of non-Hermiticity γ. While the same model is investigated in Sec. 2.3.2 to understand the bulk Fermi arc, we here focus on its topological characterization. The eigenenergy is

$$E_{\pm}(\boldsymbol{k}) = \pm\sqrt{\boldsymbol{k}^2 - \gamma^2 + 2\mathrm{i}\gamma k_y} \tag{2.108}$$

with the square root singularity around the exceptional points

$$\boldsymbol{k}_{\mathrm{EP}} = (\pm\gamma, 0)\,. \tag{2.109}$$

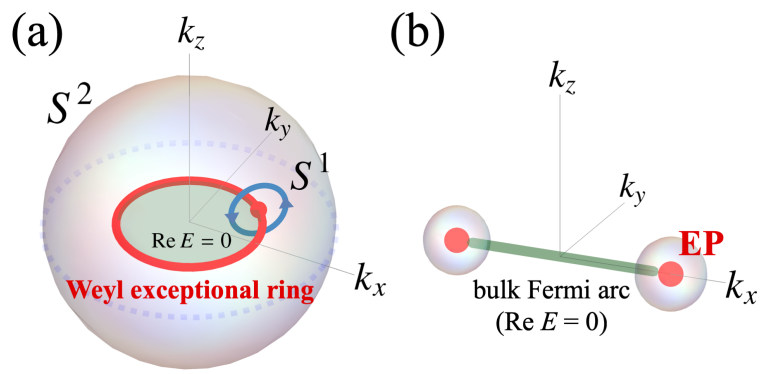

Figure 2.4: Non-Hermitian topological semimetals. (a) Weyl exceptional ring (red ring) with the two independent topological charges, the Chern number defined on the surface S^2 that encloses the ring ($p = 3$, line gap) and the winding number defined on the loop S^1 across the ring ($p = 2$, point gap). (b) Topological dumbbell of exceptional points in three dimensions. The bulk Fermi arc with $\mathrm{Re}\, E = 0$ connects a pair of exceptional points (EPs, red points). Reproduced from Fig. 2 of Ref. [KBS19]. Copyright 2019 by the American Physical Society.

As a direct consequence of this singularity, a branch cut and a self-intersecting Riemann surface appear in the complex-energy plane. Thus, $E_+(\boldsymbol{k})$ and $E_-(\boldsymbol{k})$ are swapped when we go around a loop S^1 in momentum space that encircles one of the exceptional points. Importantly, a point gap for the reference point $E(\boldsymbol{k}_{\mathrm{EP}})$ is open but a line gap is closed on S^1. As a result, the determinant of $H(\boldsymbol{k}) - E(\boldsymbol{k}_{\mathrm{EP}})$ does not vanish on S^1, which enables us to define the winding number for a point gap as

$$W := -\oint_{S^1} \frac{d\boldsymbol{k}}{2\pi \mathrm{i}} \cdot \nabla_{\boldsymbol{k}} \log \det \left[H(\boldsymbol{k}) - E(\boldsymbol{k}_{\mathrm{EP}}) \right]. \tag{2.110}$$

An exceptional point with $W \neq 0$ is topologically stable. For the above representative model, the exceptional points $\boldsymbol{k}_{\mathrm{EP}} = (\pm\gamma, 0)$ are characterized by $W = \mp 1$, respectively.

Multiple topological structure Because of the two types of complex-energy gaps, exceptional points can be characterized by a couple of independent topological charges. A prime example is the Weyl exceptional ring in three-dimensional systems with no symmetry [Fig. 2.4 (a)] [Ber04, XWD17]. For the Hermitian case, the topological stability of a Weyl point in three dimensions is ensured by the Chern number defined on an enclosing surface [AMV18]. In the presence of non-Hermiticity, such a Weyl point morphs into an exceptional ring. A representative model is

$$H(\boldsymbol{k}) = k_x \sigma_x + k_y \sigma_y + (k_z + \mathrm{i}\gamma)\, \sigma_z \tag{2.111}$$

with a Weyl exceptional ring at

$$k_x^2 + k_y^2 = \gamma^2. \tag{2.112}$$

On a sphere [S^2 in Fig. 2.4 (a)] that encloses the ring, a line gap is open, and the Chern number remains to be well defined unless it annihilates with another ring (this Chern number corresponds to the $\mathbb{Z}$ index for a line gap with codimensions $p = 3$; see Table A.10 with no symmetry). Moreover, on S^1 across the ring, a point gap is open and the winding number in Eq. (2.110) is well defined (this winding number corresponds to the $\mathbb{Z}$ index for a point gap with codimensions $p = 2$). Notably, the two topological charges are independent of each other and individually ensure the topological stability of the Weyl exceptional ring. Such a

multiple topological structure is a general hallmark of non-Hermitian topological semimetals. For example, symmetry-protected exceptional rings in two dimensions [ZHI+15,BCKB19,OY19, ZLLZ19, YPKH19] may host different topological charges.

Topological classification of exceptional points We can also classify exceptional points and non-Hermitian topological semimetals according to symmetry and complex-energy gaps. The results are summarized in Table A.10 in Appendix A.3 (see also Tables S2-S7 in Supplemental Material of Ref. [KBS19] for all the 38 symmetry classes). This classification specifies exceptional points and non-Hermitian topological semimetals in a general manner and describes their unconventional nodal structures. The unique nodal structures, as well as the concomitant physical phenomena, are topologically protected against symmetry-preserving perturbations.

The classification also predicts unknown non-Hermitian topological semimetals and nodal superconductors. As an illustrative example, we consider an exceptional point in three dimensions ($p = 3$) protected by chiral symmetry. Although exceptional rings [Ber04, XWD17] and surfaces [OY19, ZLLZ19] were discussed before, such an exceptional point in three dimensions was first discussed in Ref. [KBS19]. A representative model is systematically constructed in the following manner. We begin with a Hermitian gapless system in four dimensions

$$H(\boldsymbol{k}) = k_x\sigma_x\tau_x + k_y\sigma_x\tau_y + k_z\sigma_x\tau_z + k_w\sigma_y \tag{2.113}$$

with Pauli matrices σ_i's and τ_i's. Corresponding to the $\mathbb{Z}$ index for a real line gap with codimensions $p = 4$ (see Table A.10 with chiral symmetry), it possesses a topologically stable gapless point at $\boldsymbol{k} = 0$, around which the three-dimensional winding number [SRFL08, RSFL10, QHZ10] is defined because of chiral symmetry with $\Gamma = \sigma_z$. Now, we add a non-Hermitian perturbation $\mathrm{i}\gamma\sigma_z\tau_x$ to this Hermitian model. Similarly to the Weyl exceptional ring, non-Hermiticity spawns an exceptional ring. The complex spectrum is obtained as

$$E(\boldsymbol{k}) = \pm\sqrt{k_x^2 + k_w^2 + (\sqrt{k_y^2 + k_z^2} \pm \mathrm{i}\gamma)^2}, \tag{2.114}$$

and an exceptional ring appears at

$$k_x^2 + k_w^2 = \gamma^2, \quad k_y = k_z = 0. \tag{2.115}$$

Finally, we take $k_w = 0$ and regard this four-dimensional model as a three-dimensional one,

$$H(\boldsymbol{k}) = k_x\sigma_x\tau_x + k_y\sigma_x\tau_y + k_z\sigma_x\tau_z + \mathrm{i}\gamma\sigma_z\tau_x, \tag{2.116}$$

which has a pair of exceptional points at

$$\boldsymbol{k}_{\mathrm{EP}} = (\pm\gamma, 0, 0). \tag{2.117}$$

As illustrated in Fig. 2.4 (b), these exceptional points are connected by a Fermi arc with $\mathrm{Re}\, E = 0$, forming a topologically stable dumbbell configuration. The topological stability of the exceptional points is ensured by the $\mathbb{Z}$ index, which is given as the Chern number ± 1 of the Hermitian matrix $\mathrm{i}H(\boldsymbol{k})\Gamma$ defined on a surface that encloses each of the exceptional points (see also Table A.10 with chiral symmetry, $p = 3$, and point gap).

Notably, topologically stable gapless points are absent in Hermitian three-dimensional systems with chiral symmetry. The above gapless structures are thus unique to non-Hermitian systems. Furthermore, the above recipe is widely applicable to different symmetry classes and spatial dimensions. Unknown exceptional points and non-Hermitian topological semimetals can be systematically predicted, which is one of the advantages of the classification.

Chapter 3

Non-Hermitian skin effect

As discussed in Chap. 2, much recent research has focused on the distinctive characteristics of non-Hermitian topological phases. The rich non-Hermitian topology is attributed to the complex-valued nature of the spectrum, which enables two types of complex-energy gaps [KSUS19]: line gap and point gap. Since a non-Hermitian Hamiltonian with a line gap is continuously deformed to a Hermitian one without closing the line gap [KSUS19], topology for a line gap describes the robustness of conventional topological phases against non-Hermitian perturbations. On the other hand, a non-Hermitian Hamiltonian with a point gap is allowed to be deformed to a unitary one [GAK+18, KSUS19]. As a result, point-gapped topological phases cannot always be continuously deformed into any Hermitian counterpart; the topology for a point gap is intrinsic to non-Hermitian systems in sharp contrast to a line gap.

A hallmark of topological phases is the presence of localized states at the boundaries as a result of nontrivial topology of the bulk [HK10, QZ11, CTSR16]. Remarkably, non-Hermiticity alters the nature of the bulk-boundary correspondence. The critical distinction is the extreme sensitivity of the bulk to the boundary conditions, which is called the non-Hermitian skin effect [Lee16, YW18, KEBB18]. It accompanies the localization of bulk eigenstates as well as the clear distinction of bulk spectra according to the boundary conditions, which forces us to redefine the bulk topology so as to be suitable for the open boundary conditions. In particular, although the skin effect invalidates the conventional Bloch band theory, researchers formulated a non-Bloch band theory that works even under arbitrary boundary conditions [YW18, YM19]. Recent experimental observations confirmed the skin effect and the non-Bloch band theory in mechanical metamaterials [BLLC19, GBvWC20], electrical circuits [HHI+20, HHS+20], quantum walk [XDW+20], and photonic lattices [WKH+20]. The skin effect plays a crucial role in a general understanding about topological phases of non-Hermitian systems, especially their bulk-boundary correspondence [Lee16, Xio18, MABVFT18, GAK+18, YW18, YSW18b, KEBB18, KSU18, MPBC18, LT19, JS19, LZA+19, LLG19, KD19, EKB19, KSUS19, HBR19, ZRR21, BKS20, YM19, OS19, SYW19a, SYW19b, Lon19b, RHS19, Sch20, IT19, HRB19, CYWR20]. Even if the skin effect occurs, the bulk-boundary correspondence persists in the presence of a line gap since non-Hermitian Hamiltonians with a line gap can be continuously deformed to Hermitian ones. However, the bulk-boundary correspondence for a point gap has yet to be clarified. Since a point gap describes intrinsic non-Hermitian topology, the nature of the bulk-boundary correspondence may be distinct from the Hermitian counterpart. Even when a point gap is open under the periodic boundary conditions, it can be closed under the open boundary conditions [GAK+18, Xio18, LT19]. Thus, the non-Hermitian skin effect obscures point-gap topology.

In this chapter, we provide a unified understanding about the bulk-boundary correspondence

and the skin effect in non-Hermitian systems [OKSS20]. We show that the bulk-boundary correspondence holds even for a point gap in semi-infinite systems with only one boundary. In finite systems with open boundaries, by contrast, we demonstrate that the point-gap topology inevitably induces the non-Hermitian skin effect. Thus, the skin effect originates from intrinsic non-Hermitian topology. On the basis of such a topological origin, we reveal new types of the skin effects protected by symmetry, as illustrated in the next chapter (Chap. 4).

This chapter, especially Secs. 3.3 and 3.4, is based on Ref. [OKSS20].

3.1 Hatano-Nelson model

We begin with reviewing the non-Hermitian skin effect. It accompanies the emergence of an extensive number of skin modes localized at arbitrary boundaries; $\mathcal{O}\left(L^d\right)$ skin modes appear in d dimensions. This sharply contrasts with Hermitian systems, in which the bulk is insensitive to boundary conditions, and there appear $\mathcal{O}\left(L^{d-1}\right)$ boundary modes under the open boundary conditions. The extensive number of boundary modes are unique to non-Hermitian systems.

A prototypical model that exhibits the skin effect is the Hatano-Nelson model [HN96,HN97]:

$$\hat{H}_{\mathrm{HN}}=\sum_n\left[\left(t+g\right)\hat{c}_{n+1}^\dagger\hat{c}_n+\left(t-g\right)\hat{c}_n^\dagger\hat{c}_{n+1}\right], \tag{3.1}$$

where $t,g\in\mathbb{R}$ are the hopping amplitudes, and $\hat{c}_n$ ($\hat{c}_n^\dagger$) annihilates (creates) a particle on site n. We assume $t\geq g\geq 0$ for simplicity. The corresponding Bloch Hamiltonian reads

$$\begin{aligned}H_{\mathrm{HN}}\left(k\right)&=\left(t+g\right)e^{-\mathrm{i}k}+\left(t-g\right)e^{\mathrm{i}k}\\&=2t\cos k-2\mathrm{i}g\sin k.\end{aligned} \tag{3.2}$$

Under the periodic boundary conditions, the system is described by $H_{\mathrm{HN}}\left(k\right)$ with real wave numbers $k\in[0,2\pi]$. The spectrum forms a loop in the complex-energy plane, and the eigenstates are delocalized in the bulk.

Under the open boundary conditions, by contrast, the system is no longer described by $H_{\mathrm{HN}}\left(k\right)$. To understand this, let us consider the following similarity transformation (imaginary gauge transformation [HN96,HN97]):

$$\hat{V}_r^{-1}\hat{c}_i\hat{V}_r=r^{-i}\hat{c}_i,\quad \hat{V}_r^{-1}\hat{c}_i^\dagger\hat{V}_r=r^i\hat{c}_i^\dagger\quad\left(0<r<\infty\right). \tag{3.3}$$

The Hamiltonian $\hat{H}_{\mathrm{HN}}$ transforms into

$$\hat{V}_r^{-1}\hat{H}_{\mathrm{HN}}\hat{V}_r=\sum_n\left[r\left(t+g\right)\hat{c}_{n+1}^\dagger\hat{c}_n+\frac{t-g}{r}\hat{c}_n^\dagger\hat{c}_{n+1}\right]. \tag{3.4}$$

In particular, for

$$r_\times\coloneqq\sqrt{\frac{t-g}{t+g}}, \tag{3.5}$$

we have

$$\hat{V}_{r_\times}^{-1}\hat{H}_{\mathrm{HN}}\hat{V}_{r_\times}=\sqrt{t^2-g^2}\sum_n\left(\hat{c}_{n+1}^\dagger\hat{c}_n+\hat{c}_n^\dagger\hat{c}_{n+1}\right), \tag{3.6}$$

which is Hermitian. Importantly, this transformation does not change the spectrum since it is a similarity transformation under the open boundary conditions. Hence, the non-Hermitian

Hamiltonian $\hat{H}_{\mathrm{HN}}$ with open boundaries has the same spectrum as the Hermitian Hamiltonian $\hat{V}_{r_\times}^{-1}\hat{H}_{\mathrm{HN}}\hat{V}_{r_\times}$, which is given as

$$E(k) = 2\sqrt{t^2 - g^2}\cos k, \quad k \in [0, 2\pi]. \tag{3.7}$$

This spectrum is entirely real and lies on the real axis in the complex-energy plane. Since $\hat{V}_{r_\times}^{-1}\hat{H}_{\mathrm{HN}}\hat{V}_{r_\times}$ has delocalized eigenstates, all the eigenstates of $\hat{H}_{\mathrm{HN}}$ are localized at the left edge as $\sim e^{-n/\xi}$ with the localization length $\xi = |\log r_\times|^{-1}$. Clearly, the spectrum and the eigenstates of the bulk are dramatically sensitive to the boundary conditions, which is impossible in Hermitian systems. This is the non-Hermitian skin effect in the Hatano-Nelson model. In a similar manner, the skin effect generally occurs in non-Hermitian systems. In d dimensions, the $\mathcal{O}(L^d)$ skin modes can appear at arbitrary boundaries including edges and corners.

Meanwhile, the Hatano-Nelson model is also a prototypical example that is characterized by intrinsic non-Hermitian topology. Let us consider a generic one-dimensional system with a point gap [GAK+18, KSUS19]:

$$\forall\, k \in [0, 2\pi] \quad \det(H(k) - E) \neq 0. \tag{3.8}$$

Here, $E \in \mathbb{C}$ is reference energy, and $H(k)$ is the Bloch Hamiltonian. For this one-dimensional system, the topological invariant is given as the following winding number $W(E) \in \mathbb{Z}$:

$$W(E) \coloneqq -\oint_0^{2\pi} \frac{dk}{2\pi \mathrm{i}} \frac{d}{dk} \log\det(H(k) - E). \tag{3.9}$$

This topological invariant is well defined as long as the spectrum of $H(k)$ does not cross the given energy E [i.e., $H(k)$ is point-gapped in terms of a reference point E]. Importantly, the topological invariant $W(E)$ is intrinsic to non-Hermitian systems [GAK+18, KSUS19]. In fact, without symmetry protection, no topological invariant is well defined in Hermitian systems in one dimension [HK10, QZ11, CTSR16].

The non-Hermitian topology of $H(k)$ can also be understood on the basis of the extended Hermitian Hamiltonian

$$\tilde{H}(k, E) \coloneqq \begin{pmatrix} 0 & H(k) - E \\ H^\dagger(k) - E^* & 0 \end{pmatrix}. \tag{3.10}$$

By construction, $\tilde{H}(k, E)$ respects chiral symmetry

$$\Gamma \tilde{H}(k, E) \Gamma^{-1} = -\tilde{H}(k, E), \qquad \Gamma \coloneqq \sigma_z. \tag{3.11}$$

If the non-Hermitian Hamiltonian $H(k)$ is topologically nontrivial for E, the extended Hermitian Hamiltonian $\tilde{H}(k, E)$ is also topologically nontrivial under the open boundary conditions. For the Hatano-Nelson model, we have $W(E) = \mathrm{sgn}(g)$ as long as E is inside the loop described by Eq. (3.2). The extended Hermitian Hamiltonian in Eq. (3.10) is similar to the Su-Schrieffer-Heeger model [SSH79].

Both complex-energy winding and skin effect have no counterparts in Hermitian systems and are intrinsic to non-Hermitian systems. Below in this chapter, we show that these two non-Hermitian phenomena are actually closely related to each other: the skin effect originates from the intrinsic non-Hermitian topology [ZYF20, OKSS20]. If $W(E)$ is nonzero, the skin effect occurs; otherwise, no skin effect occurs. The skin modes in the Hatano-Nelson model correspond to a pair of zero modes in the Su-Schrieffer-Heeger model. This understanding constitutes a universal feature of non-Hermitian topology.

3.2 Non-Bloch band theory

Because of the non-Hermitian skin effect, the conventional Bloch band theory is not generally applicable to non-Hermitian systems. The Bloch band theory works only under the periodic boundary conditions, and the skin effect invalidates it under the open boundary conditions. To overcome this difficulty, recent works have developed a non-Bloch band theory that works even under the open boundary conditions [YW18, YM19].

The non-Bloch band theory is formulated as follows. We consider a generic non-Hermitian Hamiltonian in one dimension described by

$$\hat{H} = \sum_{n} \sum_{j=-l}^{l} \sum_{\mu,\nu=1}^{q} H_{j,\mu\nu} \hat{c}^{\dagger}_{n+j,\mu} \hat{c}_{n,\nu}, \tag{3.12}$$

where $\hat{c}_{n,\mu}$ ($\hat{c}^{\dagger}_{n,\mu}$) is the annihilation (creation) operator at site n, and $H_{j,\mu\nu}$ is the single-particle Hamiltonian. Here, n describes the spatial degrees of freedom, l describes the hopping range, and μ, ν describe the internal degrees of freedom per unit cell. We assume translation invariance under the periodic boundary conditions. Thus, $H_{j,\mu\nu}$ is independent of sites n away from the edges. Because of the noninteracting (quadratic) nature of the Hamiltonian, the diagonalization of the many-body Hamiltonian $\hat{H}$ reduces to diagonalization of the single-particle Hamiltonian H, whose elements are given by $H_{j,\mu\nu}$. Let $E \in \mathbb{C}$ be complex eigenenergy of H and $|\phi\rangle$ ($|\chi\rangle$) be the corresponding right (left) eigenstate [Bro14]:

$$H |\phi\rangle = E |\phi\rangle , \quad H^{\dagger} |\chi\rangle = E^{*} |\chi\rangle . \tag{3.13}$$

Because of translation invariance of H away from the edges, the eigenstates are given by a linear combination of fundamental solutions

$$\sum_{n=1}^{L} \beta_i^n |n\rangle |\phi_i\rangle \coloneqq \sum_{n=1}^{L} \sum_{\mu=1}^{q} \beta_i^n \phi_{\mu}^{(i)} |n\rangle |\mu\rangle , \quad \beta_i, \phi_{\mu}^{(i)} \in \mathbb{C}, \tag{3.14}$$

where L is the number of unit cells, $|n\rangle$ is a state localized at site n, and $|\mu\rangle$ is a state with the internal degree μ. This wave function is delocalized through the bulk for $|\beta| = 1$, while it is localized around the edge $n = 1$ ($n = L$) for $|\beta| < 1$ ($|\beta| > 1$). The corresponding bulk Hamiltonian is described by

$$H(\beta) \coloneqq \sum_{j=-l}^{l} H_j \beta^j, \tag{3.15}$$

where H_j is a $q \times q$ matrix defined by $(H_j)_{\mu\nu} \coloneqq H_{j,\mu\nu}$ and satisfies

$$H(\beta_i) |\phi_i\rangle = E |\phi_i\rangle . \tag{3.16}$$

In the presence of Hermiticity, Eq. (3.14) is just a plane wave and $H(\beta)$ is a conventional Bloch Hamiltonian because of $|\beta| = 1$. The possible β_i's for given E are determined by the characteristic equation

$$\det [H(\beta) - E] = 0, \tag{3.17}$$

which is the $2lq$-th-order algebraic equation in terms of β. For these β_i's ($i = 1, 2, \cdots, 2lq$), the right eigenstate $|\phi\rangle$ in real space can be represented as

$$|\phi\rangle = \sum_{i=1}^{2lq} \sum_{n=1}^{L} \beta_i^n |n\rangle |\phi_i\rangle . \tag{3.18}$$

Now, it is nontrivial how to determine β_i's for the continuum bands of systems. While we have $|\beta_i| = 1$ (i.e., plane waves) for Hermitian systems, this is not necessarily the case for non-Hermitian systems with open boundaries. Importantly, the non-Bloch band theory developed in Refs. [YW18, YM19] provides a general condition for the continuum bands of non-Hermitian systems, summarized as follows:

Non-Bloch band theory [YW18, YM19]

Suppose that $H(\beta)$ denotes a bulk Hamiltonian in one dimension with $\beta := e^{ik}$ and complex-valued wave numbers $k \in \mathbb{C}$. Moreover, β_i's ($i = 1, 2, \cdots, 2M$; $|\beta_1| \leq |\beta_2| \leq \cdots \leq |\beta_{2M}|$) denote the solutions to the characteristic equation

$$\det[H(\beta) - E] = 0 \tag{3.19}$$

in terms of β for the given eigenenergy $E \in \mathbb{C}$. Then, the continuum bands are formed by $H(\beta)$ with the trajectory of β_M and β_{M+1} satisfying

$$|\beta_M| = |\beta_{M+1}|. \tag{3.20}$$

For example, in the Hatano-Nelson model, the bulk Hamiltonian reads

$$H(\beta) = (t+g)\beta^{-1} + (t-g)\beta. \tag{3.21}$$

The characteristic equation $\det[H(\beta) - E] = 0$ gives the quadratic equation

$$(t-g)\beta^2 - E\beta + t + g = 0. \tag{3.22}$$

Since β_1 and β_2 are the two solutions to this quadratic equation, we have

$$\beta_1 + \beta_2 = \frac{E}{t-g}, \quad \beta_1\beta_2 = \frac{t+g}{t-g}. \tag{3.23}$$

Then, the condition (3.20) leads to

$$|\beta_1| = |\beta_2| = \sqrt{\frac{t+g}{t-g}} =: r_\times^{-1}, \tag{3.24}$$

which reproduces the skin modes in Sec. 3.1.

In general, if a right eigenstate $|\phi\rangle$ is localized at one end, the corresponding left eigenstate $|\chi\rangle$ is localized at the other end. To see this property, we notice that $|\chi\rangle^*$ is, by definition, a right eigenstate of H^T with the eigenenergy E. Then, let us consider transposition $H \to H^T$, which leads to the transformations

$$H_{j,\mu\nu} \to H_{-j,\nu\mu}, \tag{3.25}$$

and

$$H(\beta) \to \sum_{j=-l}^{l} H_{-j}^T \beta^{-j} = \sum_{j=-l}^{l} H_j^T \beta^{-j} = H^T(\beta^{-1}). \tag{3.26}$$

This result implies that if β satisfies Eq. (3.17) for H, β^{-1} satisfies Eq. (3.17) for H^T, and vice versa. Recalling that $|\chi\rangle^*$ is a right eigenstate of H^T, we conclude that if $|\phi\rangle$ is localized at one end, $|\chi\rangle$ is localized at the other end, and vice versa. This also means that delocalization of $|\phi\rangle$ occurs simultaneously with delocalization of $|\chi\rangle$.

Notably, the above non-Bloch band theory implicitly assumes the absence of symmetry and can break down in the presence of symmetry. In Sec. 4.2, we demonstrate that it is indeed modified in the symplectic class [YY20, KOS20], which accounts for the $\mathbb{Z}_2$ reciprocal skin effect [OKSS20]. Furthermore, the non-Bloch band theory is not directly applicable if the open boundary conditions are imposed in more than one direction. Thus, the non-Bloch band theory can be modified in higher dimensions. In Sec. 4.4, we demonstrate that such a modification in higher dimensions indeed arises and underlies the higher-order skin effect.

3.3 Index theorem

While the skin effect obscures the bulk-boundary correspondence for finite non-Hermitian systems, we still have the bulk-boundary correspondence for semi-infinite non-Hermitian systems, as demonstrated below. Similarly to the Hermitian case, the bulk-boundary correspondence for semi-infinite non-Hermitian systems is formulated as the index theorem.

3.3.1 Class A

As discussed previously, non-Hermitian Hamiltonian H is defined to have a point gap if and only if its complex spectrum does not cross a reference point $E \in \mathbb{C}$ [GAK+18, KSUS19]. The simplest nontrivial example of the point-gapped topological phases appears in one-dimensional systems with no symmetry. While $\det(H - E)$ is always real for Hermitian Hamiltonians H, it can be complex for non-Hermitian Hamiltonians H, for which the winding number $W(E) \in \mathbb{Z}$ is defined as Eq. (3.9). Topological phases are absent in one-dimensional Hermitian systems without symmetry protection [HK10, QZ11, CTSR16]; the point-gap topology characterized by $W(E)$ is intrinsic to non-Hermitian systems.

Corresponding to $W(E) \neq 0$, the boundary modes with the eigenenergy E can appear in semi-infinite systems with only one boundary. Suppose that the non-Hermitian system has a boundary on the left but no boundary on the right (the same semi-infinite boundary conditions are chosen below unless otherwise stated). An important observation is that the Hermitian Hamiltonian $\tilde{H}$ is constructed from H as [GAK+18, KSUS19]

$$\tilde{H} \coloneqq \begin{pmatrix} 0 & H - E \\ H^\dagger - E^* & 0 \end{pmatrix}. \tag{3.27}$$

Under the periodic boundary conditions, when a point gap is open for the non-Hermitian Hamiltonian $H(k)$, a real energy gap is also open for the Hermitian Hamiltonian $\tilde{H}(k)$, and vice versa. In addition, $\tilde{H}$ respects additional chiral symmetry by construction:

$$\Gamma \tilde{H} \Gamma^{-1} = -\tilde{H} \tag{3.28}$$

with $\Gamma \coloneqq \sigma_z$. As a result of the conventional bulk-boundary correspondence for Hermitian Hamiltonians, $\tilde{H}$ with the semi-infinite boundary possesses topologically protected zero modes localized at the boundary [HK10, QZ11, CTSR16] in a manner similar to the Su-Schrieffer-Heeger model [SSH79]. The corresponding topological invariant coincides with $W(E)$ in Eq. (3.9). For

$W(E) > 0$, there appear boundary modes $(0 \ \ |E\rangle)^T$ with negative chirality, i.e.,

$$\Gamma \begin{pmatrix} 0 \\ |E\rangle \end{pmatrix} = - \begin{pmatrix} 0 \\ |E\rangle \end{pmatrix}, \tag{3.29}$$

which implies that $|E\rangle$ is a right eigenstate of non-Hermitian H (i.e., $H|E\rangle = E|E\rangle$) localized at the boundary. For $W(E) < 0$, on the other hand, the boundary modes $(|E\rangle \ \ 0)^T$ have positive chirality, i.e.,

$$\Gamma \begin{pmatrix} |E\rangle \\ 0 \end{pmatrix} = + \begin{pmatrix} |E\rangle \\ 0 \end{pmatrix}, \tag{3.30}$$

which in turn implies that $|E\rangle$ is a right eigenstate of $H^\dagger$, i.e., a left eigenstate of H (i.e., $\langle E| H = \langle E| E$) [Bro14].

The above discussion is valid for arbitrary $E \in \mathbb{C}$ in the complex-energy plane satisfying $W(E) \neq 0$. Thus, in semi-infinite systems H_{SIBC}, an infinite number of boundary modes emerges as a result of the nontrivial winding number $W(E) \neq 0$. This conclusion leads to the following index theorem in spectral theory [BG05, TE05]:

Index theorem

Let $\sigma(H(k))$ be the spectrum of $H(k)$ with $k \in [0, 2\pi]$, which generally forms closed curves in the complex-energy plane (Fig. 3.1). Then, the spectrum of the semi-infinite Hamiltonian H_{SIBC} with only one boundary is equal to $\sigma(H(k))$ together with the whole area of $E \in \mathbb{C}$ enclosed by $\sigma(H(k))$ with $W(E) \neq 0$. For $W(E) > 0$ [$W(E) < 0$], there appears a right (left) eigenstate $|E\rangle$ of H_{SIBC} localized at the boundary:

$$H_{\mathrm{SIBC}}|E\rangle = E|E\rangle \quad (\langle E| H_{\mathrm{SIBC}} = \langle E| E). \tag{3.31}$$

Similar index theorems are considered in Refs. [LBH+17, GAK+18].

The index theorem is illustrated with the Hatano-Nelson model [HN96, HN97] in Eq. (3.1). The spectrum of the Bloch Hamiltonian

$$H_{\mathrm{HN}}(k) = (t+g)\, e^{-\mathrm{i}k} + (t-g)\, e^{\mathrm{i}k} \tag{3.32}$$

forms an ellipse in the complex-energy plane, and we have

$$W(E) = \mathrm{sgn}(g) \tag{3.33}$$

for $E \in \mathbb{C}$ inside this ellipse. In fact, the hopping from the left to the right dominates the hopping from the right to the left for $g > 0$, which leads to the emergence of the boundary modes.

We can confirm the emergence of boundary modes by directly solving the Schrödinger equation. We assume $t > g \geq 0$ for the sake of simplicity. Suppose that the system has a boundary on the left but no boundary on the right. If a state $|E\rangle = (\psi_1 \ \psi_2 \ \psi_3 \ \cdots)^T$ is an eigenstate with eigenenergy E, the Schrödinger equation reads

$$(t+g)\,\psi_{i-1} + (t-g)\,\psi_{i+1} = E\psi_i \tag{3.34}$$

in the bulk and

$$\psi_0 = \lim_{i\to\infty} \psi_i = 0 \tag{3.35}$$

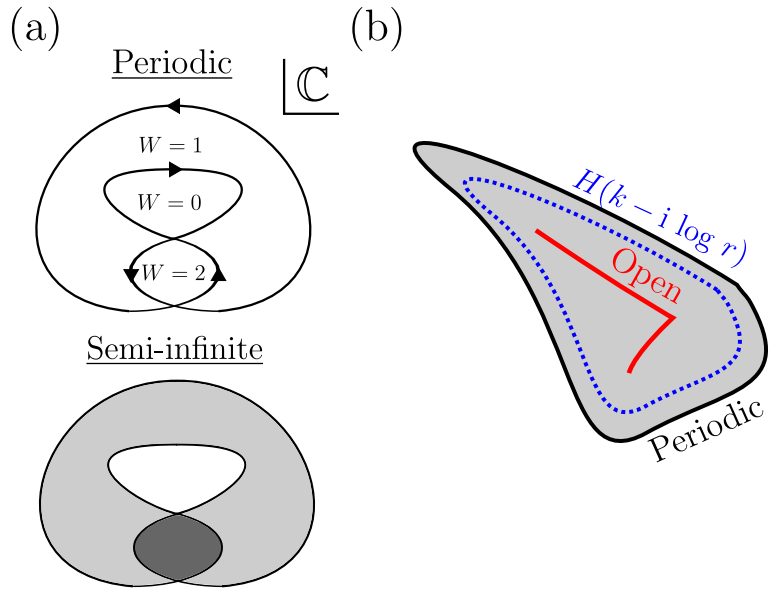

Figure 3.1: Complex spectra of non-Hermitian systems with periodic, open, and semi-infinite boundaries. (a) A semi-infinite system possesses an infinite number of boundary modes due to the nonzero winding number $W \neq 0$ in the corresponding periodic system. (b) The spectrum of a semi-infinite system shrinks through the imaginary gauge transformation, resulting in an arc of the open-boundary system. Reproduced from Fig. 1 of Ref. [OKSS20]. Copyright 2020 by the American Physical Society.

at the boundaries. We take an ansatz $\psi_i \sim \beta^i$ ($\beta \in \mathbb{C}$). From the bulk equation (3.34), we have

$$\frac{t+g}{\beta} + (t-g)\,\beta = E, \quad \text{i.e.,} \quad \beta = \beta_\pm(E) := \frac{E \pm \sqrt{E^2 - (t^2 - g^2)}}{2(t-g)}. \tag{3.36}$$

Here, the absolute values of both $|\beta_+(E)|$ and $|\beta_-(E)|$ should be less than 1 so that $|E\rangle$ can satisfy the semi-infinite boundary conditions (3.35). To see this fact, suppose, for example, that $|\beta_+(E)|$ is larger than 1. We note that $|\beta_+(E)| = 1$ describes delocalized states, in which we are not interested here. Now, a generic eigenstate is given as $\psi_i = c_+\beta_+^i(E) + c_-\beta_-^i(E)$ with some coefficients $c_+, c_- \in \mathbb{C}$. However, because of $|\beta_+(E)| > 1$, the boundary conditions given by Eq. (3.35) lead to $c_+ + c_- = 0$, as well as $c_+ = 0$ or $\beta_+ = \beta_-$, either of which results in $\psi_i = 0$. Therefore, we need both $|\beta_+(E)| < 1$ and $|\beta_-(E)| < 1$ to obtain eigenstates, which in turn leads to

$$1 > |\beta_+(E)\,\beta_-(E)| = \left|\frac{t+g}{t-g}\right|, \quad \text{i.e.,} \quad g < 0. \tag{3.37}$$

Moreover, introducing $\varphi \in [0, 2\pi]$ by $\beta =: |\beta|\,e^{\mathrm{i}\varphi}$, we have

$$E = \left[\frac{t+g}{|\beta|} + (t-g)\,|\beta|\right]\cos\varphi + \mathrm{i}\left[-\frac{t+g}{|\beta|} + (t-g)\,|\beta|\right]\sin\varphi, \tag{3.38}$$

which leads to

$$\frac{(\mathrm{Re}\,E)^2}{(2t)^2} + \frac{(\mathrm{Im}\,E)^2}{(2g)^2} = \frac{1}{(2t)^2}\left[\frac{t+g}{|\beta|} + (t-g)\,|\beta|\right]^2\cos^2\varphi + \frac{1}{(2g)^2}\left[-\frac{t+g}{|\beta|} + (t-g)\,|\beta|\right]^2\sin^2\varphi. \tag{3.39}$$

The right-hand side of this equation reaches a maximum for $\cos\varphi = 0$ or $\sin\varphi = 0$. Hence, we have

$$\frac{(\mathrm{Re}\, E)^2}{(2t)^2} + \frac{(\mathrm{Im}\, E)^2}{(2g)^2} \leq \max\left\{ \frac{1}{(2t)^2}\left[\frac{t+g}{|\beta|} + (t-g)\,|\beta|\right]^2, \frac{1}{(2g)^2}\left[-\frac{t+g}{|\beta|} + (t-g)\,|\beta|\right]^2 \right\}. \tag{3.40}$$

Since both of the two in the right-hand side reach a maximum for $|\beta| = 1$ because of Eq. (3.37), we have

$$\frac{(\mathrm{Re}\, E)^2}{(2t)^2} + \frac{(\mathrm{Im}\, E)^2}{(2g)^2} \leq 1. \tag{3.41}$$

Thus, the semi-infinite Hatano-Nelson model indeed has an infinite number of boundary states for $E \in \mathbb{C}$ with the nontrivial winding number $W(E) = \mathrm{sgn}(g) = +1$. Remarkably, the above discussions are not necessarily applicable to finite systems with open boundaries, in which a stricter boundary condition $\psi_0 = \psi_{N+1} = 0$ is imposed instead of Eq. (3.35).

3.3.2 Class AII†

We have a different type of index theorems in the presence of symmetry. For example, non-Hermitian Hamiltonians H in class AII† respect reciprocity [KSUS19]:

$$\mathcal{T} H^T(k)\,\mathcal{T}^{-1} = H(-k), \quad \mathcal{T}\mathcal{T}^* = -1, \tag{3.42}$$

where $\mathcal{T}$ is a unitary operator. A set of Hamiltonians with this symmetry is called the symplectic class. In the presence of a point gap for reference energy $E \in \mathbb{C}$, the following $\mathbb{Z}_2$ topological invariant $\nu(E) \in \{0, 1\}$ is defined:

$$(-1)^{\nu(E)} \coloneqq \mathrm{sgn}\left\{ \frac{\mathrm{Pf}\left[(H(\pi) - E)\,\mathcal{T}\right]}{\mathrm{Pf}\left[(H(0) - E)\,\mathcal{T}\right]} \times \exp\left[-\frac{1}{2}\int_{k=0}^{k=\pi} d \log\det\left[(H(k) - E)\,\mathcal{T}\right]\right]\right\}. \tag{3.43}$$

In a semi-infinite system H_{SIBC}, the index theorem reads

$$\#\left[\text{zero modes of } (H_{\mathrm{SIBC}} - E)\right] \equiv \nu(E) \pmod 2. \tag{3.44}$$

To see this index theorem, we consider the extended Hermitian Hamiltonian

$$\tilde{H} \coloneqq \begin{pmatrix} 0 & H - E \\ H^\dagger - E^* & 0 \end{pmatrix}, \tag{3.45}$$

which belongs to symmetry class DIII [QHZ10, SR11, BA13] with chiral and time-reversal symmetry described by

$$\Gamma \coloneqq \begin{pmatrix} 1 & 0 \\ 0 & -1 \end{pmatrix}, \quad \tilde{\mathcal{T}} \coloneqq \begin{pmatrix} 0 & \mathcal{T} \\ \mathcal{T} & 0 \end{pmatrix} \mathcal{K}, \tag{3.46}$$

where $\mathcal{K}$ denotes complex conjugation. The conventional bulk-boundary correspondence for the Hermitian Hamiltonian $\tilde{H}$ states that $\tilde{H}$ has a Kramers pair of zero modes localized at the boundary for $\nu(E) = 1$. One of the zero modes has positive chirality (i.e., $\Gamma|\varphi_+\rangle = +|\varphi_+\rangle$), and the other has negative chirality (i.e., $\Gamma|\varphi_-\rangle = -|\varphi_-\rangle$), both of which are related by time reversal (i.e., $\tilde{\mathcal{T}}|\varphi_-\rangle = |\varphi_+\rangle$). Thus, these zero modes are represented as

$$|\varphi_-\rangle = \begin{pmatrix} 0 \\ |E\rangle \end{pmatrix}, \quad |\varphi_+\rangle = \tilde{\mathcal{T}}|\varphi_-\rangle = \begin{pmatrix} \mathcal{T}|E\rangle^* \\ 0 \end{pmatrix}, \tag{3.47}$$

which leads to

$$H\left|E\right\rangle = E\left|E\right\rangle, \quad H^{\dagger}\left(\mathcal{T}\left|E\right\rangle^{*}\right) = E^{*}\left(\mathcal{T}\left|E\right\rangle^{*}\right). \tag{3.48}$$

These equations imply that $\left|E\right\rangle$ $\left(\mathcal{T}\left|E\right\rangle^{*}\right)$ is a right (left) eigenstate of the semi-infinite non-Hermitian Hamiltonian with $\nu\left(E\right) = 1$. Because of the $\mathbb{Z}_2$ nature of topology, only the parity of the boundary modes is relevant. This different type of index theorems is relevant to the $\mathbb{Z}_2$ skin effect protected by reciprocity, as discussed in Sec. 4.1.

3.3.3 Class D

Non-Hermitian Hamiltonians H in class D respect particle-hole symmetry [KSUS19]:

$$\mathcal{C}H^{T}\left(k\right)\mathcal{C}^{-1} = -H\left(-k\right), \quad \mathcal{C}\mathcal{C}^{*} = +1, \tag{3.49}$$

where $\mathcal{C}$ is a unitary operator. Particle-hole symmetry creates opposite-energy pairs $(E, -E)$ and makes zero energy a special symmetric point in the complex-energy plane. Hence, we take a reference point as zero energy so that it will respect particle-hole symmetry. In the presence of the point gap, the following $\mathbb{Z}_2$ topological invariant $\nu \in \{0, 1\}$ is defined:

$$\left(-1\right)^{\nu} \coloneqq \mathrm{sgn}\left\{\frac{\mathrm{Pf}\left[H\left(\pi\right)\mathcal{C}\right]}{\mathrm{Pf}\left[H\left(0\right)\mathcal{C}\right]} \times \exp\left[-\frac{1}{2}\int_{k=0}^{k=\pi} d\log\det\left[H\left(k\right)\mathcal{C}\right]\right]\right\}. \tag{3.50}$$

In semi-infinite systems H_{SIBC}, the index theorem reads

$$\#\left[\text{zero modes of } H_{\mathrm{SIBC}}\right] \equiv \nu \pmod 2. \tag{3.51}$$

To see this index theorem, we consider the extended Hermitian Hamiltonian $\tilde{H}$ in Eq. (3.45) with $E = 0$, which belongs to symmetry class DIII [QHZ10, SR11, BA13] in a manner similar to non-Hermitian Hamiltonians in class AII†. For $\tilde{H}$, particle-hole symmetry is described by

$$\tilde{\mathcal{C}} \coloneqq \begin{pmatrix} 0 & \mathcal{C} \\ \mathcal{C} & 0 \end{pmatrix}\mathcal{K}, \tag{3.52}$$

and time-reversal symmetry is described as a combination of particle-hole and chiral symmetries by

$$\tilde{\mathcal{T}} \coloneqq \mathrm{i}\Gamma\tilde{\mathcal{C}} = \mathrm{i}\begin{pmatrix} 0 & \mathcal{C} \\ -\mathcal{C} & 0 \end{pmatrix}\mathcal{K}. \tag{3.53}$$

Here, $\tilde{\mathcal{T}}$ is chosen so that it will commute with $\tilde{\mathcal{C}}$ (i.e., $\tilde{\mathcal{C}}\tilde{\mathcal{T}} = \tilde{\mathcal{T}}\tilde{\mathcal{C}}$). The bulk-boundary correspondence for the Hermitian Hamiltonian $\tilde{H}$ states that $\tilde{H}$ has a Kramers pair of zero modes localized at the boundary for $\nu = 1$. One of the zero modes has positive chirality (i.e., $\Gamma\left|\varphi_{+}\right\rangle = +\left|\varphi_{+}\right\rangle$) and the other has negative chirality (i.e., $\Gamma\left|\varphi_{-}\right\rangle = -\left|\varphi_{-}\right\rangle$), both of which are related by time reversal (i.e., $\tilde{\mathcal{T}}\left|\varphi_{-}\right\rangle = \left|\varphi_{+}\right\rangle$). Thus, these zero modes are represented as

$$\left|\varphi_{-}\right\rangle = \begin{pmatrix} 0 \\ \left|0\right\rangle \end{pmatrix}, \quad \left|\varphi_{+}\right\rangle = \tilde{\mathcal{T}}\left|\varphi_{-}\right\rangle = \begin{pmatrix} \mathrm{i}\mathcal{C}\left|0\right\rangle^{*} \\ 0 \end{pmatrix}, \tag{3.54}$$

which leads to

$$H\left|0\right\rangle = H^{\dagger}\left(\mathcal{C}\left|0\right\rangle^{*}\right) = 0. \tag{3.55}$$

These equations imply that $\left|0\right\rangle$ $\left(\mathcal{C}\left|0\right\rangle^{*}\right)$ is a right (left) eigenstate with zero energy of the semi-infinite non-Hermitian Hamiltonian with $\nu = 1$. We discuss consequences of this index theorem for class D also in Sec. 4.3.

3.4 Topological origin of non-Hermitian skin effects

3.4.1 Skin effect as intrinsic non-Hermitian topology

The index theorem for semi-infinite systems is not directly applicable to finite systems with open boundaries. In fact, an infinite number of boundary modes is impossible in finite systems. Furthermore, an additional boundary condition is imposed because of the other boundary, which may forbid some of the boundary states appearing in semi-infinite systems. For example, the spectrum of the Hatano-Nelson model $(H_{\mathrm{HN}})_{\mathrm{OBC}}$ with open boundaries forms not a loop but a line on the real axis in the complex-energy plane, which signals the non-Hermitian skin effect. As discussed in Sec. 3.1, using an imaginary gauge transformation [HN96, HN97, YW18, LT19]

$$V_r^{-1} c_i^\dagger V_r = r^i c_i^\dagger, \quad V_r^{-1} c_i V_r = r^{-i} c_i, \quad (0 < r < \infty), \tag{3.56}$$

we have a Hermitian Hamiltonian $\bar{H} \coloneqq V_{r_\times}^{-1} (H_{\mathrm{HN}})_{\mathrm{OBC}} V_{r_\times}$ for $r_\times \coloneqq \sqrt{|(t-g)/(t+g)|}$. Here, Eq. (3.56) shifts the momentum from k to $k - \mathrm{i} \log r$. Since this similarity transformation does not change the spectrum, $(H_{\mathrm{HN}})_{\mathrm{OBC}}$ has the entirely real spectrum and hence no longer retains the point gap. Importantly, such a non-Hermitian skin effect is a general non-Hermitian topological phenomenon as a direct consequence of point-gap topology, as summarized in the following theorem:

Theorem: topological origin of non-Hermitian skin effects [OKSS20]

A finite Hamiltonian H_{OBC} with open boundaries is always topologically trivial in terms of a point gap. Consequently, if the corresponding Hamiltonian $H(k)$ under the periodic boundary conditions is gapped and topological with respect to a point gap, the non-Hermitian skin effect inevitably occurs with a topological phase transition.

To see the theorem, we begin with

$$\lim_{N \to \infty} \sigma (H_{\mathrm{OBC}}) \subset \sigma (H_{\mathrm{SIBC}}), \tag{3.57}$$

where $\sigma (H_{\mathrm{OBC}})$ is the spectrum of a non-Hermitian system H_{OBC} with open boundaries and N unit cells, and $\sigma (H_{\mathrm{SIBC}})$ is the spectrum of the corresponding semi-infinite system H_{SIBC}. In fact, an approximate eigenstate of H_{SIBC} can be obtained from an eigenstate of H_{OBC}, which becomes an exact eigenstate for $N \to \infty$ (this statement can be made more rigorous in terms of pseudospectra in spectral theory [BG05, TE05]; see Supplemental Material of Ref. [OKSS20] for a rigorous proof). The contrary is not always true: even if an approximate eigenstate of H_{OBC} is constructed from an eigenstate of H_{SIBC}, it is not necessarily an exact eigenstate of H_{OBC}.

A crucial step is again the imaginary gauge transformation:

$$H_{\mathrm{OBC}} \to V_r^{-1} H_{\mathrm{OBC}} V_r, \quad H_{\mathrm{SIBC}} \to V_r^{-1} H_{\mathrm{SIBC}} V_r \quad (0 < r < \infty). \tag{3.58}$$

For each transformation, we still have the inclusion in Eq. (3.57):

$$\lim_{N \to \infty} \sigma \left(V_r^{-1} H_{\mathrm{OBC}} V_r \right) \subset \sigma \left(V_r^{-1} H_{\mathrm{SIBC}} V_r \right). \tag{3.59}$$

This imaginary gauge transformation does not change the spectrum of H_{OBC}. However, it changes the spectrum of H_{SIBC} since H_{SIBC} has no boundary on the right because of the semi-infinite nature [Fig. 3.1 (b)]. In fact, $H(k)$ changes to $H(k - \mathrm{i} \log r)$ through V_r. Nevertheless,

Eq. (3.59) implies that the transformed semi-infinite spectrum includes the spectrum of H_{OBC} for any transformation V_r. Thus, we have

$$\lim_{N\to\infty}\sigma\left(H_{\mathrm{OBC}}\right)\subset\bigcap_{r\in(0,\infty)}\sigma\left(V_r^{-1}H_{\mathrm{SIBC}}V_r\right). \tag{3.60}$$

Because of the index theorem for semi-infinite systems, when $H\left(k\right)$ has a point gap and $W\left(E\right)>0$ ($W\left(E\right)<0$), right (left) boundary modes with eigenenergy E appear in the semi-infinite system. Let us choose an appropriate imaginary gauge V_r such that these boundary modes are transformed to delocalized bulk modes. Then, E is on the edges of $\sigma\left(V_r^{-1}H_{\mathrm{SIBC}}V_r\right)$, whereas it is originally located inside $\sigma\left(H_{\mathrm{SIBC}}\right)$. Thus, the intersection of $\sigma\left(H_{\mathrm{SIBC}}\right)$ and $\sigma\left(V_r^{-1}H_{\mathrm{SIBC}}V_r\right)$ is strictly smaller than $\sigma\left(H_{\mathrm{SIBC}}\right)$ (see Supplemental Material of Ref. [OKSS20] for a rigorous proof). Repeating this procedure for all V_r with $r\in(0,\infty)$, the right-hand side of Eq. (3.60) reaches an open curve or a topologically trivial area for which the interior satisfies $W(E)=0$, otherwise a contradiction arises (see Supplemental Material of Ref. [OKSS20] for a rigorous proof). Since this region includes $\lim_{N\to\infty}\sigma\left(H_{\mathrm{OBC}}\right)$ because of Eq. (3.60), H_{OBC} is also topologically trivial and different from $H\left(k\right)$ with nontrivial topology. Furthermore, $\sigma\left(H_{\mathrm{OBC}}\right)$ is indeed distinct from $\sigma\left(H\left(k\right)\right)$, which implies the inevitable occurrence of the non-Hermitian skin effect due to the point-gap topology.

It should be noted that an observation similar to our theorem is also made in Ref. [LT19], which is made rigorous by our results. Moreover, we identify the non-Hermitian skin effect as the point-gap topology. Here, the intrinsic point-gap topology is the only origin of the non-Hermitian skin effect. Suppose that a non-Hermitian system with open boundaries exhibits the skin effect and that its spectrum is different from $\sigma\left(H\left(k\right)\right)$. This, together with Eq. (3.57), implies the presence of boundary states under the semi-infinite boundary conditions, which in turn requires nontrivial point-gap topology of $H\left(k\right)$ from the index theorem for semi-infinite systems. The topological origin constitutes a universal feature of the non-Hermitian skin effect. Furthermore, based on this general understanding, new types of the skin effects—symmetry-protected skin effects—are discovered, as illustrated in the next chapter (Chap. 4).

3.4.2 Relationship with the non-Bloch band theory

As summarized in Sec. 3.2, Refs. [YW18, YM19] determine the conditions for the spectra of open-boundary systems and develop the non-Bloch band theory of non-Hermitian systems. Their conditions are actually equivalent to the set in the right-hand side of Eq. (3.60). On the basis of spectral theory [BG05, TE05], together with the results in Refs. [YW18, YM19], we show

$$\lim_{N\to\infty}\sigma\left(H_{\mathrm{OBC}}\right)=\bigcap_{r\in(0,\infty)}\sigma\left(V_r^{-1}H_{\mathrm{SIBC}}V_r\right). \tag{3.61}$$

Here, the hopping range of the system is $l<\infty$, and the number of internal degrees of freedom is m. We prove Eq. (3.61) by contraposition, i.e.,

$$E\notin\lim_{N\to\infty}\sigma\left(H_{\mathrm{OBC}}\right)\quad\Longleftrightarrow\quad E\notin\bigcap_{r\in(0,\infty)}\sigma\left(V_r^{-1}H_{\mathrm{SIBC}}V_r\right). \tag{3.62}$$

The non-Bloch band theory developed in Refs. [YW18, YM19] demonstrates that the spectrum of a non-Hermitian Hamiltonian H_{OBC} with open boundaries satisfies

$$\lim_{N\to\infty}\sigma\left(H_{\mathrm{OBC}}\right)=\{E\in\mathbb{C}\mid|\beta_{lm}(E)|=|\beta_{lm+1}(E)|\}, \tag{3.63}$$

where $\beta_i(E)$'s $(i = 1, \cdots, 2lm)$ with $|\beta_1(E)| \leq \cdots \leq |\beta_{2lm}(E)|$ are the zeros of the $2lm$-th polynomial $\beta^{lm} \det(H(\beta) - E)$. In the following, we assume this result. The previous argument in Sec. 3.4.1 only derives the inclusion relation of Eq. (3.60). On the other hand, Eq. (3.63) leads to the stronger relation of Eq. (3.61), as shown below.

We first notice

$$E \notin \sigma(H_{\mathrm{SIBC}}) \quad \Longleftrightarrow \quad W(E) = 0, \text{ and } \det(H(\beta) - E) \neq 0 \text{ for } \beta \in \mathbb{T} \coloneqq \{\beta \in \mathbb{C} \mid |\beta| = 1\} \tag{3.64}$$

because of the index theorem for semi-infinite systems. Here, $\beta^{lm} \det(H(\beta) - E)$ is the $2lm$-th polynomial for β such that

$$\det(H(\beta) - E) = a_{-lm}\beta^{-lm} + a_{-lm+1}\beta^{-lm+1} + \cdots a_{lm}\beta^{lm}, \quad a_i \in \mathbb{C}. \tag{3.65}$$

Because of the argument principle, the winding number $W(E)$ for $H(\beta)$ with $\beta \in \mathbb{T}$ is given by the difference of the numbers of the zeros and the poles of $\det(H(\beta) - E)$ inside the disk $\mathbb{D} \coloneqq \{\beta \in \mathbb{C} \mid |\beta| < 1\}$. Hence, the numbers of the zeros and the poles in $\mathbb{D}$ coincide with each other for $W(E) = 0$. In addition, $\beta = 0$ is the only pole of $\det(H(\beta) - E)$ with the multiplicity lm. Thus, we have the following lemma:

> **Lemma** We have $E \notin \sigma(H_{\mathrm{SIBC}})$ if and only if the $2lm$-th polynomial $\beta^{lm} \det(H(\beta) - E)$ has no zeros on $\mathbb{T}$ and has lm zeros in $\mathbb{D}$. Similarly, we have $E \notin \sigma(V_r^{-1} H_{\mathrm{SIBC}} V_r)$ if and only if $\beta^{lm} \det(H(\beta) - E)$ has no zeros on $r^{-1}\mathbb{T} \coloneqq \{\beta \in \mathbb{C} \mid |\beta| = r^{-1}\}$ and has lm zeros in $r^{-1}\mathbb{D} \coloneqq \{\beta \in \mathbb{C} \mid |\beta| < r^{-1}\}$.

We note that Eq. (3.57) immediately follows from the former part of this lemma. For $E \notin \sigma(H_{\mathrm{SIBC}})$, the lemma leads to $|\beta_{lm}(E)| \neq |\beta_{lm+1}(E)|$. Then, we have $E \notin \lim_{N\to\infty} \sigma(H_{\mathrm{OBC}})$ because of Eq. (3.63), which implies Eq. (3.57).

Now, we show Eq. (3.61). If we have $E \notin \lim_{N\to\infty} \sigma(H_{\mathrm{OBC}})$, Eq. (3.63) implies that there exists $r_\times > 0$ such that

$$|\beta_{lm}(E)| < r_\times^{-1} < |\beta_{lm+1}(E)|, \tag{3.66}$$

and vice versa. Equation (3.66) implies that $\beta^{lm} \det(H(\beta) - E)$ has no zeros on $r_\times^{-1}\mathbb{T}$ and lm zeros in $r_\times^{-1}\mathbb{D}$. Then, Eq. (3.66) also means $E \notin \sigma(V_{r_\times}^{-1} H_{\mathrm{SIBC}} V_{r_\times})$ and hence $E \notin \bigcap_{r\in(0,\infty)} \sigma(V_r^{-1} H_{\mathrm{SIBC}} V_r)$ because of the lemma, resulting in Eq. (3.62). We thus have Eq. (3.61).

Recently, a similar result has been obtained in a related work [ZYF20].

Chapter 4

Symmetry-protected non-Hermitian skin effects

A unique feature of non-Hermitian systems is the skin effect, which is the extreme sensitivity to boundary conditions. In Chap. 3, we reveal that the skin effect originates from intrinsic non-Hermitian topology. In this chapter, we demonstrate that such a topological origin not merely explains the universal feature of the known skin effect, but also leads to new types of the skin effects—symmetry-protected skin effects. In Sec. 4.1, we discover the $\mathbb{Z}_2$ skin effect protected by reciprocity and discuss its unique properties that are distinct from the conventional skin effect [OKSS20]. As shown in Sec. 4.2, this $\mathbb{Z}_2$ skin effect accompanies a modification of the non-Bloch band theory [KOS20]. In Sec. 4.3, we clarify the bulk-boundary correspondence of non-Hermitian systems and discuss possible other skin effects in arbitrary dimensions on the basis of topological classification. Intrinsic non-Hermitian topology leads to the skin effects also in higher dimensions. As prime examples, in Secs. 4.4 and 4.5, we discuss the higher-order counterparts of the non-Hermitian skin effects in higher dimensions [KSS20]. The discussions in this chapter provide a unified understanding about the bulk-boundary correspondence and the skin effects in non-Hermitian systems, as well as new nonequilibrium topological phenomena unique to open systems.

This chapter is based on Refs. [OKSS20, KOS20, KSS20].

4.1 $\mathbb{Z}_2$ skin effect protected by reciprocity

The point-gap topology and the corresponding skin effect are enriched by symmetry. Reciprocity is one of such important symmetry, which is defined by the transposition version of time-reversal symmetry [KSUS19]:

$$\mathcal{T} H^T(\boldsymbol{k}) \mathcal{T}^{-1} = H(-\boldsymbol{k}), \quad \mathcal{T}\mathcal{T}^* = -1, \tag{4.1}$$

where $\mathcal{T}$ is a unitary operator. This symmetry is fundamental as reciprocity in non-Hermitian spinful systems and naturally appears, for example, in mesoscopic systems [Bee97, Bee15] and open quantum systems [HKKU20, LMC20, SRP20, BP07].

In conventional quantum spin Hall insulators, the integer Chern number vanishes but the Kane-Mele $\mathbb{Z}_2$ topological invariant [KM05b, KM05a] becomes nontrivial because of time-reversal symmetry [HK10, QZ11, CTSR16]. Similarly, Eq. (4.1) trivializes the winding number in Eq. (3.9), but instead, it supplies a $\mathbb{Z}_2$ invariant. The $\mathbb{Z}_2$ topological invariant $\nu(E) \in \{0, 1\}$

for a reference point $E \in \mathbb{C}$ is given by [KSUS19]

$$(-1)^{\nu(E)} := \operatorname{sgn}\left\{\frac{\operatorname{Pf}\left[\left(H\left(\pi\right)-E\right)\mathcal{T}\right]}{\operatorname{Pf}\left[\left(H\left(0\right)-E\right)\mathcal{T}\right]} \times \exp\left[-\frac{1}{2}\int_{k=0}^{k=\pi} d\log\det\left[\left(H\left(k\right)-E\right)\mathcal{T}\right]\right]\right\}. \tag{4.2}$$

Corresponding to the $\mathbb{Z}_2$ topological invariant $\nu\left(E\right)$, we have an index theorem similar to the standard class without symmetry (i.e., class A) (see Sec. 3.3.2 for details). A clear distinction from the standard class is the Kramers degeneracy due to Eq. (4.1) [ESHK11, KSUS19, ZLLZ19]. The extended Hermitian Hamiltonian $\tilde{H}$ in Eq. (3.27) respects time-reversal symmetry as well as the additional chiral symmetry Γ, analogous to time-reversal-invariant topological superconductors [QHRZ09, QHZ10, SR11, BA13]. The index theorem states that the semi-infinite system $\tilde{H}$ hosts an odd number of boundary Majorana Kramers pairs for each E with $\nu\left(E\right)=1$. In terms of the original non-Hermitian Hamiltonian H, the Kramers pair reduces to a pair of right and left eigenstates of H localized at the same boundary. Using the transposition version of time reversal in Eq. (4.1), we can convert the left eigenmode into a right one in the oppositely extended semi-infinite system (i.e., semi-infinite system with a boundary only on the right). As a result, finite systems with open boundaries host localized modes at both ends, as explicitly shown in the following model.

We recall that a quantum spin Hall insulator [KM05b, KM05a] can be constructed from a pair of time-reversed quantum Hall insulators [Hal88] with the spin-orbit coupling. Similarly, combining the Hatano-Nelson model $H_{\mathrm{HN}}\left(k\right)$ and its reciprocal partner $H_{\mathrm{HN}}^{T}\left(-k\right)$ (see Sec. 3.1 for details on the Hatano-Nelson model), we have a canonical model that exhibits the $\mathbb{Z}_2$ skin effect:

$$\begin{aligned} H\left(k\right) &= \begin{pmatrix} H_{\mathrm{HN}}\left(k\right) & -2\Delta\sin k \\ -2\Delta\sin k & H_{\mathrm{HN}}^{T}\left(-k\right) \end{pmatrix} \\ &= 2t\cos k - 2\Delta\left(\sin k\right)\sigma_x - 2\mathrm{i}g\left(\sin k\right)\sigma_z, \end{aligned} \tag{4.3}$$

with $t, g, \Delta \geq 0$. Here, Δ describes the spin-orbit coupling. In real space, the Hamiltonian reads

$$\hat{H} = \sum_n \left[\hat{c}_{n+1}^{\dagger}\left(t - \mathrm{i}\Delta\sigma_x + g\sigma_z\right)\hat{c}_n + \hat{c}_n^{\dagger}\left(t + \mathrm{i}\Delta\sigma_x - g\sigma_z\right)\hat{c}_{n+1}\right], \tag{4.4}$$

where $\hat{c}_n$ ($\hat{c}_n^{\dagger}$) annihilates (creates) a spinful particle with two components. It indeed respects reciprocity with $\mathcal{T} = \mathrm{i}\sigma_y$. Under the periodic boundary conditions, the spectrum is given as

$$E_{\pm}\left(k\right) = 2t\cos k \pm 2\mathrm{i}\sqrt{g^2-\Delta^2}\sin k, \tag{4.5}$$

which is entirely real for $|g| < |\Delta|$ and forms a loop in the complex-energy plane for $|g| > |\Delta|$ (Fig. 4.1). Thus, for $|g| > |\Delta|$, $H\left(k\right)$ retains a point gap. Since it can be continuously deformed to $H\left(k\right)$ with $t = g$ and $\Delta = 0$ while keeping the point gap, the $\mathbb{Z}_2$ invariant in Eq. (4.2) is obtained as $\nu\left(E\right) = 1$ when E is in the area enclosed by $\sigma\left(H(k)\right)$.

As well as the periodic-boundary spectra, the open-boundary spectra are shown in Fig. 4.1. The open-boundary spectrum is clearly different from the periodic-boundary counterpart, which indicates the non-Hermitian skin effect. Each complex eigenenergy consists of a Kramers pair, one of which is localized at the left boundary and the other at the right boundary. Because of the $\mathbb{Z}_2$ nature, the point-gap topology becomes trivial and no skin effect occurs if the two nontrivial systems are stacked. Such a stacked system is explicitly constructed, for example, as

$$H^{\mathrm{stack}}\left(k\right) = \begin{pmatrix} H\left(k\right) & \mathrm{i}\boldsymbol{\delta}\cdot\boldsymbol{\sigma} \\ -\mathrm{i}\boldsymbol{\delta}\cdot\boldsymbol{\sigma} & H\left(k\right) \end{pmatrix}, \tag{4.6}$$

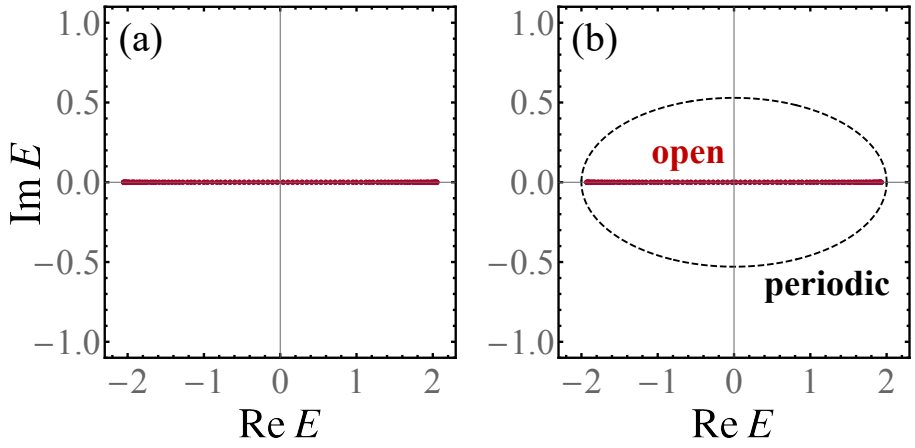

Figure 4.1: Complex spectra of the symplectic Hatano-Nelson model. The black dashed curves denote the spectra under the periodic boundary conditions, and the red dots denote the spectra under the open boundary conditions ($L = 100$). (a) The periodic-boundary spectrum and the open-boundary spectrum coincide with each other, and no skin effect occurs ($t = 1.0$, $\Delta = 0.3$, $g = 0.2$). (b) The periodic-boundary spectrum forms a loop in the complex plane, but the open-boundary spectrum lies on the real axis, which is a signature of the skin effect ($t = 1.0$, $\Delta = 0.3$, $g = 0.4$). Reproduced from Fig. 1 of Ref. [KOS20]. Copyright 2020 by the American Physical Society.

where the off-diagonal terms are symmetry-preserving couplings. Consistently, the skin effect no longer survives in this stacked system [OKSS20].

Since the $\mathbb{Z}_2$ skin effect is topologically protected by reciprocity, it breaks down by a symmetry-breaking perturbation including $(\delta h)\,\sigma_z$. In particular, such a local perturbation, which does not connect the ends, may be infinitesimal for the breakdown of the skin effect [OS19]. This local infinitesimal instability is unique to symmetry-protected non-Hermitian skin effects (see Appendix B.2 for details).

4.2 Non-Bloch band theory in the symplectic class

As summarized in Sec. 3.2, recent works [YW18, YM19] have developed a non-Bloch band theory that works even under arbitrary boundary conditions to elucidate the breakdown of the Bloch band theory due to the non-Hermitian skin effect. However, the validity of the non-Bloch band theory has been unclear in the presence of symmetry. Here, although the standard non-Bloch band theory [YW18, YM19] is applicable to generic non-Hermitian systems without symmetry, we demonstrate its breakdown in the symplectic class [KOS20]. For non-Hermitian Hamiltonians, the symplectic class (class AII† in Ref. [KSUS19]) is defined by reciprocity given by Eq. (4.1). Because of this symmetry, Hamiltonians exhibit Kramers degeneracy even in non-Hermitian systems, leading to the breakdown of the standard non-Bloch band theory. Instead, we generally provide a modified condition for continuum bands in the symplectic class, summarized as follows:

Non-Bloch band theory in the symplectic class [KOS20]

Suppose that non-Hermitian Hamiltonians respect reciprocity in

$$\mathcal{T}H^T\mathcal{T}^{-1} = H, \quad \mathcal{T}\mathcal{T}^* = -1 \tag{4.7}$$

and belong to the symplectic class. The solutions to the characteristic equation

$$\det\left[H\left(\beta\right) - E\right] = 0 \tag{4.8}$$

are generally denoted by

$$\beta_1, \beta_2, \cdots, \beta_{2M}; \beta_{2M}^{-1}, \beta_{2M-1}^{-1}, \cdots, \beta_1^{-1} \quad \left(|\beta_1| \leq \cdots |\beta_{2M}| \leq 1 \leq |\beta_{2M}^{-1}| \leq \cdots \leq |\beta_1^{-1}|\right). \tag{4.9}$$

Here, β_i and β_i^{-1} form a Kramers pair. Then, the condition for continuum bands is given as

$$|\beta_{2M-1}| = |\beta_{2M}|\,. \tag{4.10}$$

Notably, the standard non-Bloch band theory [YW18, YM19] predicts Eq. (3.20), i.e.,

$$|\beta_{2M}| = |\beta_{2M}^{-1}|, \tag{4.11}$$

for continuum bands, but this is not the case in the symplectic class. The condition (3.20) intuitively implies the interference between the non-Bloch waves with β_M and β_{M+1}. In the symplectic class, however, the non-Bloch waves with β_{2M} and β_{2M}^{-1} cannot interfere with each other since they form a Kramers pair; instead, the non-Bloch waves with β_{2M-1} and β_{2M} interfere, replacing the condition (3.20) with the condition (4.10). This nonstandard non-Bloch band theory underlies the $\mathbb{Z}_2$ skin effects protected by reciprocity in Sec. 4.1 [OKSS20].

More precisely, the conditions (3.20) and (4.10) are derived from the boundary conditions. In the standard (symplectic) case, boundary conditions impose a constraint on β_i's, which forms an Mth-order (a $2M$th-order) algebraic equation in terms of β_1^L, β_2^L, $\cdots$, β_M^L (β_1^L, $\cdots$, β_{2M}^L, β_{2M}^{-L}, $\cdots$, β_1^{-L}) with the system size L [see Eq. (B.20) in Appendix B.1 for the symplectic case]. In the standard case, because of the assumption $|\beta_1| \leq |\beta_2| \leq \cdots \leq |\beta_{2M}|$, the leading-order term generally includes

$$(\beta_{M+1}\beta_{M+2}\cdots\beta_{2M})^L \tag{4.12}$$

and the next-to-leading-order term includes

$$(\beta_M\beta_{M+2}\cdots\beta_{2M})^L. \tag{4.13}$$

To respect the constraint, these two terms should be comparable to each other for $L \to \infty$, which leads to Eq. (3.20). In the symplectic case, by contrast, reciprocity forbids the appearance of a term proportional to

$$(\beta_{2M}^{-1}\beta_{2M-1}^{-1}\cdots\beta_1^{-1})^L, \tag{4.14}$$

which should be dominant in the absence of symmetry (see Appendix B.1 for a detailed derivation). Consequently, the leading-order-term including

$$(\beta_{2M}\beta_{2M-1}^{-1}\beta_{2M-2}^{-1}\cdots\beta_1^{-1})^L \tag{4.15}$$

and the next-to-leading-order term including

$$(\beta_{2M-2}^{-1}\beta_{2M-3}^{-1}\cdots\beta_1^{-1})^L \tag{4.16}$$

should be comparable, which yields Eq. (4.10).

Below, we discuss several important aspects of the non-Bloch band theory in the symplectic class. In Sec. 4.2.1, we summarize the basic properties of reciprocity and how reciprocity changes the non-Bloch band theory. In Sec. 4.2.2, we investigate in detail the symplectic extension of the Hatano-Nelson model, which is a prototypical non-Hermitian system in the symplectic class. We also confirm that this model is indeed described by the non-Bloch band theory in the symplectic class. In Sec. 4.2.3, we further investigate the symplectic Hatano-Nelson model with next-nearest-neighbor hopping and numerically confirm the non-Bloch band theory in the symplectic class.

4.2.1 Reciprocity

As also described above, reciprocity is one of the fundamental internal symmetry [KSUS19]. There are two types of reciprocity according to the sign of the unitary matrix $\mathcal{T}$ (i.e., $\mathcal{T}\mathcal{T}^* = +1$ or $\mathcal{T}\mathcal{T}^* = -1$), one of which is defined by

$$\mathcal{T}H^T\mathcal{T}^{-1} = H, \quad \mathcal{T}\mathcal{T}^* = +1, \tag{4.17}$$

and the other is defined by Eq. (4.7). In Ref. [KSUS19], this symmetry is called TRS† since it is a Hermitian-conjugate counterpart of time-reversal symmetry (TRS), and non-Hermitian Hamiltonians with Eqs. (4.17) and (4.7) are defined to belong to classes AI† and AII†, respectively. Classes AI† and AII† are also called the orthogonal and symplectic classes, respectively, in a similar manner to the Hermitian case. Reciprocity appears in a variety of non-Hermitian systems. For example, time-reversal-invariant Hermitian Hamiltonians with gain or loss (i.e., complex onsite potential) respect it and belong to the orthogonal (symplectic) class in the absence (presence) of the spin degrees of freedom. In addition, it is relevant to open quantum systems described by the master equation [HKKU20, LMC20, SRP20, BP07].

Reciprocity imposes some constraints on the eigenstates $|\phi\rangle$ and $|\chi\rangle$. In the orthogonal class, Eq. (4.17) yields

$$H\left(\mathcal{T}|\chi\rangle^*\right) = \mathcal{T}H^T|\chi\rangle^* = E\left(\mathcal{T}|\chi\rangle^*\right), \tag{4.18}$$

which means that $\mathcal{T}|\chi\rangle^*$ is also a right eigenstate with the eigenenergy E. The eigenenergy is, in general, not degenerate solely in the presence of Eq. (4.17). Hence, the two right eigenstates are equivalent to each other, i.e.,

$$|\phi\rangle \propto \mathcal{T}|\chi\rangle^*. \tag{4.19}$$

Because of the relationship between $|\phi\rangle$ and $|\chi\rangle$ discussed in Sec. 3.2, they are forbidden to be localized in the orthogonal class. In fact, if $|\phi\rangle$ were localized at one end, $\mathcal{T}|\chi\rangle^*$ would be localized at the other end, which contradicts Eq. (4.19). Here, we use the fact that the internal-symmetry operation does not change the place at which eigenstates are localized. Thus, no skin effects appear in the orthogonal class, and this is why we call the symmetry in Eq. (4.17) reciprocity.

The absence of skin effects in the orthogonal class can be derived also on the basis of the non-Bloch band theory [KSUS19]. Since transposition transforms $H(\beta)$ to $H^T(\beta^{-1})$ as shown in Eq. (3.26), reciprocity for H [i.e., Eq. (4.17)] imposes

$$\mathcal{T}H^T(\beta)\mathcal{T}^{-1} = H(\beta^{-1}). \tag{4.20}$$

Then, when β is a solution to the characteristic equation (3.17), we have

$$\begin{aligned}\det\left[H\left(\beta^{-1}\right)-E\right] &= \det\left[\mathcal{T}H^{T}\left(\beta\right)\mathcal{T}^{-1}-E\right]\\ &= \det\left[H\left(\beta\right)-E\right]\\ &= 0,\end{aligned} \tag{4.21}$$

which implies that β^{-1} is another solution to Eq. (3.17). Hence, the solutions to the $2lq$-th-order equation (3.17) can be represented as

$$|\beta_1| \leq \cdots \leq |\beta_{lq}| \leq 1 \leq |\beta_{lq}^{-1}| \leq \cdots \leq |\beta_1^{-1}|. \tag{4.22}$$

Then, using Eq. (3.20), which is the salient result of the non-Bloch band theory, we have

$$|\beta_{lq}| = |\beta_{lq}^{-1}|, \quad \text{i.e.,} \quad |\beta_{lq}| = 1. \tag{4.23}$$

Consequently, bulk eigenstates are delocalized and no skin effects occur.

Notably, in Sec. 3.4 [ZYF20,OKSS20], we show that the skin effects originate from nontrivial topology that cannot be continuously deformed to any Hermitian systems. Consistently, such intrinsic non-Hermitian topology is absent in one-dimensional systems in the orthogonal class; see class AI† in Table A.5 of Appendix A.2 [KSUS19].

In the symplectic class, in which Eq. (4.7) is respected, we still have Eq. (4.18). A crucial distinction is Kramers degeneracy due to $\mathcal{T}\mathcal{T}^{*}=-1$ [ESHK11, KSUS19]. Such generic degeneracy is absent in the orthogonal class. In fact, because of $\mathcal{T}^{T}=-\mathcal{T}$, we have

$$\langle\chi|\mathcal{T}|\chi\rangle^{*} = \langle\chi|\mathcal{T}^{T}|\chi\rangle^{*} = -\langle\chi|\mathcal{T}|\chi\rangle^{*}, \tag{4.24}$$

which leads to $\langle\chi|\mathcal{T}|\chi\rangle^{*}=0$. This indicates that $|\phi\rangle$ and $\mathcal{T}|\chi\rangle^{*}$, which belong to the same eigenenergy, are biorthogonal [Bro14] to each other and linearly independent of each other. Thus, all the eigenenergy is at least twofold degenerate.

Similarly to the orthogonal class, we have Eq. (4.21) even in the symplectic class. In terms of $H\left(\beta\right)$, the non-Bloch waves $|\phi_i\rangle$ and $\mathcal{T}|\chi_i\rangle^{*}$ form a Kramers pair; the former satisfies Eq. (3.16), while the latter satisfies

$$H\left(\beta_i^{-1}\right)\left(\mathcal{T}|\chi_i\rangle^{*}\right) = E\left(\mathcal{T}|\chi_i\rangle^{*}\right). \tag{4.25}$$

Because of this Kramers degeneracy, the characteristic equation has the $4lq$-th order and its solutions are generally represented as

$$|\beta_1| \leq \cdots \leq |\beta_{2lq}| \leq 1 \leq |\beta_{2lq}^{-1}| \leq \cdots \leq |\beta_1^{-1}|. \tag{4.26}$$

If the standard non-Bloch band theory is applicable, we have $|\beta_{2lq}|=|\beta_{2lq}^{-1}|$, and hence no skin effects appear in a manner similar to the orthogonal class. However, the reciprocal skin effect is feasible in the symplectic class, as shown in Sec. 4.1 [OKSS20]. This fact implies a modification of the standard non-Bloch band theory, as discussed above.

4.2.2 Symplectic Hatano-Nelson model

Below, we investigate the symplectic Hatano-Nelson model in Eq. (4.4) and confirm the non-Bloch band theory in the symplectic class [i.e., Eq. (4.10)]. The bulk Hamiltonian of the symplectic Hatano-Nelson model reads

$$H\left(\beta\right) = \left(t-\mathrm{i}\Delta\sigma_x+g\sigma_z\right)\beta^{-1}+\left(t+\mathrm{i}\Delta\sigma_x-g\sigma_z\right)\beta. \tag{4.27}$$

This Hamiltonian respects reciprocity

$$\sigma_y H^T(\beta)\,\sigma_y^{-1} = H(\beta^{-1}), \tag{4.28}$$

and indeed belongs to the symplectic class.

Under the periodic boundary conditions, β satisfies $|\beta| = 1$ and hence is given by $\beta \coloneqq e^{\mathrm{i}k}$ with a real wave number $k \in [0, 2\pi]$. Then, the Bloch Hamiltonian is

$$H(k) = 2t\cos k - 2\left(\Delta\sigma_x + \mathrm{i}g\sigma_z\right)\sin k. \tag{4.29}$$

The spectrum of $H(k)$ is given as

$$E(k) = 2t\cos k \pm 2\mathrm{i}\sqrt{g^2 - \Delta^2}\sin k, \tag{4.30}$$

which is entirely real for $|g| \leq |\Delta|$ and forms a loop in the complex plane for $|g| > |\Delta|$ (Fig. 4.1).

Under the open boundary conditions, let $E \in \mathbb{C}$ be eigenenergy and

$$|\phi\rangle = \sum_{n=1}^{L}\sum_{s\in\{\uparrow,\downarrow\}} \phi_{n,s}\,|n\rangle\,|s\rangle \tag{4.31}$$

be the corresponding right eigenstate. The Schrödinger equation in real space reads

$$(t - \mathrm{i}\Delta\sigma_x + g\sigma_z)\begin{pmatrix}\phi_{n-1,\uparrow}\\ \phi_{n-1,\downarrow}\end{pmatrix} + (t + \mathrm{i}\Delta\sigma_x - g\sigma_z)\begin{pmatrix}\phi_{n+1,\uparrow}\\ \phi_{n+1,\downarrow}\end{pmatrix} = E\begin{pmatrix}\phi_{n,\uparrow}\\ \phi_{n,\downarrow}\end{pmatrix} \tag{4.32}$$

in the bulk ($n = 2, 3, \cdots, L-1$), and

$$(t + \mathrm{i}\Delta\sigma_x - g\sigma_z)\begin{pmatrix}\phi_{2,\uparrow}\\ \phi_{2,\downarrow}\end{pmatrix} = E\begin{pmatrix}\phi_{1,\uparrow}\\ \phi_{1,\downarrow}\end{pmatrix}, \tag{4.33}$$

$$(t - \mathrm{i}\Delta\sigma_x + g\sigma_z)\begin{pmatrix}\phi_{L-1,\uparrow}\\ \phi_{L-1,\downarrow}\end{pmatrix} = E\begin{pmatrix}\phi_{L,\uparrow}\\ \phi_{L,\downarrow}\end{pmatrix} \tag{4.34}$$

at the edges. Defining $\phi_{0,s}$ and $\phi_{L+1,s}$ by the bulk equation (4.32), the boundary equations (4.33) and (4.34) reduce to

$$\begin{pmatrix}\phi_{0,\uparrow}\\ \phi_{0,\downarrow}\end{pmatrix} = \begin{pmatrix}\phi_{L+1,\uparrow}\\ \phi_{L+1,\downarrow}\end{pmatrix} = 0. \tag{4.35}$$

Suppose that a fundamental solution is given as

$$\phi_{n,s} \propto \beta^n \phi_s. \tag{4.36}$$

From the bulk equation (4.32), we have

$$\left[H(\beta) - E\right]\begin{pmatrix}\phi_\uparrow\\ \phi_\downarrow\end{pmatrix} = 0. \tag{4.37}$$

To have a nontrivial solution $(\phi_\uparrow\ \phi_\downarrow)^T \neq 0$, the coefficient matrix $H(\beta) - E$ should not be invertible, leading to the characteristic equation

$$\det\left[H(\beta) - E\right] = 0, \tag{4.38}$$

i.e.,

$$E = t\left(\beta + \beta^{-1}\right) \pm \sqrt{g^2 - \Delta^2}\left(\beta - \beta^{-1}\right). \tag{4.39}$$

This is a quartic equation in terms of β for given E and decomposes into a pair of quadratic equations

$$\left(t + \sqrt{g^2 - \Delta^2}\right)\beta^2 - E\beta + t - \sqrt{g^2 - \Delta^2} = 0, \tag{4.40}$$

$$\left(t - \sqrt{g^2 - \Delta^2}\right)\beta^2 - E\beta + t + \sqrt{g^2 - \Delta^2} = 0. \tag{4.41}$$

Notably, when β satisfies this characteristic equation, β^{-1} also satisfies it; in particular, when β satisfies Eq. (4.40), β^{-1} satisfies Eq. (4.41), and vice versa. This is a direct consequence of reciprocity, as discussed in Sec. 4.2.1. Furthermore, a fundamental solution with β and another fundamental solution with β^{-1} are linearly independent of each other and form a Kramers pair. Now, we define the solutions to Eq. (4.40) as β_1 and β_2 ($|\beta_1| \leq |\beta_2|$), which satisfy

$$\beta_1\beta_2 = \frac{t - \sqrt{g^2 - \Delta^2}}{t + \sqrt{g^2 - \Delta^2}}. \tag{4.42}$$

The solutions to Eq. (4.41) are given as β_1^{-1} and β_2^{-1}. Since the solutions $\beta_1, \beta_2, \beta_1^{-1}, \beta_2^{-1}$ to the characteristic equation are defined so as to respect $|\beta_1| \leq |\beta_2|$, the standard non-Bloch band theory [YW18, YM19] predicts

$$|\beta_2| = |\beta_2^{-1}| \tag{4.43}$$

for continuum bands. However, this is not the case in the symplectic class; we have

$$|\beta_1| = |\beta_2|, \tag{4.44}$$

as shown below.

Now, the eigenstate $|\phi\rangle = \sum_{n=1}^{L}\sum_{s\in\{\uparrow,\downarrow\}}\phi_{n,s}|n\rangle|s\rangle$ can be obtained as a linear combination of the above fundamental solutions:

$$\begin{pmatrix}\phi_{n,\uparrow}\\ \phi_{n,\downarrow}\end{pmatrix} = \beta_1^n\begin{pmatrix}\phi_\uparrow^{(1+)}\\ \phi_\downarrow^{(1+)}\end{pmatrix} + \beta_2^n\begin{pmatrix}\phi_\uparrow^{(2+)}\\ \phi_\downarrow^{(2+)}\end{pmatrix} + \beta_1^{-n}\begin{pmatrix}\phi_\uparrow^{(1-)}\\ \phi_\downarrow^{(1-)}\end{pmatrix} + \beta_2^{-n}\begin{pmatrix}\phi_\uparrow^{(2-)}\\ \phi_\downarrow^{(2-)}\end{pmatrix} \tag{4.45}$$

for $n = 1, 2, \cdots, L$. Here, since $(\phi_\uparrow^{(i\pm)}\ \phi_\downarrow^{(i\pm)})^T$ satisfies Eq. (4.37), we have

$$\begin{pmatrix}\pm\sqrt{g^2 - \Delta^2} + g & -\mathrm{i}\Delta\\ -\mathrm{i}\Delta & \pm\sqrt{g^2 - \Delta^2} - g\end{pmatrix}\begin{pmatrix}\phi_\uparrow^{(i\pm)}\\ \phi_\downarrow^{(i\pm)}\end{pmatrix} = 0. \tag{4.46}$$

Notably, $(\phi_\uparrow^{(i\pm)}\ \phi_\downarrow^{(i\pm)})^T$ does not depend on i. Hence, Eq. (4.45) further simplifies to

$$\begin{pmatrix}\phi_{n,\uparrow}\\ \phi_{n,\downarrow}\end{pmatrix} = (\beta_1^n\bar{\phi}_{1+} + \beta_2^n\bar{\phi}_{2+})\begin{pmatrix}1\\ c_+\end{pmatrix} + (\beta_1^{-n}\bar{\phi}_{1-} + \beta_2^{-n}\bar{\phi}_{2-})\begin{pmatrix}1\\ c_-\end{pmatrix}, \tag{4.47}$$

with some constants $\bar{\phi}_{1\pm}, \bar{\phi}_{2\pm} \in \mathbb{C}$ and

$$c_\pm := -\frac{-\mathrm{i}\left(\pm\sqrt{g^2 - \Delta^2} + g\right)}{\Delta}. \tag{4.48}$$

Then, the boundary conditions (4.35) reduce to

$$(\bar{\phi}_{1+}+\bar{\phi}_{2+})\begin{pmatrix}1\\c_+\end{pmatrix}+(\bar{\phi}_{1-}+\bar{\phi}_{2-})\begin{pmatrix}1\\c_-\end{pmatrix}=0, \tag{4.49}$$

$$(\beta_1^{L+1}\bar{\phi}_{1+}+\beta_2^{L+1}\bar{\phi}_{2+})\begin{pmatrix}1\\c_+\end{pmatrix}+(\beta_1^{-(L+1)}\bar{\phi}_{1-}+\beta_2^{-(L+1)}\bar{\phi}_{2-})\begin{pmatrix}1\\c_-\end{pmatrix}=0. \tag{4.50}$$

The vectors $(1\ c_+)^T$ and $(1\ c_-)^T$ form a Kramers pair and linearly independent of each other. In particular, they are biorthogonal to each other [Bro14], i.e., the left counterpart of $(1\ c_+)^T$ is orthogonal to $(1\ c_-)^T$. As a result, we have

$$\bar{\phi}_{1\pm}+\bar{\phi}_{2\pm}=\beta_1^{\pm(L+1)}\bar{\phi}_{1\pm}+\beta_2^{\pm(L+1)}\bar{\phi}_{2\pm}=0, \tag{4.51}$$

leading to

$$\beta_1^{L+1}=\beta_2^{L+1} \tag{4.52}$$

for a nontrivial solution $\left(\bar{\phi}_{1\pm},\bar{\phi}_{2\pm}\right)\neq 0$. This equation means that the absolute values of β_1 and β_2 coincide with each other and are given, from Eq. (4.42), as

$$|\beta_1|=|\beta_2|=\sqrt{\left|\frac{t-\sqrt{g^2-\Delta^2}}{t+\sqrt{g^2-\Delta^2}}\right|}. \tag{4.53}$$

The relative phase between β_1 and β_2 can be different, resulting in the formation of continuum bands.

Equation (4.53) provides the localization length of eigenstates and the criteria of the skin effect. For $|g|\leq|\Delta|$, we have $|\beta_1|=|\beta_2|=1$, and hence eigenstates are delocalized. For $|g|>|\Delta|$, on the other hand, we have $|\beta_1|=|\beta_2|\neq 1$, and hence the eigenstates are localized at the edges. In contrast to the conventional skin effect, skin modes appear at both edges; when an eigenstate is localized at one edge, the Kramers partner is localized at the other edge. The numerical calculations shown in Fig. 4.1 confirm this result. For $|g|>|\Delta|$, the spectrum under the periodic boundary conditions forms a loop in the complex plane, but the spectrum under the open boundary conditions lies on the real axis, which is a signature of the non-Hermitian skin effect.

In the above calculations, an important distinction from the standard case is the equivalence between $(\phi_\uparrow^{(1\pm)}\ \phi_\downarrow^{(1\pm)})^T$ and $(\phi_\uparrow^{(2\pm)}\ \phi_\downarrow^{(2\pm)})^T$. In fact, if they were linearly independent, we would have $|\beta_2|=|\beta_2^{-1}|$ instead of $|\beta_1|=|\beta_2|$ in a manner similar to the standard case [YW18, YM19]. However, symplectic reciprocity makes $(\phi_\uparrow^{(1\pm)}\ \phi_\downarrow^{(1\pm)})^T$ and $(\phi_\uparrow^{(2\pm)}\ \phi_\downarrow^{(2\pm)})^T$ linearly depend on each other and changes the condition for continuum bands (see Appendix B.1 for a general proof).

4.2.3 Symplectic Hatano-Nelson model with next-nearest-neighbor hopping

To further verify the nonstandard non-Bloch band theory, we consider the symplectic Hatano-Nelson model with next-nearest-neighbor hopping:

$$\hat{H}=\sum_n\left[\hat{c}_{n+1}^\dagger\left(t-\mathrm{i}\Delta\sigma_x+g\sigma_z\right)\hat{c}_n+\hat{c}_n^\dagger\left(t+\mathrm{i}\Delta\sigma_x-g\sigma_z\right)\hat{c}_{n+1}+t'\left(\hat{c}_{n+2}^\dagger\hat{c}_n+\hat{c}_n^\dagger\hat{c}_{n+2}\right)\right], \tag{4.54}$$

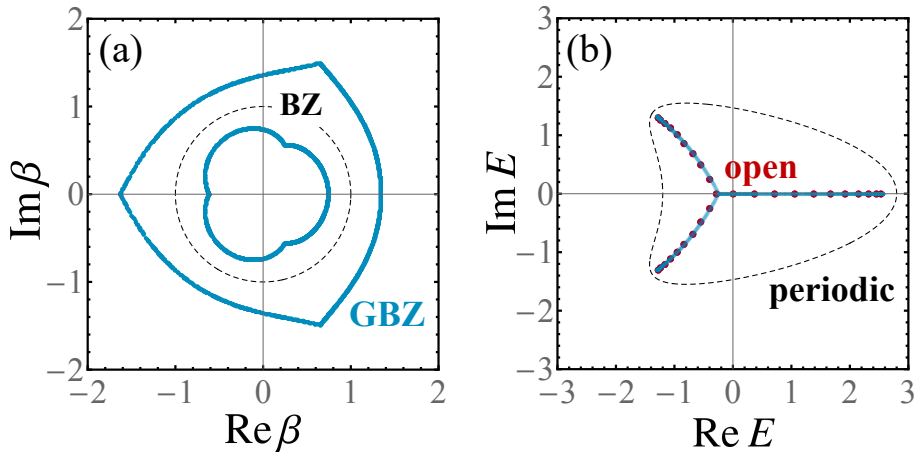

Figure 4.2: Symplectic Hatano-Nelson model with next-nearest-neighbor hopping ($t = 1.0$, $\Delta = 0.2$, $g = 0.8$, $t' = 0.4$). (a) Brillouin zone (BZ) and generalized Brillouin zone (GBZ). The system with periodic boundaries is described by the BZ (black dashed loop), which forms the unit circle in the complex β plane. By contrast, the system with open boundaries is described by the GBZ (blue solid loops), which is determined by the non-Bloch band theory in the symplectic class. (b) Complex spectra. The open-boundary spectrum ($L = 30$, red dots) coincides with the non-Bloch bands determined by the GBZ (blue solid curves), which is different from the periodic-boundary spectrum (black dashed loop). Reproduced from Fig. 2 of Ref. [KOS20]. Copyright 2020 by the American Physical Society.

where t' denotes the amplitude of the next-nearest-neighbor hopping. The bulk Hamiltonian reads

$$H(\beta) = (t - \mathrm{i}\Delta\sigma_x + g\sigma_z)\beta^{-1} + (t + \mathrm{i}\Delta\sigma_x - g\sigma_z)\beta + t'\left(\beta^2 + \beta^{-2}\right), \tag{4.55}$$

and the energy dispersion is given by the characteristic equation $\det[H(\beta) - E] = 0$, i.e.,

$$E = t\left(\beta + \beta^{-1}\right) + t'\left(\beta^2 + \beta^{-2}\right) \pm \sqrt{g^2 - \Delta^2}\left(\beta - \beta^{-1}\right). \tag{4.56}$$

The characteristic equation is eighth order and decomposes into a pair of quartic equations in terms of β, while it reduces to a pair of quadratic equations for $t' = 0$ as investigated in Sec. 4.2.2. Consequently, the analytical solutions are not simple.

We numerically investigate the symplectic Hatano-Nelson model with the next-nearest-neighbor hopping in a similar manner to Ref. [YM19] and confirm that it is indeed described by the nonstandard non-Bloch band theory. Figure 4.2 (a) shows the Brillouin zone and the generalized Brillouin zone of this model. The system with periodic boundaries is described by the Brillouin zone, which forms the unit circle $|\beta| = 1$ in the complex β plane. By contrast, the system with open boundaries is described by the generalized Brillouin zone, which is determined by Eq. (4.10) of the non-Bloch band theory in the symplectic class. In this model, Eq. (4.10) means

$$|\beta_3| = |\beta_4|, \tag{4.57}$$

where the eight solutions to Eq. (4.56) for given $E \in \mathbb{C}$ are denoted by β_1, β_2, β_3, β_4; β_4^{-1}, β_3^{-1}, β_2^{-1}, β_1^{-1} with $|\beta_1| \le |\beta_2| \le |\beta_3| \le |\beta_4|$. In the presence of non-Hermiticity, the generalized Brillouin zone does not necessarily form the unit circle, which is a direct manifestation of the non-Hermitian skin effect. In contrast to the standard case, the generalized Brillouin zone generally consists of a pair of loops, one of which is inside the unit circle and the other

is outside the unit circle. This is a consequence of reciprocity, and each loop describes the localized modes at the right or left edge. Figure 4.2 (b) shows the complex spectra of this model. The open-boundary spectrum cannot be described by the Bloch bands determined by the Brillouin zone, which is another signature of the skin effect. However, it is in complete agreement with the non-Bloch bands determined by the generalized Brillouin zone. It is also notable that both generalized Brillouin zone and complex spectra are symmetric about the real axis, which originates from time-reversal symmetry $\sigma_z H^* (\beta) \sigma_z^{-1} = H (\beta^*)$.

4.3 Bulk-boundary correspondence

4.3.1 Modified bulk-boundary correspondence

A non-Hermitian Hamiltonian H is defined to have a line gap if and only if its spectrum does not cross a reference line in the complex-energy plane. The modified bulk-boundary correspondence persists for a line gap because a non-Hermitian Hamiltonian with a line gap can be continuously deformed to a Hermitian one [KSUS19]. In Sec. 3.4, on the other hand, we develop a theory of the bulk-boundary correspondence for a point gap.

Importantly, point and line gaps are not necessarily independent of each other. In fact, if a line gap is open, a point gap is also open with a reference point on the reference line. Hence, a remnant of line-gap topology may survive in the presence of a point gap even if the line gap is closed. Prime examples include non-Hermitian superconductors in one dimension without time-reversal symmetry (i.e., class D). In this case, particle-hole symmetry

$$\mathcal{C} H^T (k) \mathcal{C}^{-1} = -H (-k) , \quad \mathcal{C}\mathcal{C}^* = +1 \tag{4.58}$$

lets zero energy be a special point in the complex-energy plane in contrast to reciprocity. As a result, non-Hermitian systems have the $\mathbb{Z}_2$ topological phases for both point and line gaps, and their topological invariants coincide with each other [KSUS19]. The Majorana zero modes in Hermitian topological superconductors survive as long as the point gap at $E = 0$ is open. Correspondingly, an index theorem states the emergence of the zero modes localized at the boundary (see Sec. 3.3.3 for details).

By contrast, point-gap topology can be nontrivial even if line-gap topology is trivial. For example, while line-gap topology is absent in one dimension with and without reciprocity [KSUS19], the point-gap topology characterized by Eqs. (3.9) and (4.2) is present. As shown above, such intrinsic point-gap topology in finite systems leads to the non-Hermitian skin effect.

4.3.2 Non-Hermitian Su-Schrieffer-Heeger model

As a prototypical non-Hermitian model that exhibits both skin effect and modified bulk-boundary correspondence, we here investigate a non-Hermitian extension of the Su-Schrieffer-Heeger model [SSH79] with asymmetric hopping [Lee16, KEBB18, YW18, YM19]. It exhibits the skin effect under the open boundary conditions due to the point-gap topology under the periodic boundary conditions. Still, a line gap can be open and the corresponding topological invariant protected by sublattice symmetry can be well defined under the open boundary conditions. As a result, topologically protected zero modes can emerge because of this line-gap topology.

The Hamiltonian of the non-Hermitian Su-Schrieffer-Heeger model reads

$$H_{\mathrm{SSH}} (k) = (v + w \cos k) \sigma_x + (w \sin k + \mathrm{i} g) \sigma_y = \begin{pmatrix} 0 & v + g + w e^{-\mathrm{i}k} \\ v - g + w e^{\mathrm{i}k} & 0 \end{pmatrix} , \tag{4.59}$$

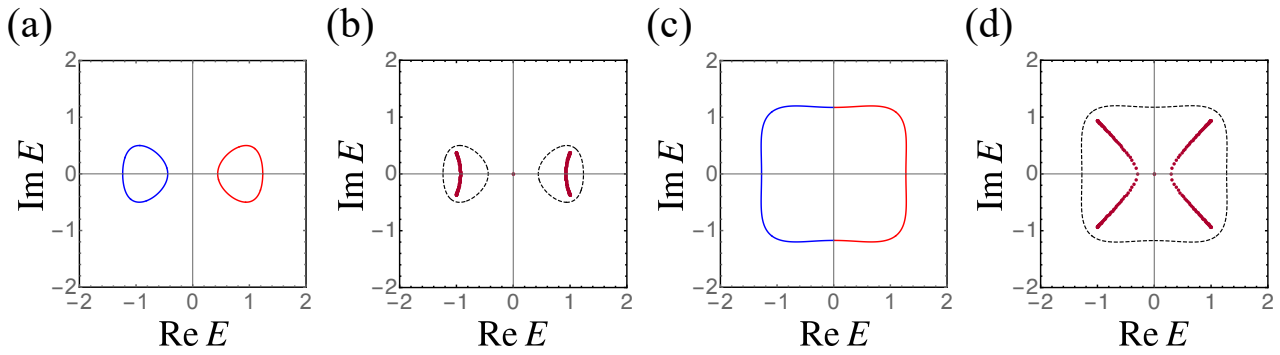

Figure 4.3: Non-Hermitian Su-Schrieffer-Heeger model with asymmetric hopping. (a, b) Complex spectra under the (a) periodic and (b) open boundary conditions ($L = 100$) with $v = 1/3$, $w = 1$, and $g = 1/2$. (a) Under the periodic boundary conditions, each of the two bands (red and blue curves) forms a loop in the complex-energy plane. (b) Under the open boundary conditions, the energy bands (red dots) form arcs and are different from those under the periodic boundary conditions (black dotted curves), which signals the non-Hermitian skin effect. Still, a line gap for the imaginary axis is open (i.e., $\mathrm{Re}\, E \neq 0$) and the zero modes appear because of the line-gap topology. (c, d) Complex spectra under the (c) periodic and (d) open boundary conditions ($L = 100$) with $v = 3/4$, $w = 1$, and $g = 6/5$.

with $v, w, g \in \mathbb{R}$ [Lee16, KEBB18, YW18, YM19]. In contrast with the Hatano-Nelson model, $H_{\mathrm{SSH}}(k)$ respects sublattice symmetry:

$$\mathcal{S} H_{\mathrm{SSH}}(k) \mathcal{S}^{-1} = -H_{\mathrm{SSH}}(k), \quad \mathcal{S}^2 = 1, \tag{4.60}$$

with $\mathcal{S} \coloneqq \sigma_z$. As a result of sublattice symmetry, $H_{\mathrm{SSH}}(k)$ possesses $\mathbb{Z}$ topological phases in the presence of a line gap [KSUS19]. The corresponding topological invariant (winding number W_{L}) has the same form as that in the Hermitian case,

$$W_{\mathrm{L}} = -\oint_{\mathrm{BZ}} \frac{dk}{4\pi \mathrm{i}} \mathrm{tr} \left[\mathcal{S} H_{\mathrm{SSH}}^{-1}(k) \frac{d H_{\mathrm{SSH}}(k)}{dk} \right]. \tag{4.61}$$

On the other hand, $H_{\mathrm{SSH}}(k)$ possesses $\mathbb{Z} \oplus \mathbb{Z}$ topological phases in the presence of a point gap, i.e., two independent $\mathbb{Z}$ topological invariants are well defined [KSUS19]. One of these invariants coincides with W_{L}, and the other is the following winding number W_{P}, which is intrinsic to point-gap topology (see also 1D class A with $\mathcal{S}$ in Table 4.3):

$$W_{\mathrm{P}} = -\oint_{\mathrm{BZ}} \frac{dk}{2\pi \mathrm{i}} \frac{d}{dk} \log \det H_{\mathrm{SSH}}(k). \tag{4.62}$$

For Hermitian systems, we have $W_{\mathrm{P}} = 0$. Notably, W_{L} can be a half integer in non-Hermitian systems, while it is always an integer for $W_{\mathrm{P}} = 0$. In the above, the reference line for the line gap is chosen as a line in the complex-energy plane that crosses $E = 0$, and the reference point for the point gap is chosen as $E = 0$ so that they will respect sublattice symmetry. While they may be chosen as lines and points away from these symmetric lines and points, respectively, the consequent topological phases reduce to those without sublattice-symmetry protection.

As shown in Fig. 4.3, the non-Hermitian Su-Schrieffer-Heeger model exhibits the skin effect under the open boundary conditions, which originates from the intrinsic point-gap topology. Consistent with our preceding discussions, each of the two energy bands forms an arc in the

complex-energy plane. Notably, we have $W_{\mathrm{P}} = 0$ in terms of the reference point $E = 0$ for Fig. 4.3 (a, b). Nevertheless, we have a nontrivial winding number when we choose a reference point as energy inside the loop determined by $H_{\mathrm{SSH}}(k)$, instead of the symmetric point $E = 0$ that respects sublattice symmetry. In this case, the topological classification reduces to that without symmetry despite sublattice symmetry of the Hamiltonian, as described above. On the other hand, we have $W_{\mathrm{P}} \neq 0$ for Fig. 4.3 (c, d), which directly leads to the skin effect.

In either case, the bulk spectrum under the open boundary conditions has a line gap for the imaginary axis (i.e., $\mathrm{Re}\, E \neq 0$). Therefore, W_{L} can be defined for the bulk Hamiltonian under the open boundary conditions. According to the non-Bloch band theory [KEBB18, YW18, YM19], the open-boundary bulk Hamiltonian is given by

$$H_{\mathrm{SSH}}(k - \mathrm{i} \log r_0) = \begin{pmatrix} 0 & v + g + w r_0^{-1} e^{-\mathrm{i}k} \\ v - g + w r_0 e^{\mathrm{i}k} & 0 \end{pmatrix}, \quad r_0 \coloneqq \sqrt{\left| \frac{v - g}{v + g} \right|}, \tag{4.63}$$

which provides a nonzero winding number W_{L} in either case of Fig. 4.3. As a result, topologically protected zero modes emerge for Fig. 4.3 (b,d).

We note in passing that sublattice symmetry in Eq. (4.60) is distinct from chiral symmetry defined by [KSUS19]

$$\Gamma H^{\dagger}(k) \Gamma^{-1} = -H(k), \quad \Gamma^2 = 1, \tag{4.64}$$

where Γ is a unitary operator. While Eqs. (4.60) and (4.64) are equivalent to each other in Hermitian systems [$H^{\dagger}(k) = H(k)$], they are not in non-Hermitian systems. Correspondingly, although $H(k)$ with chiral symmetry possesses $\mathbb{Z}$ topological phases in the presence of a line gap for the real part of the spectrum, it does not possess nontrivial point-gap topology in terms of a reference point on the symmetric line (i.e., the imaginary axis) [KSUS19]. For example, another non-Hermitian extension of the Su-Schrieffer-Heeger model [SSH79] with balanced gain and loss [ESHK11, Sch13, WKP+17, SJGG+17] respects chiral symmetry instead of sublattice symmetry.

4.3.3 Classification of skin effects

As discussed above, the skin effect originates from intrinsic non-Hermitian topology. To characterize such intrinsic non-Hermitian topology in a general manner, we here classify the homomorphisms from line-gap topology to point-gap topology for all the 38-fold internal symmetry class in arbitrary spatial dimensions [OKSS20, Shi19]. This classification allows us to know possible types of symmetry-protected skin effects for general internal-symmetry classes and arbitrary dimensions (Tables 4.1, 4.2, and 4.3).

As discussed above, if a line gap is open, a point gap is also open with a reference point on the reference line. Hence, we can define a map from a line-gapped topological phase to a point-gaped one for each spatial dimension and symmetry class. Such maps are obtained as follows. Given a non-Hermitian Hamiltonian $H(\boldsymbol{k})$ in d dimensions, we introduce an extended Hermitian Hamiltonian [GAK+18, KSUS19]

$$\tilde{H}(\boldsymbol{k}) = \begin{pmatrix} 0 & H(\boldsymbol{k}) \\ H^{\dagger}(\boldsymbol{k}) & 0 \end{pmatrix}, \tag{4.65}$$

which respects chiral symmetry $\Gamma H(\boldsymbol{k}) \Gamma^{-1} = -H(\boldsymbol{k})$ with $\Gamma \coloneqq \sigma_z$. Here, $\tilde{H}(\boldsymbol{k})$ is gapped when $H(\boldsymbol{k})$ has a point gap, and vice versa. Thus, topological classification for $H(\boldsymbol{k})$ with respect to a point gap coincides with the topological classification of Hermitian Hamiltonians

$\tilde{H}(\boldsymbol{k})$ [GAK+18, KSUS19]. The obtained topological phases are denoted by K_{P}. On the other hand, when one keeps a line gap, an additional constraint arises on $\tilde{H}(\boldsymbol{k})$. As shown in Ref. [KSUS19], a non-Hermitian Hamiltonian $H(\boldsymbol{k})$ with a real (an imaginary) line gap is continuously deformed to a Hermitian (an anti-Hermitian) Hamiltonian while keeping the line gap (and the point gap as well). Therefore, when one considers the classification of $\tilde{H}(\boldsymbol{k})$ while keeping a real (an imaginary) line gap of $H(\boldsymbol{k})$, $H(\boldsymbol{k})$ is supposed to be Hermitian (anti-Hermitian). Notably, Hermiticity (anti-Hermiticity) of $H(\boldsymbol{k})$ imposes additional chiral symmetry with $\Gamma_{\mathrm{r}} = \sigma_y$ ($\Gamma_{\mathrm{i}} = \sigma_x$) on $\tilde{H}(\boldsymbol{k})$. Because of this additional symmetry, we have a different topological phase $K_{\mathrm{L_r}}$ ($K_{\mathrm{L_i}}$) with respect to a point gap in the presence of a real (an imaginary) line gap. Leaving the additional chiral symmetry Γ_{r} (Γ_{i}) out of consideration defines a homomorphism $f_{\mathrm{r}} : K_{\mathrm{L_r}} \to K_{\mathrm{P}}$ ($f_{\mathrm{i}} : K_{\mathrm{L_i}} \to K_{\mathrm{P}}$) from $K_{\mathrm{L_r}}$ ($K_{\mathrm{L_i}}$) to K_{P}. Because of the dimensional isomorphism of the K-theory, it suffices to compute f_{r} and f_{i} in zero dimension to get the homomorphisms in arbitrary spatial dimension (see Refs. [OKSS20, Shi19] for details).

If a point-gapped non-Hermitian Hamiltonian $H(\boldsymbol{k})$ lies in the image of either homomorphism f_{r} or f_{i}, $H(\boldsymbol{k})$ can be continuously deformed to a Hermitian or anti-Hermitian Hamiltonian, and thus the topological nature is attributed to the conventional Hermitian one. By contrast, if $H(\boldsymbol{k})$ does not, its topological nature is intrinsic to non-Hermitian Hamiltonians. In other words, the quotient group $K_{\mathrm{P}}/(\mathrm{Im}\, f_{\mathrm{r}} \cup \mathrm{Im}\, f_{\mathrm{i}})$ indicates the presence of the topological nature unique to non-Hermitian systems. A prime example of such intrinsic point-gap topology is found in one-dimensional systems without symmetry (class A), where the non-Hermitian skin effect occurs as a consequence of nontrivial topology, as discussed in Sec. 3.4. Tables 4.1, 4.2, and 4.3 summarize the quotient groups $K_{\mathrm{P}}/(\mathrm{Im}\, f_{\mathrm{r}} \cup \mathrm{Im}\, f_{\mathrm{i}})$ for all fundamental symmetry classes (see also Sec. 2.4 for details about symmetry classes of non-Hermitian systems).

Like surface Dirac fermions in topological insulators, higher-dimensional skin modes appear in any boundary of the system under proper boundary conditions. For example, a two-dimensional variant of the $\mathbb{Z}_2$ skin effect is present in the symplectic class (see Supplemental Material of Ref. [OKSS20] for details). There, skin modes coexist with bulk modes under the open boundary conditions in one direction and the periodic boundary conditions in the other direction, which are the "proper boundary conditions" in this system. Notably, only $\mathcal{O}(L)$ skin modes appear from all the $\mathcal{O}(L^2)$ modes in this model (L denotes the length in one direction), which is unfeasible for the skin effects in one dimension.

Since weak topological invariants can be defined in higher dimensions, the corresponding weak skin effects can occur. For example, the two-dimensional skin effect in Ref. [HHS+20] is due to one-dimensional point-gap topology of $H(k_x, k_y)$ with fixed k_y. By contrast, the aforementioned two-dimensional skin effects in Ref. [OKSS20] originate from strong point-gap topology defined by both k_x and k_y. This strong nature is well understood by the skin effect due to a π-flux defect, in a similar manner to time-reversal-invariant topological superconductors in two dimensions [QHRZ09].

Table 4.1: Classification table of intrinsic non-Hermitian topology for the AZ symmetry class.

AZ class	$d=0$	$d=1$	$d=2$	$d=3$	$d=4$	$d=5$	$d=6$	$d=7$
A	0	$\mathbb{Z}$	0	$\mathbb{Z}$	0	$\mathbb{Z}$	0	$\mathbb{Z}$
AIII	0	0	0	0	0	0	0	0
AI	0	$\mathbb{Z}$	0	0	0	$2\mathbb{Z}$	0	0
BDI	0	0	0	0	0	0	0	0
D	0	0	0	$\mathbb{Z}$	0	0	0	$2\mathbb{Z}$
DIII	0	0	0	0	$\mathbb{Z}_2$	0	0	0
AII	0	$2\mathbb{Z}$	0	0	0	$\mathbb{Z}$	0	0
CII	0	0	0	0	0	0	0	0
C	0	0	0	$2\mathbb{Z}$	0	0	0	$\mathbb{Z}$
CI	$\mathbb{Z}_2$	0	0	0	0	0	0	0

Table 4.2: Classification table of intrinsic non-Hermitian topology for the AZ† symmetry class.

AZ† class	$d=0$	$d=1$	$d=2$	$d=3$	$d=4$	$d=5$	$d=6$	$d=7$
AI†	0	0	0	$2\mathbb{Z}$	0	$\mathbb{Z}_2$	$\mathbb{Z}_2$	$\mathbb{Z}$
BDI†	0	0	0	0	0	0	0	0
D†	0	$\mathbb{Z}$	0	0	0	$2\mathbb{Z}$	0	0
DIII†	0	$\mathbb{Z}_2$	$\mathbb{Z}_2$	0	0	0	0	0
AII†	0	$\mathbb{Z}_2$	$\mathbb{Z}_2$	$\mathbb{Z}$	0	0	0	$2\mathbb{Z}$
CII†	0	0	0	0	0	0	0	0
C†	0	$2\mathbb{Z}$	0	0	0	$\mathbb{Z}$	0	0
CI†	0	0	0	0	0	$\mathbb{Z}_2$	$\mathbb{Z}_2$	0

Table 4.3: Classification table of intrinsic non-Hermitian topology for the AZ symmetry class with additional symmetry (i.e., sublattice symmetry or pseudo-Hermiticity).

AZ class	Add. symm.	$d=0$	$d=1$	$d=2$	$d=3$	$d=4$	$d=5$	$d=6$	$d=7$
A	η	0	0	0	0	0	0	0	0
AIII	$\mathcal{S}_+$, η_+	0	0	0	0	0	0	0	0
A	$\mathcal{S}$	0	$\mathbb{Z}$	0	$\mathbb{Z}$	0	$\mathbb{Z}$	0	$\mathbb{Z}$
AIII	$\mathcal{S}_-$, η_-	$\mathbb{Z}_2$	0	$\mathbb{Z}_2$	0	$\mathbb{Z}_2$	0	$\mathbb{Z}_2$	0
AI	η_+	0	0	0	0	0	0	0	0
BDI	$\mathcal{S}_{++}$, η_{++}	0	0	0	0	0	0	0	0
D	η_+	0	0	0	0	0	0	0	0
DIII	$\mathcal{S}_{--}$,η_{++}	0	0	0	0	0	0	0	0
AII	η_+	0	0	0	0	0	0	0	0
CII	$\mathcal{S}_{++}$, η_{++}	0	0	0	0	0	0	0	0
C	η_+	0	0	0	0	0	0	0	0
CI	$\mathcal{S}_{--}$, η_{++}	0	0	0	0	0	0	0	0
AI	$\mathcal{S}_-$	0	$\mathbb{Z}$	0	0	0	$\mathbb{Z}$	0	0
BDI	$\mathcal{S}_{-+}$, η_{+-}	0	0	0	0	$\mathbb{Z}_2$	0	$\mathbb{Z}_2$	0
D	$\mathcal{S}_+$	0	0	0	$\mathbb{Z}$	0	$\mathbb{Z}_2$	0	$\mathbb{Z}$
DIII	$\mathcal{S}_{-+}$, η_{-+}	0	0	0	0	$\mathbb{Z}_2$	0	$\mathbb{Z}_2$	0
AII	$\mathcal{S}_-$	0	$\mathbb{Z}$	0	0	0	$\mathbb{Z}$	0	0
CII	$\mathcal{S}_{-+}$, η_{+-}	$\mathbb{Z}_2$	0	$\mathbb{Z}_2$	0	0	0	0	0
C	$\mathcal{S}_+$	0	$\mathbb{Z}_2$	0	$\mathbb{Z}$	0	0	0	$\mathbb{Z}$
CI	$\mathcal{S}_{-+}$, η_{-+}	$\mathbb{Z}_2$	0	$\mathbb{Z}_2$	0	0	0	0	0
AI	η_-	0	$\mathbb{Z}_2$	$\mathbb{Z}_2$	0	0	0	0	0
BDI	$\mathcal{S}_{--}$, η_{--}	0	0	0	0	0	0	0	0
D	η_-	0	0	0	0	$\mathbb{Z}_2$	0	0	0
DIII	$\mathcal{S}_{++}$, η_{--}	0	0	0	0	$\mathbb{Z}_2$	$\mathbb{Z}_2$	0	0
AII	η_-	0	0	0	0	0	$\mathbb{Z}_2$	$\mathbb{Z}_2$	0
CII	$\mathcal{S}_{--}$, η_{--}	0	0	0	0	0	0	0	0
C	η_-	$\mathbb{Z}_2$	0	0	0	0	0	0	0
CI	$\mathcal{S}_{++}$, η_{--}	$\mathbb{Z}_2$	$\mathbb{Z}_2$	0	0	0	0	0	0
AI	$\mathcal{S}_+$	$\mathbb{Z}_2$	$\mathbb{Z}$	0	0	0	$\mathbb{Z}$	0	$\mathbb{Z}_2$
BDI	$\mathcal{S}_{+-}$, η_{-+}	$\mathbb{Z}_2$	$\mathbb{Z}_2$	$\mathbb{Z}_2$	0	0	0	$\mathbb{Z}_2$	0
D	$\mathcal{S}_-$	0	$\mathbb{Z}_2$	$\mathbb{Z}_2$	$\mathbb{Z}$	0	0	0	$\mathbb{Z}$
DIII	$\mathcal{S}_{+-}$, η_{+-}	$\mathbb{Z}_2$	0	$\mathbb{Z}_2$	$\mathbb{Z}_2$	$\mathbb{Z}_2$	0	0	0
AII	$\mathcal{S}_+$	0	$\mathbb{Z}$	0	$\mathbb{Z}_2$	$\mathbb{Z}_2$	$\mathbb{Z}$	0	0
CII	$\mathcal{S}_{+-}$, $\eta-+$	0	0	$\mathbb{Z}_2$	0	$\mathbb{Z}_2$	$\mathbb{Z}_2$	$\mathbb{Z}_2$	0
C	$\mathcal{S}_-$	0	0	0	$\mathbb{Z}$	0	$\mathbb{Z}_2$	$\mathbb{Z}_2$	$\mathbb{Z}$
CI	$\mathcal{S}_{+-}$, η_{+-}	$\mathbb{Z}_2$	0	0	0	$\mathbb{Z}_2$	0	$\mathbb{Z}_2$	$\mathbb{Z}_2$

4.4 Second-order skin effect

Recently, higher-order counterparts of topological phases were revealed and investigated extensively [BBH17a, BBH17b, LPT+17, SFF17, FF19, KvMB18, SCV+18, Kha18, KPVW18, YSW18a, MW18, TB19, LVK19, BLH19]. Higher-order topological phases are protected by spatial symmetry such as inversion, mirror, and rotation symmetry. Importantly, the nature of the bulk-boundary correspondence is changed for higher-order topological phases. In two dimensions, second-order topology leads to $\mathcal{O}(1)$ zero modes localized at the corners, which is to be contrasted with $\mathcal{O}(L)$ chiral or helical edge modes accompanied by first-order topology. Similarly, in three dimensions, third-order topology leads to $\mathcal{O}(1)$ zero modes localized at the corners, instead of $\mathcal{O}(L^2)$ surface modes in first-order topological insulators. Higher-order topology was observed in various experiments [SGPS+18, IBB+18, PBHB18, SWV+18, XYG+19, NWAK19, MOZ+19, HKM+19, PLB+20], and may lead to unique phenomena and functionalities due to its new boundary physics.

As discussed previously, topological phases and their boundary physics are enriched also by non-Hermiticity. Despite the rich physics of non-Hermitian topological systems, little research has hitherto addressed non-Hermitian topological phenomena in higher dimensions. In particular, the non-Hermitian skin effect has been investigated mainly in one dimension and has remained largely unknown in higher dimensions. Similarly, the non-Bloch band theory in Refs. [YW18, YM19] is applicable only to one dimension, and its validity in higher dimensions has remained elusive.

Here, we discover higher-order counterparts of the non-Hermitian skin effect. They give rise to new types of boundary modes as a result of higher-order non-Hermitian topology (Fig. 4.4). In two-dimensional systems with the system size $L \times L$ and open boundaries along both directions, the conventional skin effect accompanies $\mathcal{O}(L^2)$ skin modes at arbitrary boundaries [Fig. 4.4 (c)]. In the second-order skin effect, by contrast, $\mathcal{O}(L)$ skin modes appear at the corners [Fig. 4.4 (d)]. This is also distinct from Hermitian second-order topological insulators, in which only $\mathcal{O}(1)$ corner modes appear as a result of Hermitian topology [Fig. 4.4 (b)]. We demonstrate that the higher-order skin effect cannot be described by the conventional non-Bloch band theory, which implies its inevitable modification in higher dimensions.

Notably, the higher-order non-Hermitian skin effect is distinct from non-Hermitian extensions of higher-order topological insulators [LZA+19, LLG19, EKB19, ZRLC+19, LZ19, YJS21]. There, even in the presence of non-Hermiticity, the corner modes have the same topological nature as the Hermitian counterparts. Consequently, the number of these corner modes is $\mathcal{O}(1)$. Moreover, the other modes typically exhibit the first-order skin effect and are also localized at boundaries. In the second-order skin effect, by contrast, the corner skin modes originate from intrinsic non-Hermitian topology that has no counterpart in Hermitian systems. Almost all the $\mathcal{O}(L^2)$ modes are delocalized through the bulk, and only $\mathcal{O}(L)$ skin modes appear at the corners.

In Sec. 4.4.1, we introduce a non-Hermitian model in two dimensions that exhibits the second-order skin effect [Eq. (4.66)]. This model is systematically constructed on the basis of a Hermitian second-order topological insulator [BBH17a, BBH17b]. The spectra and wave functions of this system are investigated in Sec. 4.4.2. Then, in Sec. 4.4.3, we identify the topological origin of the second-order non-Hermitian skin effect as the Wess-Zumino term [WZ71]. This topological invariant is protected by four-fold-rotation-type symmetry in Eqs. (4.80) and (4.90). The second-order skin effect requires a modification of the non-Bloch band theory, as demonstrated in Sec. 4.4.4. Furthermore, we investigate the third-order non-Hermitian skin effect in Sec. 4.5.

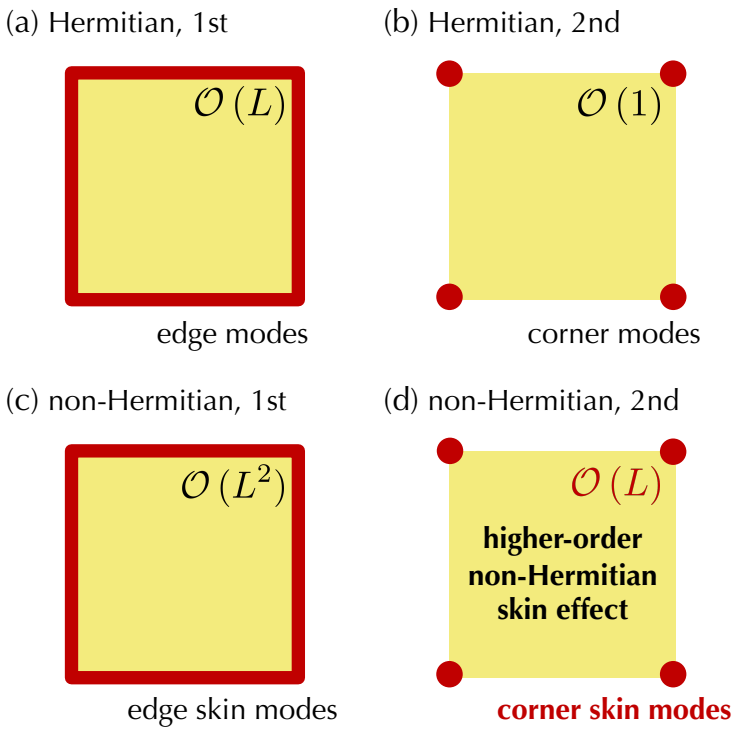

Figure 4.4: Higher-order non-Hermitian skin effect. Boundary modes (red lines or dots) are shown in a two-dimensional system with the system size $L \times L$. (a) Hermitian first-order topological insulator. At the edges, $\mathcal{O}(L)$ chiral or helical modes appear. (b) Hermitian second-order topological insulator. At the corners, $\mathcal{O}(1)$ zero modes appear. (c) First-order non-Hermitian skin effect. At arbitrary boundaries, $\mathcal{O}(L^2)$ skin modes appear because of intrinsic non-Hermitian topology. (d) Second-order non-Hermitian skin effect. At the corners, $\mathcal{O}(L)$ skin modes appear because of intrinsic non-Hermitian topology. Reproduced from Fig. 1 of Ref. [KSS20]. Copyright 2020 by the American Physical Society.

It is notable that similar results have been obtained in a recent related work [OTY20]. While the second-order skin effect here is protected by rotation-type symmetry, the second-order skin effect in Ref. [OTY20] is protected by inversion-type symmetry. Moreover, on the basis of our theoretical results, the second-order skin effect has been observed in the recent experiments of active particles [PTG+20] and acoustic materials [ZTJ+21]. These recent experiments show the utility of non-Hermitian topology for active control of materials.

4.4.1 Model and symmetry

We provide a model that exhibits the second-order non-Hermitian skin effect. The Bloch Hamiltonian reads

$$H(\boldsymbol{k}) = -\mathrm{i}(\gamma + \lambda\cos k_x) + \lambda(\sin k_x)\sigma_z + (\gamma + \lambda\cos k_y)\sigma_y + \lambda(\sin k_y)\sigma_x, \tag{4.66}$$

where γ and λ are real parameters, and σ_i's $(i = x, y, z)$ are Pauli matrices. As discussed previously, the Hatano-Nelson model is closely related to the Su-Schrieffer-Heeger model. Similarly, this model is constructed on the basis of a Hermitian second-order topological insulator. In

fact, the extended Hermitian Hamiltonian is given as

$$\begin{aligned}\tilde{H}_{\mathrm{BBH}}(\boldsymbol{k}) &= \begin{pmatrix} 0 & H(\boldsymbol{k}) \\ H^{\dagger}(\boldsymbol{k}) & 0 \end{pmatrix} \\ &= (\gamma + \lambda\cos k_x)\,\tau_y + \lambda(\sin k_x)\,\sigma_z\tau_x + (\gamma + \lambda\cos k_y)\,\sigma_y\tau_x + \lambda(\sin k_y)\,\sigma_x\tau_x, \end{aligned} \tag{4.67}$$

where τ_i's ($i = x, y, z$) are Pauli matrices that describe the additional degrees of freedom. This Hermitian Hamiltonian is a prototypical model of a second-order topological insulator that was first introduced by Benalcazar, Bernevig, and Hughes [BBH17a, BBH17b]. There, no edge modes appear under the open boundary conditions solely along one direction. Nevertheless, under the open boundary conditions along both directions, zero-energy modes appear at the corners for $|\gamma/\lambda| < 1$.

Spatial symmetry plays a crucial role in the second-order topological phase of $\tilde{H}_{\mathrm{BBH}}(\boldsymbol{k})$ and the second-order non-Hermitian skin effect of $H(\boldsymbol{k})$. First, both $\tilde{H}_{\mathrm{BBH}}(\boldsymbol{k})$ and $H(\boldsymbol{k})$ respect spatial-inversion (parity) symmetry:

$$\sigma_y \tilde{H}_{\mathrm{BBH}}(\boldsymbol{k})\,\sigma_y^{-1} = \tilde{H}_{\mathrm{BBH}}(-\boldsymbol{k}), \tag{4.68}$$

$$\sigma_y H(\boldsymbol{k})\,\sigma_y^{-1} = H(-\boldsymbol{k}). \tag{4.69}$$

In addition, $\tilde{H}_{\mathrm{BBH}}(\boldsymbol{k})$ respects mirror symmetry:

$$(\sigma_z\tau_y)\,\tilde{H}_{\mathrm{BBH}}(k_x, k_y)\,(\sigma_z\tau_y)^{-1} = \tilde{H}_{\mathrm{BBH}}(-k_x, k_y), \tag{4.70}$$

$$(\sigma_x\tau_y)\,\tilde{H}_{\mathrm{BBH}}(k_x, k_y)\,(\sigma_x\tau_y)^{-1} = \tilde{H}_{\mathrm{BBH}}(k_x, -k_y). \tag{4.71}$$

Correspondingly, $H(\boldsymbol{k})$ respects

$$\sigma_z H^{\dagger}(k_x, k_y)\,\sigma_z^{-1} = -H(-k_x, k_y), \tag{4.72}$$

$$\sigma_x H^{\dagger}(k_x, k_y)\,\sigma_x^{-1} = -H(k_x, -k_y). \tag{4.73}$$

They also respect the following transposition-associated mirror symmetry

$$\sigma_x \tilde{H}^{T}_{\mathrm{BBH}}(k_x, k_y)\,\sigma_x^{-1} = \tilde{H}_{\mathrm{BBH}}(-k_x, k_y), \tag{4.74}$$

$$\sigma_z \tilde{H}^{T}_{\mathrm{BBH}}(k_x, k_y)\,\sigma_z^{-1} = \tilde{H}_{\mathrm{BBH}}(k_x, -k_y), \tag{4.75}$$

and

$$\sigma_x H^{T}(k_x, k_y)\,\sigma_x^{-1} = H(-k_x, k_y), \tag{4.76}$$

$$\sigma_z H^{T}(k_x, k_y)\,\sigma_z^{-1} = H(k_x, -k_y). \tag{4.77}$$

The combination of Eqs. (4.72) and (4.73), or the combination of Eqs. (4.76) and (4.77) reduces to Eq. (4.69). As shown in Sec. 4.4.4, the symmetry in Eqs. (4.76) and (4.77) vanishes the first-order skin effect in $H(\boldsymbol{k})$ along the x and y directions, respectively. Furthermore, $\tilde{H}_{\mathrm{BBH}}(\boldsymbol{k})$ respects four-fold-rotation symmetry:

$$\mathcal{R}_4 \tilde{H}_{\mathrm{BBH}}(k_x, k_y)\,\mathcal{R}_4^{-1} = \tilde{H}_{\mathrm{BBH}}(-k_y, k_x), \tag{4.78}$$

where $\mathcal{R}_4$ is a unitary matrix given as

$$\mathcal{R}_4 = \begin{pmatrix} 0 & -\mathrm{i}\sigma_y \\ 1 & 0 \end{pmatrix}. \tag{4.79}$$

Correspondingly, $H(\boldsymbol{k})$ respects

$$-\mathrm{i}\sigma_y H^{\dagger}(k_x, k_y) = H(-k_y, k_x). \tag{4.80}$$

This rotation-type symmetry protects the second-order skin effect, as shown in Sec. 4.4.3.

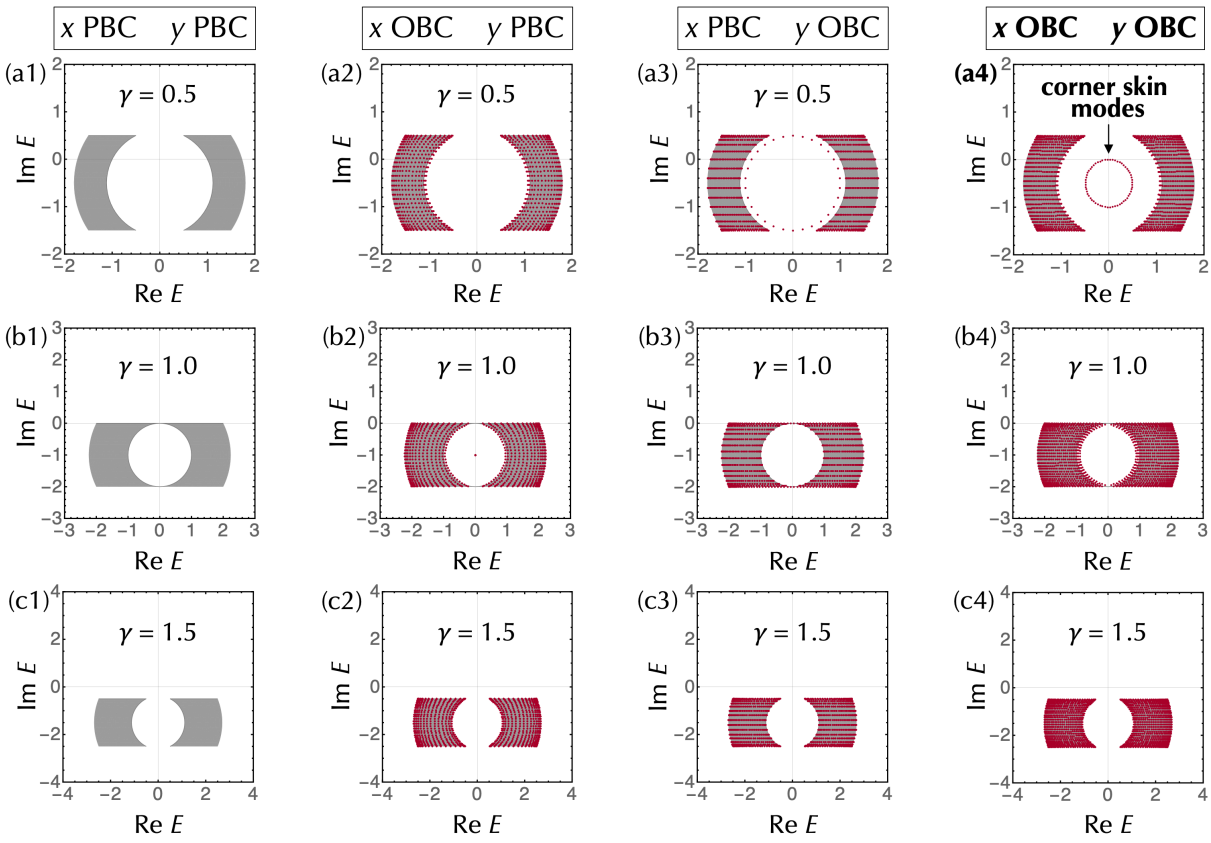

Figure 4.5: Second-order non-Hermitian skin effect. The complex spectra of the non-Hermitian model in two dimensions [Eq. (4.66)] are shown for 30×30 sites. The parameters are given as $\lambda = 1.0$, as well as (a1, a2, a3, a4) $\gamma = 0.5$, (b1, b2, b3, b4) $\gamma = 1.0$, or (c1, c2, c3, c4) $\gamma = 1.5$. The open boundary conditions are imposed along none of the directions for (a1, b1, c1), only along the x direction for (a2, b2, c2), only along the y direction for (a3, b3, c3), and both of the directions for (a4, b4, c4). The spectra for the periodic boundary conditions are shown as the grey regions, while the spectra for the open boundary conditions are shown as the red dots. For $|\gamma/\lambda| < 1$, the corner skin modes appear under the open boundary conditions along all the directions, as shown in (a4). The spectrum of these corner skin modes is given as $E = -\mathrm{i}\gamma\left(1 + e^{\mathrm{i}\theta}\right)$ with $\theta \in [0, 2\pi]$. Reproduced from Fig. 2 of Ref. [KSS20]. Copyright 2020 by the American Physical Society.

4.4.2 Corner skin effect

We numerically obtain the complex spectrum of the non-Hermitian model under various boundary conditions, as shown in Fig. 4.5. Under the periodic boundary conditions, eigenstates are delocalized through the bulk and form two bands [Fig. 4.5 (a1, b1, c1)]; the bulk spectrum is given as

$$E\left(\boldsymbol{k}\right) = \pm\sqrt{\lambda^2 \sin^2 k_x + \left(\gamma + \lambda\cos k_y\right)^2 + \lambda^2 \sin^2 k_y} - \mathrm{i}\left(\gamma + \lambda\cos k_x\right). \tag{4.81}$$

The complex-energy gap between the two bands is closed at $|\gamma| = |\lambda|$. Similarly, under the open boundary conditions solely along the x direction [Fig. 4.5 (a2, b2, c2)] or solely along the y direction [Fig. 4.5 (a3, b3, c3)], no skin effect occurs, in general. This corresponds to the absence of zero modes in $\tilde{H}_{\mathrm{BBH}}$ under these boundary conditions.

Under the open boundary conditions in both directions, by contrast, skin modes appear for $|\gamma| < |\lambda|$ [Fig. 4.5 (a4)]. These skin modes are not included in the bulk spectrum and localized

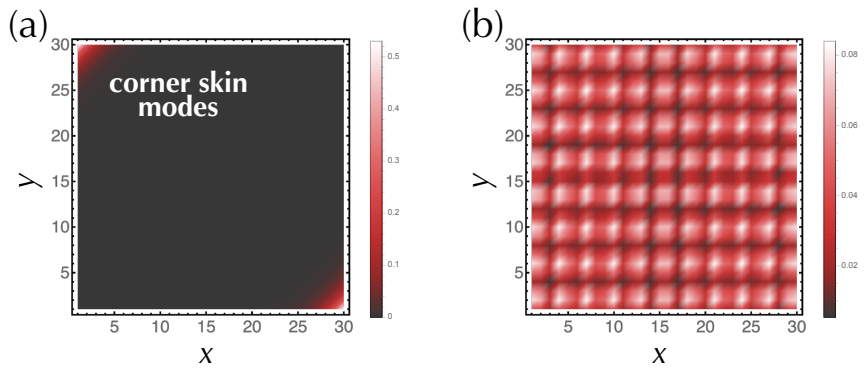

Figure 4.6: Wave functions for the second-order non-Hermitian skin effect. Under the open boundary conditions along both x and y directions, eigenstates of the non-Hermitian model in two dimensions [Eq. (4.66)] are shown for $L = 30$, $\gamma = 0.5$, and $\lambda = 1.0$. (a) Corner skin modes ($E = -0.027 - 0.0008\mathrm{i}$). (b) Delocalized bulk modes ($E = -1.64 - 0.94\mathrm{i}$). Reproduced from Fig. 3 of Ref. [KSS20]. Copyright 2020 by the American Physical Society.

at boundaries. In particular, the skin modes are localized at the corners, while the other bulk modes are delocalized (Fig. 4.6). For all the $2L^2$ eigenstates, the number of the corner skin modes is $2L$, while the number of the delocalized bulk modes is $2L\,(L-1)$. Notably, the skin spectrum forms a loop in the complex-energy plane even under the open boundary conditions, which is forbidden for the conventional skin effect [ZYF20, OKSS20].

This model can be solved also in an analytical manner (see Appendix C.1 for details). In particular, for sufficiently large L, the spectrum of the corner skin modes is given as

$$E = -\mathrm{i}\gamma\left(1 + e^{\mathrm{i}\theta}\right), \quad \theta \in [0, 2\pi], \tag{4.82}$$

and their localization lengths ξ_x and ξ_y along the x and y directions are given as

$$\xi_x = \xi_y = \left(\log\left|\frac{\lambda}{\gamma}\right|\right)^{-1}. \tag{4.83}$$

These analytical results are consistent with the numerical results.

The corner skin modes are a new type of boundary modes unique to non-Hermitian systems in higher dimensions. They are distinct from both $\mathcal{O}(L^2)$ skin modes for the conventional skin effect and $\mathcal{O}(1)$ corner modes in Hermitian second-order topological insulators. We call this new type of the skin effect the second-order skin effect. It originates from second-order non-Hermitian topology protected by spatial symmetry, as shown in Sec. 4.4.3.

Notably, Ref. [LLG19] provided another non-Hermitian model in two dimensions that exhibits corner skin modes. Similarly to our model, the $\mathcal{O}(L)$ skin modes are localized at the corners, while the other $\mathcal{O}(L^2)$ modes are delocalized through the bulk. However, this model is characterized by the bulk Chern number, and under the open boundary conditions, there appear chiral edge modes closing the line gap. Non-Hermiticity further pushes these chiral edge modes to the corners, resulting in the corner skin modes. Thus, the corner skin modes in Ref. [LLG19] arise from the combination of Hermitian topology (i.e., Chern number) and non-Hermiticity. On the other hand, the Chern number vanishes for our model in Eq. (4.66). Instead, the corner skin modes in our model are characterized solely by intrinsic non-Hermitian topology in terms of a point gap, as discussed in Sec. 4.4.3.

We also note in passing that different types of boundary modes appear for other boundary conditions. Even under the periodic boundary conditions along the x direction, there appear

$\mathcal{O}(L)$ modes away from the bulk bands as long as the open boundary conditions are imposed along the y direction, as shown in Fig. 4.5 (a3). These modes are localized at both edges with the localization length ξ_y in Eq. (4.83) (see Appendix C.2.1 for details), and their spectrum is given as

$$E = -\mathrm{i}\gamma - \mathrm{i}\lambda e^{-\mathrm{i}k_x}. \tag{4.84}$$

These edge modes do not touch the bulk bands, which contrasts with the chiral edge states in Chern insulators. On the other hand, even if the open boundary conditions are imposed along the x direction, no edge modes generally appear under the periodic boundary conditions along the y direction. Even under these boundary conditions, boundary modes appear for $|\gamma/\lambda| = 1$ [Fig. 4.5 (b2)]. Anomalously, they belong to the same wave number $k_y = \pi$ and the same eigenenergy $E = -\mathrm{i}\gamma$, and form exceptional points; $2L$ eigenstates coalesce into only 2 eigenstates, one of which is localized at the left edge and the other of which is localized at the right edge (see Appendix C.2.2 for details). The relationship between these boundary modes and the corner skin modes may merit further investigation.

4.4.3 Wess-Zumino term

The second-order non-Hermitian skin effect originates from the $\mathbb{Z}_2$-quantized Wess-Zumino (WZ) term introduced in the following. In two dimensions, we can define the one-dimensional winding numbers

$$W_i \coloneqq -\oint_0^{2\pi} \frac{dk_i}{2\pi\mathrm{i}} \frac{\partial}{\partial k_i} \log\det\left[H\left(k_x, k_y\right)\right] \quad (i = x, y), \tag{4.85}$$

along the x and y directions, respectively. As shown below, given a non-Hermitian Hamiltonian $H(k_x, k_y)$ which is invertible and has no one-dimensional winding numbers $W_x = W_y = 0$, we can define a geometric quantity $\mathrm{WZ}[H]$ called the WZ term which takes a value in the circle $[0, 1]$. The absence of the one-dimensional winding numbers ensures the existence of a smooth path of invertible Hamiltonians $H(k_x, k_y, t)$ from the original one

$$H\left(k_x, k_y, t = 0\right) \coloneqq H\left(k_x, k_y\right) \tag{4.86}$$

to another constant one

$$H\left(k_x, k_y, t = 1\right) \coloneqq H_{\mathrm{const}} \tag{4.87}$$

at the end. The WZ term is defined by [WZ71]

$$\mathrm{WZ}[H] \coloneqq \frac{1}{24\pi^2} \oint_{[0,2\pi]^2\times[0,1]} \mathrm{tr}\left[H^{-1}dH\right]^3. \tag{4.88}$$

While the WZ term is a real number, it is not quantized in the absence of symmetry.

Although the extension $H(k_x, k_y) \to H(k_x, k_y, t)$ is not unique, the difference $\mathrm{WZ}[H] - \mathrm{WZ}[H']$ between the two extensions $H(k_x, k_y, t)$ and $H'(k_x, k_y, t)$ is the integer-valued three-dimensional winding number of the third homotopy class

$$\pi_3\left(\mathrm{GL}_N(\mathbb{C})\right) = \mathbb{Z}, \tag{4.89}$$

where $N \geq 2$ is the dimension of the matrix $H(k_x, k_y)$. Thus, the WZ term in Eq. (4.88) does not depend on extensions of $H(k_x, k_y)$ as a quantity in the circle $[0, 1]$. It is a two-dimensional analog of the Berry-phase formula of the electric polarization [Van18].

Spatial symmetry can quantize the WZ term, similarly to the quantization of the electric polarization due to spatial-inversion symmetry. Here, we focus on the following four-fold-rotation-type symmetry:

$$UH^{\dagger}\left(k_x, k_y\right) V^{-1} = H\left(-k_y, k_x\right), \quad (UV)^2 = 1, \tag{4.90}$$

where U and V are unitary matrices that are, in general, independent of each other. The two-dimensional model in Eq. (4.66) respects this symmetry with [i.e., Eq. (4.80)]

$$U = -\mathrm{i}e^{\mathrm{i}\pi/4}\sigma_y, \quad V = e^{\mathrm{i}\pi/4}. \tag{4.91}$$

We show that this rotation-type symmetry indeed quantizes the WZ term to the $\mathbb{Z}_2$ values

$$\mathrm{WZ}\left[H\right] \in \{0, 1/2\}. \tag{4.92}$$

For an extension $H\left(k_x, k_y\right) \to H\left(k_x, k_y, t\right)$ for $t \in [0, 1]$, we introduce a different extension by

$$H'\left(k_x, k_y, t\right) \coloneqq UH^{\dagger}\left(k_y, -k_x, t\right) V^{-1} \quad (t \in [0, 1]). \tag{4.93}$$

Because of rotation-type symmetry in Eq. (4.90), $H'\left(k_x, k_y, t\right)$ at $t = 0$ coincides with the original Hamiltonian:

$$H'\left(k_x, k_y, t = 0\right) = H\left(k_x, k_y\right). \tag{4.94}$$

In a straightforward manner, we can also show

$$\mathrm{WZ}\left[H'\right] = -\mathrm{WZ}\left[H\right], \tag{4.95}$$

and

$$2\mathrm{WZ}\left[H\right] = \mathrm{WZ}\left[H\right] - \mathrm{WZ}\left[H'\right]. \tag{4.96}$$

The right-hand side of this equation gives the integer-valued three-dimensional winding number, which proves that the WZ term $\mathrm{WZ}\left[H\right]$ is quantized to the $\mathbb{Z}_2$ value. For our model in Eq. (4.66), the WZ term takes the nontrivial value

$$\mathrm{WZ}\left[H\right] = 1/2 \quad \text{for} \quad |\gamma/\lambda| < 1. \tag{4.97}$$

Thus, the $\mathbb{Z}_2$-quantized WZ term is a meaningful topological invariant of two-dimensional non-Hermitian systems, as long as four-fold-rotation-type symmetry in Eq. (4.90) is respected.

In general, the WZ term is quantized to the $\mathbb{Z}_2$ value when either rotation-type symmetry

$$UH^{\dagger}\left(\boldsymbol{k}\right) V^{-1} = H\left(c_n\boldsymbol{k}\right) \tag{4.98}$$

or reflection symmetry

$$UH\left(\boldsymbol{k}\right) V^{-1} = H\left(m\boldsymbol{k}\right) \tag{4.99}$$

is respected, where $\boldsymbol{k} \mapsto c_n\boldsymbol{k}$ is an n-fold rotation and $\boldsymbol{k} \mapsto m\boldsymbol{k}$ is a reflection on an axis. It can be proven in the same way as four-fold-rotation-type symmetry in Eq. (4.90).

It should also be noted that four-fold-rotation-type symmetry in Eq. (4.90) vanishes the one-dimensional winding numbers in Eq. (4.85). In fact, we have

$$W_x = -\oint_0^{2\pi} \frac{dk_x}{2\pi\mathrm{i}} \frac{\partial}{\partial k_x} \log\det\left[H^{\dagger}\left(-k_y, k_x\right)\right] = -W_y, \tag{4.100}$$

and on the other hand, we have

$$W_y = -\oint_0^{2\pi} \frac{dk_y}{2\pi \mathrm{i}} \frac{\partial}{\partial k_y} \log \det \left[H^\dagger \left(-k_y, k_x \right) \right] = W_x. \tag{4.101}$$

These equations result in

$$W_x = W_y = 0. \tag{4.102}$$

The quantization of the WZ term is closely related to the corner skin effect. This can be understood in view of the topological invariant in momentum space and the adiabatic parameter by Teo and Kane [TK10]. Let us consider a point defect and a circle S^1 that encloses this point defect. We consider a non-Hermitian Hamiltonian $H\left(k_x, k_y, s\right)$ and the corresponding extended Hermitian Hamiltonian $\tilde{H}\left(k_x, k_y, s\right)$ defined with the adiabatic parameter $s \in S^1$ that characterizes the spatial modulation of the Hamiltonians far from the point defect. The zero modes of $\tilde{H}\left(k_x, k_y, s\right)$ at the point defect are detected by the three-dimensional winding number W_3, which is in turn given as the winding of the WZ term

$$W_3 = \oint_0^1 ds \frac{d}{ds} \mathrm{WZ}\left[H\left(s\right) \right]. \tag{4.103}$$

In $\tilde{H}\left(k_x, k_y, s\right)$, there appear W_3 zero modes localized at the point defect. In a similar manner to the Hatano-Nelson model, these zero modes accompany the skin modes at the same defect in the original non-Hermitian Hamiltonian $H\left(k_x, k_y, s\right)$.

In the following, we show that the nonzero WZ term $\mathrm{WZ}\left[H\right]$ leads to the presence of the corner zero modes in the extended Hermitian Hamiltonian, and consequently, the presence of the corner skin modes in the original non-Hermitian Hamiltonian. Let us impose the open boundary conditions along both x and y directions. Near the edges, no zero modes appear because of the vanishing one-dimensional winding numbers in Eq. (4.102), allowing us to consider the adiabatic changes of the microscopic Hamiltonian near the edges into a slowly varying Hamiltonian while keeping the topological phase. In doing so, we can define a family of Hamiltonians $\tilde{H}\left(k_x, k_y, s\right)$ for each edge such that $\tilde{H}\left(k_x, k_y, s = 0\right)$ is the Hamiltonian deep inside the bulk and that $\tilde{H}\left(k_x, k_y, s = 1\right)$ is outside the finite system. For example, $\tilde{H}\left(k_x, k_y, s = 1\right)$ can be chosen as the vacuum Hamiltonian $\tilde{H}_{\mathrm{vac}}$. Let the families of the edge Hamiltonians be $\tilde{H}_{\mathrm{l}}\left(k_x, k_y, s\right)$, $\tilde{H}_{\mathrm{r}}\left(k_x, k_y, s\right)$, $\tilde{H}_{\mathrm{u}}\left(k_x, k_y, s\right)$, and $\tilde{H}_{\mathrm{d}}\left(k_x, k_y, s\right)$ for the left, right, up, and down edges, respectively. We assume that the edge Hamiltonians, as well as the bulk Hamiltonian, enjoy four-fold-rotation-type symmetry, meaning that they are related in a four-fold-symmetric way. For example, the up-edge Hamiltonian is related to the right-edge one by

$$H_{\mathrm{u}}\left(k_x, k_y, s\right) = U H_{\mathrm{r}}^\dagger \left(k_x, k_y, s\right) V^{-1} \tag{4.104}$$

for the off-diagonal parts.

Then, the changes in the WZ terms

$$\Delta \mathrm{WZ}_\nu \coloneqq \oint_0^1 ds \frac{d}{ds} \mathrm{WZ}\left[H_\nu \left(s\right) \right] \quad \left(\nu \in \{\mathrm{l}, \mathrm{r}, \mathrm{u}, \mathrm{d}\}\right), \tag{4.105}$$

from the bulk to the vacuum for the four edges satisfy

$$\Delta \mathrm{WZ}_{\mathrm{l}} = -\Delta \mathrm{WZ}_{\mathrm{u}} = \Delta \mathrm{WZ}_{\mathrm{r}} = -\Delta \mathrm{WZ}_{\mathrm{d}}. \tag{4.106}$$

Here, the vacuum Hamiltonian $\tilde{H}_{\mathrm{vac}}$ is assumed to be in common for all the edges. This structure gives a constraint on the three-dimensional winding numbers in Eq. (4.103) of the four corners: W_3 of the upper-right corner is given as

$$W_3 = \Delta \mathrm{WZ}_{\mathrm{r}} - \Delta \mathrm{WZ}_{\mathrm{u}} = 2 \Delta \mathrm{WZ}_{\mathrm{r}} \equiv -2 \mathrm{WZ}\left[H\right] \tag{4.107}$$

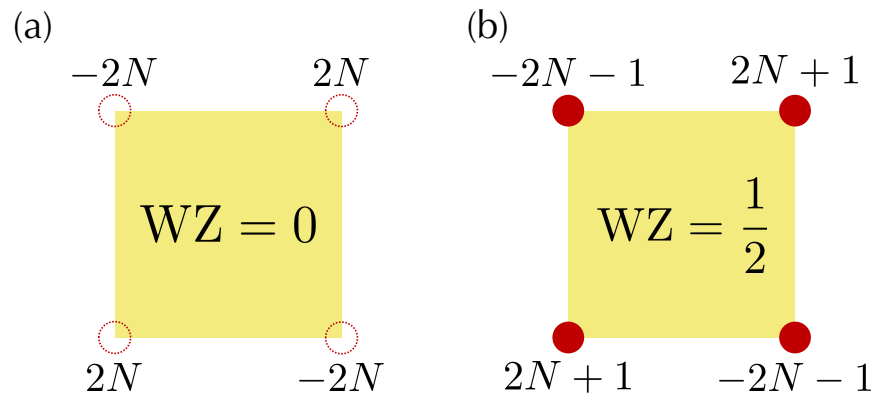

Figure 4.7: Wess-Zumino (WZ) term and corner zero modes. The numbers of the zero modes in the extended Hermitian Hamiltonian $\tilde{H}(k_x, k_y)$ with four-fold-rotation symmetry are shown as the even and odd integers at each corner. (a) and (b) correspond to the trivial (WZ = 0) and nontrivial (WZ = 1/2) WZ terms, respectively. Reproduced from Fig. 4 of Ref. [KSS20]. Copyright 2020 by the American Physical Society.

modulo 2. This implies that if the quantized WZ term of the bulk is nontrivial (i.e., $\mathrm{WZ}[H] = 1/2$), the three-dimensional winding number W_3 of the four corners should be odd, especially nonzero, and hence the extended Hermitian Hamiltonian should have zero modes localized at the corners. Figure 4.7 shows possible quartets of the numbers of the corner zero modes accompanied by the trivial and nontrivial bulk WZ terms. Since the presence of the zero modes in the extended Hermitian Hamiltonian leads to the skin effect in the non-Hermitian Hamiltonian [OKSS20], the bulk WZ term leads to the corner skin effect. Similar $\mathbb{Z}_2$ quantization for corner zero modes was recently discussed for Hermitian second-order topological superconductors [TJWar].

It should be noted that the nontrivial WZ term does not always imply the corner skin effect. Suppose that a real line gap is open and that the Chern number Ch is well defined for each band. Then, under rotation-type symmetry in Eq. (4.90), or more generally Eq. (4.98), with a common unitary matrix $U = V$, we have the equality

$$2\mathrm{WZ} \equiv \mathrm{Ch} \tag{4.108}$$

modulo 2. This is because the inverse of the Green's function $G(\boldsymbol{k}, \omega) \coloneqq [\mathrm{i}\omega - H(\boldsymbol{k})]^{-1}$ plays the role of the Hamiltonian $H(\boldsymbol{k}, s)$ introduced before, and the Chern number is given as the three-dimensional winding number

$$\mathrm{Ch} = \frac{1}{24\pi^2} \oint_{[0,2\pi]^2 \times [-\infty,\infty]} \mathrm{tr}\left[G dG^{-1}\right]^3 \tag{4.109}$$

of $G^{-1}(\boldsymbol{k}, \omega)$. The condition $U = V$ is crucial in Eq. (4.108); for $U \neq V$, the gluing condition $U[G^{-1}(\boldsymbol{k}, \omega = 0)]^{\dagger} V^{-1} = G^{-1}(\boldsymbol{k}, \omega = 0)$ at $\omega = 0$ does not hold. As a corollary, Hermitian Hamiltonians always satisfy Eq. (4.108) since Hermiticity is equivalent to the trivial rotation (i.e., $c_1 \boldsymbol{k} = \boldsymbol{k}$) with $U = V = 1$. Thus, Chern insulators can also have the nontrivial WZ term regardless of the presence or absence of the corner skin modes.

On the other hand, even though the non-Hermitian model in Eq. (4.66) takes the nontrivial WZ term $\mathrm{WZ} = 1/2$ for $|\gamma| < |\lambda|$, it has a nonzero real line gap except for $|\gamma| = |\lambda|$, and the Chern number vanishes. While this difference between the WZ term and the Chern number

may seem like a contradiction, we do not actually have any contradictions. First, Eq. (4.108) is not always true for generic unitary matrices U and V. In fact, the non-Hermitian model in Eq. (4.66), for which we have $U \neq V$ [see Eq. (4.80)], does not satisfy Eq. (4.108). Moreover, we inevitably have an obstacle to having a continuous path from the non-Hermitian model in Eq. (4.66) to a Hermitian Hamiltonian while keeping the real line gap and rotation-type symmetry in Eq. (4.80): if a Hermitian Hamiltonian $H(\boldsymbol{k}) = H^{\dagger}(\boldsymbol{k})$ respects Eq. (4.80), it is subject to the constraint $-\mathrm{i}\sigma_y H(\boldsymbol{k}_*) = H(\boldsymbol{k}_*)$ and hence vanishes [i.e., $H(\boldsymbol{k}_*) = 0$] at the symmetric points $\boldsymbol{k}_* = (0,0), (\pi,\pi)$, meaning closing of both point and line gaps. This fact implies intrinsic non-Hermitian topology of the model in Eq. (4.66).

4.4.4 Non-Bloch band theory in higher dimensions

While symmetry can protect skin effects, it can also vanish skin effects. Prime examples include orthogonal reciprocity, as discussed in Sec. 4.2.1. Other prime examples are spatial-inversion (parity) symmetry

$$\mathcal{P} H(\boldsymbol{k}) \mathcal{P}^{-1} = H(-\boldsymbol{k}) \tag{4.110}$$

with a unitary matrix $\mathcal{P}$ respecting $\mathcal{P}^2 = 1$, and transposition-associated mirror symmetry

$$\mathcal{M}_i H^T(\boldsymbol{k}) \mathcal{M}_i^{-1} = H(m_i \boldsymbol{k}) \tag{4.111}$$

with a unitary matrix $\mathcal{M}_i$ respecting $\mathcal{M}_i^2 = 1$. Here, m_i denotes a reflection that changes k_i into $-k_i$; in two dimensions, for example, we have $m_x(k_x, k_y) = (-k_x, k_y)$ and $m_y(k_x, k_y) = (k_x, -k_y)$. Our model with the corner skin modes indeed respects these symmetry with $\mathcal{P} = \sigma_y$ [i.e., Eq. (4.69)], $\mathcal{M}_x = \sigma_x$ [i.e., Eq. (4.76)], and $\mathcal{M}_y = \sigma_z$ [i.e., Eq. (4.77)]. In one dimension, no skin effect occurs in the presence of these symmetry [KSUS19]. This is compatible with the vanishing winding number in the presence of these symmetry. Even in higher dimensions, mirror-type symmetry in Eq. (4.111) vanishes the winding number and the consequent skin effect along the i direction.

The absence of the skin effect in one dimension can be shown on the basis of

$$|\beta_M| = |\beta_{M+1}|, \tag{4.112}$$

which is the salient result of the non-Bloch band theory (see Sec. 3.2 for details) [YW18, YM19]. We begin with the characteristic equation

$$\det[H(\beta) - E] = 0. \tag{4.113}$$

In terms of $H(\beta)$, spatial-inversion symmetry in Eq. (4.110) imposes

$$\mathcal{P} H(\beta) \mathcal{P}^{-1} = H(\beta^{-1}), \tag{4.114}$$

and hence leads to

$$\det\left[H(\beta^{-1}) - E\right] = 0. \tag{4.115}$$

This equation implies that β^{-1} is another solution to the characteristic equation (4.113) if β is a solution. Because of the assumption $|\beta_1| \leq |\beta_2| \leq \cdots |\beta_{2M}|$, we then have

$$\beta_{2M-i+1} = \beta_i^{-1} \quad (i = 1, 2, \cdots, M). \tag{4.116}$$

Now, using Eq. (4.112), we finally have

$$|\beta_M| = |\beta_{M+1}| = 1, \tag{4.117}$$

showing that continuum bands are formed by delocalized eigenstates. Similarly, transposition-associated symmetry in Eq. (4.111) also leads to the absence of the skin effect in one dimension.

Importantly, the above discussion is not directly applicable in higher dimensions. This is because the non-Bloch band theory in Refs. [YW18, YM19], especially Eq. (4.112), is inapplicable under the open boundary conditions along more than one direction. Remarkably, the higher-order skin effect requires a modification of the non-Bloch band theory in higher dimensions. In fact, if Eq. (4.112) were valid even in higher dimensions, transposition-associated mirror symmetry in Eq. (4.111) leads to the absence of the skin effect along the i direction. However, this would contradict the emergence of the corner skin effect in our two-dimensional model with Eq. (4.111) for both x and y directions. Hence, the non-Bloch band theory is indeed modified in higher dimensions.

Nevertheless, it is naturally expected that Eq. (4.112) is valid for an extensive number of eigenstates even in higher dimensions. This is consistent with delocalization of the $\mathcal{O}(L^2)$ bulk modes in our model. On the other hand, the $\mathcal{O}(L)$ corner skin modes cannot be described by the current non-Bloch band theory. It is thus important to develop a non-Bloch band theory in higher dimensions in a general manner, which we leave for future work.

4.5 Third-order skin effect

The non-Hermitian skin effect can even have the third-order nature in three dimensions. For the third-order non-Hermitian skin effect, $\mathcal{O}(L)$ corner skin modes emerge from all the $\mathcal{O}(L^3)$ modes. We provide a model that exhibits the third-order skin effect. The Bloch Hamiltonian reads

$$\begin{aligned} H(\boldsymbol{k}) = {} & \mathrm{i}\lambda(\sin k_y)\sigma_x + \mathrm{i}(\gamma + \lambda\cos k_y)\sigma_y + \mathrm{i}\lambda(\sin k_x)\sigma_z \\ & + (\gamma + \lambda\cos k_x)\tau_z + \lambda(\sin k_z)\tau_y + (\gamma + \lambda\cos k_z)\tau_x, \end{aligned} \tag{4.118}$$

where γ and λ are real parameters, and σ_i's and τ_i's ($i = x, y, z$) are Pauli matrices. The extended Hermitian Hamiltonian reads

$$\begin{aligned} \tilde{H}_{\mathrm{BBH}}(\boldsymbol{k}) = {} & \begin{pmatrix} 0 & H(\boldsymbol{k}) \\ H^\dagger(\boldsymbol{k}) & 0 \end{pmatrix} \\ = {} & -\lambda(\sin k_y)\rho_y\sigma_x - (\gamma + \lambda\cos k_y)\rho_y\sigma_y - \lambda(\sin k_x)\rho_y\sigma_z \\ & + (\gamma + \lambda\cos k_x)\rho_x\tau_z + \lambda(\sin k_z)\rho_x\tau_y + (\gamma + \lambda\cos k_z)\rho_x\tau_x, \end{aligned} \tag{4.119}$$

where ρ_i's ($i = x, y, z$) are Pauli matrices that account for the additional degrees of freedom. Similarly to the second-order topological insulator, $\tilde{H}_{\mathrm{BBH}}(\boldsymbol{k})$ is a prototypical example of a third-order topological insulator that was first proposed by Benalcazar, Bernevig, and Hughes [BBH17a, BBH17b]. It can exhibit zero-energy modes localized at the corners under the open boundary conditions along all the three directions, although no boundary modes appear under other boundary conditions.

The Hermitian model $\tilde{H}_{\mathrm{BBH}}(\boldsymbol{k})$ respects spatial-inversion symmetry:

$$(\rho_y\sigma_y\tau_y)\,\tilde{H}_{\mathrm{BBH}}(\boldsymbol{k})\,(\rho_y\sigma_y\tau_y)^{-1} = \tilde{H}_{\mathrm{BBH}}(-\boldsymbol{k}). \tag{4.120}$$

Correspondingly, $H(\boldsymbol{k})$ respects

$$(\sigma_y\tau_y)\,H^\dagger(\boldsymbol{k})\,(\sigma_y\tau_y)^{-1} = -H(-\boldsymbol{k}). \tag{4.121}$$

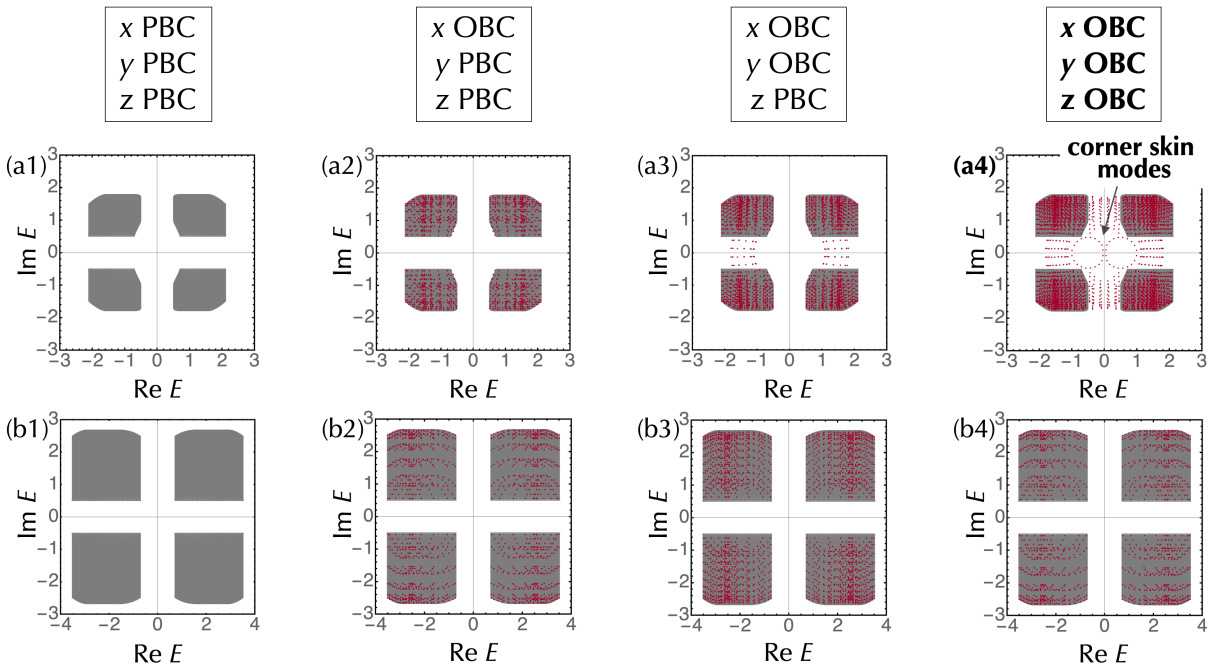

Figure 4.8: Third-order non-Hermitian skin effect. The complex spectra of the non-Hermitian model in three dimensions [Eq. (4.118)] are shown for $10 \times 10 \times 10$ sites. The parameters are given as $\lambda = 1.0$, as well as (a1, a2, a3, a4) $\gamma = 0.5$ or (b1, b2, b3, b4) $\gamma = 1.5$. The open boundary conditions are imposed along none of the directions for (a1, b1), only along the x direction for (a2, b2), only along the x and y directions for (a3, b3), and along all the directions for (a4, b4). The spectra for the periodic boundary conditions are shown as the grey regions, while the spectra for the open boundary conditions are shown as the red dots. The corner skin modes appear under the open boundary conditions along all the directions, as shown in (a4). Reproduced from Fig. 5 of Ref. [KSS20]. Copyright 2020 by the American Physical Society.

Moreover, $\tilde{H}_{\mathrm{BBH}}(\boldsymbol{k})$ respects mirror symmetry:

$$(\rho_x\sigma_z)\,\tilde{H}_{\mathrm{BBH}}(k_x,k_y,k_z)\,(\rho_x\sigma_z)^{-1} = \tilde{H}_{\mathrm{BBH}}(-k_x,k_y,k_z)\,, \tag{4.122}$$

$$(\rho_x\sigma_x)\,\tilde{H}_{\mathrm{BBH}}(k_x,k_y,k_z)\,(\rho_x\sigma_x)^{-1} = \tilde{H}_{\mathrm{BBH}}(k_x,-k_y,k_z)\,, \tag{4.123}$$

$$(\rho_y\tau_y)\,\tilde{H}_{\mathrm{BBH}}(k_x,k_y,k_z)\,(\rho_y\tau_y)^{-1} = \tilde{H}_{\mathrm{BBH}}(k_x,k_y,-k_z)\,. \tag{4.124}$$

Correspondingly, $H(\boldsymbol{k})$ respects

$$\sigma_z H^\dagger(k_x,k_y,k_z)\,\sigma_z^{-1} = H(-k_x,k_y,k_z)\,, \tag{4.125}$$

$$\sigma_x H^\dagger(k_x,k_y,k_z)\,\sigma_x^{-1} = H(k_x,-k_y,k_z)\,, \tag{4.126}$$

$$\tau_y H^\dagger(k_x,k_y,k_z)\,\tau_y^{-1} = -H(k_x,k_y,-k_z)\,. \tag{4.127}$$

Such spatial symmetry plays a crucial role in the third-order skin effect.

The third-order topological insulator $\tilde{H}_{\mathrm{BBH}}(\boldsymbol{k})$ with $|\gamma/\lambda| < 1$ exhibits zero-energy corner modes. Correspondingly, corner skin modes appear in the non-Hermitian model $H(\boldsymbol{k})$ with open boundaries along all the directions. In Fig. 4.8, we show the numerically obtained spectra for various boundary conditions. Under the periodic boundary conditions, no skin effect occurs, and all the eigenstates are delocalized through the bulk. The bulk forms four bands and their

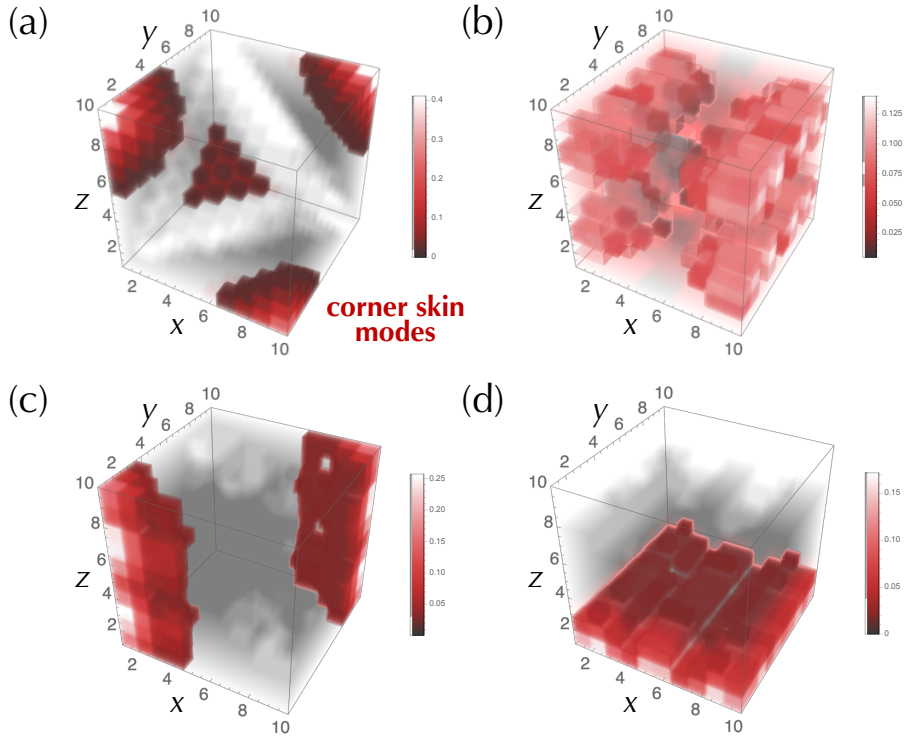

Figure 4.9: Wave functions for the third-order non-Hermitian skin effect. Under the open boundary conditions along all the directions, eigenstates of the non-Hermitian model in three dimensions [Eq. (4.118)] are shown for $L = 10$, $\gamma = 0.5$, and $\lambda = 1.0$. (a) Corner skin modes ($E = -0.050 - 0.086\mathrm{i}$). (b) Delocalized bulk modes ($E = -1.49 - 1.34\mathrm{i}$). (c) Edge modes ($E = -1.15 - 0.36\mathrm{i}$). (d) Surface modes ($E = -0.13 - 1.20\mathrm{i}$). Reproduced from Fig. 6 of Ref. [KSS20]. Copyright 2020 by the American Physical Society.

spectrum is given as

$$E(\boldsymbol{k}) = \pm\sqrt{(\gamma + \lambda\cos k_x)^2 + (\gamma + \lambda\cos k_z)^2 + \lambda^2 \sin^2 k_z} \\ \pm \mathrm{i}\sqrt{\lambda^2 \sin^2 k_x + (\gamma + \lambda\cos k_y)^2 + \lambda^2 \sin^2 k_y}. \tag{4.128}$$

Under the open boundary conditions along all the directions, an extensive number of eigenstates remain delocalized and form the bulk bands [Fig. 4.9 (b)]. However, some of the eigenstates exhibit the skin effect and are localized at the four corners [Figs. 4.8 (a4) and 4.9 (a)]. For the conventional skin effect, there appear $\mathcal{O}(L^3)$ skin modes in a three-dimensional system with the system size $L \times L \times L$; for the third-order skin effect, by contrast, only $\mathcal{O}(L)$ skin modes appear at the corners. This also contrasts with zero-energy corner modes in Hermitian third-order topological insulators, the number of which is $\mathcal{O}(1)$. Thus, the third-order non-Hermitian skin effect gives rise to a new type of boundary physics in three dimensions.

Finally, it is notable that the three-dimensional model in Eq. (4.118) exhibits different types of boundary modes in addition to the corner skin modes. As shown in Fig. 4.8 (a3), gapless modes appear as long as the open boundary conditions are imposed for both x and y directions. These gapless modes appear even though the periodic boundary conditions are imposed along the z direction. Their spectrum crosses $\mathrm{Im}\, E = 0$, i.e., the imaginary line gap is closed. Consistently, they are localized at the corners on the xy plane, but delocalized along the z direction [Fig. 4.9 (c)]. Moreover, other gapless modes appear as long as the open boundary

conditions are imposed in the z direction [Fig. 4.8 (a4)]. Their spectrum crosses $\mathrm{Re}\, E = 0$, i.e., the real line gap is closed. These gapless modes are localized on the surface perpendicular to the z axis [Fig. 4.9 (d)].

Chapter 5

Topological field theory of non-Hermitian systems

Topology plays a key role in modern physics. Topological phases of matter have been arguably one of the most actively studied condensed-matter systems in recent years [HK10, QZ11, CTSR16]. A universal understanding of topological phases is obtained by topological field theory in spacetime. For example, the Chern-Simon theory describes the quantum Hall effect [Red84, NS83, ZHK89, FK91, LF91, WZ92a], and the axion electrodynamics describes the magnetoelectric effect [QHZ08, EMV09]. One of the consequences of the topological field theory description is the bulk-boundary correspondence: in the presence of a boundary, a topological field theory is gauge dependent at the boundary, and this gauge noninvariance must be compensated by an anomaly at the boundary [CH85].

While topological phases were mainly investigated for Hermitian systems at equilibrium, topological phases of non-Hermitian systems have attracted growing interest [BBK21]. However, topological field theories have yet to be established for non-Hermitian systems. Field-theoretical characterization of intrinsic non-Hermitian topology has remained elusive, although it is crucial for understanding and exploring non-Hermitian topological phenomena including the skin effect.

Here, we develop a field-theoretical description of the intrinsic non-Hermitian topological phases. Because of the dissipative and nonequilibrium nature of non-Hermiticity, our theory is formulated solely in terms of spatial degrees of freedom, which contrasts with the conventional theory defined in spacetime. It provides a universal understanding about non-Hermitian topological phenomena, such as the unidirectional transport in one dimension and the chiral magnetic skin effect in three dimensions. Furthermore, it systematically predicts new physics; we illustrate this by revealing transport phenomena and skin effects in two dimensions induced by a perpendicular spatial texture. From the field-theoretical perspective, the non-Hermitian skin effect, which is anomalous localization due to non-Hermiticity, is shown to be a signature of an anomaly. As a virtue of the field-theoretical description, our theory is relevant not only to noninteracting systems but also to disordered and interacting systems, as well as open quantum systems described by master equations.

This chapter is based on Refs. [KSR21].

5.1 Topological field theory

As discussed in the preceding chapters, non-Hermitian systems give rise to unique topological phases that have no counterparts in Hermitian systems. For convenience, we first summarize

such intrinsic non-Hermitian topology in band theory, for which we develop a field-theoretical description. Suppose that a non-Hermitian Bloch Hamiltonian $H(k)$ has a point gap, i.e., it is invertible in terms of reference energy $E \in \mathbb{C}$ [GAK+18, KSUS19]:

$$\forall\, k \quad \det\left(H(k) - E\right) \neq 0. \tag{5.1}$$

Then, the following winding number $W_1(E) \in \mathbb{Z}$ is well defined:

$$W_1(E) := -\oint_{\mathrm{BZ}} \frac{dk}{2\pi \mathrm{i}} \left(\frac{d}{dk} \log \det\left(H(k) - E\right) \right). \tag{5.2}$$

A prototypical lattice model with nontrivial W_1 is the Hatano-Nelson model [HN96, HN97], described by the Hamiltonian

$$\hat{H} = -\frac{1}{2} \sum_n \left[(1+\gamma)\, \hat{c}_{n+1}^\dagger \hat{c}_n + (1-\gamma)\, \hat{c}_n^\dagger \hat{c}_{n+1} \right], \tag{5.3}$$

where $\hat{c}_n$ ($\hat{c}_n^\dagger$) annihilates (creates) a particle on site n, and $\gamma \in \mathbb{R}$ denotes the asymmetry of the hopping amplitudes and describes the degree of non-Hermiticity. The corresponding Bloch Hamiltonian reads

$$H(k) = -\cos k + \mathrm{i}\gamma \sin k \tag{5.4}$$

and winds around the origin in the complex energy plane. Consequently, we have

$$W_1(E) = \mathrm{sgn}\,(\gamma) \tag{5.5}$$

as long as the reference energy E is inside the region surrounded by the loop of $H(k)$. Despite the presence of a point gap, an energy gap for the real part of the spectrum closes at $k = \pm\pi/2$, i.e., $\mathrm{Re}\, H\,(k = \pm\pi/2) = 0$; this type of energy gap is called a line gap [SZF18, KSUS19]. To understand a universal feature of non-Hermitian topology, let us consider the continuum Dirac Hamiltonian around the line-gap-closing points:

$$H(k) = k + \mathrm{i}\gamma. \tag{5.6}$$

This non-Hermitian Dirac Hamiltonian, similarly to its lattice counterpart, is characterized by the nonzero winding number

$$W_1(E) = \frac{1}{2}\, \mathrm{sgn}\,(\gamma - \mathrm{Im}\, E)\,. \tag{5.7}$$

An important consequence of nontrivial W_1 is the non-Hermitian skin effect [ZYF20, OKSS20]. In the presence of a boundary, there appear $|W_1(E)|$ eigenstates with the eigenenergy E at the boundary. Notably, $W_1(E)$ can be nontrivial for many choices of the reference energy E, and consequently, an extensive number of eigenstates are localized at the boundary. In the lattice model in Eq. (5.3), all the eigenstates are localized at the right (left) edge for $\gamma > 0$ ($\gamma < 0$). Such anomalous localization is impossible in Hermitian systems and hence presents a unique non-Hermitian topological phenomenon.

5.1.1 Spacetime field theory for Hermitian systems

Before developing effective field theories for intrinsic non-Hermitian topology, let us briefly recall the Hermitian case. The effective field theories for Hermitian systems are obtained by introducing a gauge potential $(\boldsymbol{A}, \phi)$ to a microscopic Hamiltonian and integrating out matter

degrees of freedom. The quantum partition function of a Hamiltonian $H(\boldsymbol{k})$ is given by the path integral as

$$Z[\boldsymbol{A},\phi] = \int \mathcal{D}\bar{\psi}\mathcal{D}\psi\, e^{\mathrm{i}\mathcal{S}} \tag{5.8}$$

with the (real-time) action

$$\mathcal{S} = \int \bar{\psi}\left[\mathrm{i}\partial_t + \phi - H(-\mathrm{i}\partial_{\boldsymbol{x}} - \boldsymbol{A})\right]\psi\, d^d x dt. \tag{5.9}$$

Here, ψ and $\bar{\psi}$ describe matter degrees of freedom, and ϕ and $\boldsymbol{A}$ are scalar and vector potentials, respectively. Integrating over the matter field, we obtain the effective action $S[\boldsymbol{A},\phi]$ for the external field,

$$e^{\mathrm{i}S[\boldsymbol{A},\phi]} := \frac{Z[\boldsymbol{A},\phi]}{Z[0]}, \tag{5.10}$$

with

$$Z[\boldsymbol{A},\phi] = \det\left(\mathrm{i}\omega + \phi - H(\boldsymbol{k} - \boldsymbol{A})\right). \tag{5.11}$$

In the presence of an energy gap, the effective action is given by a local functional of $(\boldsymbol{A},\phi)$. The response of the system to the external field can be read off from the current density

$$\boldsymbol{j} := \frac{\delta S}{\delta \boldsymbol{A}}. \tag{5.12}$$

In this formulation, the topological invariant that appears in the topological term of the effective action is given by the Green's function [IM87, Vol03, QHZ08]

$$G_0(\boldsymbol{k},\omega) := \left(\mathrm{i}\omega - H(\boldsymbol{k})\right)^{-1}, \tag{5.13}$$

which is a non-Hermitian matrix. For example, if we consider the two-dimensional Dirac Hamiltonian

$$H(\boldsymbol{k}) = k_x\sigma_x + k_y\sigma_y + m\sigma_z, \tag{5.14}$$

we obtain the $(2+1)$-dimensional Chern-Simons theory

$$S[\boldsymbol{A},\phi] = \frac{C_1}{4\pi}\sum_{\mu\nu\tau\in\{x,y,t\}}\int \varepsilon_{\mu\nu\tau}A_\mu(\boldsymbol{x},t)\partial_\nu A_\tau(\boldsymbol{x},t)d^2x dt \quad (A_t := -\phi), \tag{5.15}$$

where C_1 is the Chern number defined by the Green's function in Eq. (5.13):

$$C_1 := -\sum_{\mu\nu\tau}\oint \frac{d^2k d\omega}{24\pi^2}\,\varepsilon_{\mu\nu\tau}\,\mathrm{tr}\left[\left(G_0\frac{\partial G_0^{-1}}{\partial k_\mu}\right)\left(G_0\frac{\partial G_0^{-1}}{\partial k_\nu}\right)\left(G_0\frac{\partial G_0^{-1}}{\partial k_\tau}\right)\right] \quad (k_t := \omega). \tag{5.16}$$

The current corresponding to this topological action reads

$$j_i = \frac{C_1}{2\pi}\sum_{j=x,y}\varepsilon_{ij}E_j \quad (i = x, y), \tag{5.17}$$

which is the quantum Hall effect.

The above path integral, in its Euclidean version, assumes the Gibbs state as an equilibrium density matrix. On the other hand, for the non-Hermitian case, the thermal equilibrium is no longer achieved, and it is generally unclear what kind of path integral one should set up. This constitutes a fundamental difficulty for developing effective field theories. This may be tackled,

for example, by the Schwinger-Keldysh approach [Kam11, SBD16]. Nevertheless, as long as an energy gap for the real part of the spectrum (i.e., line gap) stays open, the above procedure gives rise to topological field theories even for non-Hermitian systems. In this case, non-Hermitian topological phases are continuously deformable to their Hermitian counterparts [KSUS19], and share the same topological field theory. For example, for non-Hermitian Chern insulators, the above procedure delivers the $(2+1)$-dimensional Chern-Simons theory in Eq. (5.15) [HPG19]. However, this is not the case for intrinsic non-Hermitian topology. For the non-Hermitian Dirac Hamiltonian in Eq. (5.6), the line gap vanishes, and the matter degrees of freedom cannot be integrated out safely; if we calculate $S[\boldsymbol{A}, \phi]$ from Eq. (5.11), it is ill defined. We also note that the quantization of $W_1(E)$ in Eq. (5.2) is guaranteed by the point gap $E(k) \neq E$ instead of the line gap $\mathrm{Re}\, E(k) \neq E$, which is a unique gap structure due to the complex-valued nature of the spectrum [GAK+18, KSUS19, KBS19].

5.1.2 Space field theory for non-Hermitian systems

We thus seek a different formulation of field theory for intrinsic non-Hermitian topological phases. Since these phases arise out of equilibrium, the temporal degree of freedom should play a special role. Then, let us Fourier transform the field operator in time by

$$\psi(\boldsymbol{x}, t) = \int \psi_E(\boldsymbol{x}) e^{-\mathrm{i}Et} dE \tag{5.18}$$

and focus on fixed energy E. We also switch off the scalar potential ϕ and focus on a time-independent vector potential $\boldsymbol{A}(\boldsymbol{x})$. The action in Eq. (5.9) in spacetime reduces to

$$\mathcal{S}_E = \int \bar{\psi}_E \left[H(-\mathrm{i}\partial_{\boldsymbol{x}} - \boldsymbol{A}) - E \right] \psi_E \, d^d x. \tag{5.19}$$

In contrast to Eq. (5.9), this action is written solely in terms of the spatial degrees of freedom. The functional integral

$$Z_E[\boldsymbol{A}] = \int \mathcal{D}\bar{\psi}_E \mathcal{D}\psi_E \, e^{\mathrm{i}\mathcal{S}_E} = \det \left(H(\boldsymbol{k} - \boldsymbol{A}) - E \right) \tag{5.20}$$

serves as a generating functional of the single-particle Green's function $(E - H(\boldsymbol{k}))^{-1}$ with reference energy E. It is therefore expected to capture all physical information—including the topological one such as the non-Hermitian skin effect. From this generating functional $Z_E[\boldsymbol{A}]$, we define the effective action $S_E[\boldsymbol{A}]$ by

$$e^{\mathrm{i}S_E[\boldsymbol{A}]} := \frac{Z_E[\boldsymbol{A}]}{Z_E[0]}. \tag{5.21}$$

This type of spatial field theory is commonly used for Anderson localization [Efe97a, AS06] and also for Hermitian topological systems in odd dimensions [SRFL08]. It is discussed also for Floquet systems and their boundary unitary operators [GGR21, LSGR21].

To further emphasize the special role played by the temporal direction, we note that one of the wave numbers, such as k in Eq. (5.6), plays a role similar to frequency ω for Hermitian systems; the inverse of the Green's function $G_0(\boldsymbol{k}, \omega)$ in Eq. (5.13) for a Hermitian Hamiltonian is identified with a non-Hermitian Hamiltonian $H(\boldsymbol{k})$ in Eq. (5.20) by replacing ω with k. Thus, the effective action of a non-Hermitian system in $d+0$ dimensions is mathematically equivalent to that of a Hermitian system in $(d-1)+1$ dimensions. Consistently, d-dimensional

non-Hermitian systems are topologically classified in the same manner as $(d-1)$-dimensional Hermitian systems in the same symmetry class. In fact, non-Hermitian Bloch Hamiltonians $H(\boldsymbol{k})$ in d dimensions with Altland-Zirnbauer symmetry have the same topological classification as Hermitian Bloch Hamiltonians in $d-1$ dimensions with the same symmetry class [KSUS19]. The difference of one dimension corresponds to time. The degree of a point gap, such as γ in Eq. (5.6), gives a relevant energy scale and ensures the local expansion of the effective action by the gauge potential.

Reference [XZGC21] argues that topological classification of non-Hermitian systems in one dimension is the same as the Hermitian case from the field-theoretical perspective. At the face value, this result may contradict the intrinsic non-Hermitian topological phases in one dimension [GAK+18, KSUS19]. However, since Ref. [XZGC21] assumes a line gap and a spacetime formulation, it is not incompatible with our space formulation for a point gap.

5.2 One dimension

5.2.1 $(1+0)$-dimensional Chern-Simons theory

Below, we explicitly provide field theories of intrinsic non-Hermitian topology and discuss unique phenomena including the skin effect. For the non-Hermitian Dirac Hamiltonian in Eq. (5.6), the effective action is

$$S_E[A] \simeq \mathrm{i}\,\mathrm{tr}\left[(H(-\mathrm{i}\partial_x) - E)^{-1} A(x)\right], \tag{5.22}$$

where the vector potential A is assumed to be sufficiently small. After taking the sum explicitly, this reduces to

$$S_E[A] = W_1(E) \int A(x)dx, \tag{5.23}$$

where the winding number $W_1(E)$ is defined for reference energy E as Eq. (5.2). This is the $(1+0)$-dimensional Chern-Simons theory. As discussed above, replacing x with t, we have the $(0+1)$-dimensional Chern-Simons theory, which describes Hermitian systems in zero dimension.

5.2.2 Unidirectional transport

From this effective action, the current is obtained as

$$j(x, E) \coloneqq \frac{\delta S_E[A]}{\delta A(x)} = W_1(E). \tag{5.24}$$

Thus, particles unidirectionally flow from the left to the right (from the right to the left) for $W_1 > 0$ ($W_1 < 0$). Consistently, in the lattice model in Eq. (5.3), the hopping amplitude from the left to the right is greater (smaller) than that from the right to the left for $W_1 > 0$ ($W_1 < 0$). This type of directional amplification ubiquitously appears, for example, in open photonic systems [LGV15, GAK+18, WBN20, XLH+21], parametrically driven bosonic systems [MPBC18], and active matter [YHU+ar]. The topological field theory in Eq. (5.23) underlies such unidirectional transport induced by asymmetric hopping.

The unidirectional dynamics in one dimension is confirmed also for non-Hermitian lattice models. Figure 5.1 shows the single-particle dynamics of the Hatano-Nelson model in Eq. (5.3).

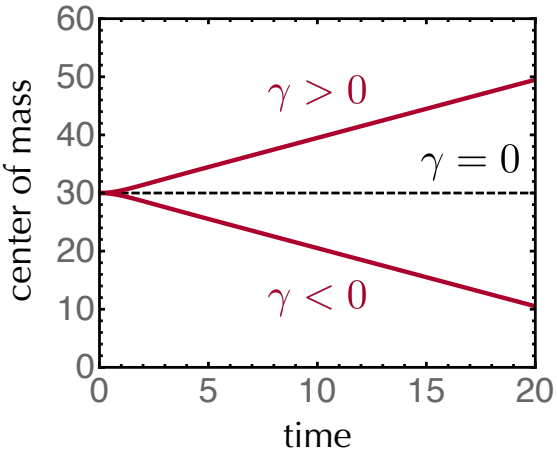

Figure 5.1: Unidirectional transport in the Hatano-Nelson model. The time evolution of the center of mass of a wave packet is shown for the Hermitian case ($\gamma = 0$, black dashed line) and the non-Hermitian case ($\gamma = \pm 0.5$, red solid lines). The periodic boundary conditions are imposed with $L = 60$. The initial state is chosen as the single-site excitation $|\psi(0)\rangle = |x_0\rangle$ with $x_0 = L/2 = 30$. While the wave packet does not move in the Hermitian case, it moves unidirectionally in the non-Hermitian case. The direction of the unidirectional transport depends on the sign of the non-Hermiticity γ. Reproduced from Fig. S1 of Supplemental Material of Ref. [KSR21]. Copyright 2021 by the American Physical Society.

While the wave packet does not move in the Hermitian case, it moves unidirectionally in the non-Hermitian case. The velocity of the wave packet coincides with the group velocity

$$\frac{\partial}{\partial k}\mathrm{Re}E(k) = \sin k \quad \text{for} \quad k = \mathrm{sgn}(\gamma)\,(\pi/2), \tag{5.25}$$

where the direction of the wave packet depends on the sign of the non-Hermiticity γ. These results are consistent with the topological field theory, which describes the unidirectional particle flow in Eq. (5.24).

It should be noted that the topological invariant W_1 may not necessarily lead to a quantized observable despite the quantization of W_1. This is partly due to the difference between right and left eigenstates of non-Hermitian Hamiltonians [Bro14], similarly to the nonquantization of the Hall conductance in a non-Hermitian Chern insulator [HPG19]. Nevertheless, the qualitative behavior of non-Hermitian systems is correctly described by the topological field theory.

5.2.3 Anomaly inflow and skin effect

In the presence of a boundary, the topological action is no longer gauge invariant. Suppose that the system described by Eq. (5.23) is confined to the region $x_\mathrm{L} \le x \le x_\mathrm{R}$, outside of which is the vacuum. Then, under the gauge transformation

$$A \quad \mapsto \quad A + \frac{df}{dx} \tag{5.26}$$

with an arbitrary function f, the effective action S_E changes by

$$S_E \quad \mapsto \quad S_E + W_1(E)\,[f(x_\mathrm{R}) - f(x_\mathrm{L})] \tag{5.27}$$

and explicitly depends on the choice of the gauge f. To retain gauge invariance, an additional degree of freedom is required at the boundaries $x = x_{\mathrm{L}}, x_{\mathrm{R}}$. This boundary system reads

$$S_E^{\mathrm{boundary}} = -W_1(E)\left[\varphi(x_{\mathrm{R}}) - \varphi(x_{\mathrm{L}})\right], \tag{5.28}$$

where $\varphi(x)$ denotes the phase of the wavefunction at x. Since φ changes to $\varphi + f$ through the gauge transformation, S_E^{boundary} changes by

$$S_E^{\mathrm{boundary}} \quad \mapsto \quad S_E^{\mathrm{boundary}} - W_1(E)\left[f(x_{\mathrm{R}}) - f(x_{\mathrm{L}})\right]. \tag{5.29}$$

Thus, while S_E and S_E^{boundary} are individually gauge dependent, their combination $S_E + S_E^{\mathrm{boundary}}$ is indeed gauge invariant.

The boundary action in Eq. (5.28) describes a pair of the charges $W_1(E)$ and $-W_1(E)$ at $x = x_{\mathrm{R}}$ and $x = x_{\mathrm{L}}$, respectively. These charges correspond to skin modes. Importantly, the reference energy E can be chosen arbitrarily as long as $W_1(E)$ is nontrivial. An extensive number of the charges appear at the boundary, which correspond to an extensive number of skin modes. Thus, the skin effect originates from a non-Hermitian anomaly. This contrasts with Hermitian systems in one dimension, in which an anomaly results in only a finite number of symmetry-protected zero-energy modes at the boundary.

It is also notable that the boundary charges create a potential gradient in the opposite direction from the current in Eq. (5.24). This is in balance with the current-driving internal field. Consequently, the system reaches a nonequilibrium steady state in contrast to the thermal equilibrium state realized in Hermitian systems. We note that the anomaly discussed here is distinct from a dynamical anomaly in Refs. [LAZV19, TK20, BS21, OS21].

5.3 Three dimensions: chiral magnetic skin effect

5.3.1 $(3+0)$-dimensional Chern-Simons theory

Topological field theories are formulated also in higher dimensions. In general, non-Hermitian systems in d dimensions are described by the $(d+0)$-dimensional Chern-Simons theory for odd d. This contrasts with Hermitian systems, which are described by the $(d+1)$-dimensional Chern-Simons theory for even d. Using topological field theories, we understand non-Hermitian topological phenomena in a universal manner.

In three dimensions, the non-Hermitian Dirac Hamiltonian

$$H(\boldsymbol{k}) = k_x\sigma_x + k_y\sigma_y + k_z\sigma_z + \mathrm{i}\gamma \tag{5.30}$$

results in the $(3+0)$-dimensional Chern-Simons theory:

$$S_E[\boldsymbol{A}] = \frac{W_3(E)}{4\pi}\sum_{ijk}\int \varepsilon_{ijk}A_i(\boldsymbol{x})\partial_j A_k(\boldsymbol{x})d^3x. \tag{5.31}$$

Here, W_3 is the three-dimensional winding number [KSUS19]

$$W_3 := -\sum_{ijk}\oint_{\mathrm{BZ}}\frac{d^3k}{24\pi^2}\varepsilon_{ijk}\,\mathrm{tr}\left[\left(H^{-1}(\boldsymbol{k})\frac{\partial H(\boldsymbol{k})}{\partial k_i}\right)\left(H^{-1}(\boldsymbol{k})\frac{\partial H(\boldsymbol{k})}{\partial k_j}\right)\left(H^{-1}(\boldsymbol{k})\frac{\partial H(\boldsymbol{k})}{\partial k_k}\right)\right], \tag{5.32}$$

where reference energy is assumed to be zero for simplicity. The current density of this theory is

$$\boldsymbol{j}(\boldsymbol{x}, E) \coloneqq \frac{\delta S_E[\boldsymbol{A}]}{\delta \boldsymbol{A}(\boldsymbol{x})} = \frac{W_3(E)}{2\pi}\boldsymbol{B}(\boldsymbol{x}), \tag{5.33}$$

where $\boldsymbol{B} \coloneqq \nabla \times \boldsymbol{A}$ is a magnetic field. Thus, particles flow along the direction of the magnetic field $\boldsymbol{B}$. This is the chiral magnetic effect [FKW08] in which non-Hermiticity induces chirality imbalance in a manner similar to an electric field. This further implies that the direction of amplification can be controlled by a magnetic field, which is a unique property of three-dimensional systems. It is also remarkable that Ref. [BS21] recently constructed a lattice model that exhibits the non-Hermitian chiral magnetic effect. Our discussions give a field-theoretical understanding about it.

Under the open boundary conditions, S_E is gauge dependent. For the quantum Hall effect, which is described by the $(2+1)$-dimensional Chern-Simons theory in Eq. (5.15), the gauge noninvariance is balanced with an anomaly of chiral fermions at the boundary [CH85]. In the non-Hermitian case, the boundary degrees of freedom are described by a Hamiltonian with a single exceptional point,

$$H(\boldsymbol{k}) = \pm k_x - \mathrm{i}k_y, \tag{5.34}$$

for $|W_3(E)| = 1$ [DSS+21]. In general, the number of exceptional points at the boundary is $|W_3(E)|$. This boundary Hamiltonian reduces to the inverse of the Green's function of the conventional chiral fermions by replacing k_y with frequency ω. In $1+1$ dimensions, a chiral anomaly is described by

$$\partial_x j_x^A + \partial_t j_t^A = \frac{E}{\pi} \tag{5.35}$$

with an axial current $\left(j_x^A, j_t^A\right)$ and an electric field $E \coloneqq \partial_x A_t - \partial_t A_x$ [Adl69, BJ69, PS95]. Replacing time with another spatial component y, we have the following non-Hermitian analog of the anomaly equation:

$$\nabla \cdot \boldsymbol{j}^A(\boldsymbol{x}, E) = \frac{W_3(E)B(\boldsymbol{x})}{\pi}, \tag{5.36}$$

where $B \coloneqq \partial_x A_y - \partial_y A_x$ is a magnetic field perpendicular to the surface. In terms of the global quantities such as the charge N_R (N_L) of the right-moving (left-moving) particle $H(\boldsymbol{k}) = k_x - \mathrm{i}k_y$ [$H(\boldsymbol{k}) = -k_x - \mathrm{i}k_y$], as well as the magnetic flux $\Phi \coloneqq \int B(\boldsymbol{x})d^2x$, this anomaly equation reduces to

$$N_\mathrm{R}(E) - N_L(E) = \frac{W_3(E)\Phi}{\pi}. \tag{5.37}$$

Combining it with the global conservation law $N_\mathrm{R} + N_\mathrm{L} = 0$ due to U(1) symmetry, we have

$$N_\mathrm{R}(E) = \frac{W_3(E)\Phi}{2\pi}, \quad N_\mathrm{L}(E) = -\frac{W_3(E)\Phi}{2\pi}. \tag{5.38}$$

Here, $\Phi/2\pi$ is the number of the fluxes since 2π denotes the flux quantum in the natural units (i.e., $e = \hbar = 1$). Thus, a signature of the topological action in three dimensions appears as the skin effect induced by a magnetic field. The number of the skin modes is given by the topological invariant W_3 and the number of fluxes. While Ref. [BS21] predicted this three-dimensional version of the skin effect—chiral magnetic skin effect—on the basis of the bulk topological invariant, we here derive it from a chiral anomaly at boundaries.

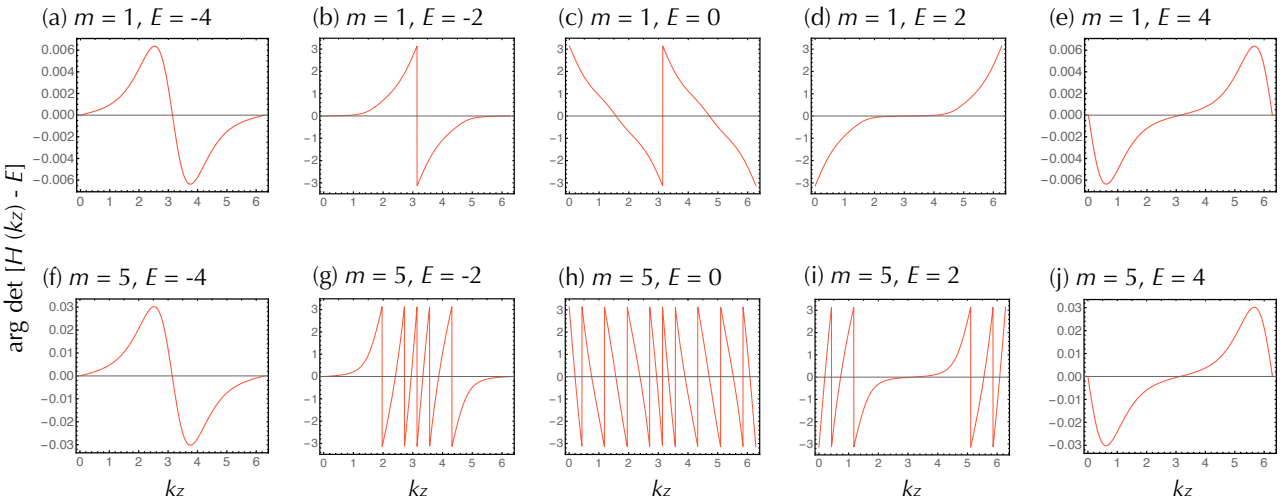

Figure 5.2: Winding number $W_1(E)$ in the presence of magnetic fluxes. For the non-Hermitian Hamiltonian in Eq. (5.39) with the vector potential in Eq. (5.40), the argument of $\det\left[H\left(k_z\right)-E\right]$ is shown as a function of the wavenumber k_z. The parameters are chosen as $\gamma = 0.5$ and $L_x = L_y = 10$. The periodic boundary conditions are imposed along all the directions. The number of the magnetic fluxes is $m = 1$ for (a-e) and $m = 5$ for (f-j). The reference energy is $E = -4$ for (a, f), $E = -2$ for (b, g), $E = 0$ for (c, h), $E = 2$ for (d, i), and $E = 4$ for (e, j). The winding numbers are given as $W_1(E) = 0$ for $E = \pm 4$ (a, e, f, j), $W_1(E) = -m$ for (b, d, g, i), and $W_1(E) = 2m$ for (c, h). Reproduced from Fig. S3 of Supplemental Material of Ref. [KSR21]. Copyright 2021 by the American Physical Society.

5.3.2 Chiral magnetic skin effect

As discussed above, a chiral anomaly of $(2+0)$-dimensional boundary states results in the chiral magnetic skin effect. This result can also be confirmed in a lattice model. Here, we investigate the following non-Hermitian system in three dimensions:

$$H\left(\boldsymbol{k}\right) = \cos k_x + \cos k_y + \cos k_z + \mathrm{i}\gamma\left(\sigma_x \sin k_x + \sigma_y \sin k_y + \sigma_z \sin k_z\right), \tag{5.39}$$

where $\gamma \in \mathbb{R}$ denotes the degree of non-Hermiticity. Let us impose a magnetic field along the z direction. In particular, we consider the vector potential

$$A_x = -\frac{2\pi m y}{L_x L_y}, \quad A_y = \begin{cases} 0 & (y = 1, \cdots, L-1), \\ \dfrac{2\pi m x}{L_x} & (y = L), \end{cases} \quad A_z = 0, \tag{5.40}$$

where m is an integer, and L_x and L_y denote the lengths of the system along the x and y directions, respectively. This vector potential gives

$$\int B_z dx dy = 2\pi m, \tag{5.41}$$

which means the presence of m magnetic fluxes (note that 2π is the flux quantum in the natural units).

In the presence of a magnetic field, the three-dimensional winding number of $H\left(\boldsymbol{k}\right)$ leads to the one-dimensional winding number along the direction parallel to the magnetic field. In

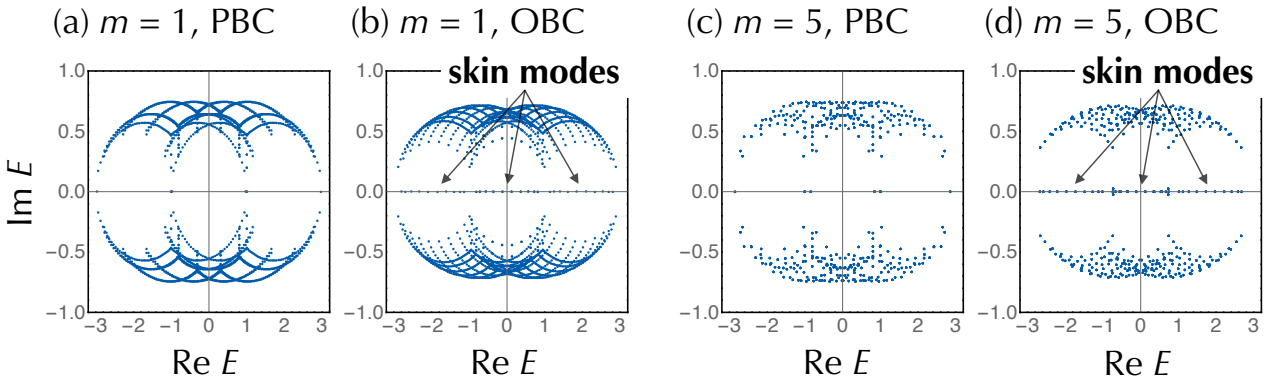

Figure 5.3: Chiral magnetic skin effect. Complex spectra of the non-Hermitian Hamiltonian in Eq. (5.39) with the vector potential in Eq. (5.40) are shown. The parameters are chosen as $\gamma = 0.5$ and $L_x = L_y = L_z = 10$. The number of magnetic fluxes is $m = 1$ for (a, b) and $m = 5$ for (c, d). The periodic boundary conditions are imposed along the x and y directions. Along the z direction, the periodic boundary conditions are imposed for (a, c), and the open boundary conditions are imposed for (b, d). Skin modes appear under the open boundary conditions (b, d). Reproduced from Fig. S4 of Supplemental Material of Ref. [KSR21]. Copyright 2021 by the American Physical Society.

particular, if a magnetic field is imposed along the z direction, the one-dimensional winding number

$$W_1(E) = -\oint_0^{2\pi} \frac{dk_z}{2\pi} \left(\frac{d}{dk_z} \arg \det \left(H\left(k_z\right) - E \right) \right) \tag{5.42}$$

can be nontrivial. Here, arg denotes the argument of a complex number. Figure 5.2 shows the winding numbers $W_1(E)$ for various choices of the reference energy E and the number m of magnetic flux. While $W_1(E)$ vanishes for E such that the three-dimensional winding number $W_3(E)$ vanishes, $W_1(E)$ is nonzero for E such that $W_3(E)$ is nonzero. Notably, $W_1(E)$ is proportional to m.

According to the field-theoretical discussions, skin modes generally appear at a boundary perpendicular to a magnetic field when the three-dimensional system supports the nontrivial winding number. Consistently, under the magnetic field along the z direction, skin modes appear under the open boundary conditions along the z direction (Fig. 5.3). This is also consistent with the nontrivial (one-dimensional) winding number shown in Fig. 5.2. A similar result has recently been reported in Ref. [NBS20].

We note that the number of skin modes is not necessarily proportional to the number of magnetic fluxes in finite systems. The field-theoretical discussions assume infinite degrees of freedom and do not strictly apply to finite systems. Nevertheless, they explain qualitative behavior of non-Hermitian topological phenomena even in finite systems, as shown here for the chiral magnetic skin effect. Similarly, in one dimension, the number of skin modes is not necessarily proportional to the winding number W_1 in finite systems, although we strictly have this proportional relationship in semi-infinite systems (see Chap. 3 for details) [OKSS20].

5.4 Two dimensions: spatial-texture-induced skin effect

5.4.1 Wess-Zumino term

Lower-dimensional topological field theories are derived from higher-dimensional ones. Topological field theories of Hermitian superconductors in $0+1$ and $1+1$ dimensions, and Hermitian insulators in $2+1$ and $3+1$ dimensions are derived from the Chern-Simons theories in $2+1$ and $4+1$ dimensions, respectively [QHZ08]. Topological field theories of non-Hermitian systems in even dimensions are also derived from higher-dimensional ones. Let us reduce the z direction of the $(3+0)$-dimensional theory in Eq. (5.31) by considering z to be a parameter and making the gauge potential $\boldsymbol{A}$ be independent of z. Then, the effective action in Eq. (5.31) reduces to

$$\begin{aligned} S_E[\boldsymbol{A}] &= \frac{1}{2\pi}\sum_{ij}\int \theta(\boldsymbol{x},E)\varepsilon_{ij}\partial_i A_j(\boldsymbol{x})d^2x \\ &= \frac{1}{2\pi}\int \theta(\boldsymbol{x},E)B(\boldsymbol{x})d^2x. \end{aligned} \tag{5.43}$$

This is the effective action of non-Hermitian systems in two dimensions. Here, θ is a non-Hermitian analog of the electric polarization in $(1+1)$-dimensional Hermitian systems [Van18]. It can be identified with the Wess-Zumino term [WZ71]:

$$\theta = -\frac{1}{24\pi^2}\oint_{\mathrm{BZ}\times[0,1]} \mathrm{tr}[H^{-1}dH]^3 \in \mathbb{R}/\mathbb{Z}, \tag{5.44}$$

where $\tilde{H}=\tilde{H}(\boldsymbol{k},s)$ is an extension of the two-dimensional Hamiltonian $H(\boldsymbol{k})$ that satisfies

$$\tilde{H}(\boldsymbol{k},s=0)=H(\boldsymbol{k}), \quad \tilde{H}(\boldsymbol{k},s=1)=H_0 \tag{5.45}$$

with a constant Hamiltonian H_0. In other words, θ gives the integral of the three-dimensional winding number density for an extension $\tilde{H}(k_x,k_y,s)$. Here, for simplicity, we set reference energy E to zero and assume the absence of the one-dimensional winding number.

While Eq. (5.43) generally describes non-Hermitian systems in two dimensions, certain symmetry is needed for the quantization of θ. For example, suppose that the system is invariant under reciprocity

$$\mathcal{T}H^T(\boldsymbol{k})\mathcal{T}^{-1}=H(\boldsymbol{k}), \quad \mathcal{T}\mathcal{T}^*=-1 \tag{5.46}$$

with a unitary matrix $\mathcal{T}$ (i.e., class AII† [KSUS19]). In terms of reciprocity, a magnetic field B is odd. Hence, θ should also be odd under reciprocity so that the action will be reciprocal. Since θ is well defined only modulo 1, it is quantized to be the $\mathbb{Z}_2$ values

$$\theta = 0, 1/2, \tag{5.47}$$

which gives the $\mathbb{Z}_2$ classification of the topological phase. Moreover, θ is quantized also in spinless superconductors that respect particle-hole symmetry (i.e., class D [KSUS19]). The $\mathbb{Z}_2$ quantization is reminiscent of the quantized polarization in particle-hole-symmetric topological insulators in $1+1$ dimensions and time-reversal-invariant topological insulators in $3+1$ dimensions [QHZ08].

5.4.2 Skin effect induced by a spatial texture

The action in Eq. (5.43) generally describes non-Hermitian topological phenomena in two dimensions. The current density is

$$j_i(\boldsymbol{x}, E) = \frac{1}{2\pi} \sum_j \varepsilon_{ij} \partial_j \theta(\boldsymbol{x}, E), \tag{5.48}$$

which shows a particle flow in the direction perpendicular to the gradient of θ. Now, suppose that θ is spatially modulated along the y direction. Naively, such a y-dependent texture leads to a flow along the y direction and is irrelevant to transport along the x direction. However, Eq. (5.48) describes a perpendicular flow along the x direction as a result of non-Hermitian topology.

To understand this non-Hermitian topological phenomenon, we here consider the two-dimensional non-Hermitian system $H = H_0 + V$ with

$$H_0(\boldsymbol{k}) = \sigma_x \sin k_x + \sigma_y \sin k_y + \mathrm{i}\gamma \left(\cos k_x + \cos k_y\right), \tag{5.49}$$

$$V(\boldsymbol{x}) = \sigma_z \sin \phi(\boldsymbol{x}) + \mathrm{i}\gamma \cos \phi(\boldsymbol{x}). \tag{5.50}$$

We assume that V is translationally invariant along the x direction and modulated only along the y direction. In particular, we consider

$$\phi(\boldsymbol{x}) = \frac{\pi}{2} - \frac{2\pi\Theta}{L_y} y, \tag{5.51}$$

where Θ describes the spatial gradient of the texture along the y direction. This spatial texture induces nontrivial θ, which in turn leads to the unidirectional transport and the skin effect along the x direction. For $\gamma = 0$, the spectrum is entirely real and no skin effect occurs even in the presence of the spatial texture [Fig. 5.4 (a, b)]. The transport phenomenon is understood by the wave packet dynamics in a manner similar to the one-dimensional case (see Sec. 5.2.2 for details). Consistently with the absence of the complex-spectral winding and the skin effect, the center of mass of a wave packet does not move under the time evolution [Fig. 5.4 (c)]. For $\gamma \neq 0$, the spectrum generally becomes complex, but neither skin effect nor unidirectional transport arises in the absence of the spatial texture [Fig. 5.4 (d, e, f)]. In the simultaneous presence of γ and the spatial texture, on the other hand, the system exhibits the non-Hermitian topological phenomenon due to the nontrivial Wess-Zumino term. Under the periodic boundary conditions, the spectrum is characterized by the nontrivial winding numbers in the complex energy plane [Fig. 5.4 (g)], which induce the skin effect under the open boundary conditions [Fig. 5.4 (h)]. Accordingly, the center of mass of a wave packet moves unidirectionally [Fig. 5.4 (i)]. Notably, this transport along the x direction arises from the spatial texture along the y direction, which is a unique feature of the two-dimensional case that is distinct from the one-dimensional case. The topological field theory in Eq. (5.43) correctly describes this non-Hermitian topological phenomenon.

Moreover, Fig. 5.5 shows the skin effect for various choices of the spatial gradient Θ. For sufficiently small Θ ($\lesssim 1/4$), no skin effect occurs [Fig. 5.5 (a)]. With increasing Θ, skin modes gradually appear [Fig. 5.5 (b)]. We count the skin modes as a function of Θ [Fig. 5.5 (c)]. Here, we investigate the inverse participation ratios $\sum_{x,y} |\psi(x,y)|^4 / \sum_{x,y} |\psi(x,y)|^2$ for all the eigenstates ψ. They decrease with $\propto 1/L_x L_y$ for delocalized eigenstates but remain to be approximately one for localized eigenstates, and hence measure the degree of localization. It is notable that the skin effect along the y direction or Anderson localization may arise since

the texture breaks translation invariance along the y direction. Still, as long as the periodic boundary conditions are imposed along the x direction, the inverse participation ratios are small for all the eigenstates even under the open boundary conditions along the y direction. Thus, no localization phenomena occur except for the skin effect along the x direction. The number of the skin modes is compatible with the change of the Wess-Zumino term. As demonstrated by these results, the spatial texture enables the control of the skin modes, which is also a unique feature of two-dimensional systems.

After the present work [KSR21], a recent work [SZH21] used our topological field theory descriptions and studied the geometric response of non-Hermitian systems in three dimensions. In particular, Ref. [SZH21] used the Euclidean version of the Wen-Zee action [WZ92b] and found a new type of non-Hermitian skin effects induced by disclination. Similarly, dislocation-induced skin effects were proposed [PMRar, SP21, BFvdBM21]. These results also show the universality and utility of our topological field theory descriptions.

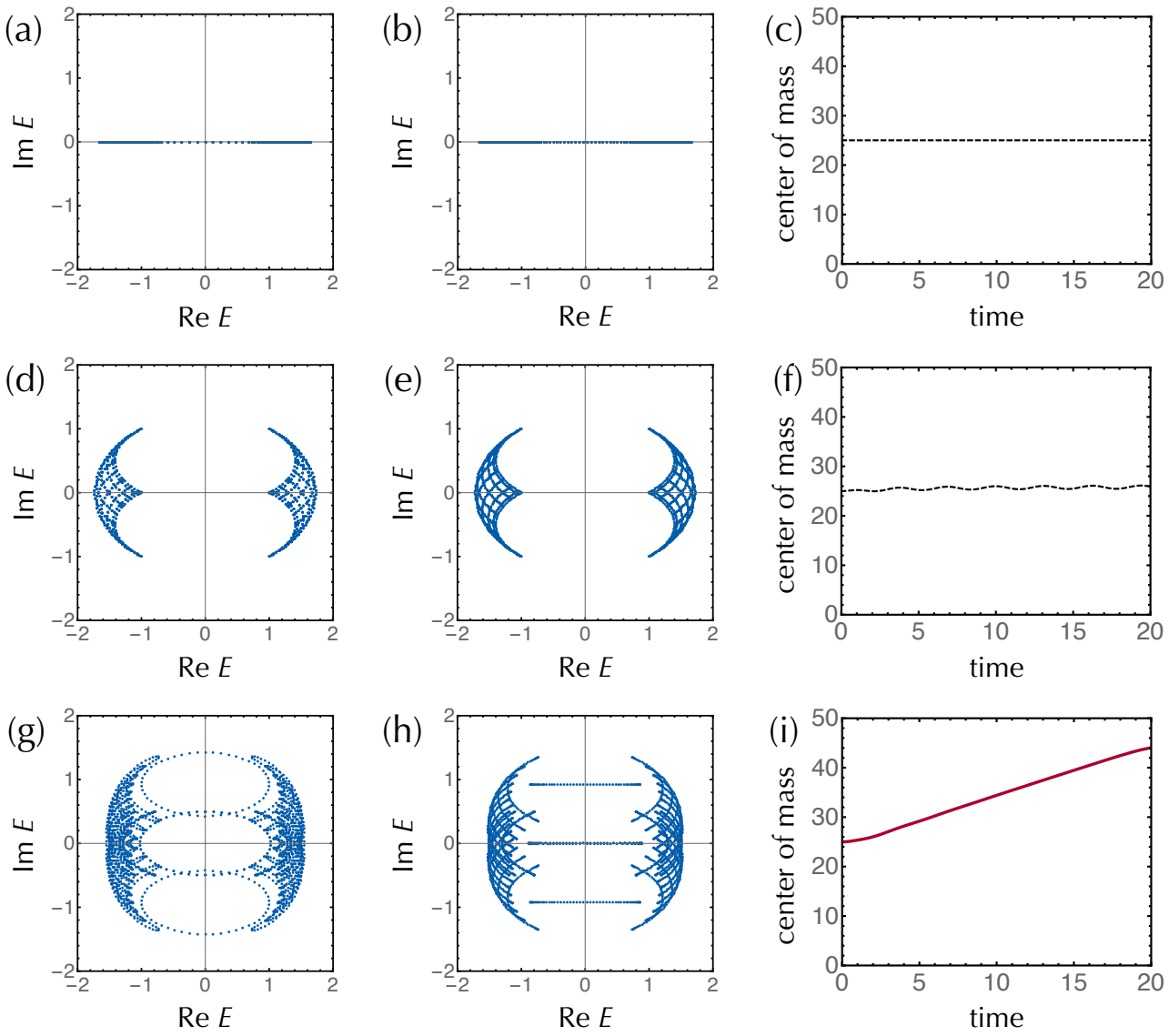

Figure 5.4: Non-Hermitian topological phenomena in two dimensions. Complex spectra of the non-Hermitian Hamiltonian in Eq. (5.50) with $L_x = 50$ and $L_y = 20$ are shown under the periodic boundary conditions for (a, d, g) and under the open boundary conditions along the x direction for (b, e, h). The corresponding time evolution of the center of mass of a wave packet along the x direction is shown for (c, f, i), where the periodic boundary conditions are imposed, and the initial state is prepared to be $|\psi(0)\rangle \propto \sum_y |x = L_x/2, y\rangle$. (a, b, c) Hermitian system with the spatial texture ($\gamma = 0$ and $\Theta = 1$). (d, e, f) Non-Hermitian system without the spatial texture ($\gamma = 0.5$ and $\Theta = 0$). (g, h, i) Non-Hermitian system with the spatial texture ($\gamma = 0.5$ and $\Theta = 1$). Under the periodic boundary conditions, the complex spectrum is characterized by nontrivial winding numbers, which lead to the skin effect under the open boundary conditions. Consistently, the center of mass of a wave packet moves unidirectionally. Reproduced from Fig. S5 of Supplemental Material of Ref. [KSR21]. Copyright 2021 by the American Physical Society.

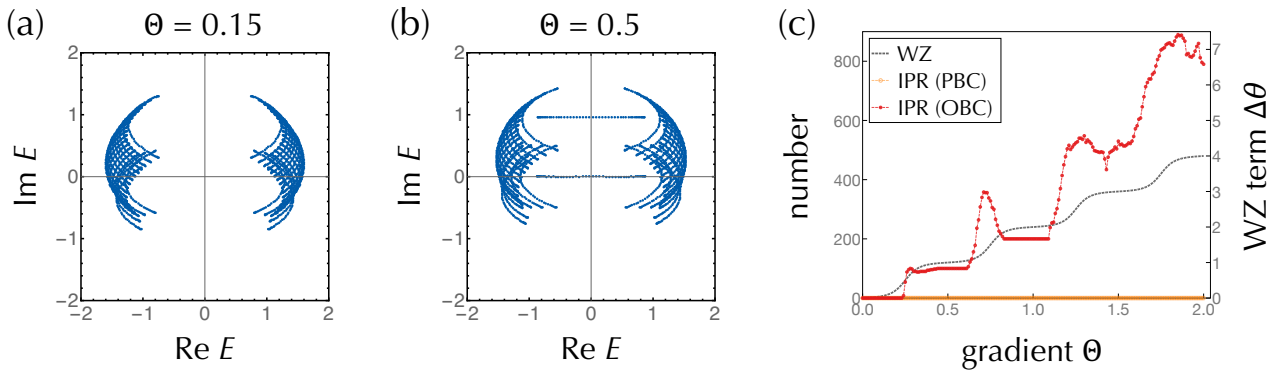

Figure 5.5: Non-Hermitian skin effect in two dimensions. Complex spectra and wavefunctions of the non-Hermitian Hamiltonian in Eq. (5.50) with $L_x = 50$, $L_y = 20$, and $\gamma = 0.5$ are investigated for various choices of the spatial gradient Θ. The open boundary conditions are imposed along both x and y directions. (a) Complex spectrum for $\Theta = 0.15$. (b) Complex spectrum for $\Theta = 0.5$. (c) Number of the skin modes. The localized eigenstates whose inverse participation ratios (IPRs) are less than 0.015 are counted as a function of Θ for the periodic (orange dots) and open (red dots) boundary conditions, which are compatible with the change of the Wess-Zumino (WZ) term along the y direction [$\Delta\theta := \theta\,(y = L_y) - \theta\,(y = 0)$; black curve]. The reference energy of the WZ term is chosen to be zero energy. Reproduced from Fig. S6 of Supplemental Material of Ref. [KSR21]. Copyright 2021 by the American Physical Society.

Chapter 6

Nonunitary scaling theory of non-Hermitian localization

Anderson localization [And58] is the disorder-induced localization of coherent waves and plays an important role in transport phenomena of condensed matter [LR85, EM08], light [SBFS07, LAP+08, SSC13], and cold atoms [BJZ+08, RDF+08]. A unified understanding of Anderson localization is provided by the scaling theory [Tho74, AALR79, ATAF80]. Based on the one-parameter-scaling hypothesis of the conductance with respect to to the system size, the scaling theory describes the criticality of localization transitions in three dimensions and predicts the absence of delocalization in one and two dimensions. Symmetry further changes the universality class of localization. For example, time-reversal symmetry (reciprocity) in the presence of spin-orbit interaction enables delocalization even in two dimensions [HLN80]; chiral (sublattice) symmetry enables delocalization of zero modes even in one dimension [Dys53, SJ81, GW91, Gad93, AZ97, BF97, BMSA98, BFGM00].

As discussed in the preceding chapters, the physics of non-Hermitian systems has attracted considerable interest in recent years [KYZ16, EGMK+18, BBK21]. Anderson localization was also investigated in non-Hermitian systems with asymmetric hopping [HN96, Efe97b, FZ97, HN97, BSB97, FZ99, GK98, NS98, MSA98, HN98, YL99, LGV15, AHN16, GAK+18, MPBC18, HKU19, ZYX20, JLY+19] and gain or loss [FPY94, BPB96, BC96, PMB96, Lon19a, Lon19c, TME20, HS20], the latter of which is directly relevant to random lasers [Wie08, Wie13]. Even in the presence of non-Hermiticity, random lasers in one dimension never exhibit delocalization similarly to the Hermitian case. By contrast, a non-Hermitian extension of the Anderson model with asymmetric hopping, which was first investigated by Hatano and Nelson [HN96, HN97, HN98], exhibits delocalization in one dimension. Importantly, this implies the breakdown of the conventional scaling theory of localization, which predicts the absence of delocalization in one dimension. In fact, since Anderson localization results from the destructive interference of coherent waves, non-Hermiticity should lead to decoherence and destroy Anderson localization. However, it remains unclear how non-Hermiticity changes the scaling theory of localization, and a unified understanding of non-Hermitian localization has yet to be obtained.

In this chapter, we develop a scaling theory of localization in non-Hermitian disordered systems. On the basis of the random-matrix approach for nonunitary scattering matrices, we reveal that non-Hermiticity introduces a new scale and breaks down the one-parameter-scaling hypothesis. Instead, we demonstrate the two-parameter scaling (Fig. 6.1), which is the origin of the unconventional non-Hermitian delocalization. Furthermore, we establish the threefold universality of non-Hermitian localization according to reciprocity (Table 6.1). While non-

Hermitian systems exhibit unidirectional delocalization in the absence of symmetry, reciprocity forbids it without internal degrees of freedom, which explains the absence of delocalization in random lasers. We also find a new universality class of localization transitions: bidirectional delocalization protected by symplectic reciprocity.

This chapter is based on Ref. [KR21].

6.1 Nonunitary scaling theory

6.1.1 Non-Hermitian delocalization

In the conventional scaling theory of localization [AALR79], we consider the dependence of the conductance G on the length scale L. A sufficiently small system is diffusive and described by Ohm's law (Boltzmann transport theory [AM76, Abr88]), leading to

$$G \propto L^{d-2} \tag{6.1}$$

in d dimensions. For a sufficiently large system, on the other hand, the wave coherence can lead to Anderson localization and hence

$$G \propto e^{-\alpha L} \tag{6.2}$$

with $\alpha > 0$. The transition between these two regimes is understood by the scaling function

$$\beta(G) \coloneqq \frac{d \log G}{d \log L}. \tag{6.3}$$

In the localized regime, it is given as

$$\beta(G) = \log G < 0, \tag{6.4}$$

and hence the conductance G gets smaller with increasing the system length L. In the diffusive regime, we have

$$\beta(G) = d - 2, \tag{6.5}$$

which is positive (negative) for $d > 2$ ($d < 2$). Consequently, a localization transition occurs in three dimensions at $G = G_c$ where $\beta(G_c) = 0$; by contrast, no transitions occur in one dimension since $\beta(G)$ is always negative and G monotonically decreases in both diffusive and localized regimes.

Non-Hermiticity gives rise to a new regime that has no analogs in particle-number-conserving systems. In fact, it describes coupling to an external environment and can lead to amplification (lasing), resulting in

$$G \propto e^{\gamma L} \tag{6.6}$$

with the amplification rate $\gamma > 0$. In such a regime, we have

$$\beta(G) = \log G > 0 \tag{6.7}$$

in arbitrary dimensions, and hence delocalization is possible even in one dimension. The amplifying regime can arise from nonunitarity of scattering matrices. In Hermitian systems, unitarity is imposed on scattering matrices as a direct consequence of current conservation, and the transmission amplitudes cannot exceed one (see Appendix D.1). In non-Hermitian systems,

by contrast, such a constraint is absent and the conductance G can be arbitrarily large, which enables the amplification as $G \propto e^{\gamma L}$.

The delocalization in the amplifying regime can also be understood by the Thouless criterion [Tho74, Ham20]. In the diffusive regime, it takes the Thouless time

$$t_{\mathrm{Th}} \propto L^2 \tag{6.8}$$

for a particle to reach one end from the other in a system of size L^d. To realize this diffusive transport, t_{Th} should be smaller than the time scale

$$\Delta t \propto \frac{1}{\Delta E} \propto L^d \tag{6.9}$$

determined by the level spacing $\Delta E \propto L^{-d}$ of the spectrum. Since we have

$$\frac{t_{\mathrm{Th}}}{\Delta t} \propto L^{2-d}, \tag{6.10}$$

this is possible in three dimensions (i.e., $t_{\mathrm{Th}}/\Delta t \propto L^{-1} \ll 1$) but impossible in one dimension (i.e., $t_{\mathrm{Th}}/\Delta t \propto L \gg 1$). In the amplifying regime, on the other hand, particle inflow from the environment enables the ballistic transport, and the relevant time scale is

$$t_{\mathrm{N}} \propto L. \tag{6.11}$$

Since we have

$$\frac{t_{\mathrm{N}}}{\Delta t} \propto L^{1-d}, \tag{6.12}$$

t_{N} is comparable to Δt even in one dimension (i.e., $t_{\mathrm{N}}/\Delta t \sim 1$), which enables delocalization. Notably, an additional relevant scale emerges in the amplifying regime, which implies the breakdown of the one-parameter-scaling hypothesis [Tho74, AALR79], as discussed below.

6.1.2 Scaling equations

To uncover universal behavior of Anderson localization in non-Hermitian systems, we revisit the Hatano-Nelson model [HN96, HN97, HN98] and derive the scaling equations for transport properties. We show that the scaling behavior should be understood in terms of two parameters rather than one. On the basis of this understanding, we later discuss Anderson localization for other symmetry classes and find new universality classes. Our scaling theory also explains the different universality classes between the Hatano-Nelson model and random lasers.

The Hatano-Nelson model [HN96, HN97, HN98] reads

$$\hat{H} = \sum_n \left\{ -\frac{1}{2} \left[\left(J + \frac{\gamma}{2} \right) \hat{c}_{n+1}^\dagger \hat{c}_n + \left(J - \frac{\gamma}{2} \right) \hat{c}_n^\dagger \hat{c}_{n+1} \right] + m_n \hat{c}_n^\dagger \hat{c}_n \right\}, \tag{6.13}$$

where $\hat{c}_n$ ($\hat{c}_n^\dagger$) annihilates (creates) a fermion at site n, $J + \gamma/2$ ($J - \gamma/2$) $\in \mathbb{R}$ describes the hopping from the left to the right (from the right to the left), and $m_n \in \mathbb{R}$ is the random potential at site n. The asymmetry γ of the hopping can be introduced in various open classical systems such as photonic systems [LGV15, COZ+17, WKH+20, WKLS21, WDY+21, WDWF21], mechanical metamaterials [BLLC19, GBvWC20], and electrical circuits [HHI+20, HHS+20]. In open quantum systems, it can be realized with cold atoms [GAK+18], quantum walk [XDW+20], and solid-state spins [ZOH+21]. Whereas eigenstates are localized for weak γ, they can be

delocalized for strong γ. In the literature, the complex spectrum [HN96, FZ97, HN97, BSB97, FZ99, GK98, HN98, HKU19], the conductance [BSB97, YL99], and the chiral transport [LGV15, MPBC18] were investigated for this lattice model. Nevertheless, the scaling theory has not been fully developed.

The nature of the non-Hermitian delocalization should not depend on specific details of the model but solely on symmetry. To understand such a universal feature, we construct a continuum model from the Hatano-Nelson model. To this end, we focus on a narrow shell around the band center $\operatorname{Re} E = 0$ and decompose the fermions by

$$\hat{c}_n = e^{\mathrm{i}k_{\mathrm{F}}n}\hat{\psi}_{\mathrm{R}} + e^{-\mathrm{i}k_{\mathrm{F}}n}\hat{\psi}_{\mathrm{L}} \quad (k_{\mathrm{F}} \coloneqq \pi/2)\,. \tag{6.14}$$

Here, $\hat{\psi}_{\mathrm{R}}$ and $\hat{\psi}_{\mathrm{L}}$ are the right-moving and left-moving fermions on the two Fermi points (valleys), respectively. Assuming that $\hat{\psi}_{\mathrm{R}}$ and $\hat{\psi}_{\mathrm{L}}$ vary slowly in space, we have the continuum model

$$\hat{H} = \int dx \begin{pmatrix} \hat{\psi}_{\mathrm{R}}^\dagger & \hat{\psi}_{\mathrm{L}}^\dagger \end{pmatrix} h_{\mathrm{A}} \begin{pmatrix} \hat{\psi}_{\mathrm{R}} \\ \hat{\psi}_{\mathrm{L}} \end{pmatrix} \tag{6.15}$$

with

$$h_{\mathrm{A}} = (-\mathrm{i}\partial_x + \mathrm{i}\gamma/2)\,\tau_z + m_0(x) + m_1(x)\,\tau_x, \tag{6.16}$$

where Pauli matrices τ_i's describe the two valley degrees of freedom. We assume that m_0 and m_1 are the Gaussian disorder that satisfies

$$\langle m_i(x)\rangle = 0, \quad \langle m_i(x)\, m_j(x')\rangle = 2\mu_i\delta_{ij}\delta(x-x') \tag{6.17}$$

with $\mu_i > 0$ and the ensemble average $\langle\star\rangle$. Although we begin with the Hatano-Nelson model, we emphasize that h_{A} does not depend on its specific details but universally on symmetry. Generic non-Hermitian systems without symmetry including h_{A} are defined to belong to class A in the 38-fold classification of internal symmetry (see Sec. 2.4 for details) [BL02, KSUS19]. We note in passing that time-reversal symmetry of h_{A} (i.e., $\tau_x h_{\mathrm{A}}^* \tau_x^{-1} = h_{\mathrm{A}}$) does not change the universality of localization.

Now, we formulate the scaling equations (functional renormalization group equations). The conductance G_{R} from the left to the right (G_{L} from the right to the left) is given by the corresponding transmission eigenvalue T_{R} (T_{L}) according to the Landauer formula [Dat95, Imr97]. Then, we consider the incremental changes of $T_{\mathrm{R/L}}$, in addition to the reflection eigenvalue R_{L} from the left to the left (R_{R} from the right to the right), upon attachment of a thin slice in which the scattering can be treated perturbatively. Such attachment renormalizes the probability distribution of $T_{\mathrm{R/L}}$ and $R_{\mathrm{L/R}}$, resulting in its scaling (Fokker-Planck) equation according to the system size L. It provides all the information about the transmission eigenvalues $T_{\mathrm{R/L}}$ and the conductances $G_{\mathrm{R/L}}$. In the Hermitian case, the scaling equations were obtained by Dorokhov, and by Mello, Pereyra, and Kumar [Dor82, MPK88, Bee97, Bee15].

For the continuum model h_{A}, we find that non-Hermiticity γ amplifies one of T_{R} and T_{L} and attenuates the other, but does not have significant influence on their phases. As a result, we have

$$\frac{\langle dT_{\mathrm{R/L}}\rangle}{dL} = \pm\gamma T_{\mathrm{R/L}} - \frac{T_{\mathrm{R/L}}\left(1 - R_{\mathrm{L/R}}\right)}{\ell}, \tag{6.18}$$

where

$$\ell \coloneqq \frac{1}{2\mu_1} \tag{6.19}$$

is the mean free path determined by the disorder strength (see Appendix D.4 for detailed derivations). The ensemble average $\langle\star\rangle$ is taken over the attached thin slice and the phases

of the scattered waves for given $T_{\mathrm{R/L}}$ and $R_{\mathrm{L/R}}$. This scaling equation (6.18) implies that the transmission amplitudes are given as

$$T_{\mathrm{R/L}} = e^{\pm\gamma L}\tilde{T} \tag{6.20}$$

with the transmission amplitude $\tilde{T}$ in Hermitian systems. For $L \gg \ell$, the conductance fluctuations become as large as the averages $\langle G\rangle$, which no longer represent the conductances of a single sample. In fact, the conductance distributions are broad and asymmetric, and follow the log-normal distributions. Consequently, the typical conductances are $G^{\mathrm{typ}} \coloneqq e^{\langle \log G\rangle}$ instead of $\langle G\rangle$. Because of

$$\frac{\tilde{G}^{\mathrm{typ}}}{G_{\mathrm{c}}} \sim e^{-L/\ell} \quad (L \gg \ell) \tag{6.21}$$

in the Hermitian case [Dor82, MPK88, Bee97, Bee15], the typical conductances in the non-Hermitian case are

$$\frac{G^{\mathrm{typ}}_{\mathrm{R/L}}}{G_{\mathrm{c}}} \sim e^{(\pm\gamma - 1/\ell)L}. \tag{6.22}$$

Thus, either one of the two conductances exhibits delocalization. For $\gamma \geq 0$, for example, $G^{\mathrm{typ}}_{\mathrm{R}}$ diverges for $L \to \infty$ above the transition point

$$\gamma = \gamma_{\mathrm{c}} \coloneqq \frac{1}{\ell}, \tag{6.23}$$

around which the critical behavior

$$\frac{|G^{\mathrm{typ}}_{\mathrm{R}} - G_{\mathrm{c}}|}{G_{\mathrm{c}}} \propto |\gamma - \gamma_{\mathrm{c}}| \tag{6.24}$$

appears.

6.1.3 Two-parameter scaling

In Hermitian systems, the scaling equations and the conductance $\tilde{G}$ depend solely on L/ℓ. This confirms the one-parameter-scaling hypothesis, which underlies the absence of delocalization in one dimension [Tho74, AALR79]. However, the obtained scaling equation (6.18) clearly indicates the emergence of the additional scale γ due to non-Hermiticity. In fact, non-Hermiticity leads to the distinction between G_{R} and G_{L}, which is impossible in Hermitian systems by current conservation. From Eq. (6.18), we show in Fig. 6.1 the renormalization-group flow based on both G_{R} and G_{L}. In addition to the fixed point

$$(G_{\mathrm{R}}, G_{\mathrm{L}}) = (0, 0) \tag{6.25}$$

for the localized phase, a pair of additional fixed points

$$(G_{\mathrm{R}}, G_{\mathrm{L}}) = (G_{\mathrm{c}}, 0)\,, (0, G_{\mathrm{c}}) \tag{6.26}$$

emerges away from $G_{\mathrm{R}} = G_{\mathrm{L}}$. As a result, delocalization with

$$(G_{\mathrm{R}}, G_{\mathrm{L}}) = (\infty, 0)\,, (0, \infty) \tag{6.27}$$

is possible for sufficiently strong non-Hermiticity. Therefore, the emergence of the new scale and the breakdown of the one-parameter scaling are the origin of the non-Hermitian delocalization in one dimension.

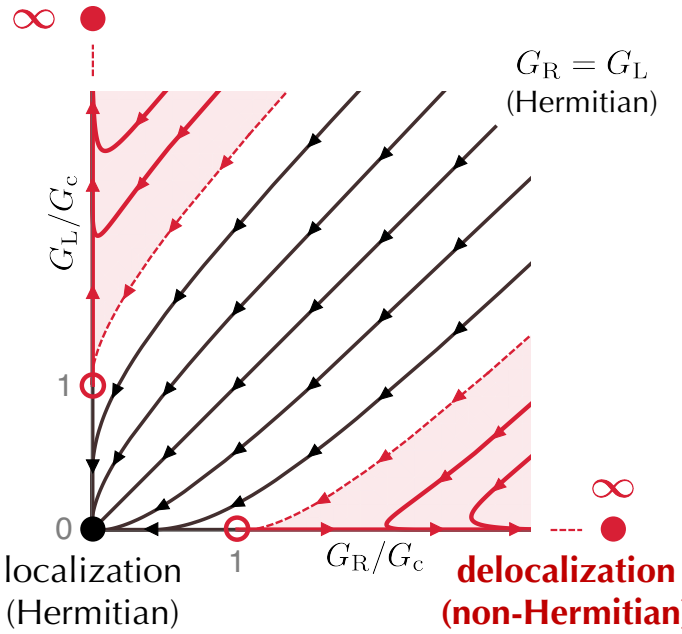

Figure 6.1: Two-parameter scaling of non-Hermitian localization. The renormalization-group flow is shown according to the conductance $G_{\rm R}$ from the left to the right and the conductance $G_{\rm L}$ from the right to the left. The system size L increases along with the arrows. While localization with $(G_{\rm R}, G_{\rm L}) = (0, 0)$ (black dot) occurs in Hermitian systems ($G_{\rm R} = G_{\rm L}$), delocalization with $(G_{\rm R}, G_{\rm L}) = (\infty, 0), (0, \infty)$ (red dots) arises for sufficiently strong non-Hermiticity. Reproduced from Fig. 1 of Ref. [KR21]. Copyright 2021 by the American Physical Society.

It is also notable that the average conductances are

$$\frac{\langle G_{\rm R/L} \rangle}{G_{\rm c}} \sim e^{(\pm\gamma - 1/4\ell)L} \tag{6.28}$$

since the Hermitian counterpart is $\langle \tilde{G} \rangle / G_{\rm c} \sim e^{-L/4\ell}$ [Dor82, MPK88, Bee97, Bee15]. Hence, $\langle G_{\rm R} \rangle$ exhibits critical behavior at

$$\gamma = \frac{1}{4\ell}, \tag{6.29}$$

which is different from the critical point

$$\gamma = \frac{1}{\ell} \tag{6.30}$$

of the typical conductance $G_{\rm R}^{\rm typ}$ [YL99]. Such a difference in the critical points is another manifestation of the breakdown of the one-parameter scaling. In fact, if the scaling equations are described solely by a single parameter ℓ, both $\langle G_{\rm R} \rangle$ and $G_{\rm R}^{\rm typ}$ are functions of L/ℓ, and hence their critical points should coincide with each other. The different critical points of $\langle G_{\rm R} \rangle$ and $G_{\rm R}^{\rm typ}$ imply the two different length scales ℓ and γ^{-1}.

In our nonunitary two-parameter scaling, the critical exponents are integers, which contrast with the more complicated exponents in the two-parameter scaling of the quantum Hall transition [PG87, Huc95, KOK05]. The simple scaling dimensions appear to be due to one dimension. Several recent works [LOS21a, LOS21b, LXKKSar, LYRF21], which appeared after the present work [KR21], numerically demonstrated that non-Hermiticity leads to the new universality classes of localization transitions also in higher dimensions. There, the universality classes are characterized by complicated critical exponents in contrast to the one-dimensional case. It is worthwhile to study these new universality classes in terms of the renormalization group.

6.2 Symmetry

6.2.1 Threefold universality by reciprocity

Symmetry can further change the universality class of Anderson localization. In particular, reciprocity, defined by

$$\mathcal{T}H^{T}\mathcal{T}^{-1}=H,\quad \mathcal{T}\mathcal{T}^{*}=\pm 1, \tag{6.31}$$

with a unitary matrix $\mathcal{T}$, is fundamental symmetry relevant to localization. For example, reciprocity with $\mathcal{T}\mathcal{T}^{*}=+1$ (-1) enhances (suppresses) the localization and shortens (lengthens) the localization length in Hermitian wires in quasi-one dimension [Dor82,MPK88,Bee97,Bee15]. Moreover, symplectic reciprocity with $\mathcal{T}\mathcal{T}^{*}=-1$ enables delocalization even in two dimensions [HLN80], although delocalization is forbidden without symmetry protection. Here, we uncover the threefold universality of non-Hermitian localization based on reciprocity (Table 6.1). As demonstrated below, the influence of reciprocity is more dramatic than the Hermitian case.

We consider a non-Hermitian continuum model

$$h_{\mathrm{AI}^{\dagger}}=-\mathrm{i}\tau_{z}\partial_{x}+m_{0}\left(x\right)+\left(m_{1}\left(x\right)+\mathrm{i}\gamma/2\right)\tau_{x}, \tag{6.32}$$

which respects

$$\tau_{x}h_{\mathrm{AI}^{\dagger}}^{T}\tau_{x}^{-1}=h \tag{6.33}$$

and hence belongs to class $\mathrm{AI}^{\dagger}$ (orthogonal class; see Sec. 2.4 for details) [KSUS19]. Notably, the asymmetry between the valleys [i.e., $\mathrm{i}\left(\gamma/2\right)\tau_{z}$ term in Eq. (6.16)] is forbidden because of reciprocity, which leads to

$$G_{\mathrm{R}}=G_{\mathrm{L}} \tag{6.34}$$

even in non-Hermitian systems. Thus, the nonunitary fixed points away from $G_{\mathrm{R}}=G_{\mathrm{L}}$ in Fig. 6.1 cannot be reached, and the unidirectional delocalization is forbidden. In terms of the scaling equations, reciprocity-preserving non-Hermiticity is irrelevant by the ensemble average over disorder, whereas reciprocity-breaking non-Hermiticity gives rise to an additional scale (see Appendix D.4 for detailed derivations). Consequently, the universality in class $\mathrm{AI}^{\dagger}$ is the same as the Hermitian counterpart, which contrasts with class A. The continuum model in Eq. (6.32) describes disordered wires with gain or loss (i.e., complex onsite potential), including random lasers [Wie08,Wie13]. Reciprocity underlies the absence of delocalization in random lasers.

On the other hand, reciprocal systems with $\mathcal{T}\mathcal{T}^{*}=-1$ instead of $\mathcal{T}\mathcal{T}^{*}=+1$ are defined to belong to class $\mathrm{AII}^{\dagger}$ (symplectic class) [KSUS19]. Although reciprocity imposes $G_{\mathrm{R}}=G_{\mathrm{L}}$ also in this case, an important distinction in the symplectic class is the Kramers degeneracy, which gives rise to a new type of non-Hermitian delocalization protected by reciprocity. The corresponding continuum model is

$$h_{\mathrm{AII}^{\dagger}}=\left(-\mathrm{i}\partial_{x}+\Delta\sigma_{x}+\mathrm{i}\left(\gamma/2\right)\sigma_{z}\right)\tau_{z}+m_{0}\left(x\right)+m_{1}\left(x\right)\tau_{x}, \tag{6.35}$$

which respects

$$\left(\sigma_{y}\tau_{x}\right)h_{\mathrm{AII}^{\dagger}}^{T}\left(\sigma_{y}\tau_{x}\right)^{-1}=h_{\mathrm{AII}^{\dagger}}. \tag{6.36}$$

Here, Pauli matrices σ_{i}'s describe the internal degrees of freedom such as spin. The scaling equations can be obtained in a manner similar to class A (see Appendix D.4 for detailed derivations). In this case, one of the Kramers pair is amplified to the right while the other is amplified to the left because of non-Hermiticity. We then have

$$\frac{G_{\mathrm{R}}^{\mathrm{typ}}}{G_{\mathrm{c}}}=\frac{G_{\mathrm{L}}^{\mathrm{typ}}}{G_{\mathrm{c}}}\sim\left(e^{\gamma L}+e^{-\gamma L}\right)e^{-L/\ell}\sim e^{\left(|\gamma|-1/\ell\right)L} \tag{6.37}$$

Table 6.1: Threefold universality of non-Hermitian localization based on reciprocity. The types of delocalization and the typical conductances for $L \gg \ell$ are shown according to non-Hermiticity γ and the mean free path $\ell > 0$.

Class	Symmetry	Delocalization	Conductances
A	No	Unidirectional	$e^{(\pm\gamma-1/\ell)L}$
AI†	$H^T = H$	No	$e^{-L/\ell}$
AII†	$\sigma_y H^T \sigma_y^{-1} = H$	Bidirectional	$e^{(\lvert\gamma\rvert-1/\ell)L}$

for $L \gg \ell$. Thus, the eigenstates are bidirectionally delocalized in contrast to classes A and AI†. Without symmetry, one of the transmitted channels dominates the other, and non-Hermitian delocalization is unidirectional. Hence, the bidirectional delocalization arises only in the presence of symplectic reciprocity. Despite $G_{\mathrm{R}} = G_{\mathrm{L}}$, the conductance of one channel serves as G_{R} and that of the corresponding Kramers partner serves as G_{L} in the two-parameter scaling shown in Fig. 6.1, the sum of which yields the total conductance.

While reciprocity is equivalent to time-reversal symmetry

$$\mathcal{T} H^* \mathcal{T}^{-1} = H \tag{6.38}$$

in Hermitian systems, this is not the case in non-Hermitian systems. The corresponding symmetry classes with time-reversal symmetry are classes AI and AII [KSUS19]. The universality of non-Hermitian localization is also different depending on whether one imposes time-reversal symmetry or reciprocity. In fact, time-reversal symmetry does not change the universality of the non-Hermitian localization (see Appendix D.4 for details), whereas reciprocity can forbid or enhance it as discussed above.

As discussed in Chap. 4, reciprocity enriches non-Hermitian topology and skin effects. While reciprocity with $\mathcal{T}\mathcal{T}^* = +1$ eliminates the skin effect, reciprocity with $\mathcal{T}\mathcal{T}^* = -1$ gives rise to the $\mathbb{Z}_2$ skin effect, which is compatible with the aforementioned threefold universality of non-Hermitian localization. It is worthwhile to clarify the analogy between the non-Hermitian delocalization and skin effects. Reciprocity also leads to threefold universality of non-Hermitian random matrices [HKKU20].

6.2.2 Chiral and sublattice symmetry

In the presence of chiral or sublattice symmetry, zero modes can be delocalized even in Hermitian systems in one dimension, accompanied by the Dyson singularity [Dys53]. Similarly to time-reversal symmetry and reciprocity, chiral symmetry and sublattice symmetry are distinct from each other in non-Hermitian systems, the former (latter) of which corresponds to class AIII (AIII†) [KSUS19]. For example, a random hopping model with gain or loss respects chiral symmetry, while a random asymmetric hopping model respects sublattice symmetry. In the presence of chiral symmetry

$$\tau_x h_{\mathrm{AIII}}^\dagger \tau_x^{-1} = -h_{\mathrm{AIII}}, \tag{6.39}$$

non-Hermiticity is found not to change the universality of delocalization (see Appendix D.4 for detailed derivations); by contrast, in the presence of sublattice symmetry

$$\tau_x h_{\mathrm{AIII}^\dagger} \tau_x^{-1} = -h_{\mathrm{AIII}^\dagger}, \tag{6.40}$$

non-Hermiticity enables the unidirectional delocalization in a manner similar to class A. In fact, the asymmetry between the valleys is allowed for sublattice symmetry, but forbidden for chiral symmetry.

It is also notable that the non-Hermitian delocalization shares the same nature with the delocalization of zero modes due to chiral symmetry. To see this correspondence, we notice the following Hermitian Hamiltonian $\tilde{H}(E)$ constructed from a non-Hermitian Hamiltonian H and $E \in \mathbb{C}$ [FZ97, BMSA98, GAK+18, KSUS19, OKSS20]:

$$\tilde{H}(E) \coloneqq \begin{pmatrix} 0 & H - E \\ H^\dagger - E^* & 0 \end{pmatrix}. \tag{6.41}$$

As discussed in the preceding chapters, this Hermitization procedure plays a key role also in non-Hermitian random matrices [FZ97] and non-Hermitian topological phases [GAK+18, KSUS19, OKSS20]. When E is eigenenergy of H and $|\psi\rangle$ is the corresponding right eigenstate, $(0 \;\; |\psi\rangle)^T$ is a zero mode of $\tilde{H}(E)$. Thus, delocalized eigenstates can appear in H even in the presence of disorder if the corresponding zero modes are delocalized in $\tilde{H}(E)$. Consistently, when H belongs to class A or AII† (AI†), $\tilde{H}(E)$ belongs to class AIII or DIII (CI) [KSUS19], for which delocalization of zero modes is possible (impossible) [BMSA98, BFGM00].

Non-Hermitian disordered systems and the corresponding Hermitian systems also share the same critical exponents of the localization transitions. As discussed above, the localization transitions in one-dimensional non-Hermitian systems in classes A and AII† are characterized by the critical exponent $\nu = 1$, which coincides with the critical behavior in the corresponding Hermitian systems with chiral symmetry [MSHSP14, ABF+14]. A recent work [LXKKSar] further confirmed this correspondence for non-Hermitian disordered systems in two and three dimensions with extensive numerical calculations. A remarkable consequence of this correspondence is superuniversality: the localization transitions in some different symmetry classes of non-Hermitian disordered systems are characterized by the same critical exponent. Furthermore, this correspondence is helpful in predicting the unknown critical exponents in Hermitian systems, which paves a new efficient way to study the localization transitions of Hermitian systems by the corresponding non-Hermitian systems.

6.3 Lattice models

To confirm our nonunitary scaling theory, we generalize the transfer-matrix method [KMOS10] to the non-Hermitian case and numerically investigate non-Hermitian lattice models. We consider generic one-dimensional Hamiltonians with onsite disorder described by

$$\hat{H} = \sum_n \left[-\frac{1}{2} \left(\hat{c}_{n+1}^\dagger J_\mathrm{R} \hat{c}_n + \hat{c}_n^\dagger J_\mathrm{L} \hat{c}_{n+1} \right) + \hat{c}_n^\dagger M_n \hat{c}_n \right], \tag{6.42}$$

where $\hat{c}_n$ ($\hat{c}_n^\dagger$) annihilates (creates) an N-component fermion at site n, and J_R (J_L) and M_n are $N \times N$ matrices that describe the hopping from the left to the right (from the right to the left) and the disordered potential at site n, respectively. This Hamiltonian reduces to the Hatano-Nelson model in Eq. (6.13) for $J_\mathrm{R} = J + \gamma/2$, $J_\mathrm{L} = J - \gamma/2$, and $M_n = m_n$. In the presence of Hermiticity $\hat{H}^\dagger = \hat{H}$, we have

$$J_\mathrm{R}^\dagger = J_\mathrm{L}, \quad M_n^\dagger = M_n. \tag{6.43}$$

When the disorder is sufficiently strong, the eigenstates are localized. The site-n component of an eigenstate localized around $n = n_0$ is generally described by

$$\psi_n \sim \begin{cases} e^{-|n-n_0|/\xi_\mathrm{L}} & (n < n_0), \\ e^{-|n-n_0|/\xi_\mathrm{R}} & (n > n_0). \end{cases} \tag{6.44}$$

To efficiently obtain the localization lengths ξ_{L} and ξ_{R}, we begin with the Schrödinger equation

$$-\frac{J_{\mathrm{R}}}{2}\psi_{n-1}-\frac{J_{\mathrm{L}}}{2}\psi_{n+1}+M_n\psi_n=E\,\psi_n, \tag{6.45}$$

where $E\in\mathbb{C}$ is eigenenergy and ψ_n is the site-n component of the corresponding eigenstate. This leads to

$$\begin{pmatrix}\psi_{n+1}\\ \psi_n\end{pmatrix}=M_{\mathrm{L}n}\begin{pmatrix}\psi_n\\ \psi_{n-1}\end{pmatrix},\quad M_{\mathrm{L}n}\coloneqq\begin{pmatrix}-2J_{\mathrm{L}}^{-1}\left(E-M_n\right) & -J_{\mathrm{L}}^{-1}J_{\mathrm{R}}\\ 1 & 0\end{pmatrix}. \tag{6.46}$$

In this representation, the Schrödinger equation is viewed as the spatial evolution of the wave function $(\psi_n\ \psi_{n-1})^T$ from the left to the right through the system described by the transfer matrix $M_{\mathrm{L}n}$. Then, the left localization length ξ_{L} is given as the inverse of the smallest positive eigenvalue of the $2N\times 2N$ matrix

$$\frac{1}{2L}\log\left[\left(\prod_{n=1}^{L}M_{\mathrm{L}n}\right)\left(\prod_{n=1}^{L}M_{\mathrm{L}n}\right)^{\dagger}\right]. \tag{6.47}$$

Similarly, we have

$$\begin{pmatrix}\psi_{n-1}\\ \psi_n\end{pmatrix}=M_{\mathrm{R}n}\begin{pmatrix}\psi_n\\ \psi_{n+1}\end{pmatrix},\quad M_{\mathrm{R}n}\coloneqq\begin{pmatrix}-2J_{\mathrm{R}}^{-1}\left(E-M_n\right) & -J_{\mathrm{R}}^{-1}J_{\mathrm{L}}\\ 1 & 0\end{pmatrix}, \tag{6.48}$$

from which we can obtain the right localization length ξ_{R}. While $M_{\mathrm{L}n}$ describes the spatial evolution of the wave function from the left to the right, $M_{\mathrm{R}n}$ describes that from the right to the left.

In Hermitian systems, we have $J_{\mathrm{R}}^{\dagger}=J_{\mathrm{L}}$ and hence $\xi_{\mathrm{L}}=\xi_{\mathrm{R}}$. In non-Hermitian systems, on the other hand, we can have two different localization lengths (i.e., $\xi_{\mathrm{L}}\neq\xi_{\mathrm{R}}$). This is similar to the conductances G_{L} and G_{R}. As discussed above, the distinction between ξ_{L} and ξ_{R} leads to the two-parameter scaling of non-Hermitian localization. Moreover, we have $|\det M_{\mathrm{L}n}|=|\det M_{\mathrm{R}n}|=1$ in Hermitian systems, which ensures $\xi_{\mathrm{L}}=\xi_{\mathrm{R}}<\infty$ and hence the absence of delocalization in one dimension. However, this is not the case in non-Hermitian systems, which enables the divergence of the localization length and the consequent delocalization even in one dimension.

Figure 6.2 (a) shows the localization lengths for the Hatano-Nelson model in Eq. (6.13). For $\gamma\geq 0$, the right localization length ξ_{R} diverges at a critical point, whereas the left localization length ξ_{L} remains finite, which is a signature of the unidirectional delocalization. Around the critical point, ξ_{R} diverges as

$$\xi_{\mathrm{R}}\propto\frac{1}{|\gamma-\gamma_{\mathrm{c}}|}. \tag{6.49}$$

A symplectic extension of the Hatano-Nelson model is given by

$$\hat{H}=\sum_n\left\{-\frac{1}{2}\left[\hat{c}_{n+1}^{\dagger}\left(J+\frac{\gamma\sigma_3}{2}-\mathrm{i}\Delta\sigma_1\right)\hat{c}_n+\hat{c}_n^{\dagger}\left(J-\frac{\gamma\sigma_3}{2}+\mathrm{i}\Delta\sigma_1\right)\hat{c}_{n+1}\right]+\hat{c}_n^{\dagger}\left(m_n+h\sigma_3\right)\hat{c}_n\right\}. \tag{6.50}$$

The non-Hermitian skin effect of this model without disorder ($W=0$) is investigated in Chap. 4 [OKSS20, KOS20]. This lattice model with $h=0$ corresponds to the continuum model in Eq. (6.35). In contrast to the original Hatano-Nelson model, we have $\xi_{\mathrm{L}}=\xi_{\mathrm{R}}$ for $h=0$ because of reciprocity. As a result, both ξ_{L} and ξ_{R} diverge at a critical point [Fig. 6.2 (b)], which is a

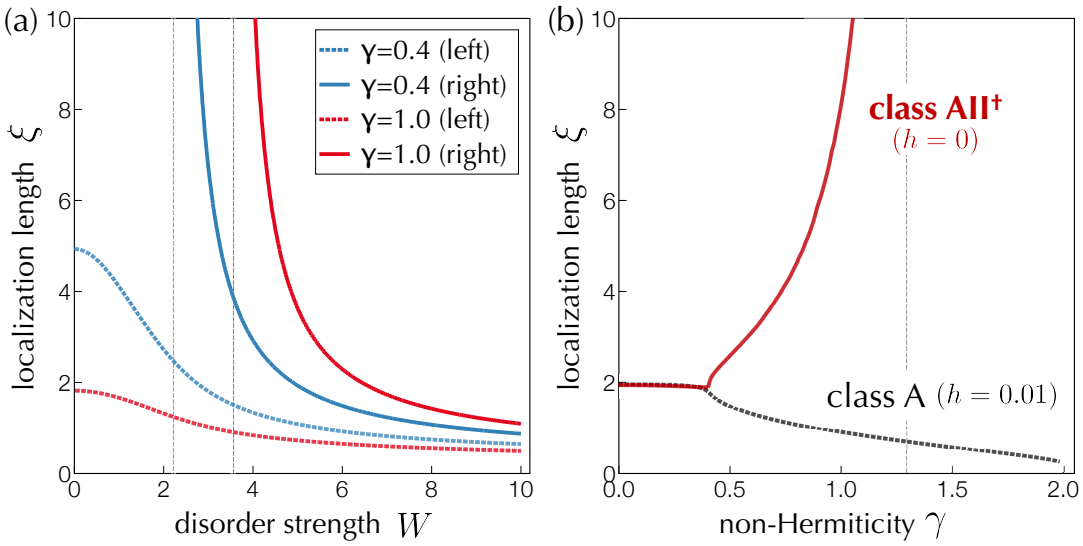

Figure 6.2: Non-Hermitian localization on lattices ($L = 5000$, $J = 1.0$, $E = 0$). The disordered onsite potential is uniformly distributed over $[-W/2, W/2]$, and each datum shows the average over 1000 samples. (a) Hatano-Nelson model (class A). For $\gamma > 0$, the right localization length diverges at a transition point, whereas the left localization length remains finite. The transition points are $W_c = 2.22$ ($\gamma = 0.4$) and $W_c = 3.56$ ($\gamma = 1.0$). (b) Symplectic Hatano-Nelson model (class AII†; $\Delta = 0.2$, $W = 4.0$). Both right and left localization lengths diverge at the transition point $\gamma_c = 1.30$ (red solid curve). The delocalization vanishes in the presence of a reciprocity-breaking perturbation $h = 0.01$ (black dotted curve). Reproduced from Fig. 2 of Ref. [KR21]. Copyright 2021 by the American Physical Society.

signature of the bidirectional delocalization. Because of the reciprocity-protected nature, the delocalization vanishes even in the presence of a small reciprocity-breaking perturbation $h \neq 0$, which is unique to the symplectic class.

In Appendix D.5, we provide additional numerical results of non-Hermitian disordered systems in one dimension. The localization transitions of non-Hermitian disordered systems in higher dimensions were also investigated by the transfer-matrix method in recent works [LOS21b, LXKKSar, LYRF21].

6.4 Discussions

Transport phenomena of disordered systems, including Anderson localization and transitions, enjoy universality in various scaling limits that is governed only by a few physical parameters. This is embodied by the one-parameter scaling of localization [Tho74, AALR79]. In this chapter, we have demonstrated that non-Hermiticity makes it break down and leads to the two-parameter scaling, which generally describes the unconventional non-Hermitian delocalization.

While we here restrict ourselves to the single-channel case, it is meaningful to consider the limit of thick wires to fully uncover universal properties—we leave this as a future problem. Moreover, a random-matrix theory underlies Anderson localization [Bee97, Bee15], and it merits further research to generalize this relationship to non-Hermitian systems. Notably, a recent work [HKKU20] showed the threefold universality of complex-level-spacing distributions for non-Hermitian random matrices.

From a topological perspective, our nonunitary two-parameter scaling shares similarities

with the two-parameter scaling of the quantum Hall transition [PG87, Huc95, KOK05]. As discussed in the preceding chapters, the Hatano-Nelson model is characterized by a topological invariant unique to non-Hermitian systems [GAK+18, KSUS19]. In our continuum model, this topological invariant is $\operatorname{sgn}\gamma$, similar to the Hall conductivity given by the Dirac mass term. An open problem is to formulate an effective field theory for the nonunitary two-parameter scaling, akin to the nonlinear sigma model augmented with a topological term for the quantum Hall transition. This should also give a unified understanding about topology and localization in open systems. In this regard, the topological field theory for non-Hermitian systems in Chap. 5 [KSR21] should play a key role.

Chapter 7

Conclusion

We have developed a general theory of open systems and established their universality. We have demonstrated that non-Hermiticity, which is the hallmark of open systems, induces new nonequilibrium physics in various aspects. Our theory has direct relevance to experiments in view of recent experimental advances. For example, on the basis of our theory in Chap. 4 [KSS20], the higher-order non-Hermitian skin effect has been observed in recent experiments of active particles [PTG+20] and acoustic materials [ZTJ+21]. Similarly, other non-Hermitian topological phenomena, such as the chiral magnetic skin effect in three dimensions, are expected to be experimentally realized in the near future. Such new nonequilibrium topological phenomena should also open a new way of actively controlling materials. The universality of our theory manifests itself as robustness against disorder. In fact, in Chap. 6, we have developed a scaling theory of non-Hermitian disordered systems and elucidated the universality classes of Anderson localization in open systems. Notably, the competition between nonreciprocity and disorder has been experimentally observed in open photonic systems in one dimension [WKH+20]. Similarly, new universality classes of non-Hermitian disordered systems should be confirmed in future experiments. Furthermore, the topological field theory developed in Chap. 5 is universally applicable even in the presence of disorder and many-body interaction since it is solely based on the gauge principle. It merits further research to explore the quantum many-body physics of open systems on the basis of our topological field theory.

In this thesis, we aim to significantly advance nonequilibrium physics and further push it into a new direction with new concepts. Our theory tells us a new characterization and classification of phases of matter far from equilibrium. Conventionally, we focus only on states when we discuss phases of matter. For example, we study spontaneous symmetry breaking and topological phases of thermal equilibrium states or ground states. Such a state-based characterization assumes that we are interested only in physics at equilibrium. Even far from equilibrium, it is arguably important to characterize states such as stationary states. However, universal features of nonequilibrium phases appear not only in states but also in dynamics. In fact, the intrinsic non-Hermitian topology cannot be captured only by states. Instead, it is characterized by operators themselves, which contain information about both spectra and states. Consequently, intrinsic non-Hermitian topology describes dynamical phenomena in open systems, prime examples of which include the skin effects and the anomalous delocalization. Such operator-based characterization also underlies the new formulation of a field theory developed in Chap. 5 [KSR21]. These discussions show that new physics actually hides in apparently complicated nonequilibrium dynamics. To unveil it, we should further develop fundamental concepts [DG91]. We hope that the development of nonequilibrium physics, including a theory of life [Sch44], will herald a new perspective on the world.

Appendix A

Periodic table of topological phases

A.1 Hermitian systems

The topological classification of Hermitian insulators and superconductors is shown in the periodic table A.1 [SRFL08, Kit09, RSFL10, CTSR16]. The classification procedure is based on the following two steps:

- Identify the classifying spaces and topology (homotopy group) of Hermitian insulators and superconductors in zero dimension (i.e., Hermitian matrices).
- Reduce the topological problem to an extension of the Clifford algebra and determine the topology of insulators and superconductors in nonzero dimensions.

To classify topological phases of Hermitian insulators and superconductors, we first determine the topology of Hermitian matrices in each Altland-Zirnbauer (AZ) symmetry class [AZ97]. For example, let us consider a Hermitian matrix without any symmetry (i.e., class A). We assume the presence of an energy gap, i.e.,

$$\forall\, n \quad E_n \neq 0 \qquad \Longleftrightarrow \qquad \det H \neq 0. \tag{A.1}$$

Here, topology of this Hermitian matrix can be captured only by its wave function. Then, we can generally flatten its energy spectrum without closing the energy gap so that the energy of empty (occupied) bands is -1 $(+1)$. After this spectral flattening, the Hermitian Hamiltonian is expressed as

$$H = U \begin{pmatrix} 1_m & 0 \\ 0 & -1_n \end{pmatrix} U^{-1}, \quad U \in \mathrm{U}\,(m+n)\,, \tag{A.2}$$

where the number of the empty (occupied) bands is assumed to be m (n), and U is the unitary group. The topology of the Hermitian Hamiltonian is solely determined by the unitary matrix U. Notably, U has the following gauge ambiguity:

$$U \to U \begin{pmatrix} \tilde{U}_m & 0 \\ 0 & \tilde{U}_n \end{pmatrix}, \quad \tilde{U}_i \in \mathrm{U}\,(i)\,. \tag{A.3}$$

Then, U belongs to a parameter space

$$\mathcal{C}_0 \coloneqq \frac{\mathrm{U}\,(m+n)}{\mathrm{U}\,(m) \times \mathrm{U}\,(n)}. \tag{A.4}$$

Table A.1: Topological classification table for Hermitian insulators and superconductors in the tenfold Altland-Zirnbauer (AZ) symmetry class [SRFL08, Kit09, RSFL10]. Topological phases are classified according to the AZ symmetry class and the spatial dimensions d. The entries $\mathbb{Z}$, $\mathbb{Z}_2$, $2\mathbb{Z}$, or 0 represent the presence or absence of nontrivial topological insulators and superconductors, and types of these systems when they exist.

AZ class	Classifying space	$d=0$	$d=1$	$d=2$	$d=3$	$d=4$	$d=5$	$d=6$	$d=7$
A	$\mathcal{C}_0$	$\mathbb{Z}$	0	$\mathbb{Z}$	0	$\mathbb{Z}$	0	$\mathbb{Z}$	0
AIII	$\mathcal{C}_1$	0	$\mathbb{Z}$	0	$\mathbb{Z}$	0	$\mathbb{Z}$	0	$\mathbb{Z}$
AI	$\mathcal{R}_0$	$\mathbb{Z}$	0	0	0	$2\mathbb{Z}$	0	$\mathbb{Z}_2$	$\mathbb{Z}_2$
BDI	$\mathcal{R}_1$	$\mathbb{Z}_2$	$\mathbb{Z}$	0	0	0	$2\mathbb{Z}$	0	$\mathbb{Z}_2$
D	$\mathcal{R}_2$	$\mathbb{Z}_2$	$\mathbb{Z}_2$	$\mathbb{Z}$	0	0	0	$2\mathbb{Z}$	0
DIII	$\mathcal{R}_3$	0	$\mathbb{Z}_2$	$\mathbb{Z}_2$	$\mathbb{Z}$	0	0	0	$2\mathbb{Z}$
AII	$\mathcal{R}_4$	$2\mathbb{Z}$	0	$\mathbb{Z}_2$	$\mathbb{Z}_2$	$\mathbb{Z}$	0	0	0
CII	$\mathcal{R}_5$	0	$2\mathbb{Z}$	0	$\mathbb{Z}_2$	$\mathbb{Z}_2$	$\mathbb{Z}$	0	0
C	$\mathcal{R}_6$	0	0	$2\mathbb{Z}$	0	$\mathbb{Z}_2$	$\mathbb{Z}_2$	$\mathbb{Z}$	0
CI	$\mathcal{R}_7$	0	0	0	$2\mathbb{Z}$	0	$\mathbb{Z}_2$	$\mathbb{Z}_2$	$\mathbb{Z}$

Table A.2: Classifying spaces of Hermitian matrices and extension of Clifford algebra in the Altland-Zirnbauer (AZ) symmetry classes.

AZ class		Classifying space	π_0	Extension
A	$\mathcal{C}_0$	$\mathrm{U}(m+n)/\mathrm{U}(m)\times\mathrm{U}(n)$	$\mathbb{Z}$	$Cl_0 \to Cl_1$
AIII	$\mathcal{C}_1$	$\mathrm{U}(n)$	0	$Cl_1 \to Cl_2$
AI	$\mathcal{R}_0$	$\mathrm{O}(m+n)/\mathrm{O}(m)\times\mathrm{O}(n)$	$\mathbb{Z}$	$Cl_{0,2} \to Cl_{1,2}$
BDI	$\mathcal{R}_1$	$\mathrm{O}(n)$	$\mathbb{Z}_2$	$Cl_{1,2} \to Cl_{1,3}$
D	$\mathcal{R}_2$	$\mathrm{O}(2n)/\mathrm{U}(n)$	$\mathbb{Z}_2$	$Cl_{0,2} \to Cl_{0,3}$
DIII	$\mathcal{R}_3$	$\mathrm{U}(2n)/\mathrm{Sp}(n)$	0	$Cl_{0,3} \to Cl_{0,4}$
AII	$\mathcal{R}_4$	$\mathrm{Sp}(m+n)/\mathrm{Sp}(m)\times\mathrm{Sp}(n)$	$\mathbb{Z}$	$Cl_{2,0} \to Cl_{3,0}$
CII	$\mathcal{R}_5$	$\mathrm{Sp}(n)$	0	$Cl_{3,0} \to Cl_{3,1}$
C	$\mathcal{R}_6$	$\mathrm{Sp}(n)/\mathrm{U}(n)$	0	$Cl_{2,0} \to Cl_{2,1}$
CI	$\mathcal{R}_7$	$\mathrm{U}(n)/\mathrm{O}(n)$	0	$Cl_{2,1} \to Cl_{2,2}$

The disconnected components of this parameter space $\mathcal{C}_0$ determine the topological phases of the Hermitian matrix, which are calculated by its zeroth homotopy group $\pi_0(\mathcal{C}_0)$. Because of the mathematical fact

$$\pi_0(\mathcal{C}_0) = \mathbb{Z}, \tag{A.5}$$

a topological phase characterized by an integer is well defined. This $\mathbb{Z}$ topological invariant is given as the number of the occupied bands

$$\mathrm{Ch}_0 \coloneqq n, \tag{A.6}$$

which is also known as the zeroth Chern number. The parameter space that determines the topology of the system is called classifying space (e.g., $\mathcal{C}_0$ in class A). Additional symmetry can change the classifying space, as well as the corresponding topological phase. The classifying spaces in all the AZ symmetry classes are summarized in Table A.2.

We can determine the topology of Hermitian systems in an alternative algebraic way. To see this algebraic approach, we consider the following low-energy description of the Hamiltonian in

momentum space near the relevant momentum point:

$$H(\boldsymbol{k}) = \sum_{i=1}^{d} k_i \Gamma_i + m\Gamma_0, \tag{A.7}$$

where $\boldsymbol{k} \coloneqq (k_1, \cdots, k_d)$ is the deviation of the momentum, and $\Gamma_0, \Gamma_1, \cdots, \Gamma_d$ form Clifford algebra:

$$\{\Gamma_i, \Gamma_j\} = 2\delta_{ij}. \tag{A.8}$$

In the presence of the AZ symmetry [AZ97] defined by

$$\mathcal{T} H \mathcal{T}^{-1} = H, \quad \mathcal{T}^2 = \pm 1, \tag{A.9}$$
$$\mathcal{C} H \mathcal{C}^{-1} = -H, \quad \mathcal{C}^2 = \pm 1, \tag{A.10}$$
$$\mathcal{S} H \mathcal{S}^{-1} = -H, \quad \mathcal{S}^2 = 1, \tag{A.11}$$

the Dirac matrices respect

$$\mathcal{T}\,\Gamma_0\,\mathcal{T} = \Gamma_0, \quad \mathcal{T}\,\Gamma_i\,\mathcal{T} = -\Gamma_i \quad (i \neq 0), \tag{A.12}$$
$$\mathcal{C}\,\Gamma_0\,\mathcal{C} = -\Gamma_0, \quad \mathcal{C}\,\Gamma_i\,\mathcal{C} = \Gamma_i \quad (i \neq 0), \tag{A.13}$$
$$\mathcal{S}\,\Gamma_0\,\mathcal{S} = -\Gamma_0, \quad \mathcal{S}\,\Gamma_i\,\mathcal{S} = -\Gamma_i \quad (i \neq 0). \tag{A.14}$$

The Dirac mass term $m\Gamma_0$ is responsible for a bulk energy gap and lives in the classifying space discussed before. The topology of the original Hermitian system can be characterized by the mass term $m\Gamma_0$.

This topological problem can reduce to an extension problem of Clifford algebra. For example, let us consider Hermitian systems without any symmetry (i.e., class A). In this symmetry class, the Dirac matrices in the kinetic term satisfy

$$Cl_d \coloneqq \{\Gamma_i \mid \{\Gamma_i, \Gamma_j\} = 2\delta_{ij},\ i, j \in \{1, \cdots, d\}\} \tag{A.15}$$

The mass term anticommutes with all the Dirac matrices in the kinetic term, i.e.,

$$\{\Gamma_0, \Gamma_i\} = 0 \quad (i = 1, \cdots, d), \tag{A.16}$$

which leads to Cl_{d+1}. We thus consider the mass as a generator that extends the algebra as

$$Cl_d \to Cl_{d+1}. \tag{A.17}$$

Counting different ways to extend the algebra means counting unitary equivalent masses that determine topological phases. The classifying space $\mathcal{C}_0$ in Eq. (A.4) corresponds to the extension of Clifford algebra in Eq. (A.17).

The above discussions can be applied to all the other symmetry classes, as summarized in Table A.2. The two symmetry classes without antiunitary symmetry (complex class) form the complex Clifford algebra which leads to

$$\mathcal{C}_{d+2} \simeq \mathcal{C}_d, \tag{A.18}$$

while the other eight symmetry classes with antiunitary symmetry (real class) form the real Clifford algebra which leads to

$$\mathcal{R}_{d+8} \simeq \mathcal{R}_d. \tag{A.19}$$

As a consequence, the classification table A.1 for topological insulators and superconductors has a periodic structure in terms of spatial dimensions: the complex class has a period of two, and the real class has a period of eight.

A.2 Non-Hermitian systems

The topological classification of non-Hermitian systems [KSUS19] is listed in the periodic tables for the complex AZ symmetry class (Table A.3), the real AZ symmetry class (Table A.4), the real AZ† symmetry class (Table A.5), the complex AZ symmetry class with sublattice symmetry (Table A.6), and the real AZ symmetry class with sublattice symmetry (Table A.7). In addition to this 38-fold topological classification, we provide the periodic tables for the AZ symmetry class with pseudo-Hermiticity (Tables A.8 and A.9).

Table A.3: Topological classification table for non-Hermitian systems in the complex AZ symmetry class [KSUS19]. Non-Hermitian topological phases are classified according to the AZ symmetry class, the spatial dimensions d, and the definition of a complex-energy point (P) or line (L) gap. The subscript of L specifies the line gap for the real or imaginary part of the complex spectrum.

AZ class	Gap	Classifying space	$d=0$	$d=1$	$d=2$	$d=3$	$d=4$	$d=5$	$d=6$	$d=7$
A	P	$\mathcal{C}_1$	0	$\mathbb{Z}$	0	$\mathbb{Z}$	0	$\mathbb{Z}$	0	$\mathbb{Z}$
	L	$\mathcal{C}_0$	$\mathbb{Z}$	0	$\mathbb{Z}$	0	$\mathbb{Z}$	0	$\mathbb{Z}$	0
AIII	P	$\mathcal{C}_0$	$\mathbb{Z}$	0	$\mathbb{Z}$	0	$\mathbb{Z}$	0	$\mathbb{Z}$	0
	$\mathrm{L_r}$	$\mathcal{C}_1$	0	$\mathbb{Z}$	0	$\mathbb{Z}$	0	$\mathbb{Z}$	0	$\mathbb{Z}$
	$\mathrm{L_i}$	$\mathcal{C}_0 \times \mathcal{C}_0$	$\mathbb{Z}\oplus\mathbb{Z}$	0	$\mathbb{Z}\oplus\mathbb{Z}$	0	$\mathbb{Z}\oplus\mathbb{Z}$	0	$\mathbb{Z}\oplus\mathbb{Z}$	0

Table A.4: Topological classification table for non-Hermitian systems in the real AZ symmetry class [KSUS19]. Non-Hermitian topological phases are classified according to the AZ symmetry class, the spatial dimensions d, and the definition of a complex-energy point (P) or line (L) gap. The subscript of L specifies the line gap for the real or imaginary part of the complex spectrum.

AZ class	Gap	Classifying space	$d=0$	$d=1$	$d=2$	$d=3$	$d=4$	$d=5$	$d=6$	$d=7$
AI	P	$\mathcal{R}_1$	$\mathbb{Z}_2$	$\mathbb{Z}$	0	0	0	$2\mathbb{Z}$	0	$\mathbb{Z}_2$
	$\mathrm{L_r}$	$\mathcal{R}_0$	$\mathbb{Z}$	0	0	0	$2\mathbb{Z}$	0	$\mathbb{Z}_2$	$\mathbb{Z}_2$
	$\mathrm{L_i}$	$\mathcal{R}_2$	$\mathbb{Z}_2$	$\mathbb{Z}_2$	$\mathbb{Z}$	0	0	0	$2\mathbb{Z}$	0
BDI	P	$\mathcal{R}_2$	$\mathbb{Z}_2$	$\mathbb{Z}_2$	$\mathbb{Z}$	0	0	0	$2\mathbb{Z}$	0
	$\mathrm{L_r}$	$\mathcal{R}_1$	$\mathbb{Z}_2$	$\mathbb{Z}$	0	0	0	$2\mathbb{Z}$	0	$\mathbb{Z}_2$
	$\mathrm{L_i}$	$\mathcal{R}_2 \times \mathcal{R}_2$	$\mathbb{Z}_2\oplus\mathbb{Z}_2$	$\mathbb{Z}_2\oplus\mathbb{Z}_2$	$\mathbb{Z}\oplus\mathbb{Z}$	0	0	0	$2\mathbb{Z}\oplus 2\mathbb{Z}$	0
D	P	$\mathcal{R}_3$	0	$\mathbb{Z}_2$	$\mathbb{Z}_2$	$\mathbb{Z}$	0	0	0	$2\mathbb{Z}$
	L	$\mathcal{R}_2$	$\mathbb{Z}_2$	$\mathbb{Z}_2$	$\mathbb{Z}$	0	0	0	$2\mathbb{Z}$	0
DIII	P	$\mathcal{R}_4$	$2\mathbb{Z}$	0	$\mathbb{Z}_2$	$\mathbb{Z}_2$	$\mathbb{Z}$	0	0	0
	$\mathrm{L_r}$	$\mathcal{R}_3$	0	$\mathbb{Z}_2$	$\mathbb{Z}_2$	$\mathbb{Z}$	0	0	0	$2\mathbb{Z}$
	$\mathrm{L_i}$	$\mathcal{C}_0$	$\mathbb{Z}$	0	$\mathbb{Z}$	0	$\mathbb{Z}$	0	$\mathbb{Z}$	0
AII	P	$\mathcal{R}_5$	0	$2\mathbb{Z}$	0	$\mathbb{Z}_2$	$\mathbb{Z}_2$	$\mathbb{Z}$	0	0
	$\mathrm{L_r}$	$\mathcal{R}_4$	$2\mathbb{Z}$	0	$\mathbb{Z}_2$	$\mathbb{Z}_2$	$\mathbb{Z}$	0	0	0
	$\mathrm{L_i}$	$\mathcal{R}_6$	0	0	$2\mathbb{Z}$	0	$\mathbb{Z}_2$	$\mathbb{Z}_2$	$\mathbb{Z}$	0
CII	P	$\mathcal{R}_6$	0	0	$2\mathbb{Z}$	0	$\mathbb{Z}_2$	$\mathbb{Z}_2$	$\mathbb{Z}$	0
	$\mathrm{L_r}$	$\mathcal{R}_5$	0	$2\mathbb{Z}$	0	$\mathbb{Z}_2$	$\mathbb{Z}_2$	$\mathbb{Z}$	0	0
	$\mathrm{L_i}$	$\mathcal{R}_6 \times \mathcal{R}_6$	0	0	$2\mathbb{Z}\oplus 2\mathbb{Z}$	0	$\mathbb{Z}_2\oplus\mathbb{Z}_2$	$\mathbb{Z}_2\oplus\mathbb{Z}_2$	$\mathbb{Z}\oplus\mathbb{Z}$	0
C	P	$\mathcal{R}_7$	0	0	0	$2\mathbb{Z}$	0	$\mathbb{Z}_2$	$\mathbb{Z}_2$	$\mathbb{Z}$
	L	$\mathcal{R}_6$	0	0	$2\mathbb{Z}$	0	$\mathbb{Z}_2$	$\mathbb{Z}_2$	$\mathbb{Z}$	0
CI	P	$\mathcal{R}_0$	$\mathbb{Z}$	0	0	0	$2\mathbb{Z}$	0	$\mathbb{Z}_2$	$\mathbb{Z}_2$
	$\mathrm{L_r}$	$\mathcal{R}_7$	0	0	0	$2\mathbb{Z}$	0	$\mathbb{Z}_2$	$\mathbb{Z}_2$	$\mathbb{Z}$
	$\mathrm{L_i}$	$\mathcal{C}_0$	$\mathbb{Z}$	0	$\mathbb{Z}$	0	$\mathbb{Z}$	0	$\mathbb{Z}$	0

Table A.5: Topological classification table for non-Hermitian systems in the real AZ† symmetry class [KSUS19]. Non-Hermitian topological phases are classified according to the AZ† symmetry class, the spatial dimensions d, and the definition of a complex-energy point (P) or line (L) gap. The subscript of L specifies the line gap for the real or imaginary part of the complex spectrum.

AZ† class	Gap	Classifying space	$d=0$	$d=1$	$d=2$	$d=3$	$d=4$	$d=5$	$d=6$	$d=7$
AI†	P	$\mathcal{R}_7$	0	0	0	$2\mathbb{Z}$	0	$\mathbb{Z}_2$	$\mathbb{Z}_2$	$\mathbb{Z}$
	L	$\mathcal{R}_0$	$\mathbb{Z}$	0	0	0	$2\mathbb{Z}$	0	$\mathbb{Z}_2$	$\mathbb{Z}_2$
BDI†	P	$\mathcal{R}_0$	$\mathbb{Z}$	0	0	0	$2\mathbb{Z}$	0	$\mathbb{Z}_2$	$\mathbb{Z}_2$
	$\mathrm{L_r}$	$\mathcal{R}_1$	$\mathbb{Z}_2$	$\mathbb{Z}$	0	0	0	$2\mathbb{Z}$	0	$\mathbb{Z}_2$
	$\mathrm{L_i}$	$\mathcal{R}_0\times\mathcal{R}_0$	$\mathbb{Z}\oplus\mathbb{Z}$	0	0	0	$2\mathbb{Z}\oplus2\mathbb{Z}$	0	$\mathbb{Z}_2\oplus\mathbb{Z}_2$	$\mathbb{Z}_2\oplus\mathbb{Z}_2$
D†	P	$\mathcal{R}_1$	$\mathbb{Z}_2$	$\mathbb{Z}$	0	0	0	$2\mathbb{Z}$	0	$\mathbb{Z}_2$
	$\mathrm{L_r}$	$\mathcal{R}_2$	$\mathbb{Z}_2$	$\mathbb{Z}_2$	$\mathbb{Z}$	0	0	0	$2\mathbb{Z}$	0
	$\mathrm{L_i}$	$\mathcal{R}_0$	$\mathbb{Z}$	0	0	0	$2\mathbb{Z}$	0	$\mathbb{Z}_2$	$\mathbb{Z}_2$
DIII†	P	$\mathcal{R}_2$	$\mathbb{Z}_2$	$\mathbb{Z}_2$	$\mathbb{Z}$	0	0	0	$2\mathbb{Z}$	0
	$\mathrm{L_r}$	$\mathcal{R}_3$	0	$\mathbb{Z}_2$	$\mathbb{Z}_2$	$\mathbb{Z}$	0	0	0	$2\mathbb{Z}$
	$\mathrm{L_i}$	$\mathcal{C}_0$	$\mathbb{Z}$	0	$\mathbb{Z}$	0	$\mathbb{Z}$	0	$\mathbb{Z}$	0
AII†	P	$\mathcal{R}_3$	0	$\mathbb{Z}_2$	$\mathbb{Z}_2$	$\mathbb{Z}$	0	0	0	$2\mathbb{Z}$
	L	$\mathcal{R}_4$	$2\mathbb{Z}$	0	$\mathbb{Z}_2$	$\mathbb{Z}_2$	$\mathbb{Z}$	0	0	0
CII†	P	$\mathcal{R}_4$	$2\mathbb{Z}$	0	$\mathbb{Z}_2$	$\mathbb{Z}_2$	$\mathbb{Z}$	0	0	0
	$\mathrm{L_r}$	$\mathcal{R}_5$	0	$2\mathbb{Z}$	0	$\mathbb{Z}_2$	$\mathbb{Z}_2$	$\mathbb{Z}$	0	0
	$\mathrm{L_i}$	$\mathcal{R}_4\times\mathcal{R}_4$	$2\mathbb{Z}\oplus2\mathbb{Z}$	0	$\mathbb{Z}_2\oplus\mathbb{Z}_2$	$\mathbb{Z}_2\oplus\mathbb{Z}_2$	$\mathbb{Z}\oplus\mathbb{Z}$	0	0	0
C†	P	$\mathcal{R}_5$	0	$2\mathbb{Z}$	0	$\mathbb{Z}_2$	$\mathbb{Z}_2$	$\mathbb{Z}$	0	0
	$\mathrm{L_r}$	$\mathcal{R}_6$	0	0	$2\mathbb{Z}$	0	$\mathbb{Z}_2$	$\mathbb{Z}_2$	$\mathbb{Z}$	0
	$\mathrm{L_i}$	$\mathcal{R}_4$	$2\mathbb{Z}$	0	$\mathbb{Z}_2$	$\mathbb{Z}_2$	$\mathbb{Z}$	0	0	0
CI†	P	$\mathcal{R}_6$	0	0	$2\mathbb{Z}$	0	$\mathbb{Z}_2$	$\mathbb{Z}_2$	$\mathbb{Z}$	0
	$\mathrm{L_r}$	$\mathcal{R}_7$	0	0	0	$2\mathbb{Z}$	0	$\mathbb{Z}_2$	$\mathbb{Z}_2$	$\mathbb{Z}$
	$\mathrm{L_i}$	$\mathcal{C}_0$	$\mathbb{Z}$	0	$\mathbb{Z}$	0	$\mathbb{Z}$	0	$\mathbb{Z}$	0

Table A.6: Topological classification table for non-Hermitian systems in the complex AZ symmetry class with sublattice symmetry (SLS) [KSUS19]. Non-Hermitian topological phases are classified according to the AZ symmetry class with additional SLS, the spatial dimensions d, and the definition of a complex-energy point (P) or line (L) gap. The subscript of $\mathcal{S}_\pm$ specifies the commutation (+) or anticommutation (−) relation to chiral symmetry: $\Gamma\mathcal{S}_\pm = \pm\mathcal{S}_\pm\Gamma$. The subscript of L specifies the line gap for the real or imaginary part of the complex spectrum.

SLS	AZ class	Gap	Classifying space	$d=0$	$d=1$	$d=2$	$d=3$	$d=4$	$d=5$	$d=6$	$d=7$
$\mathcal{S}_+$	AIII	P	$\mathcal{C}_1$	0	$\mathbb{Z}$	0	$\mathbb{Z}$	0	$\mathbb{Z}$	0	$\mathbb{Z}$
		$\mathrm{L_r}$	$\mathcal{C}_1\times\mathcal{C}_1$	0	$\mathbb{Z}\oplus\mathbb{Z}$	0	$\mathbb{Z}\oplus\mathbb{Z}$	0	$\mathbb{Z}\oplus\mathbb{Z}$	0	$\mathbb{Z}\oplus\mathbb{Z}$
		$\mathrm{L_i}$	$\mathcal{C}_1\times\mathcal{C}_1$	0	$\mathbb{Z}\oplus\mathbb{Z}$	0	$\mathbb{Z}\oplus\mathbb{Z}$	0	$\mathbb{Z}\oplus\mathbb{Z}$	0	$\mathbb{Z}\oplus\mathbb{Z}$
$\mathcal{S}$	A	P	$\mathcal{C}_1\times\mathcal{C}_1$	0	$\mathbb{Z}\oplus\mathbb{Z}$	0	$\mathbb{Z}\oplus\mathbb{Z}$	0	$\mathbb{Z}\oplus\mathbb{Z}$	0	$\mathbb{Z}\oplus\mathbb{Z}$
		L	$\mathcal{C}_1$	0	$\mathbb{Z}$	0	$\mathbb{Z}$	0	$\mathbb{Z}$	0	$\mathbb{Z}$
$\mathcal{S}_-$	AIII	P	$\mathcal{C}_0\times\mathcal{C}_0$	$\mathbb{Z}\oplus\mathbb{Z}$	0	$\mathbb{Z}\oplus\mathbb{Z}$	0	$\mathbb{Z}\oplus\mathbb{Z}$	0	$\mathbb{Z}\oplus\mathbb{Z}$	0
		$\mathrm{L_r}$	$\mathcal{C}_0$	$\mathbb{Z}$	0	$\mathbb{Z}$	0	$\mathbb{Z}$	0	$\mathbb{Z}$	0
		$\mathrm{L_i}$	$\mathcal{C}_0$	$\mathbb{Z}$	0	$\mathbb{Z}$	0	$\mathbb{Z}$	0	$\mathbb{Z}$	0

Table A.7: Topological classification table for non-Hermitian systems in the real AZ symmetry class with sublattice symmetry (SLS) [KSUS19]. Non-Hermitian topological phases are classified according to the AZ symmetry class with additional SLS, the spatial dimensions d, and the definition of a complex-energy point (P) or line (L) gap. The subscript of $\mathcal{S}$ specifies the commutation (+) or anticommutation (−) relation to time-reversal symmetry and/or particle-hole symmetry; for the symmetry classes that involve both time-reversal symmetry and particle-hole symmetry (BDI, DIII, CII, and CI), the first subscript specifies the relation to time-reversal symmetry and the second one to particle-hole symmetry. The subscript of L specifies the line gap for the real or imaginary part of the complex spectrum.

SLS	AZ class	Gap	Classifying space	$d=0$	$d=1$	$d=2$	$d=3$	$d=4$	$d=5$	$d=6$	$d=7$
$\mathcal{S}_{++}$	BDI	P	$\mathcal{R}_1$	$\mathbb{Z}_2$	$\mathbb{Z}$	0	0	0	$2\mathbb{Z}$	0	$\mathbb{Z}_2$
		$\mathrm{L_r}$	$\mathcal{R}_1\times\mathcal{R}_1$	$\mathbb{Z}_2\oplus\mathbb{Z}_2$	$\mathbb{Z}\oplus\mathbb{Z}$	0	0	0	$2\mathbb{Z}\oplus2\mathbb{Z}$	0	$\mathbb{Z}_2\oplus\mathbb{Z}_2$
		$\mathrm{L_i}$	$\mathcal{R}_1\times\mathcal{R}_1$	$\mathbb{Z}_2\oplus\mathbb{Z}_2$	$\mathbb{Z}\oplus\mathbb{Z}$	0	0	0	$2\mathbb{Z}\oplus2\mathbb{Z}$	0	$\mathbb{Z}_2\oplus\mathbb{Z}_2$
$\mathcal{S}_{--}$	DIII	P	$\mathcal{R}_3$	0	$\mathbb{Z}_2$	$\mathbb{Z}_2$	$\mathbb{Z}$	0	0	0	$2\mathbb{Z}$
		$\mathrm{L_r}$	$\mathcal{R}_3\times\mathcal{R}_3$	0	$\mathbb{Z}_2\oplus\mathbb{Z}_2$	$\mathbb{Z}_2\oplus\mathbb{Z}_2$	$\mathbb{Z}\oplus\mathbb{Z}$	0	0	0	$2\mathbb{Z}\oplus2\mathbb{Z}$
		$\mathrm{L_i}$	$\mathcal{C}_1$	0	$\mathbb{Z}$	0	$\mathbb{Z}$	0	$\mathbb{Z}$	0	$\mathbb{Z}$
$\mathcal{S}_{++}$	CII	P	$\mathcal{R}_5$	0	$2\mathbb{Z}$	0	$\mathbb{Z}_2$	$\mathbb{Z}_2$	$\mathbb{Z}$	0	0
		$\mathrm{L_r}$	$\mathcal{R}_5\times\mathcal{R}_5$	0	$2\mathbb{Z}\oplus2\mathbb{Z}$	0	$\mathbb{Z}_2\oplus\mathbb{Z}_2$	$\mathbb{Z}_2\oplus\mathbb{Z}_2$	$\mathbb{Z}\oplus\mathbb{Z}$	0	0
		$\mathrm{L_i}$	$\mathcal{R}_5\times\mathcal{R}_5$	0	$2\mathbb{Z}\oplus2\mathbb{Z}$	0	$\mathbb{Z}_2\oplus\mathbb{Z}_2$	$\mathbb{Z}_2\oplus\mathbb{Z}_2$	$\mathbb{Z}\oplus\mathbb{Z}$	0	0
$\mathcal{S}_{--}$	CI	P	$\mathcal{R}_7$	0	0	0	$2\mathbb{Z}$	0	$\mathbb{Z}_2$	$\mathbb{Z}_2$	$\mathbb{Z}$
		$\mathrm{L_r}$	$\mathcal{R}_7\times\mathcal{R}_7$	0	0	0	$2\mathbb{Z}\oplus2\mathbb{Z}$	0	$\mathbb{Z}_2\oplus\mathbb{Z}_2$	$\mathbb{Z}_2\oplus\mathbb{Z}_2$	$\mathbb{Z}\oplus\mathbb{Z}$
		$\mathrm{L_i}$	$\mathcal{C}_1$	0	$\mathbb{Z}$	0	$\mathbb{Z}$	0	$\mathbb{Z}$	0	$\mathbb{Z}$
$\mathcal{S}_{-}$	AI	P	$\mathcal{C}_1$	0	$\mathbb{Z}$	0	$\mathbb{Z}$	0	$\mathbb{Z}$	0	$\mathbb{Z}$
		$\mathrm{L_r}$	$\mathcal{R}_7$	0	0	0	$2\mathbb{Z}$	0	$\mathbb{Z}_2$	$\mathbb{Z}_2$	$\mathbb{Z}$
		$\mathrm{L_i}$	$\mathcal{R}_3$	0	$\mathbb{Z}_2$	$\mathbb{Z}_2$	$\mathbb{Z}$	0	0	0	$2\mathbb{Z}$
$\mathcal{S}_{-+}$	BDI	P	$\mathcal{C}_0$	$\mathbb{Z}$	0	$\mathbb{Z}$	0	$\mathbb{Z}$	0	$\mathbb{Z}$	0
		$\mathrm{L_r}$	$\mathcal{R}_0$	$\mathbb{Z}$	0	0	0	$2\mathbb{Z}$	0	$\mathbb{Z}_2$	$\mathbb{Z}_2$
		$\mathrm{L_i}$	$\mathcal{R}_2$	$\mathbb{Z}_2$	$\mathbb{Z}_2$	$\mathbb{Z}$	0	0	0	$2\mathbb{Z}$	0
$\mathcal{S}_{+}$	D	P	$\mathcal{C}_1$	0	$\mathbb{Z}$	0	$\mathbb{Z}$	0	$\mathbb{Z}$	0	$\mathbb{Z}$
		L	$\mathcal{R}_1$	$\mathbb{Z}_2$	$\mathbb{Z}$	0	0	0	$2\mathbb{Z}$	0	$\mathbb{Z}_2$
$\mathcal{S}_{-+}$	DIII	P	$\mathcal{C}_0$	$\mathbb{Z}$	0	$\mathbb{Z}$	0	$\mathbb{Z}$	0	$\mathbb{Z}$	0
		$\mathrm{L_r}$	$\mathcal{R}_2$	$\mathbb{Z}_2$	$\mathbb{Z}_2$	$\mathbb{Z}$	0	0	0	$2\mathbb{Z}$	0
		$\mathrm{L_i}$	$\mathcal{R}_0$	$\mathbb{Z}$	0	0	0	$2\mathbb{Z}$	0	$\mathbb{Z}_2$	$\mathbb{Z}_2$
$\mathcal{S}_{-}$	AII	P	$\mathcal{C}_1$	0	$\mathbb{Z}$	0	$\mathbb{Z}$	0	$\mathbb{Z}$	0	$\mathbb{Z}$
		$\mathrm{L_r}$	$\mathcal{R}_3$	0	$\mathbb{Z}_2$	$\mathbb{Z}_2$	$\mathbb{Z}$	0	0	0	$2\mathbb{Z}$
		$\mathrm{L_i}$	$\mathcal{R}_7$	0	0	0	$2\mathbb{Z}$	0	$\mathbb{Z}_2$	$\mathbb{Z}_2$	$\mathbb{Z}$
$\mathcal{S}_{-+}$	CII	P	$\mathcal{C}_0$	$\mathbb{Z}$	0	$\mathbb{Z}$	0	$\mathbb{Z}$	0	$\mathbb{Z}$	0
		$\mathrm{L_r}$	$\mathcal{R}_4$	$2\mathbb{Z}$	0	$\mathbb{Z}_2$	$\mathbb{Z}_2$	$\mathbb{Z}$	0	0	0
		$\mathrm{L_i}$	$\mathcal{R}_6$	0	0	$2\mathbb{Z}$	0	$\mathbb{Z}_2$	$\mathbb{Z}_2$	$\mathbb{Z}$	0
$\mathcal{S}_{+}$	C	P	$\mathcal{C}_1$	0	$\mathbb{Z}$	0	$\mathbb{Z}$	0	$\mathbb{Z}$	0	$\mathbb{Z}$
		L	$\mathcal{R}_5$	0	$2\mathbb{Z}$	0	$\mathbb{Z}_2$	$\mathbb{Z}_2$	$\mathbb{Z}$	0	0
$\mathcal{S}_{-+}$	CI	P	$\mathcal{C}_0$	$\mathbb{Z}$	0	$\mathbb{Z}$	0	$\mathbb{Z}$	0	$\mathbb{Z}$	0
		$\mathrm{L_r}$	$\mathcal{R}_6$	0	0	$2\mathbb{Z}$	0	$\mathbb{Z}_2$	$\mathbb{Z}_2$	$\mathbb{Z}$	0
		$\mathrm{L_i}$	$\mathcal{R}_4$	$2\mathbb{Z}$	0	$\mathbb{Z}_2$	$\mathbb{Z}_2$	$\mathbb{Z}$	0	0	0

continued on next page

TABLE A.7 — continued

$\mathcal{S}_{--}$	BDI	P	$\mathcal{R}_3$	0	$\mathbb{Z}_2$	$\mathbb{Z}_2$	$\mathbb{Z}$	0	0	0	$2\mathbb{Z}$
		L_r	$\mathcal{C}_1$	0	$\mathbb{Z}$	0	$\mathbb{Z}$	0	$\mathbb{Z}$	0	$\mathbb{Z}$
		L_i	$\mathcal{R}_3 \times \mathcal{R}_3$	0	$\mathbb{Z}_2 \oplus \mathbb{Z}_2$	$\mathbb{Z}_2 \oplus \mathbb{Z}_2$	$\mathbb{Z} \oplus \mathbb{Z}$	0	0	0	$2\mathbb{Z} \oplus 2\mathbb{Z}$
$\mathcal{S}_{++}$	DIII	P	$\mathcal{R}_5$	0	$2\mathbb{Z}$	0	$\mathbb{Z}_2$	$\mathbb{Z}_2$	$\mathbb{Z}$	0	0
		L_r	$\mathcal{C}_1$	0	$\mathbb{Z}$	0	$\mathbb{Z}$	0	$\mathbb{Z}$	0	$\mathbb{Z}$
		L_i	$\mathcal{C}_1$	0	$\mathbb{Z}$	0	$\mathbb{Z}$	0	$\mathbb{Z}$	0	$\mathbb{Z}$
$\mathcal{S}_{--}$	CII	P	$\mathcal{R}_7$	0	0	0	$2\mathbb{Z}$	0	$\mathbb{Z}_2$	$\mathbb{Z}_2$	$\mathbb{Z}$
		L_r	$\mathcal{C}_1$	0	$\mathbb{Z}$	0	$\mathbb{Z}$	0	$\mathbb{Z}$	0	$\mathbb{Z}$
		L_i	$\mathcal{R}_7 \times \mathcal{R}_7$	0	0	0	$2\mathbb{Z} \oplus 2\mathbb{Z}$	0	$\mathbb{Z}_2 \oplus \mathbb{Z}_2$	$\mathbb{Z}_2 \oplus \mathbb{Z}_2$	$\mathbb{Z} \oplus \mathbb{Z}$
$\mathcal{S}_{++}$	CI	P	$\mathcal{R}_1$	$\mathbb{Z}_2$	$\mathbb{Z}$	0	0	0	$2\mathbb{Z}$	0	$\mathbb{Z}_2$
		L_r	$\mathcal{C}_1$	0	$\mathbb{Z}$	0	$\mathbb{Z}$	0	$\mathbb{Z}$	0	$\mathbb{Z}$
		L_i	$\mathcal{C}_1$	0	$\mathbb{Z}$	0	$\mathbb{Z}$	0	$\mathbb{Z}$	0	$\mathbb{Z}$
$\mathcal{S}_{+}$	AI	P	$\mathcal{R}_1 \times \mathcal{R}_1$	$\mathbb{Z}_2 \oplus \mathbb{Z}_2$	$\mathbb{Z} \oplus \mathbb{Z}$	0	0	0	$2\mathbb{Z} \oplus 2\mathbb{Z}$	0	$\mathbb{Z}_2 \oplus \mathbb{Z}_2$
		L_r	$\mathcal{R}_1$	$\mathbb{Z}_2$	$\mathbb{Z}$	0	0	0	$2\mathbb{Z}$	0	$\mathbb{Z}_2$
		L_i	$\mathcal{R}_1$	$\mathbb{Z}_2$	$\mathbb{Z}$	0	0	0	$2\mathbb{Z}$	0	$\mathbb{Z}_2$
$\mathcal{S}_{+-}$	BDI	P	$\mathcal{R}_2 \times \mathcal{R}_2$	$\mathbb{Z}_2 \oplus \mathbb{Z}_2$	$\mathbb{Z}_2 \oplus \mathbb{Z}_2$	$\mathbb{Z} \oplus \mathbb{Z}$	0	0	0	$2\mathbb{Z} \oplus 2\mathbb{Z}$	0
		L_r	$\mathcal{R}_2$	$\mathbb{Z}_2$	$\mathbb{Z}_2$	$\mathbb{Z}$	0	0	0	$2\mathbb{Z}$	0
		L_i	$\mathcal{R}_2$	$\mathbb{Z}_2$	$\mathbb{Z}_2$	$\mathbb{Z}$	0	0	0	$2\mathbb{Z}$	0
$\mathcal{S}_{-}$	D	P	$\mathcal{R}_3 \times \mathcal{R}_3$	0	$\mathbb{Z}_2 \oplus \mathbb{Z}_2$	$\mathbb{Z}_2 \oplus \mathbb{Z}_2$	$\mathbb{Z} \oplus \mathbb{Z}$	0	0	0	$2\mathbb{Z} \oplus 2\mathbb{Z}$
		L	$\mathcal{R}_3$	0	$\mathbb{Z}_2$	$\mathbb{Z}_2$	$\mathbb{Z}$	0	0	0	$2\mathbb{Z}$
$\mathcal{S}_{+-}$	DIII	P	$\mathcal{R}_4 \times \mathcal{R}_4$	$2\mathbb{Z} \oplus 2\mathbb{Z}$	0	$\mathbb{Z}_2 \oplus \mathbb{Z}_2$	$\mathbb{Z}_2 \oplus \mathbb{Z}_2$	$\mathbb{Z} \oplus \mathbb{Z}$	0	0	0
		L_r	$\mathcal{R}_4$	$2\mathbb{Z}$	0	$\mathbb{Z}_2$	$\mathbb{Z}_2$	$\mathbb{Z}$	0	0	0
		L_i	$\mathcal{R}_4$	$2\mathbb{Z}$	0	$\mathbb{Z}_2$	$\mathbb{Z}_2$	$\mathbb{Z}$	0	0	0
$\mathcal{S}_{+}$	AII	P	$\mathcal{R}_5 \times \mathcal{R}_5$	0	$2\mathbb{Z} \oplus 2\mathbb{Z}$	0	$\mathbb{Z}_2 \oplus \mathbb{Z}_2$	$\mathbb{Z}_2 \oplus \mathbb{Z}_2$	$\mathbb{Z} \oplus \mathbb{Z}$	0	0
		L_r	$\mathcal{R}_5$	0	$2\mathbb{Z}$	0	$\mathbb{Z}_2$	$\mathbb{Z}_2$	$\mathbb{Z}$	0	0
		L_i	$\mathcal{R}_5$	0	$2\mathbb{Z}$	0	$\mathbb{Z}_2$	$\mathbb{Z}_2$	$\mathbb{Z}$	0	0
$\mathcal{S}_{+-}$	CII	P	$\mathcal{R}_6 \times \mathcal{R}_6$	0	0	$2\mathbb{Z} \oplus 2\mathbb{Z}$	0	$\mathbb{Z}_2 \oplus \mathbb{Z}_2$	$\mathbb{Z}_2 \oplus \mathbb{Z}_2$	$\mathbb{Z} \oplus \mathbb{Z}$	0
		L_r	$\mathcal{R}_6$	0	0	$2\mathbb{Z}$	0	$\mathbb{Z}_2$	$\mathbb{Z}_2$	$\mathbb{Z}$	0
		L_i	$\mathcal{R}_6$	0	0	$2\mathbb{Z}$	0	$\mathbb{Z}_2$	$\mathbb{Z}_2$	$\mathbb{Z}$	0
$\mathcal{S}_{-}$	C	P	$\mathcal{R}_7 \times \mathcal{R}_7$	0	0	0	$2\mathbb{Z} \oplus 2\mathbb{Z}$	0	$\mathbb{Z}_2 \oplus \mathbb{Z}_2$	$\mathbb{Z}_2 \oplus \mathbb{Z}_2$	$\mathbb{Z} \oplus \mathbb{Z}$
		L	$\mathcal{R}_7$	0	0	0	$2\mathbb{Z}$	0	$\mathbb{Z}_2$	$\mathbb{Z}_2$	$\mathbb{Z}$
$\mathcal{S}_{+-}$	CI	P	$\mathcal{R}_0 \times \mathcal{R}_0$	$\mathbb{Z} \oplus \mathbb{Z}$	0	0	0	$2\mathbb{Z} \oplus 2\mathbb{Z}$	0	$\mathbb{Z}_2 \oplus \mathbb{Z}_2$	$\mathbb{Z}_2 \oplus \mathbb{Z}_2$
		L_r	$\mathcal{R}_0$	$\mathbb{Z}$	0	0	0	$2\mathbb{Z}$	0	$\mathbb{Z}_2$	$\mathbb{Z}_2$
		L_i	$\mathcal{R}_0$	$\mathbb{Z}$	0	0	0	$2\mathbb{Z}$	0	$\mathbb{Z}_2$	$\mathbb{Z}_2$

Table A.8: Topological classification table for non-Hermitian systems in the complex AZ symmetry class with pseudo-Hermiticity (pH) [KSUS19]. Non-Hermitian topological phases are classified according to the AZ symmetry class with additional pH, the spatial dimensions d, and the definition of a complex-energy point (P) or line (L) gap. The subscript of $\eta_\pm$ specifies the commutation (+) or anticommutation (−) relation to chiral symmetry: $\Gamma\eta_\pm = \pm\eta_\pm\Gamma$. The subscript of L specifies the line gap for the real or imaginary part of the complex spectrum.

pH	AZ class	Gap	Classifying space	$d=0$	$d=1$	$d=2$	$d=3$	$d=4$	$d=5$	$d=6$	$d=7$
η	A	P	$\mathcal{C}_0$	$\mathbb{Z}$	0	$\mathbb{Z}$	0	$\mathbb{Z}$	0	$\mathbb{Z}$	0
		L_r	$\mathcal{C}_0 \times \mathcal{C}_0$	$\mathbb{Z} \oplus \mathbb{Z}$	0	$\mathbb{Z} \oplus \mathbb{Z}$	0	$\mathbb{Z} \oplus \mathbb{Z}$	0	$\mathbb{Z} \oplus \mathbb{Z}$	0
		L_i	$\mathcal{C}_1$	0	$\mathbb{Z}$	0	$\mathbb{Z}$	0	$\mathbb{Z}$	0	$\mathbb{Z}$
η_+	AIII	P	$\mathcal{C}_1$	0	$\mathbb{Z}$	0	$\mathbb{Z}$	0	$\mathbb{Z}$	0	$\mathbb{Z}$
		L_r	$\mathcal{C}_1 \times \mathcal{C}_1$	0	$\mathbb{Z} \oplus \mathbb{Z}$	0	$\mathbb{Z} \oplus \mathbb{Z}$	0	$\mathbb{Z} \oplus \mathbb{Z}$	0	$\mathbb{Z} \oplus \mathbb{Z}$
		L_i	$\mathcal{C}_1 \times \mathcal{C}_1$	0	$\mathbb{Z} \oplus \mathbb{Z}$	0	$\mathbb{Z} \oplus \mathbb{Z}$	0	$\mathbb{Z} \oplus \mathbb{Z}$	0	$\mathbb{Z} \oplus \mathbb{Z}$
η_-	AIII	P	$\mathcal{C}_0 \times \mathcal{C}_0$	$\mathbb{Z} \oplus \mathbb{Z}$	0	$\mathbb{Z} \oplus \mathbb{Z}$	0	$\mathbb{Z} \oplus \mathbb{Z}$	0	$\mathbb{Z} \oplus \mathbb{Z}$	0
		L_r	$\mathcal{C}_0$	$\mathbb{Z}$	0	$\mathbb{Z}$	0	$\mathbb{Z}$	0	$\mathbb{Z}$	0
		L_i	$\mathcal{C}_0$	$\mathbb{Z}$	0	$\mathbb{Z}$	0	$\mathbb{Z}$	0	$\mathbb{Z}$	0

Table A.9: Topological classification table for non-Hermitian systems in the real AZ symmetry class with pseudo-Hermiticity (pH) [KSUS19]. Non-Hermitian topological phases are classified according to the AZ symmetry class with additional pH, the spatial dimensions d, and the definition of a complex-energy point (P) or line (L) gap. The subscript of η specifies the commutation (+) or anticommutation (−) relation to time-reversal symmetry and/or particle-hole symmetry; for the symmetry classes that involve both time-reversal symmetry and particle-hole symmetry (BDI, DIII, CII, and CI), the first subscript specifies the relation to time-reversal symmetry and the second one to particle-hole symmetry. The subscript of L specifies the line gap for the real or imaginary part of the complex spectrum.

pH	AZ class	Gap	Classifying space	$d=0$	$d=1$	$d=2$	$d=3$	$d=4$	$d=5$	$d=6$	$d=7$
η_+	AI	P	$\mathcal{R}_0$	$\mathbb{Z}$	0	0	0	$2\mathbb{Z}$	0	$\mathbb{Z}_2$	$\mathbb{Z}_2$
		L_r	$\mathcal{R}_0 \times \mathcal{R}_0$	$\mathbb{Z}\oplus\mathbb{Z}$	0	0	0	$2\mathbb{Z}\oplus 2\mathbb{Z}$	0	$\mathbb{Z}_2\oplus\mathbb{Z}_2$	$\mathbb{Z}_2\oplus\mathbb{Z}_2$
		L_i	$\mathcal{R}_1$	$\mathbb{Z}_2$	$\mathbb{Z}$	0	0	0	$2\mathbb{Z}$	0	$\mathbb{Z}_2$
η_{++}	BDI	P	$\mathcal{R}_1$	$\mathbb{Z}_2$	$\mathbb{Z}$	0	0	0	$2\mathbb{Z}$	0	$\mathbb{Z}_2$
		L_r	$\mathcal{R}_1 \times \mathcal{R}_1$	$\mathbb{Z}_2\oplus\mathbb{Z}_2$	$\mathbb{Z}\oplus\mathbb{Z}$	0	0	0	$2\mathbb{Z}\oplus 2\mathbb{Z}$	0	$\mathbb{Z}_2\oplus\mathbb{Z}_2$
		L_i	$\mathcal{R}_1 \times \mathcal{R}_1$	$\mathbb{Z}_2\oplus\mathbb{Z}_2$	$\mathbb{Z}\oplus\mathbb{Z}$	0	0	0	$2\mathbb{Z}\oplus 2\mathbb{Z}$	0	$\mathbb{Z}_2\oplus\mathbb{Z}_2$
η_+	D	P	$\mathcal{R}_2$	$\mathbb{Z}_2$	$\mathbb{Z}_2$	$\mathbb{Z}$	0	0	0	$2\mathbb{Z}$	0
		L_r	$\mathcal{R}_2 \times \mathcal{R}_2$	$\mathbb{Z}_2\oplus\mathbb{Z}_2$	$\mathbb{Z}_2\oplus\mathbb{Z}_2$	$\mathbb{Z}\oplus\mathbb{Z}$	0	0	0	$2\mathbb{Z}\oplus 2\mathbb{Z}$	0
		L_i	$\mathcal{R}_1$	$\mathbb{Z}_2$	$\mathbb{Z}$	0	0	0	$2\mathbb{Z}$	0	$\mathbb{Z}_2$
η_{++}	DIII	P	$\mathcal{R}_3$	0	$\mathbb{Z}_2$	$\mathbb{Z}_2$	$\mathbb{Z}$	0	0	0	$2\mathbb{Z}$
		L_r	$\mathcal{R}_3 \times \mathcal{R}_3$	0	$\mathbb{Z}_2\oplus\mathbb{Z}_2$	$\mathbb{Z}_2\oplus\mathbb{Z}_2$	$\mathbb{Z}\oplus\mathbb{Z}$	0	0	0	$2\mathbb{Z}\oplus 2\mathbb{Z}$
		L_i	$\mathcal{C}_1$	0	$\mathbb{Z}$	0	$\mathbb{Z}$	0	$\mathbb{Z}$	0	$\mathbb{Z}$
η_+	AII	P	$\mathcal{R}_4$	$2\mathbb{Z}$	0	$\mathbb{Z}_2$	$\mathbb{Z}_2$	$\mathbb{Z}$	0	0	0
		L_r	$\mathcal{R}_4 \times \mathcal{R}_4$	$2\mathbb{Z}\oplus 2\mathbb{Z}$	0	$\mathbb{Z}_2\oplus\mathbb{Z}_2$	$\mathbb{Z}_2\oplus\mathbb{Z}_2$	$\mathbb{Z}\oplus\mathbb{Z}$	0	0	0
		L_i	$\mathcal{R}_5$	0	$2\mathbb{Z}$	0	$\mathbb{Z}_2$	$\mathbb{Z}_2$	$\mathbb{Z}$	0	0
η_{++}	CII	P	$\mathcal{R}_5$	0	$2\mathbb{Z}$	0	$\mathbb{Z}_2$	$\mathbb{Z}_2$	$\mathbb{Z}$	0	0
		L_r	$\mathcal{R}_5 \times \mathcal{R}_5$	0	$2\mathbb{Z}\oplus 2\mathbb{Z}$	0	$\mathbb{Z}_2\oplus\mathbb{Z}_2$	$\mathbb{Z}_2\oplus\mathbb{Z}_2$	$\mathbb{Z}\oplus\mathbb{Z}$	0	0
		L_i	$\mathcal{R}_5 \times \mathcal{R}_5$	0	$2\mathbb{Z}\oplus 2\mathbb{Z}$	0	$\mathbb{Z}_2\oplus\mathbb{Z}_2$	$\mathbb{Z}_2\oplus\mathbb{Z}_2$	$\mathbb{Z}\oplus\mathbb{Z}$	0	0
η_+	C	P	$\mathcal{R}_6$	0	0	$2\mathbb{Z}$	0	$\mathbb{Z}_2$	$\mathbb{Z}_2$	$\mathbb{Z}$	0
		L_r	$\mathcal{R}_6 \times \mathcal{R}_6$	0	0	$2\mathbb{Z}\oplus 2\mathbb{Z}$	0	$\mathbb{Z}_2\oplus\mathbb{Z}_2$	$\mathbb{Z}_2\oplus\mathbb{Z}_2$	$\mathbb{Z}\oplus\mathbb{Z}$	0
		L_i	$\mathcal{R}_5$	0	$2\mathbb{Z}$	0	$\mathbb{Z}_2$	$\mathbb{Z}_2$	$\mathbb{Z}$	0	0
η_{++}	CI	P	$\mathcal{R}_7$	0	0	0	$2\mathbb{Z}$	0	$\mathbb{Z}_2$	$\mathbb{Z}_2$	$\mathbb{Z}$
		L_r	$\mathcal{R}_7 \times \mathcal{R}_7$	0	0	0	$2\mathbb{Z}\oplus 2\mathbb{Z}$	0	$\mathbb{Z}_2\oplus\mathbb{Z}_2$	$\mathbb{Z}_2\oplus\mathbb{Z}_2$	$\mathbb{Z}\oplus\mathbb{Z}$
		L_i	$\mathcal{C}_1$	0	$\mathbb{Z}$	0	$\mathbb{Z}$	0	$\mathbb{Z}$	0	$\mathbb{Z}$
η_{+-}	BDI	P	$\mathcal{C}_0$	$\mathbb{Z}$	0	$\mathbb{Z}$	0	$\mathbb{Z}$	0	$\mathbb{Z}$	0
		L_r	$\mathcal{R}_0$	$\mathbb{Z}$	0	0	0	$2\mathbb{Z}$	0	$\mathbb{Z}_2$	$\mathbb{Z}_2$
		L_i	$\mathcal{R}_2$	$\mathbb{Z}_2$	$\mathbb{Z}_2$	$\mathbb{Z}$	0	0	0	$2\mathbb{Z}$	0
η_{-+}	DIII	P	$\mathcal{C}_0$	$\mathbb{Z}$	0	$\mathbb{Z}$	0	$\mathbb{Z}$	0	$\mathbb{Z}$	0
		L_r	$\mathcal{R}_2$	$\mathbb{Z}_2$	$\mathbb{Z}_2$	$\mathbb{Z}$	0	0	0	$2\mathbb{Z}$	0
		L_i	$\mathcal{R}_0$	$\mathbb{Z}$	0	0	0	$2\mathbb{Z}$	0	$\mathbb{Z}_2$	$\mathbb{Z}_2$
η_{+-}	CII	P	$\mathcal{C}_0$	$\mathbb{Z}$	0	$\mathbb{Z}$	0	$\mathbb{Z}$	0	$\mathbb{Z}$	0
		L_r	$\mathcal{R}_4$	$2\mathbb{Z}$	0	$\mathbb{Z}_2$	$\mathbb{Z}_2$	$\mathbb{Z}$	0	0	0
		L_i	$\mathcal{R}_6$	0	0	$2\mathbb{Z}$	0	$\mathbb{Z}_2$	$\mathbb{Z}_2$	$\mathbb{Z}$	0
η_{-+}	CI	P	$\mathcal{C}_0$	$\mathbb{Z}$	0	$\mathbb{Z}$	0	$\mathbb{Z}$	0	$\mathbb{Z}$	0
		L_r	$\mathcal{R}_6$	0	0	$2\mathbb{Z}$	0	$\mathbb{Z}_2$	$\mathbb{Z}_2$	$\mathbb{Z}$	0
		L_i	$\mathcal{R}_4$	$2\mathbb{Z}$	0	$\mathbb{Z}_2$	$\mathbb{Z}_2$	$\mathbb{Z}$	0	0	0

continued on next page

TABLE A.9 — continued

η_-	AI	P	$\mathcal{R}_2$	$\mathbb{Z}_2$	$\mathbb{Z}_2$	$\mathbb{Z}$	0	0	0	$2\mathbb{Z}$	0
		L_r	$\mathcal{C}_0$	$\mathbb{Z}$	0	$\mathbb{Z}$	0	$\mathbb{Z}$	0	$\mathbb{Z}$	0
		L_i	$\mathcal{R}_3$	0	$\mathbb{Z}_2$	$\mathbb{Z}_2$	$\mathbb{Z}$	0	0	0	$2\mathbb{Z}$
η_{--}	BDI	P	$\mathcal{R}_3$	0	$\mathbb{Z}_2$	$\mathbb{Z}_2$	$\mathbb{Z}$	0	0	0	$2\mathbb{Z}$
		L_r	$\mathcal{C}_1$	0	$\mathbb{Z}$	0	$\mathbb{Z}$	0	$\mathbb{Z}$	0	$\mathbb{Z}$
		L_i	$\mathcal{R}_3 \times \mathcal{R}_3$	0	$\mathbb{Z}_2 \oplus \mathbb{Z}_2$	$\mathbb{Z}_2 \oplus \mathbb{Z}_2$	$\mathbb{Z} \oplus \mathbb{Z}$	0	0	0	$2\mathbb{Z} \oplus 2\mathbb{Z}$
η_-	D	P	$\mathcal{R}_4$	$2\mathbb{Z}$	0	$\mathbb{Z}_2$	$\mathbb{Z}_2$	$\mathbb{Z}$	0	0	0
		L_r	$\mathcal{C}_0$	$\mathbb{Z}$	0	$\mathbb{Z}$	0	$\mathbb{Z}$	0	$\mathbb{Z}$	0
		L_i	$\mathcal{R}_3$	0	$\mathbb{Z}_2$	$\mathbb{Z}_2$	$\mathbb{Z}$	0	0	0	$2\mathbb{Z}$
η_{--}	DIII	P	$\mathcal{R}_5$	0	$2\mathbb{Z}$	0	$\mathbb{Z}_2$	$\mathbb{Z}_2$	$\mathbb{Z}$	0	0
		L_r	$\mathcal{C}_1$	0	$\mathbb{Z}$	0	$\mathbb{Z}$	0	$\mathbb{Z}$	0	$\mathbb{Z}$
		L_i	$\mathcal{C}_1$	0	$\mathbb{Z}$	0	$\mathbb{Z}$	0	$\mathbb{Z}$	0	$\mathbb{Z}$
η_-	AII	P	$\mathcal{R}_6$	0	0	$2\mathbb{Z}$	0	$\mathbb{Z}_2$	$\mathbb{Z}_2$	$\mathbb{Z}$	0
		L_r	$\mathcal{C}_0$	$\mathbb{Z}$	0	$\mathbb{Z}$	0	$\mathbb{Z}$	0	$\mathbb{Z}$	0
		L_i	$\mathcal{R}_7$	0	0	0	$2\mathbb{Z}$	0	$\mathbb{Z}_2$	$\mathbb{Z}_2$	$\mathbb{Z}$
η_{--}	CII	P	$\mathcal{R}_7$	0	0	0	$2\mathbb{Z}$	0	$\mathbb{Z}_2$	$\mathbb{Z}_2$	$\mathbb{Z}$
		L_r	$\mathcal{C}_1$	0	$\mathbb{Z}$	0	$\mathbb{Z}$	0	$\mathbb{Z}$	0	$\mathbb{Z}$
		L_i	$\mathcal{R}_7 \times \mathcal{R}_7$	0	0	0	$2\mathbb{Z} \oplus 2\mathbb{Z}$	0	$\mathbb{Z}_2 \oplus \mathbb{Z}_2$	$\mathbb{Z}_2 \oplus \mathbb{Z}_2$	$\mathbb{Z} \oplus \mathbb{Z}$
η_-	C	P	$\mathcal{R}_0$	$\mathbb{Z}$	0	0	0	$2\mathbb{Z}$	0	$\mathbb{Z}_2$	$\mathbb{Z}_2$
		L_r	$\mathcal{C}_0$	$\mathbb{Z}$	0	$\mathbb{Z}$	0	$\mathbb{Z}$	0	$\mathbb{Z}$	0
		L_i	$\mathcal{R}_7$	0	0	0	$2\mathbb{Z}$	0	$\mathbb{Z}_2$	$\mathbb{Z}_2$	$\mathbb{Z}$
η_{--}	CI	P	$\mathcal{R}_1$	$\mathbb{Z}_2$	$\mathbb{Z}$	0	0	0	$2\mathbb{Z}$	0	$\mathbb{Z}_2$
		L_r	$\mathcal{C}_1$	0	$\mathbb{Z}$	0	$\mathbb{Z}$	0	$\mathbb{Z}$	0	$\mathbb{Z}$
		L_i	$\mathcal{C}_1$	0	$\mathbb{Z}$	0	$\mathbb{Z}$	0	$\mathbb{Z}$	0	$\mathbb{Z}$
η_{-+}	BDI	P	$\mathcal{R}_2 \times \mathcal{R}_2$	$\mathbb{Z}_2 \oplus \mathbb{Z}_2$	$\mathbb{Z}_2 \oplus \mathbb{Z}_2$	$\mathbb{Z} \oplus \mathbb{Z}$	0	0	0	$2\mathbb{Z} \oplus 2\mathbb{Z}$	0
		L_r	$\mathcal{R}_2$	$\mathbb{Z}_2$	$\mathbb{Z}_2$	$\mathbb{Z}$	0	0	0	$2\mathbb{Z}$	0
		L_i	$\mathcal{R}_2$	$\mathbb{Z}_2$	$\mathbb{Z}_2$	$\mathbb{Z}$	0	0	0	$2\mathbb{Z}$	0
η_{+-}	DIII	P	$\mathcal{R}_4 \times \mathcal{R}_4$	$2\mathbb{Z} \oplus 2\mathbb{Z}$	0	$\mathbb{Z}_2 \oplus \mathbb{Z}_2$	$\mathbb{Z}_2 \oplus \mathbb{Z}_2$	$\mathbb{Z} \oplus \mathbb{Z}$	0	0	0
		L_r	$\mathcal{R}_4$	$2\mathbb{Z}$	0	$\mathbb{Z}_2$	$\mathbb{Z}_2$	$\mathbb{Z}$	0	0	0
		L_i	$\mathcal{R}_4$	$2\mathbb{Z}$	0	$\mathbb{Z}_2$	$\mathbb{Z}_2$	$\mathbb{Z}$	0	0	0
η_{-+}	CII	P	$\mathcal{R}_6 \times \mathcal{R}_6$	0	0	$2\mathbb{Z} \oplus 2\mathbb{Z}$	0	$\mathbb{Z}_2 \oplus \mathbb{Z}_2$	$\mathbb{Z}_2 \oplus \mathbb{Z}_2$	$\mathbb{Z} \oplus \mathbb{Z}$	0
		L_r	$\mathcal{R}_6$	0	0	$2\mathbb{Z}$	0	$\mathbb{Z}_2$	$\mathbb{Z}_2$	$\mathbb{Z}$	0
		L_i	$\mathcal{R}_6$	0	0	$2\mathbb{Z}$	0	$\mathbb{Z}_2$	$\mathbb{Z}_2$	$\mathbb{Z}$	0
η_{+-}	CI	P	$\mathcal{R}_0 \times \mathcal{R}_0$	$\mathbb{Z} \oplus \mathbb{Z}$	0	0	0	$2\mathbb{Z} \oplus 2\mathbb{Z}$	0	$\mathbb{Z}_2 \oplus \mathbb{Z}_2$	$\mathbb{Z}_2 \oplus \mathbb{Z}_2$
		L_r	$\mathcal{R}_0$	$\mathbb{Z}$	0	0	0	$2\mathbb{Z}$	0	$\mathbb{Z}_2$	$\mathbb{Z}_2$
		L_i	$\mathcal{R}_0$	$\mathbb{Z}$	0	0	0	$2\mathbb{Z}$	0	$\mathbb{Z}_2$	$\mathbb{Z}_2$

A.3 Exceptional points

Table A.10 provides the classification of exceptional points and non-Hermitian topological semimetals [KBS19]; see also Tables S2-S7 in Supplemental Material of Ref. [KBS19] for all the 38 symmetry classes. This periodic table specifies exceptional points and non-Hermitian topological semimetals in a general manner and describes their unconventional nodal structures.

Table A.10: Classification table of topologically stable exceptional points at generic momentum points [KBS19]. The codimensions p are defined as $p := d - d_{\mathrm{EP}}$ with the spatial dimensions d and the dimensions d_{EP} of the gapless region; exceptional points, lines, and surfaces are described by $d_{\mathrm{EP}} = 0, 1, 2$, respectively. Complex-energy gaps have two distinct types, a point (P) or line (L) gap, and the subscript of L specifies a line gap for the real or imaginary part of the complex spectrum. The sign of $\mathcal{PT}$ ($\mathcal{CP}$) symmetry means $(\mathcal{PT})\,(\mathcal{PT})^*$ [$(\mathcal{CP})\,(\mathcal{CP})^*$].

Symmetry	Gap	Classifying space	$p=0$	$p=1$	$p=2$	$p=3$	$p=4$	$p=5$	$p=6$	$p=7$
No	P	$\mathcal{C}_p$	$\mathbb{Z}$	0	$\mathbb{Z}$	0	$\mathbb{Z}$	0	$\mathbb{Z}$	0
	L	$\mathcal{C}_{p+1}$	0	$\mathbb{Z}$	0	$\mathbb{Z}$	0	$\mathbb{Z}$	0	$\mathbb{Z}$
Chiral	P	$\mathcal{C}_{p+1}$	0	$\mathbb{Z}$	0	$\mathbb{Z}$	0	$\mathbb{Z}$	0	$\mathbb{Z}$
	L_r	$\mathcal{C}_p$	$\mathbb{Z}$	0	$\mathbb{Z}$	0	$\mathbb{Z}$	0	$\mathbb{Z}$	0
	L_i	$\mathcal{C}_{p+1} \times \mathcal{C}_{p+1}$	0	$\mathbb{Z} \oplus \mathbb{Z}$	0	$\mathbb{Z} \oplus \mathbb{Z}$	0	$\mathbb{Z} \oplus \mathbb{Z}$	0	$\mathbb{Z} \oplus \mathbb{Z}$
Sublattice	P	$\mathcal{C}_p \times \mathcal{C}_p$	$\mathbb{Z} \oplus \mathbb{Z}$	0	$\mathbb{Z} \oplus \mathbb{Z}$	0	$\mathbb{Z} \oplus \mathbb{Z}$	0	$\mathbb{Z} \oplus \mathbb{Z}$	0
	L	$\mathcal{C}_p$	$\mathbb{Z}$	0	$\mathbb{Z}$	0	$\mathbb{Z}$	0	$\mathbb{Z}$	0
$\mathcal{PT}$, $+1$	P	$\mathcal{R}_p$	$\mathbb{Z}$	$\mathbb{Z}_2$	$\mathbb{Z}_2$	0	$2\mathbb{Z}$	0	0	0
	L_r	$\mathcal{R}_{p+7}$	0	$\mathbb{Z}$	$\mathbb{Z}_2$	$\mathbb{Z}_2$	0	$2\mathbb{Z}$	0	0
	L_i	$\mathcal{R}_{p+1}$	$\mathbb{Z}_2$	$\mathbb{Z}_2$	0	$2\mathbb{Z}$	0	0	0	$\mathbb{Z}$
$\mathcal{PT}$, -1	P	$\mathcal{R}_{p+4}$	$2\mathbb{Z}$	0	0	0	$\mathbb{Z}$	$\mathbb{Z}_2$	$\mathbb{Z}_2$	0
	L_r	$\mathcal{R}_{p+3}$	0	$2\mathbb{Z}$	0	0	0	$\mathbb{Z}$	$\mathbb{Z}_2$	$\mathbb{Z}_2$
	L_i	$\mathcal{R}_{p+5}$	0	0	0	$\mathbb{Z}$	$\mathbb{Z}_2$	$\mathbb{Z}_2$	0	$2\mathbb{Z}$
$\mathcal{CP}$, $+1$	P	$\mathcal{R}_{p+2}$	$\mathbb{Z}_2$	0	$2\mathbb{Z}$	0	0	0	$\mathbb{Z}$	$\mathbb{Z}_2$
	L	$\mathcal{R}_{p+1}$	$\mathbb{Z}_2$	$\mathbb{Z}_2$	0	$2\mathbb{Z}$	0	0	0	$\mathbb{Z}$
$\mathcal{CP}$, -1	P	$\mathcal{R}_{p+6}$	0	0	$\mathbb{Z}$	$\mathbb{Z}_2$	$\mathbb{Z}_2$	0	$2\mathbb{Z}$	0
	L	$\mathcal{R}_{p+5}$	0	0	0	$\mathbb{Z}$	$\mathbb{Z}_2$	$\mathbb{Z}_2$	0	$2\mathbb{Z}$

Appendix B

Non-Bloch band theory with symmetry

B.1 Derivation of the non-Bloch band theory in the symplectic class

We develop the non-Bloch band theory in the symplectic class in a general manner [KOS20]. We consider a generic non-Hermitian Hamiltonian described by

$$\hat{H} = \sum_{n} \sum_{j=-l}^{l} \sum_{\mu,\nu=1}^{q} \sum_{s,t\in\{\uparrow,\downarrow\}} H_{j,\mu\nu,st} \hat{c}^{\dagger}_{n+j,\mu,s} \hat{c}_{n,\nu,t}. \tag{B.1}$$

In comparison with the standard class discussed in Sec. 3.2, the indices $s, t \in \{\uparrow, \downarrow\}$ are added to Eq. (3.12) to account for the internal degrees of freedom arising from reciprocity in Eq. (4.7). A prime example of such internal degrees of freedom is the spin degrees of freedom. Correspondingly, the eigenstates are given by a linear combination of fundamental solutions

$$\sum_{n=1}^{L} |n\rangle \left(\beta_i^n |\phi_{i+}\rangle + \beta_i^{-n} |\phi_{i-}\rangle\right), \tag{B.2}$$

where $|\phi_{i\pm}\rangle$ can be expanded as

$$|\phi_{i\pm}\rangle \coloneqq \sum_{\mu=1}^{q} \sum_{s\in\{\uparrow,\downarrow\}} \phi_{\mu s}^{(i\pm)} |\mu\rangle |s\rangle, \tag{B.3}$$

and is a right eigenstate of $H(\beta_i^{\pm})$:

$$H(\beta_i^{\pm}) |\phi_{i\pm}\rangle = E |\phi_{i\pm}\rangle. \tag{B.4}$$

The corresponding left eigenstate $|\chi_{i\pm}\rangle$ of $H(\beta_i^{\pm})$ is defined by

$$H^{\dagger}(\beta_i^{\pm}) |\chi_{i\pm}\rangle = E^* |\chi_{i\pm}\rangle. \tag{B.5}$$

Here, $\{\pm\}$ reduces to $\{\uparrow, \downarrow\}$ in the absence of perturbations that mix $\uparrow$ and $\downarrow$, including spin-orbit interaction; however, $\{\pm\}$ does not necessarily reduce to $\{\uparrow, \downarrow\}$ in the presence of spin-orbit coupling. In addition, β_i's and β_i^{-1}'s ($i = 1, 2, \cdots, 2lq$) are the solutions to the characteristic equation

$$\det[H(\beta) - E] = 0. \tag{B.6}$$

Without loss of generality, they can be chosen to satisfy

$$|\beta_1| \leq \cdots \leq |\beta_{2lq}| \leq 1 \leq |\beta_{2lq}^{-1}| \leq \cdots \leq |\beta_1^{-1}|. \tag{B.7}$$

As described in Sec. 4.2.1, $|\phi_{i+}\rangle$ and $|\phi_{i-}\rangle$ are biorthogonal to each other and form a Kramers pair. Specifically, we have

$$|\phi_{i-}\rangle = \mathcal{T}\,|\chi_{i+}\rangle^*, \quad |\phi_{i+}\rangle = -\mathcal{T}\,|\chi_{i-}\rangle^* \tag{B.8}$$

under the appropriate choice of the gauges. Generally, the left eigenstates $|\chi_{i\pm}\rangle$'s are determined when the right eigenstates $|\phi_{i\pm}\rangle$'s are given, except for the arbitrariness of normalization [Bro14]. In this respect, Eq. (B.8) provides the normalization conditions of $|\chi_{i\pm}\rangle$'s. From these fundamental solutions, the right eigenstate $|\phi\rangle$ and the left eigenstate $|\chi\rangle$ in real space can be given as

$$|\phi\rangle = \sum_{i=1}^{2lq}\sum_{n=1}^{L} |n\rangle \left(\beta_i^n\,|\phi_{i+}\rangle + \beta_i^{-n}\,|\phi_{i-}\rangle\right), \tag{B.9}$$

$$|\chi\rangle = \sum_{i=1}^{2lq}\sum_{n=1}^{L} |n\rangle \left((\beta_i^*)^{-n}\,|\chi_{i+}\rangle + (\beta_i^*)^{n}\,|\chi_{i-}\rangle\right) \tag{B.10}$$

under the appropriate choice of gauges and normalization. In addition, we have from Eq. (B.8)

$$\mathcal{T}\,|\chi\rangle^* = \sum_{i=1}^{2lq}\sum_{n=1}^{L} |n\rangle \left(-\beta_i^n\,|\phi_{i+}\rangle + \beta_i^{-n}\,|\phi_{i-}\rangle\right), \tag{B.11}$$

which is the Kramers partner of $|\phi\rangle$ satisfying $\langle\chi|\mathcal{T}|\chi\rangle^* = 0$.

Generic eigenstates $|\phi\rangle$ and $\mathcal{T}\,|\chi\rangle^*$ in Eqs. (B.9) and (B.11) include $2lq \times 2 \times q \times 2$ unknown variables $\phi_{\mu s}^{(i\pm)}$ ($i = 1, 2, \cdots, 2lq$; $\mu = 1, 2, \cdots, q$; $s = \uparrow, \downarrow$) in Eq. (B.3). They reduce to $2lq \times 2$ unknown variables, for example, $\phi_{1\uparrow}^{(i\pm)}$, because of the Schrödinger equation (B.4) for the bulk Hamiltonian $H(\beta)$. Here, the rank of $H(\beta)$ is assumed appropriately in a manner similar to Ref. [YM19].

The $2lq \times 2$ unknown variables $\bar{\phi}_{i\pm} \coloneqq \phi_{1\uparrow}^{(i\pm)}$ ($i = 1, \cdots, 2lq$) are determined by boundary conditions. In general, the boundary conditions are given by details about the lq sites around each end. Hence, the boundary conditions for $|\phi\rangle$ can be represented by

$$\sum_{i=1}^{2lq} \left(f_j(\beta_i)\,\bar{\phi}_{i+} + f_j(\beta_i^{-1})\,\bar{\phi}_{i-}\right) = 0, \tag{B.12}$$

$$\sum_{i=1}^{2lq} \left(\beta_i^L g_j(\beta_i)\,\bar{\phi}_{i+} + \beta_i^{-L} g_j(\beta_i^{-1})\,\bar{\phi}_{i-}\right) = 0, \tag{B.13}$$

where $f_j(\beta_i)$ and $g_j(\beta_i)$ ($j = 1, 2, \cdots, 2lq$) are functions of β_i that do not depend on L. Importantly, the boundary conditions for the Kramers partner $\mathcal{T}\,|\chi\rangle^*$ are independent of the boundary conditions for $|\phi\rangle$, and should satisfy

$$\sum_{i=1}^{2lq} \left(-f_j(\beta_i)\,\bar{\phi}_{i+} + f_j(\beta_i^{-1})\,\bar{\phi}_{i-}\right) = 0, \tag{B.14}$$

$$\sum_{i=1}^{2lq} \left(-\beta_i^L g_j(\beta_i)\,\bar{\phi}_{i+} + \beta_i^{-L} g_j(\beta_i^{-1})\,\bar{\phi}_{i-}\right) = 0. \tag{B.15}$$

For example, when the eigenstates vanish at $n = 0$ and $n = L + 1$ in a manner similar to the example in Sec. 4.2.2, we have $\sum_{i=1}^{2lq} (|\phi_{i+}\rangle + |\phi_{i-}\rangle) = \sum_{i=1}^{2lq} (\beta_i^{L+1} |\phi_{i+}\rangle + \beta_i^{-(L+1)} |\phi_{i-}\rangle) = 0$ for $|\phi\rangle$, and $f_j(\beta_i)$ and $g_j(\beta_i)$ are given by $|\phi_{i\pm}\rangle$. Indeed, the boundary conditions (4.51) for the symplectic Hatano-Nelson model are described by these equations.

While we have $4lq$ unknown variables $\bar{\phi}_{i\pm}$, the boundary conditions (B.12)-(B.15) provide $8lq$ linear equations. This implies that Eqs. (B.12)-(B.15) are not linearly independent of each other because of some constraints on $f_j(\beta_i)$ and $g_j(\beta_i)$. To have such constraints, we notice from Eqs. (B.12) and (B.14)

$$\sum_{i=1}^{2lq} f_j(\beta_i) \bar{\phi}_{i+} = \sum_{i=1}^{2lq} f_j(\beta_i^{-1}) \bar{\phi}_{i-} = 0. \tag{B.16}$$

In matrix representation, we have

$$\begin{pmatrix} f_1(\beta_1^{\pm}) & \cdots & f_1(\beta_{2lq}^{\pm}) \\ \vdots & \ddots & \vdots \\ f_{2lq}(\beta_1^{\pm}) & \cdots & f_{2lq}(\beta_{2lq}^{\pm}) \end{pmatrix} \begin{pmatrix} \bar{\phi}_{1\pm} \\ \vdots \\ \bar{\phi}_{2lq\pm} \end{pmatrix} = 0. \tag{B.17}$$

To have a nontrivial solution, the $2lq \times 2lq$ coefficient matrix $F_\pm$ should not be invertible, i.e.,

$$\det F_\pm := \det \begin{pmatrix} f_1(\beta_1^{\pm}) & \cdots & f_1(\beta_{2lq}^{\pm}) \\ \vdots & \ddots & \vdots \\ f_{2lq}(\beta_1^{\pm}) & \cdots & f_{2lq}(\beta_{2lq}^{\pm}) \end{pmatrix} = 0. \tag{B.18}$$

Consistently, these constraints are respected in the specific example (i.e., symplectic Hatano-Nelson model) in Sec. 4.2.2 since $(\phi_\uparrow^{(1\pm)} \ \phi_\downarrow^{(1\pm)})^T$ and $(\phi_\uparrow^{(2\pm)} \ \phi_\downarrow^{(2\pm)})^T$ are linearly dependent on each other. The combination of Eqs. (B.13) and (B.15) yields similar constraints on $g_j(\beta_i)$.

Then, from Eqs. (B.12) and (B.13), we have

$$\begin{pmatrix} f_1(\beta_1) & \cdots & f_1(\beta_{2lq}) & f_1(\beta_1^{-1}) & \cdots & f_1(\beta_{2lq}^{-1}) \\ \vdots & \ddots & \vdots & \vdots & \ddots & \vdots \\ f_{2lq}(\beta_1) & \cdots & f_{2lq}(\beta_{2lq}) & f_{2lq}(\beta_1^{-1}) & \cdots & f_{2lq}(\beta_{2lq}^{-1}) \\ \beta_1^L g_1(\beta_1) & \cdots & \beta_{2lq}^L g_1(\beta_{2lq}) & \beta_1^{-L} g_1(\beta_1^{-1}) & \cdots & \beta_{2lq}^{-L} g_1(\beta_{2lq}^{-1}) \\ \vdots & \ddots & \vdots & \vdots & \ddots & \vdots \\ \beta_1^L g_{2lq}(\beta_1) & \cdots & \beta_{2lq}^L g_{2lq}(\beta_{2lq}) & \beta_1^{-L} g_{2lq}(\beta_1^{-1}) & \cdots & \beta_{2lq}^{-L} g_{2lq}(\beta_{2lq}^{-1}) \end{pmatrix} \begin{pmatrix} \bar{\phi}_{1+} \\ \vdots \\ \bar{\phi}_{2lq+} \\ \bar{\phi}_{1-} \\ \vdots \\ \bar{\phi}_{2lq-} \end{pmatrix} = 0. \tag{B.19}$$

To have a nontrivial solution, the $4lq \times 4lq$ coefficient matrix should not be invertible, i.e.,

$$\det \begin{pmatrix} f_1(\beta_1) & \cdots & f_1(\beta_{2lq}) & f_1(\beta_1^{-1}) & \cdots & f_1(\beta_{2lq}^{-1}) \\ \vdots & \ddots & \vdots & \vdots & \ddots & \vdots \\ f_{2lq}(\beta_1) & \cdots & f_{2lq}(\beta_{2lq}) & f_{2lq}(\beta_1^{-1}) & \cdots & f_{2lq}(\beta_{2lq}^{-1}) \\ \beta_1^L g_1(\beta_1) & \cdots & \beta_{2lq}^L g_1(\beta_{2lq}) & \beta_1^{-L} g_1(\beta_1^{-1}) & \cdots & \beta_{2lq}^{-L} g_1(\beta_{2lq}^{-1}) \\ \vdots & \ddots & \vdots & \vdots & \ddots & \vdots \\ \beta_1^L g_{2lq}(\beta_1) & \cdots & \beta_{2lq}^L g_{2lq}(\beta_{2lq}) & \beta_1^{-L} g_{2lq}(\beta_1^{-1}) & \cdots & \beta_{2lq}^{-L} g_{2lq}(\beta_{2lq}^{-1}) \end{pmatrix} = 0. \tag{B.20}$$

The determinant on the left-hand side is a $2lq$-th-order polynomial in terms of β_1^L, $\cdots$, β_{2lq}^L, β_{2lq}^{-L}, $\cdots$, β_1^{-L}. Because of Eq. (4.26), its leading-order term includes $(\beta_{2lq}^{-1}\beta_{2lq-1}^{-1}\cdots\beta_1^{-1})^L$

and the next-to-leading-order term includes $(\beta_{2lq}\beta_{2lq-1}^{-1}\beta_{2lq-2}^{-1}\cdots\beta_1^{-1})^L$, in general. To satisfy Eq. (B.20) for $L\to\infty$, the absolute values of these terms need to coincide with each other, which leads to the condition (3.20) for the standard case [YW18, YM19]. However, this is not the case in the symplectic class. In fact, the term including $(\beta_{2lq}^{-1}\beta_{2lq-1}^{-1}\cdots\beta_1^{-1})^L$ does not appear since it is proportional to $\det F_+$, which vanishes as shown in Eq. (B.18). As a result, the leading-order term includes $(\beta_{2lq}\beta_{2lq-1}^{-1}\beta_{2lq-2}^{-1}\cdots\beta_1^{-1})^L$ and the next-to-leading-order term includes $(\beta_{2lq-2}^{-1}\beta_{2lq-3}^{-1}\cdots\beta_1^{-1})^L$, both of which should be comparable to each other for $L\to\infty$. Therefore, it is necessary to have

$$|\beta_{2lq}\beta_{2lq-1}^{-1}\beta_{2lq-2}^{-1}\cdots\beta_1^{-1}| = |\beta_{2lq-2}^{-1}\beta_{2lq-3}^{-1}\cdots\beta_1^{-1}|, \tag{B.21}$$

leading to $|\beta_{2lq-1}| = |\beta_{2lq}|$, i.e., Eq. (4.10) with $M \coloneqq lq$.

B.2 Infinitesimal instability

The nonstandard non-Bloch band theory is relevant solely in the presence of symplectic reciprocity in Eq. (4.7). Because of this symmetry-protected nature, continuum bands in the symplectic class are fragile against a reciprocity-breaking perturbation, even if it is infinitesimal. As shown in Appendix B.1, reciprocity forbids the term proportional to $(\beta_{2M}^{-1}\beta_{2M-1}^{-1}\cdots\beta_1^{-1})^L$ for the boundary conditions. However, if we break reciprocity, such a term generally appears and becomes the leading-order term, and the standard non-Bloch band theory characterizes continuum bands.

Now, let $\epsilon>0$ be a degree of the reciprocity-breaking perturbation. Since the leading-order term $\epsilon\,(\beta_{2M}^{-1}\beta_{2M-1}^{-1}\cdots\beta_1^{-1})^L$ and the next-to-leading-order term $(\beta_{2M}\beta_{2M-1}^{-1}\cdots\beta_1^{-1})^L$ should be comparable to each other for continuum bands, we have

$$\epsilon\,|\beta_{2M}^{-1}\beta_{2M-1}^{-1}\cdots\beta_1^{-1}|^L = |\beta_{2M}\beta_{2M-1}^{-1}\cdots\beta_1^{-1}|^L. \tag{B.22}$$

Thus, for $L\to\infty$, we indeed have $|\beta_{2M}^{-1}| = |\beta_{2M}|$, i.e., Eq. (4.10). This condition is respected even for infinitesimal but nonzero $\epsilon>0$. More precisely, the reciprocity-breaking perturbation should at least exceed $\epsilon\sim\mathcal{O}\left(|\beta_{2M}|^{2L}\right)$ to satisfy Eq. (B.22). Notably, the order of the two limits $L\to\infty$ and $\epsilon\to0$ plays a decisive role. If we take $L\to\infty$ first, the standard non-Bloch band theory is relevant even for $\epsilon\to0$. By contrast, if we take $\epsilon\to0$ first, the left-hand side of Eq. (B.22) vanishes and Eq. (B.22) cannot be satisfied even for $L\to\infty$, resulting in the nonstandard non-Bloch band theory in the symplectic class.

For example, let us add a reciprocity-breaking perturbation to the symplectic Hatano-Nelson model. Physically, such a perturbation can be a magnetic field. In the absence of the perturbation, the characteristic equation is quartic and the four solutions $\beta_1,\beta_2,\beta_1^{-1},\beta_2^{-1}$ come in Kramers pairs, as investigated in Sec. 4.2.2. For $|g|>|\Delta|$, we have

$$|\beta_1| = |\beta_2| \neq 1 \neq |\beta_1^{-1}| = |\beta_2^{-1}|, \tag{B.23}$$

which is consistent with the continuum-band condition (4.10) in the symplectic class. In the presence of the perturbation, on the other hand, Eq. (3.20) of the standard non-Bloch band theory is relevant, as described above. However, Eq. (B.23) does not satisfy Eq. (3.20). As a result, the continuum bands make a dramatic difference. Even the non-Hermitian skin effect can vanish because of such an infinitesimal perturbation [OKSS20].

B.3 Other symmetry classes

B.3.1 Symplectic class with additional symmetry

We have demonstrated that the non-Bloch band theory is altered by symplectic reciprocity in Eq. (4.7). In the 38-fold classification of internal-symmetry classes [KSUS19], the simplest symmetry class relevant to this nonstandard non-Bloch band theory is class AII†, in which only symplectic reciprocity is present. The nonstandard non-Bloch band theory replaces the standard one also in other symmetry classes, as long as symplectic reciprocity is respected. For example, it is relevant even in the presence of additional sublattice symmetry $\mathcal{S}$ or pseudo-Hermiticity η. The possible symmetry classes are classified in Sec. 4.3 [OKSS20, Shi19] on the basis of the relationship between the intrinsic non-Hermitian topology and skin effects. In addition to class AII†, such symmetry classes include class DIII†, class C with $\mathcal{S}_+$, class AI with η_-, class CI with $\mathcal{S}_{++}$ or η_{--}, class BDI with $\mathcal{S}_{+-}$ or η_{-+}, and class D with $\mathcal{S}_-$ (see Tables 4.1, 4.2, and 4.3).

It should be noted that certain symmetry leads to real-valued wave numbers and restores the conventional Bloch band theory. For example, reciprocity without internal degrees of freedom leads to the absence of skin effects and replaces the non-Bloch band theory with the Bloch band theory, as discussed in Sec. 4.2.1. In a similar manner, certain additional symmetry can replace the nonstandard non-Bloch band theory with the conventional Bloch band theory even in the presence of symplectic reciprocity.

B.3.2 Particle-hole symmetry

Another important internal symmetry is particle-hole symmetry, which is defined by

$$\mathcal{C}H^T\mathcal{C}^{-1} = -H, \quad \mathcal{C}\mathcal{C}^* = \pm 1, \tag{B.24}$$

with a unitary matrix $\mathcal{C}$. This symmetry is generally relevant to non-Hermitian superconductors. For $\mathcal{C}\mathcal{C}^* = +1$ (-1), non-Hermitian Hamiltonians are defined to belong to class D (C) [KSUS19]. In terms of the bulk Hamiltonian $H(\beta)$, it imposes

$$\mathcal{C}H^T(\beta)\mathcal{C}^{-1} = -H(\beta^{-1}). \tag{B.25}$$

Now, let $E \in \mathbb{C}$ be eigenenergy of $H(\beta)$ and $|\phi\rangle$ $(|\chi\rangle)$ be the corresponding right (left) eigenstate. Then, we have

$$H(\beta^{-1})(\mathcal{C}|\chi\rangle^*) = -E(\mathcal{C}|\chi\rangle^*), \tag{B.26}$$

which means that $\mathcal{C}|\chi\rangle^*$ is an eigenstate of $H(\beta^{-1})$ with the eigenenergy $-E$. Hence, particle-hole symmetry generally creates opposite-eigenenergy pairs $(E, -E)$. This is to be contrasted with reciprocity, which imposes a constraint on each eigenenergy.

Still, particle-hole symmetry makes zero energy $E = 0$ special and imposes a constraint on zero-energy states. In particular, the zero-energy states do not exhibit skin effects for $\mathcal{C}\mathcal{C}^* = +1$ (class D). To see this, we focus on the characteristic equation $\det[H(\beta) - E] = 0$. Because of particle-hole symmetry, we have

$$\begin{aligned}\det\left[H(\beta^{-1}) - E\right] &= \det\left[-\mathcal{C}H^T(\beta)\mathcal{C}^{-1} - E\right] \\ &= \det\left[-H(\beta) - E\right].\end{aligned} \tag{B.27}$$

For generic $E \in \mathbb{C}$, this equation does not have direct relationships with the original characteristic equation $\det[H(\beta) - E] = 0$. For $E = 0$, however, we have

$$\det[H(\beta^{-1})] = \det[H(\beta)] = 0, \tag{B.28}$$

which implies that β^{-1} is another solution to the characteristic equation with $E = 0$. Thus, similarly to the orthogonal class discussed in Sec. 4.2.1, zero-energy states are delocalized and no skin effects occur in the presence of particle-hole symmetry. It should be stressed that this discussion does not necessarily mean delocalization of generic eigenstates with $E \neq 0$ even if the Hamiltonian respects particle-hole symmetry. Furthermore, it is applicable only to zero modes in continuum bands, and Majorana zero modes isolated from continuum bands can be localized.

For $\mathcal{C}\mathcal{C}^* = -1$ (class C), on the other hand, $|\phi\rangle$ and $\mathcal{C}\,|\chi\rangle^*$ with $E = 0$ form a Kramers pair, and the above discussions are not applicable in a manner similar to the symplectic class. Consequently, the zero-energy states, if present, should be described by the nonstandard non-Bloch band theory. We note, however, that such zero-energy skin states may be forbidden to appear in continuum bands for a different reason. Actually, in one-dimensional systems in class C, no zero-energy skin state is protected by intrinsic non-Hermitian topology (see Table 4.1 in Sec. 4.3). The non-Bloch band theory and the skin effects in non-Hermitian superconductors need further study, which we leave for future work.

B.3.3 Commutative unitary symmetry and spatial symmetry

A similar modification of the non-Bloch band theory can arise from symmetry that is not included in the 38-fold internal symmetry. For example, when unitary symmetry that commutes with the Hamiltonian is present, the Hamiltonian is block diagonal in the eigenbasis of the symmetry:

$$H(\beta) = \bigoplus_i H_i(\beta)\,. \tag{B.29}$$

The symplectic Hatano-Nelson model discussed in Sec. 4.2.2 respects such unitary symmetry for $\Delta = 0$. Physically, this means conservation of spin due to the absence of spin-orbit coupling. In this case, $H_i(\beta)$'s do not interact with each other. Consequently, the non-Bloch band theory should be applied not to the original Hamiltonian $H(\beta)$ but to each subspace $H_i(\beta)$. Similarly to the symplectic class discussed in Appendix B.2, non-Hermitian systems with commutative unitary symmetry are fragile even against an infinitesimal perturbation.

Spatial symmetry can also change the non-Bloch band theory. For example, Ref. [RHS19] found a reciprocal skin effect in the presence of reflection symmetry. We point out that this reflection-symmetry-protected skin effect should be accompanied by a modification of the standard non-Bloch band theory similarly to symplectic reciprocity. Our nonstandard non-Bloch band theory in the symplectic class can further be modified in the presence of such additional symmetry.

Appendix C

Exact corner and edge modes

C.1 Corner skin modes

We exactly solve the non-Hermitian Hamiltonian in Eq. (4.66) with open boundaries along both x and y directions. In particular, we obtain the corner skin modes in an analytical manner. Let $E \in \mathbb{C}$ be eigenenergy, and $\vec{\psi}\,(m,n) \in \mathbb{C}^2$ be the component of the corresponding eigenstate at the lattice site $(m,n) \in [1,L]^2$. Because of periodicity of the bulk, as well as transposition-associated mirror symmetry in Eqs. (4.76) and (4.77), $\vec{\psi}\,(m,n)$ can be described as

$$\vec{\psi}\,(m,n) = \beta_x^m \beta_y^n \vec{v}_{++} + \beta_x^m \beta_y^{L+1-n} \vec{v}_{+-} + \beta_x^{L+1-m} \beta_y^n \vec{v}_{-+} + \beta_x^{L+1-m} \beta_y^{L+1-n} \vec{v}_{--} \tag{C.1}$$

with $\beta_x, \beta_y \in \mathbb{C}$ and $\vec{v}_{\pm\pm} \in \mathbb{C}^2$. The normalization of $\vec{\psi}\,(m,n)$ requires $|\beta_x| \leq 1$ and $|\beta_y| \leq 1$.

In the bulk, the Schrödinger equation reads

$$\begin{aligned} M\vec{\psi}\,(m,n) + T_{x+}\vec{\psi}\,(m-1,n) + T_{x-}\vec{\psi}\,(m+1,n) \\ + T_{y+}\vec{\psi}\,(m,n-1) + T_{y-}\vec{\psi}\,(m,n+1) = E\,\vec{\psi}\,(m,n) \end{aligned} \tag{C.2}$$

with

$$M \coloneqq -\mathrm{i}\gamma + \gamma\sigma_y, \tag{C.3}$$

$$T_{x\pm} \coloneqq \frac{\mathrm{i}\lambda\,(-1 \pm \sigma_z)}{2}, \tag{C.4}$$

$$T_{y\pm} \coloneqq \frac{\lambda\,(\sigma_y \pm \mathrm{i}\sigma_x)}{2}. \tag{C.5}$$

With Eq. (C.1), the bulk equation leads to

$$H\,(\beta_x^{\pm 1}, \beta_y^{\pm 1})\,\vec{v}_{\pm\pm} = E\,\vec{v}_{\pm\pm}, \tag{C.6}$$

where $H\,(\beta_x, \beta_y)$ is the bulk Hamiltonian

$$H\,(\beta_x, \beta_y) = -\mathrm{i} \begin{pmatrix} \gamma + \lambda\beta_x & \gamma + \lambda\beta_y \\ -\gamma - \lambda\beta_y^{-1} & \gamma + \lambda\beta_x^{-1} \end{pmatrix}. \tag{C.7}$$

At the boundaries, on the other hand, the Schrödinger equation reads

$$T_{x+}\vec{\psi}\,(0,n) = 0, \tag{C.8}$$

$$T_{x-}\vec{\psi}\,(L+1,n) = 0, \tag{C.9}$$

$$T_{y+}\vec{\psi}\,(m,0) = 0, \tag{C.10}$$

$$T_{y-}\vec{\psi}\,(m,L+1) = 0, \tag{C.11}$$

with $m, n = 1, 2, \cdots, L$. With Eq. (C.1), these boundary equations reduce to

$$T_{x+}\left(\vec{v}_{++} + \beta_x^{L+1}\vec{v}_{-+}\right) = T_{x+}\left(\vec{v}_{+-} + \beta_x^{L+1}\vec{v}_{--}\right) = 0, \tag{C.12}$$
$$T_{x-}\left(\beta_x^{L+1}\vec{v}_{++} + \vec{v}_{-+}\right) = T_{x-}\left(\beta_x^{L+1}\vec{v}_{+-} + \vec{v}_{--}\right) = 0, \tag{C.13}$$
$$T_{y+}\left(\vec{v}_{++} + \beta_y^{L+1}\vec{v}_{+-}\right) = T_{y-}\left(\vec{v}_{-+} + \beta_y^{L+1}\vec{v}_{--}\right) = 0, \tag{C.14}$$
$$T_{y+}\left(\beta_y^{L+1}\vec{v}_{++} + \vec{v}_{+-}\right) = T_{y-}\left(\beta_y^{L+1}\vec{v}_{-+} + \vec{v}_{--}\right) = 0. \tag{C.15}$$

Now, we express $\vec{v}_{\pm\pm}$ as $\vec{v}_{\pm\pm} = (a_{\pm\pm} \;\; b_{\pm\pm})^T$. Then, these boundary equations reduce to

$$b_{++} + \beta_x^{L+1} b_{-+} = b_{+-} + \beta_x^{L+1} b_{--} = 0, \tag{C.16}$$
$$\beta_x^{L+1} a_{++} + a_{-+} = \beta_x^{L+1} a_{+-} + a_{--} = 0, \tag{C.17}$$
$$a_{++} + \beta_y^{L+1} a_{+-} = a_{-+} + \beta_y^{L+1} a_{--} = 0, \tag{C.18}$$
$$\beta_y^{L+1} b_{++} + b_{+-} = \beta_y^{L+1} b_{-+} + b_{--} = 0, \tag{C.19}$$

which are further simplified to

$$\frac{a_{+-}}{a_{++}} = \left(\frac{b_{+-}}{b_{++}}\right)^{-1} = -\beta_y^{-L-1}, \tag{C.20}$$
$$\frac{a_{-+}}{a_{++}} = \left(\frac{b_{-+}}{b_{++}}\right)^{-1} = -\beta_x^{L+1}, \tag{C.21}$$
$$\frac{a_{--}}{a_{++}} = \left(\frac{b_{--}}{b_{++}}\right)^{-1} = \beta_x^{L+1}\beta_y^{-L-1}. \tag{C.22}$$

Meanwhile, since $\vec{v}_{++}$ ($\vec{v}_{-+}$) is an eigenstate of $H(\beta_x, \beta_y)$ [$H(\beta_x^{-1}, \beta_y)$] from Eq. (C.6), we have

$$(\gamma + \lambda\beta_x - \mathrm{i}E)\, a_{++} + (\gamma + \lambda\beta_y)\, b_{++} = 0, \tag{C.23}$$
$$\left(\gamma + \lambda\beta_x^{-1} - \mathrm{i}E\right) a_{-+} + (\gamma + \lambda\beta_y)\, b_{-+} = 0. \tag{C.24}$$

Using Eq. (C.21), we have

$$\begin{pmatrix} \gamma + \lambda\beta_x - \mathrm{i}E & \gamma + \lambda\beta_y \\ \beta_x^{L+1}\left(\gamma + \lambda\beta_x^{-1} - \mathrm{i}E\right) & \beta_x^{-L-1}\left(\gamma + \lambda\beta_y\right) \end{pmatrix} \begin{pmatrix} a_{++} \\ b_{++} \end{pmatrix} = 0. \tag{C.25}$$

To have a nontrivial solution $(a_{++} \;\; b_{++}) \neq 0$, the determinant of the coefficient matrix should vanish, which results in

$$\beta_y = -\frac{\gamma}{\lambda} \tag{C.26}$$

or

$$\frac{\mathrm{i}E - \gamma}{\lambda} = \frac{\beta_x^L - \beta_x^{-L}}{\beta_x^{L+1} - \beta_x^{-L-1}}. \tag{C.27}$$

Similarly, since $\vec{v}_{++}$ ($\vec{v}_{+-}$) is an eigenstate of $H(\beta_x, \beta_y)$ [$H\left(\beta_x, \beta_y^{-1}\right)$] from Eq. (C.6), we have

$$E = -\mathrm{i}\left(\gamma + \lambda\beta_x\right) \tag{C.28}$$

or

$$-\frac{\gamma}{\lambda} = \frac{\beta_y^L - \beta_y^{-L}}{\beta_y^{L+1} - \beta_y^{-L-1}}. \tag{C.29}$$

Furthermore, since $\vec{v}_{++}$ ($\vec{v}_{--}$) is an eigenstate of $H(\beta_x, \beta_y)$ [$H(\beta_x^{-1}, \beta_y^{-1})$] from Eq. (C.6), we have

$$\begin{pmatrix} \gamma + \lambda\beta_x - \mathrm{i}E & \gamma + \lambda\beta_y \\ \beta_x^{2(L+1)}(\gamma + \lambda\beta_y) & -\beta_y^{2(L+1)}(\gamma + \lambda\beta_x - \mathrm{i}E) \end{pmatrix} \begin{pmatrix} a_{++} \\ b_{++} \end{pmatrix} = 0, \tag{C.30}$$

resulting in

$$\beta_x^{2(L+1)}(\gamma + \lambda\beta_y)^2 = -\beta_y^{2(L+1)}(\gamma + \lambda\beta_x - \mathrm{i}E)^2. \tag{C.31}$$

Importantly, we need

$$|\beta_x| = |\beta_y| \tag{C.32}$$

so that the above equation will hold for sufficiently large L.

The corner skin modes are described by Eq. (C.28). If Eq. (C.27) holds in addition to Eq. (C.28), we have $\beta_x = \pm 1$. Then, we also have $E = -\mathrm{i}(\gamma \pm \lambda)$ and $\beta_y = -\lambda/\gamma, -\gamma/\lambda$, which further leads to $|\gamma| = |\lambda|$ from Eq. (C.32). Hence, we have Eq. (C.26) as long as Eq. (C.28) and $|\gamma| \neq |\lambda|$ holds. Because of the normalization condition $|\beta_y| < 1$, we need

$$\left|\frac{\gamma}{\lambda}\right| < 1. \tag{C.33}$$

Equations (C.26) and (C.28) lead to

$$H(\beta_x, \beta_y) - E = -\mathrm{i}\begin{pmatrix} 0 & 0 \\ (\lambda^2 - \gamma^2)/\gamma & -\lambda(\beta_x - \beta_x^{-1}) \end{pmatrix}, \tag{C.34}$$

$$H(\beta_x^{-1}, \beta_y^{-1}) - E = \mathrm{i}\begin{pmatrix} \lambda(\beta_x - \beta_x^{-1}) & (\lambda^2 - \gamma^2)/\gamma \\ 0 & 0 \end{pmatrix}. \tag{C.35}$$

Since $(a_{++} \;\; b_{++})$ and $(a_{--} \;\; b_{--}) \propto (\beta_x^{2(L+1)} a_{++} \;\; \beta_y^{2(L+1)} b_{++})$ are eigenstates of $H(\beta_x, \beta_y)$ and $H(\beta_x^{-1}, \beta_y^{-1})$, respectively, we have

$$\begin{pmatrix} (\lambda^2 - \gamma^2)/\gamma & -\lambda(\beta_x - \beta_x^{-1}) \\ \beta_x^{2(L+1)}\lambda(\beta_x - \beta_x^{-1}) & \beta_y^{2(L+1)}(\lambda^2 - \gamma^2)/\gamma \end{pmatrix} \begin{pmatrix} a_{++} \\ b_{++} \end{pmatrix} = 0, \tag{C.36}$$

which leads to

$$(\beta_x - \beta_x^{-1})^2 \left(\frac{\beta_x}{\beta_y}\right)^{2(L+1)} = -\left(\frac{\lambda^2 - \gamma^2}{\lambda\gamma}\right)^2. \tag{C.37}$$

To satisfy this equation for sufficiently large L, we need $|\beta_x/\beta_y| = 1$, i.e., Eq. (C.32). Furthermore, the phase of β_x is quantized by this equation. Since we have $|\beta_x| = |\beta_y| \neq 1$, the eigenstates are localized at the corners, and the skin effect occurs. The spectrum of these corner skin modes is

$$E = -\mathrm{i}\gamma\left(1 + e^{\mathrm{i}\theta}\right), \quad \theta \in [0, 2\pi], \tag{C.38}$$

and their number is $2L$.

On the other hand, the eigenstates described by Eq. (C.29) are delocalized through the bulk. With $\beta_y = e^{\mathrm{i}k_y}$, Eq. (C.29) reduces to

$$-\frac{\gamma}{\lambda} = \frac{\sin(k_y L)}{\sin(k_y(L+1))}, \tag{C.39}$$

which quantizes the wave number $k_y \in [0, 2\pi]$. We have L real solutions in $k_y \in [0, \pi]$ for $|\gamma/\lambda| > 1$; all the $2L^2$ eigenstates do not exhibit the skin effect and are delocalized through the bulk. For $|\gamma/\lambda| < 1$, on the other hand, we have $L - 1$ real solutions in $k_y \in [0, \pi]$; the corresponding $2L(L-1)$ eigenstates are delocalized, while the other $2L$ eigenstates are the corner skin modes.

C.2 Edge modes

C.2.1 Open boundary conditions along the y direction

We consider the non-Hermitian Hamiltonian in Eq. (4.66), imposing the open boundary conditions along the y direction and the periodic boundary conditions along the x direction. The Schrödinger equation is given as

$$M_{k_x}\vec{\psi}\,(n)+T_{y+}\vec{\psi}\,(n-1)+T_{y-}\vec{\psi}\,(n+1)=E\,\vec{\psi}\,(n) \tag{C.40}$$

in the bulk ($n=2,3,\cdots,L-1$), and

$$M_{k_x}\vec{\psi}\,(1)+T_{y-}\vec{\psi}\,(2)=E\,\vec{\psi}\,(1)\,, \tag{C.41}$$

$$M_{k_x}\vec{\psi}\,(L)+T_{y+}\vec{\psi}\,(L-1)=E\,\vec{\psi}\,(L) \tag{C.42}$$

at the edges. Here, $T_{y\pm}$ is defined as Eq. (C.5), and M_{k_x} is defined as

$$M_{k_x}\coloneqq-\mathrm{i}\left(\gamma+\lambda\cos k_x\right)+\lambda\left(\sin k_x\right)\sigma_z+\gamma\sigma_y. \tag{C.43}$$

When $\vec{\psi}\,(0)$ and $\vec{\psi}\,(L+1)$ are respectively defined by the bulk equations (C.40) for $n=1$ and $n=L$, the boundary conditions in Eqs. (C.41) and (C.42) reduce to

$$T_{y+}\vec{\psi}\,(0)=T_{y-}\vec{\psi}\,(L+1)=0. \tag{C.44}$$

Now, suppose that β_y is a solution to the characteristic equation $\det\left[H\left(\beta_y\right)-E\right]=0$ for eigenenergy $E\in\mathbb{C}$, where the bulk Hamiltonian $H\left(\beta_y\right)$ is given as

$$H\left(\beta_y\right)=M_{k_x}+\beta_y T_{y-}+\beta_y^{-1}T_{y+}. \tag{C.45}$$

Because of transposition-associated mirror symmetry in Eq. (4.77), β_y^{-1} is another solution to the characteristic equation for the same eigenenergy E. Hence, the corresponding eigenstate is generally expanded as

$$\vec{\psi}\,(n)=\beta_y^n\vec{c}_+ +\beta_y^{L+1-n}\vec{c}_- \tag{C.46}$$

with $|\beta_y|\leq 1$ and $\vec{c}_\pm\in\mathbb{C}^2$. The boundary conditions (C.44) further reduce to

$$T_{y+}\left(\vec{c}_+ +\beta_y^{L+1}\vec{c}_-\right)=T_{y-}\left(\beta_y^{L+1}\vec{c}_+ +\vec{c}_-\right)=0. \tag{C.47}$$

Thus, for $|\beta_y|<1$ and sufficiently large L, we need

$$\vec{c}_+\simeq\begin{pmatrix}0\\1\end{pmatrix},\quad \vec{c}_-\simeq\begin{pmatrix}1\\0\end{pmatrix}. \tag{C.48}$$

We note that this is not necessarily required for $|\beta_y|=1$. Since $\beta_y^{\pm}\vec{c}_\pm$ is an eigenstate of the bulk Hamiltonian $H\left(\beta_y\right)$, we finally have

$$E=-\mathrm{i}\gamma-\mathrm{i}\lambda e^{-\mathrm{i}k_x}, \tag{C.49}$$

$$\beta_y=-\frac{\gamma}{\lambda}. \tag{C.50}$$

For the appearance of these edge modes, we need the normalization condition $|\beta_y|<1$, i.e.,

$$\left|\frac{\gamma}{\lambda}\right|<1. \tag{C.51}$$

The obtained analytical results are consistent with the numerical results in Fig. 4.5.

C.2.2 Open boundary conditions along the x direction

We next consider the non-Hermitian Hamiltonian in Eq. (4.66), imposing the open boundary conditions along the x direction and the periodic boundary conditions along the y direction. The Schrödinger equation is given as

$$M_{k_y}\vec{\psi}\,(n) + T_{x+}\vec{\psi}\,(n-1) + T_{x-}\vec{\psi}\,(n+1) = E\,\vec{\psi}\,(n) \tag{C.52}$$

in the bulk ($n = 1, 2, \cdots, L$), and

$$T_{x+}\vec{\psi}\,(0) = T_{x-}\vec{\psi}\,(L+1) = 0 \tag{C.53}$$

at the edges. Here, $T_{x\pm}$ is defined as Eq. (C.4), and M_{k_y} is defined as

$$M_{k_y} \coloneqq -\mathrm{i}\gamma + (\gamma + \lambda\cos k_y)\,\sigma_y + \lambda\,(\sin k_y)\,\sigma_x. \tag{C.54}$$

The bulk Hamiltonian $H\,(\beta_x)$ is given as

$$H\,(\beta_x) = M_{k_y} + \beta_x T_{x-} + \beta_x^{-1} T_{x+}. \tag{C.55}$$

Similarly to Appendix C.2.1, an eigenstate is generally expanded as

$$\vec{\psi}\,(n) = \beta_x^n \vec{c}_+ + \beta_x^{L+1-n}\vec{c}_- \tag{C.56}$$

with $|\beta_x| \leq 1$ and $\vec{c}_\pm \in \mathbb{C}^2$. The boundary conditions (C.53) further reduce to

$$T_{x+}\left(\vec{c}_+ + \beta_x^{L+1}\vec{c}_-\right) = T_{x-}\left(\beta_x^{L+1}\vec{c}_+ + \vec{c}_-\right) = 0. \tag{C.57}$$

Thus, for $|\beta_x| < 1$ and sufficiently large L, we need

$$\vec{c}_+ \simeq \begin{pmatrix} 1 \\ 0 \end{pmatrix}, \quad \vec{c}_- \simeq \begin{pmatrix} 0 \\ 1 \end{pmatrix}. \tag{C.58}$$

Since $\beta_x^\pm \vec{c}_\pm$ is an eigenstate of the bulk Hamiltonian $H\,(\beta_x)$, we have

$$E = -\mathrm{i}\gamma - \mathrm{i}\lambda\beta_x, \tag{C.59}$$

$$e^{-\mathrm{i}k_y} = -\frac{\gamma}{\lambda}. \tag{C.60}$$

To satisfy Eq. (C.60), we need $e^{-\mathrm{i}k_y} \in \mathbb{R}$, i.e., $k_y = 0, \pi$. For $k_y = 0$ ($k_y = \pi$), Eq. (C.60) leads to $\gamma = -\lambda$ ($\gamma = \lambda$). Thus, in contrast to Appendix C.2.1, the parameters γ and λ should be fine-tuned for the appearance of the edge modes. For these fine-tuned parameters, we have $M_{k_y=0,\pi} = -\mathrm{i}\gamma$, and hence $\beta_x = 0$ and $E = -\mathrm{i}\gamma$. All the $2L$ eigenstates of $H\,(\beta_x)$ with $k_y = 0, \pi$ belong to the same eigenenergy and form an exceptional point. A half of the eigenstates are localized at the left edge and the other half of them are localized at the right edge. The obtained analytical results are consistent with the numerical results in Fig. 4.5.

Appendix D

Scattering theory of non-Hermitian disordered systems

D.1 Scattering and transfer matrices

We consider a non-Hermitian disordered system H in one dimension connected to two ideal leads. A wave incident on the disordered region from the left (right) is

$$a_{\text{in}}^{+} \coloneqq \begin{pmatrix} a_1^{+} & a_2^{+} & \cdots & a_N^{+} \end{pmatrix}^T \quad \left[b_{\text{in}}^{-} \coloneqq \begin{pmatrix} b_1^{-} & b_2^{-} & \cdots & b_N^{-} \end{pmatrix}^T \right], \tag{D.1}$$

and the reflected and transmitted waves scattered to the right (left) are

$$b_{\text{out}}^{+} \coloneqq \begin{pmatrix} b_1^{+} & b_2^{+} & \cdots & b_N^{+} \end{pmatrix}^T \quad \left[a_{\text{out}}^{-} \coloneqq \begin{pmatrix} a_1^{-} & a_2^{-} & \cdots & a_N^{-} \end{pmatrix}^T \right]. \tag{D.2}$$

The scattering matrix S relates these incident and scattered waves by

$$\begin{pmatrix} a_{\text{out}}^{-} \\ b_{\text{out}}^{+} \end{pmatrix} = S \begin{pmatrix} a_{\text{in}}^{+} \\ b_{\text{in}}^{-} \end{pmatrix}, \quad S \coloneqq \begin{pmatrix} r_{\text{L}} & t_{\text{L}} \\ t_{\text{R}} & r_{\text{R}} \end{pmatrix}, \tag{D.3}$$

where r_{L} (r_{R}) is an $N \times N$ invertible matrix that describes the reflection from the left to the left (from the right to the right), and t_{R} (t_{L}) is an $N \times N$ invertible matrix that describes the transmission from the left to the right (from the right to the left). In a similar manner, the transfer matrix M is defined by

$$\begin{pmatrix} b_{\text{out}}^{+} \\ b_{\text{in}}^{-} \end{pmatrix} = M \begin{pmatrix} a_{\text{in}}^{+} \\ a_{\text{out}}^{-} \end{pmatrix}. \tag{D.4}$$

These definitions of the scattering matrix and transfer matrix mean

$$a_{\text{out}}^{-} = r_{\text{L}} a_{\text{in}}^{+} + t_{\text{L}} b_{\text{in}}^{-}, \tag{D.5}$$
$$b_{\text{out}}^{+} = t_{\text{R}} a_{\text{in}}^{+} + r_{\text{R}} b_{\text{in}}^{-}, \tag{D.6}$$
$$b_{\text{out}}^{+} = M_{11} a_{\text{in}}^{+} + M_{12} a_{\text{out}}^{-}, \tag{D.7}$$
$$b_{\text{in}}^{-} = M_{21} a_{\text{in}}^{+} + M_{22} a_{\text{out}}^{-}, \tag{D.8}$$

which leads to

$$M = \begin{pmatrix} t_{\text{R}} - r_{\text{R}} t_{\text{L}}^{-1} r_{\text{L}} & r_{\text{R}} t_{\text{L}}^{-1} \\ -t_{\text{L}}^{-1} r_{\text{L}} & t_{\text{L}}^{-1} \end{pmatrix}, \tag{D.9}$$

and

$$r_{\mathrm{L}} = -M_{22}^{-1} M_{21}, \tag{D.10}$$
$$r_{\mathrm{R}} = M_{12} M_{22}^{-1}, \tag{D.11}$$
$$t_{\mathrm{L}} = M_{22}^{-1}, \tag{D.12}$$
$$t_{\mathrm{R}} = M_{11} - M_{12} M_{22}^{-1} M_{21}. \tag{D.13}$$

Notably, we have

$$\det M = \det\left[\left(t_{\mathrm{R}} - r_{\mathrm{R}} t_{\mathrm{L}}^{-1} r_{\mathrm{L}}\right) t_{\mathrm{L}}^{-1} - \left(r_{\mathrm{R}} t_{\mathrm{L}}^{-1}\right) t_{\mathrm{L}} \left(-t_{\mathrm{L}}^{-1} r_{\mathrm{L}}\right) t_{\mathrm{L}}^{-1}\right] = \frac{\det t_{\mathrm{R}}}{\det t_{\mathrm{L}}}. \tag{D.14}$$

When the system is closed (i.e., isolated from the environment) and hence the Hamiltonian H is Hermitian, the amplitude of the waves is conserved under the scattering:

$$\left|a_{\mathrm{in}}^{+}\right|^2 + \left|b_{\mathrm{in}}^{-}\right|^2 = \left|a_{\mathrm{out}}^{-}\right|^2 + \left|b_{\mathrm{out}}^{+}\right|^2. \tag{D.15}$$

As a result, the scattering matrix S is unitary:

$$S^{\dagger} S = S S^{\dagger} = 1. \tag{D.16}$$

Unitarity of S implies that the Hermitian matrices $t_{\mathrm{L}} t_{\mathrm{L}}^{\dagger}$, $t_{\mathrm{R}} t_{\mathrm{R}}^{\dagger}$, $1 - r_{\mathrm{L}} r_{\mathrm{L}}^{\dagger}$, and $1 - r_{\mathrm{R}} r_{\mathrm{R}}^{\dagger}$ have the same set of eigenvalues. In addition, since we have

$$\left|a_{\mathrm{in}}^{+}\right|^2 - \left|a_{\mathrm{out}}^{-}\right|^2 = \left|b_{\mathrm{out}}^{+}\right|^2 - \left|b_{\mathrm{in}}^{-}\right|^2 = \begin{pmatrix} b_{\mathrm{out}}^{+} \\ b_{\mathrm{in}}^{-} \end{pmatrix}^{\dagger} \tau_z \begin{pmatrix} b_{\mathrm{out}}^{+} \\ b_{\mathrm{in}}^{-} \end{pmatrix} = \begin{pmatrix} a_{\mathrm{in}}^{+} \\ a_{\mathrm{out}}^{-} \end{pmatrix}^{\dagger} M^{\dagger} \tau_z M \begin{pmatrix} a_{\mathrm{in}}^{+} \\ a_{\mathrm{out}}^{-} \end{pmatrix} \tag{D.17}$$

with a Pauli matrix τ_z, the transfer matrix M is pseudo-unitary:

$$\tau_z M^{\dagger} \tau_z^{-1} = M^{-1}. \tag{D.18}$$

However, when the system exchanges energy or particles with the environment and hence the Hamiltonian H is non-Hermitian, the scattering matrix S and the transfer matrix M are not unitary and pseudo-unitary, respectively, which can change the universality of localization transitions.

D.2 Symmetry in scattering theory

When the system respects symmetry, certain constraints are imposed on the non-Hermitian Hamiltonian H and the nonunitary scattering matrix S. Importantly, non-Hermiticity and nonunitarity change the nature of symmetry, and the symmetry constraints become different from the conventional constraints in Hermitian systems. While the symmetry constraints for non-Hermitian Hamiltonians H are identified in Refs. [BL02, KSUS19], we here provide the symmetry constraints for nonunitary scattering matrices S (Table D.1). Our discussions are based on the relationship between H and S (Mahaux-Weidenmüller formula [Bee97, Bee15]):

$$S(E) = \frac{1 - \mathrm{i}\pi K(E)}{1 + \mathrm{i}\pi K(E)}, \quad K(E) \coloneqq W^{\dagger} \frac{1}{E - H} W, \tag{D.19}$$

where $E \in \mathbb{C}$ is energy of the incident and the scattered waves, and W describes the coupling between the system and the leads and is assumed to commute with the symmetry operations.

D.2.1 Time-reversal symmetry and reciprocity

Time-reversal symmetry for non-Hermitian Hamiltonians H is defined by

$$\mathcal{T}H^*\mathcal{T}^{-1} = H, \quad \mathcal{T}\mathcal{T}^* = \pm 1, \tag{D.20}$$

where $\mathcal{T}$ is a unitary matrix (i.e., $\mathcal{T}^\dagger\mathcal{T} = \mathcal{T}\mathcal{T}^\dagger = 1$) and commutes with the coupling matrix W (i.e., $\mathcal{T}W^*\mathcal{T}^{-1} = W$). Then, we have

$$\mathcal{T}K^*(E)\mathcal{T}^{-1} = W^\dagger \frac{1}{E^* - H} W = K(E^*), \tag{D.21}$$

and hence

$$\mathcal{T}S^*(E)\mathcal{T}^{-1} = \frac{1 + \mathrm{i}\pi K(E^*)}{1 - \mathrm{i}\pi K(E^*)} = S^{-1}(E^*). \tag{D.22}$$

For $\mathcal{T}\mathcal{T}^* = +1$ ($\mathcal{T}\mathcal{T}^* = -1$), non-Hermitian systems are defined to belong to class AI (AII) [KSUS19].

Non-Hermiticity enables a Hermitian-conjugate counterpart of time-reversal symmetry as another fundamental symmetry (TRS† in Ref. [KSUS19]). Because of the difference between complex conjugation and transposition, the symmetry defined by

$$\mathcal{T}H^T\mathcal{T}^{-1} = H, \quad \mathcal{T}\mathcal{T}^* = \pm 1, \tag{D.23}$$

is distinct from time-reversal symmetry defined by Eq. (D.20). As a consequence of this symmetry, we have

$$\mathcal{T}K^T(E)\mathcal{T}^{-1} = W^\dagger \frac{1}{E - H} W = K(E), \tag{D.24}$$

and hence

$$\mathcal{T}S^T(E)\mathcal{T}^{-1} = \frac{1 - \mathrm{i}\pi K(E)}{1 + \mathrm{i}\pi K(E^*)} = S(E). \tag{D.25}$$

For $\mathcal{T}\mathcal{T}^* = +1$ ($\mathcal{T}\mathcal{T}^* = -1$), non-Hermitian systems are defined to belong to class AI† (AII†) [KSUS19]. For $\mathcal{T} = 1$, for example, Eq. (D.25) implies

$$r_{\mathrm{L}}^T = r_{\mathrm{L}}, \quad r_{\mathrm{R}}^T = r_{\mathrm{R}}, \quad t_{\mathrm{L}}^T = t_{\mathrm{R}}, \tag{D.26}$$

and hence the transmission probability from the right to the left is equivalent to the transmission probability from the left to the right [i.e., $\mathrm{tr}\,(t_{\mathrm{L}}t_{\mathrm{L}}^\dagger) = \mathrm{tr}\,(t_{\mathrm{R}}t_{\mathrm{R}}^\dagger)$]. Thus, the symmetry defined by

Table D.1: Symmetry of non-Hermitian Hamiltonians H and nonunitary scattering matrices S. A typical representation of symmetry is shown for each class, where σ_i's and τ_i's are Pauli matrices that describe the spin and valley degrees of freedom, respectively. Furthermore, the type of delocalization and the typical conductances for sufficiently large systems $L \gg \ell$ are shown with non-Hermiticity γ and the mean free path $\ell > 0$.

Class	Symmetry of H	Symmetry of S	Delocalization	Typical conductances
A	No	No	Unidirectional	$e^{(\pm\gamma - 1/\ell)L}$
AI	$\tau_x H^* \tau_x^{-1} = H$	$S^*(E) = S^{-1}(E^*)$	Unidirectional	$e^{(\pm\gamma - 1/\ell)L}$
AI†	$\tau_x H^T \tau_x^{-1} = H$	$S^T(E) = S(E)$	No	$e^{-L/\ell}$
AII	$(\sigma_y\tau_x) H^* (\sigma_y\tau_x)^{-1} = H$	$\sigma_y S^*(E) \sigma_y^{-1} = S^{-1}(E^*)$	Unidirectional	$e^{(\pm\gamma - 1/\ell)L}$
AII†	$(\sigma_y\tau_x) H^T (\sigma_y\tau_x)^{-1} = H$	$\sigma_y S^T(E) \sigma_y^{-1} = S(E)$	Bidirectional	$e^{(\lvert\gamma\rvert - 1/\ell)L}$
AIII	$\tau_x H^\dagger \tau_x^{-1} = -H$	$S^\dagger(E) = S(-E^*)$	Bidirectional (chiral unitary)	$e^{-\sqrt{8L/\pi\ell}}$
AIII†	$\tau_x H \tau_x^{-1} = -H$	$S(E) = S^{-1}(-E)$	Unidirectional	$e^{\pm\gamma\ell - \sqrt{8L/\pi\ell}}$

Eq. (D.23) physically means reciprocity in non-Hermitian systems. Importantly, time-reversal symmetry and reciprocity are distinct from each other in non-Hermitian systems, although they are equivalent to each other in Hermitian systems; the symmetry constraints in Eqs. (D.22) and (D.25) and the consequent universality of localization transitions are different from each other.

D.2.2 Particle-hole symmetry

Particle-hole symmetry for non-Hermitian Hamiltonians H is defined by

$$\mathcal{C}H^T\mathcal{C}^{-1} = -H, \quad \mathcal{C}\mathcal{C}^* = \pm 1, \tag{D.27}$$

where $\mathcal{C}$ is a unitary matrix and commutes with the coupling matrix W (i.e., $\mathcal{C}W^T\mathcal{C}^{-1} = W$). Then, we have

$$\mathcal{C}K^T(E)\mathcal{C}^{-1} = W^\dagger \frac{1}{E+H} W = -K(-E), \tag{D.28}$$

and hence

$$\mathcal{C}S^T(E)\mathcal{C}^{-1} = \frac{1+\mathrm{i}\pi K(-E)}{1-\mathrm{i}\pi K(-E)} = S^{-1}(-E). \tag{D.29}$$

In a manner similar to time-reversal symmetry and reciprocity, non-Hermiticity enables a Hermitian-conjugate counterpart of particle-hole symmetry (PHS† in Ref. [KSUS19]):

$$\mathcal{C}H^*\mathcal{C}^{-1} = -H, \quad \mathcal{C}\mathcal{C}^* = \pm 1. \tag{D.30}$$

Then, we have

$$\mathcal{C}K^*(E)\mathcal{C}^{-1} = W^\dagger \frac{1}{E^*+H} W = -K(-E^*), \tag{D.31}$$

and hence

$$\mathcal{C}S^*(E)\mathcal{C}^{-1} = \frac{1-\mathrm{i}\pi K(-E^*)}{1+\mathrm{i}\pi K(-E^*)} = S(-E^*). \tag{D.32}$$

Whereas Eqs. (D.29) and (D.32) are equivalent to each other in the presence of unitarity, they are not in the nonunitary case.

D.2.3 Chiral symmetry and sublattice symmetry

Chiral symmetry for non-Hermitian Hamiltonians H is defined by

$$\Gamma H^\dagger \Gamma^{-1} = -H, \tag{D.33}$$

where Γ is a unitary and Hermitian matrix and commutes with the coupling matrix W (i.e., $\Gamma W\Gamma^{-1} = W$). Then, we have

$$\Gamma K^\dagger(E)\Gamma^{-1} = W^\dagger \frac{1}{E^*+H} W = -K(-E^*), \tag{D.34}$$

and hence

$$\Gamma S^\dagger(E)\Gamma^{-1} = \frac{1+\mathrm{i}\pi K(-E^*)}{1-\mathrm{i}\pi K(-E^*)} = S(-E^*). \tag{D.35}$$

On the other hand, sublattice symmetry is defined by

$$\mathcal{S}H\mathcal{S}^{-1} = -H, \tag{D.36}$$

where $\mathcal{S}$ is a unitary and Hermitian matrix and commutes with the coupling matrix W. Then, we have

$$\mathcal{S}K(E)\mathcal{S}^{-1} = W^{\dagger}\frac{1}{E+H}W = -K(-E), \tag{D.37}$$

and hence

$$\mathcal{S}S(E)\mathcal{S}^{-1} = \frac{1+\mathrm{i}\pi K(-E)}{1-\mathrm{i}\pi K(-E)} = S^{-1}(-E). \tag{D.38}$$

Whereas chiral symmetry defined by Eq. (D.35) and sublattice symmetry defined by Eq. (D.38) are equivalent to each other in the presence of unitarity, they are not in the nonunitary case. Non-Hermitian systems that respect chiral symmetry in Eq. (D.35) [sublattice symmetry in Eq. (D.38)] are defined to belong to class AIII (AIII†) [KSUS19].

D.3 Green's function

We present a scattering theory of non-Hermitian Hamiltonians in one dimension. For the non-Hermitian Hamiltonian

$$H(x) = H_0(x) + V(x), \tag{D.39}$$

let E and $\varphi(x)$ be eigenenergy and the corresponding right eigenstate, respectively:

$$[H_0(x) + V(x)]\varphi(x) = E\varphi(x). \tag{D.40}$$

For this Schrödinger equation, we define the Green's function $G_0(x)$ by

$$H_0(x)G_0(x) + \delta(x) = EG_0(x). \tag{D.41}$$

Then, the eigenstate $\varphi(x)$ satisfies

$$\varphi(x) = \varphi_0(x) + \int_{-\infty}^{\infty} dy\; G_0(x-y)V(y)\varphi(y), \tag{D.42}$$

where $\varphi_0(x)$ is a solution to the Schrödinger equation in the absence of the potential $V(x)$:

$$H_0(x)\varphi_0(x) = E\varphi_0(x). \tag{D.43}$$

For a sufficiently weak potential $V(x)$, the Born approximation is justified. Up to the second-order Born approximation, the eigenstate is given as $\varphi(x) \simeq \varphi_0(x) + \varphi_1(x) + \varphi_2(x)$ with

$$\varphi_1(x) \coloneqq \int_{-\infty}^{\infty} dy\; G_0(x-y)V(y)\varphi_0(y), \tag{D.44}$$

$$\varphi_2(x) \coloneqq \int_{-\infty}^{\infty} dy \int_{-\infty}^{\infty} dz\; G_0(x-y)V(y)G_0(y-z)V(z)\varphi_0(z). \tag{D.45}$$

In particular, we consider the scattering for

$$H_0(x) = -\mathrm{i}\tau_z\partial_x. \tag{D.46}$$

Here, τ_z is a Pauli matrix that describes the two valley degrees of freedom. Performing the Fourier transformations

$$G_0(x) = \int_{-\infty}^{\infty} \frac{dk}{2\pi}\tilde{G}_0(k)e^{\mathrm{i}kx}, \tag{D.47}$$

$$\delta(x) = \int_{-\infty}^{\infty} \frac{dk}{2\pi}e^{\mathrm{i}kx} \tag{D.48}$$

for Eq. (D.41), we have

$$\tilde{G}_0(k) = (E - k\tau_z)^{-1} = \begin{pmatrix} 1/(E-k) & 0 \\ 0 & 1/(E+k) \end{pmatrix}. \tag{D.49}$$

Using the formulas

$$\int_{-\infty}^{\infty} \frac{dk}{2\pi} \frac{e^{\mathrm{i}kx}}{E \pm \mathrm{i}\varepsilon - k} = \mp \mathrm{i} e^{\mathrm{i}Ex} \theta(\pm x), \tag{D.50}$$

$$\int_{-\infty}^{\infty} \frac{dk}{2\pi} \frac{e^{\mathrm{i}kx}}{E \pm \mathrm{i}\varepsilon + k} = \mp \mathrm{i} e^{-\mathrm{i}Ex} \theta(\mp x), \tag{D.51}$$

with a positive infinitesimal constant $\varepsilon > 0$ and the Heaviside step function θ, we have

$$G_0(x; E \pm \mathrm{i}\varepsilon) = \begin{pmatrix} \mp \mathrm{i} e^{\mathrm{i}Ex} \theta(\pm x) & 0 \\ 0 & \mp \mathrm{i} e^{-\mathrm{i}Ex} \theta(\mp x) \end{pmatrix}. \tag{D.52}$$

D.4 Scaling equations

We formulate the scaling equations (functional renormalization group equations) for non-Hermitian disordered systems in one dimension. Our formulation is based on the random-matrix approach developed for Hermitian quasi-one-dimensional systems by Dorokhov, and by Mello, Pereyra, and Kumar [Dor82, MPK88, Bee97, Bee15]. The conductance from the left to the right (from the right to the left) is given by the sum of the transmission eigenvalues from the left to the right (from the right to the left) according to the Landauer formula [Dat95, Imr97]. Then, we consider an incremental change of the transmission eigenvalues upon attachment of a thin slice of length dL to the system of length L. The transmission matrix and the reflection matrix are respectively defined as $t_{\mathrm{L/R}}(L)$ and $r_{\mathrm{L/R}}(L)$ for the original system and $t_{\mathrm{L/R}}(dL)$ and $r_{\mathrm{L/R}}(dL)$ for the attached thin slice. The transmission matrix and the reflection matrix of the combined system of length $L + dL$ are given as [Dat95, Imr97]

$$t_{\mathrm{R}}(L + dL) = t_{\mathrm{R}}(L) \left[1 - r_{\mathrm{R}}(dL)\, r_{\mathrm{L}}(L)\right]^{-1} t_{\mathrm{R}}(dL), \tag{D.53}$$

$$r_{\mathrm{L}}(L + dL) = r_{\mathrm{L}}(dL) + t_{\mathrm{L}}(dL) \left[1 - r_{\mathrm{L}}(L)\, r_{\mathrm{R}}(dL)\right]^{-1} r_{\mathrm{L}}(L)\, t_{\mathrm{R}}(dL). \tag{D.54}$$

The scattering in the thin slice can be treated perturbatively (i.e., by the Born approximation summarized in Appendix D.3) for sufficiently weak disorder such that the mean free path ℓ is much smaller than the Fermi wavelength. Moreover, the incident wave is assumed to be independently and uniformly distributed in the parameter space determined by symmetry. After the above calculations, we have the moments of the transmission eigenvalues and the reflection eigenvalues, which result in the Fokker-Planck equation (DMPK equation) of their probability distribution. This probability distribution provides all the information about the transmission eigenvalues and the conductances. In Hermitian systems, we have $t_{\mathrm{R}} t_{\mathrm{R}}^{\dagger} + r_{\mathrm{L}} r_{\mathrm{L}}^{\dagger} = 1$ as a direct result of unitarity of scattering matrices, and the Fokker-Planck equation can be described solely by the transmission eigenvalues. In non-Hermitian systems, by contrast, the transmission eigenvalues are independent of the reflection eigenvalues, and hence the Fokker-Planck equation is described by both of them. The types of delocalization and typical conductances for $L \gg \ell$ are summarized in Table D.1.

D.4.1 Class A

We investigate the following non-Hermitian continuum model with disorder:

$$h = \left(-\mathrm{i}\partial_x + \mathrm{i}\gamma_3/2\right)\tau_z + m_0\left(x\right) + \left(m_1\left(x\right) + \mathrm{i}\gamma_1/2\right)\tau_x + \left(m_2\left(x\right) + \mathrm{i}\gamma_2/2\right)\tau_y, \tag{D.55}$$

where γ_i's $(i = 1, 2, 3)$ are the degrees of non-Hermiticity, and τ_i's are Pauli matrices that describe the valley degrees of freedom. The disorder is defined to satisfy

$$\left\langle m_i\left(x\right)\right\rangle = 0, \quad \left\langle m_i\left(x\right) m_j\left(x'\right)\right\rangle = 2\mu_i\delta_{ij}\delta\left(x - x'\right), \tag{D.56}$$

where the brackets denote the ensemble average. This continuous model describes a generic non-Hermitian wire having a single channel with two valleys. For lattice models, $m_0\left(x\right)$ and $m_1\left(x\right)$ correspond to a disordered onsite potential, while $m_2\left(x\right)$ corresponds to disordered hopping. A constant imaginary term such as $\mathrm{i}\gamma_0/2$ is omitted since it does not affect the localization of eigenstates. The Hatano-Nelson model [HN96, HN97, HN98] at the band center (i.e., $\mathrm{Re}\, E = 0$) is described by $m_2 = \gamma_1 = \gamma_2 = 0$, and the asymmetry of the hopping amplitudes corresponds to non-Hermiticity γ_3.

We begin with solving a scattering problem for a thin slice of length dL. Suppose that an incident wave $e^{\mathrm{i}kx}\left|+\right\rangle$ enters the thin slice at $[0, dL]$ from the left, where $\left|\pm\right\rangle$ is the eigenstate of τ_z with the eigenvalue ±1. The incident wave satisfies $-\mathrm{i}\tau_z\partial_x\left(e^{\mathrm{i}kx}\left|+\right\rangle\right) = k\left|+\right\rangle$ and is indeed a right-moving wave with eigenenergy $E = k$. In the following, we assume $E = k \in \mathbb{R}$ so that the incident wave will be a plane wave. For $x < 0$, up to the second-order Born approximation in Eqs. (D.44) and (D.45), the eigenstate is given as $\varphi\left(x\right) \simeq e^{\mathrm{i}kx}\left|+\right\rangle + \varphi_1\left(x\right) + \varphi_2\left(x\right)$ with

$$\begin{aligned}
\varphi_1\left(x\right) &= \int_0^{dL} dy \begin{pmatrix} 0 & 0 \\ 0 & -\mathrm{i}e^{-\mathrm{i}k(x-y)} \end{pmatrix} \\
&\quad \times \begin{pmatrix} m_0\left(y\right) + \mathrm{i}\gamma_3/2 & m_1\left(y\right) - \mathrm{i}m_2\left(y\right) + \mathrm{i}\gamma_1/2 + \gamma_2/2 \\ m_1\left(y\right) + \mathrm{i}m_2\left(y\right) + \mathrm{i}\gamma_1/2 - \gamma_2/2 & m_0\left(y\right) - \mathrm{i}\gamma_3/2 \end{pmatrix} e^{\mathrm{i}ky}\left|+\right\rangle \\
&= -\mathrm{i}e^{-\mathrm{i}kx}\int_0^{dL} dy\; e^{2\mathrm{i}ky}\left(m_1\left(y\right) + \mathrm{i}m_2\left(y\right) + \mathrm{i}\gamma_1/2 - \gamma_2/2\right)\left|-\right\rangle \\
&\simeq -\mathrm{i}\left[m_1\left(dL/2\right) + \mathrm{i}m_2\left(dL/2\right) + \mathrm{i}\gamma_1/2 - \gamma_2/2\right]\left(dL\right)e^{-\mathrm{i}kx}\left|-\right\rangle,
\end{aligned} \tag{D.57}$$

$$\begin{aligned}
\varphi_2\left(x\right) &= -e^{-\mathrm{i}kx}\int_0^{dL} dy \int_0^{dL} dz\; e^{\mathrm{i}k(y+z)} \begin{pmatrix} 0 & 0 \\ m_1\left(y\right) + \mathrm{i}m_2\left(y\right) + \mathrm{i}\gamma_1/2 - \gamma_2/2 & m_0\left(y\right) - \mathrm{i}\gamma_3/2 \end{pmatrix} \\
&\quad \times \begin{pmatrix} e^{\mathrm{i}k(y-z)}\theta\left(y - z\right) & 0 \\ 0 & e^{\mathrm{i}k(z-y)}\theta\left(z - y\right) \end{pmatrix} \begin{pmatrix} m_0\left(z\right) + \mathrm{i}\gamma_3/2 \\ m_1\left(z\right) + \mathrm{i}m_2\left(y\right) + \mathrm{i}\gamma_1/2 - \gamma_2/2 \end{pmatrix} \\
&\simeq 0.
\end{aligned} \tag{D.58}$$

On the other hand, for $x > dL$, we have

$$\begin{aligned}
\varphi_1\left(x\right) &= \int_0^{dL} dy \begin{pmatrix} -\mathrm{i}e^{\mathrm{i}k(x-y)} & 0 \\ 0 & 0 \end{pmatrix} \\
&\quad \times \begin{pmatrix} m_0\left(y\right) + \mathrm{i}\gamma_3/2 & m_1\left(y\right) - \mathrm{i}m_2\left(y\right) + \mathrm{i}\gamma_1/2 + \gamma_2/2 \\ m_1\left(y\right) + \mathrm{i}m_2\left(y\right) + \mathrm{i}\gamma_1/2 - \gamma_2/2 & m_0\left(y\right) - \mathrm{i}\gamma_3/2 \end{pmatrix} e^{\mathrm{i}ky}\left|+\right\rangle \\
&= -\mathrm{i}e^{\mathrm{i}kx}\int_0^{dL} dy\left(m_0\left(y\right) + \mathrm{i}\gamma_3/2\right)\left|+\right\rangle \\
&\simeq -\mathrm{i}\left[m_0\left(dL/2\right) + \mathrm{i}\gamma_3/2\right]\left(dL\right)e^{\mathrm{i}kx}\left|+\right\rangle,
\end{aligned} \tag{D.59}$$

$$
\begin{aligned}
\varphi_2(x) = -e^{\mathrm{i}kx} \int_0^{dL} dy \int_0^{dL} dz\; e^{\mathrm{i}k(-y+z)} \begin{pmatrix} m_0(y) + \mathrm{i}\gamma_3/2 & m_1(y) - \mathrm{i}m_2(y) + \mathrm{i}\gamma_1/2 + \gamma_2/2 \\ 0 & 0 \end{pmatrix} \\
\times \begin{pmatrix} e^{\mathrm{i}k(y-z)}\theta(y-z) & 0 \\ 0 & e^{\mathrm{i}k(z-y)}\theta(z-y) \end{pmatrix} \begin{pmatrix} m_0(z) + \mathrm{i}\gamma_3/2 \\ m_1(z) + \mathrm{i}m_2(y) + \mathrm{i}\gamma_1/2 - \gamma_2/2 \end{pmatrix} \\
\simeq -e^{\mathrm{i}kx} \int_0^{dL} dy \int_0^{dL} dz \left[e^{\mathrm{i}k(y-z)}\theta(y-z)\, m_0(y)\, m_0(z) \right. \\
\left. + e^{\mathrm{i}k(z-y)}\theta(z-y) \left(m_1(y)\, m_1(z) + m_2(y)\, m_2(z) \right) \right] |+\rangle \\
\simeq -\frac{1}{2} \left[\left(m_0(dL/2) \right)^2 + \left(m_1(dL/2) \right)^2 + \left(m_2(dL/2) \right)^2 \right] (dL)^2\, e^{\mathrm{i}kx} |+\rangle . \qquad \text{(D.60)}
\end{aligned}
$$

From the above results, we have

$$
r_{\mathrm{L}}(dL) \simeq -\mathrm{i}\left(m_1 + \mathrm{i}m_2 + \mathrm{i}\gamma_1/2 - \gamma_2/2 \right) dL, \qquad \text{(D.61)}
$$

$$
t_{\mathrm{R}}(dL) \simeq 1 - \mathrm{i}\left(m_0 - E + \mathrm{i}\gamma_3/2 \right)(dL) - \frac{1}{2}\left(m_0^2 + m_1^2 + m_2^2 \right)(dL)^2 . \qquad \text{(D.62)}
$$

Similarly, for a left-moving incident wave $e^{-\mathrm{i}kx}|-\rangle$ that enters the system from the right, $r_{\mathrm{R}}(dL)$ and $t_{\mathrm{L}}(dL)$ are given as

$$
r_{\mathrm{R}}(dL) \simeq -\mathrm{i}\left(m_1 - \mathrm{i}m_2 + \mathrm{i}\gamma_1/2 + \gamma_2/2 \right) dL, \qquad \text{(D.63)}
$$

$$
t_{\mathrm{L}}(dL) \simeq 1 - \mathrm{i}\left(m_0 - E - \mathrm{i}\gamma_3/2 \right)(dL) - \frac{1}{2}\left(m_0^2 + m_1^2 + m_2^2 \right)(dL)^2 . \qquad \text{(D.64)}
$$

Thus, we have

$$
\langle |r_{\mathrm{L}}(dL)|^2 \rangle = 2\left(\mu_1 + \mu_2 \right) dL, \qquad \text{(D.65)}
$$

$$
\langle |t_{\mathrm{R}}(dL)|^2 \rangle = 1 - 2\left(\mu_1 + \mu_2 - \gamma_3/2 \right) dL, \qquad \text{(D.66)}
$$

$$
\langle |r_{\mathrm{R}}(dL)|^2 \rangle = 2\left(\mu_1 + \mu_2 \right) dL, \qquad \text{(D.67)}
$$

$$
\langle |t_{\mathrm{L}}(dL)|^2 \rangle = 1 - 2\left(\mu_1 + \mu_2 + \gamma_3/2 \right) dL. \qquad \text{(D.68)}
$$

In the absence of non-Hermiticity (i.e., $\gamma_i = 0$), we indeed have

$$
\langle |r_{\mathrm{L}}(dL)|^2 \rangle + \langle |t_{\mathrm{R}}(dL)|^2 \rangle = \langle |r_{\mathrm{R}}(dL)|^2 \rangle + \langle |t_{\mathrm{L}}(dL)|^2 \rangle = 1, \qquad \text{(D.69)}
$$

which means conservation of currents; however, it is broken by non-Hermiticity γ_3. In the following, we define the mean free path ℓ by

$$
\langle |r_{\mathrm{L}}(dL)|^2 \rangle = \langle |r_{\mathrm{R}}(dL)|^2 \rangle =: \frac{dL}{\ell}, \quad \text{i.e.,} \quad \ell := \frac{1}{2\left(\mu_1 + \mu_2 \right)}. \qquad \text{(D.70)}
$$

Now, we consider combining the system of length L and the thin slice of length dL. Using Eq. (D.53), as well as

$$
|t_{\mathrm{R}}(dL)|^2 \simeq 1 + \gamma_3\, dL - \left(m_1^2 + m_2^2 \right)(dL)^2 \qquad \text{(D.71)}
$$

and

$$
\begin{aligned}
|1 - r_{\mathrm{R}}(dL)\, r_{\mathrm{L}}(L)|^{-2} \simeq 1 + 2\sqrt{R_{\mathrm{L}}} \left[\left(m_1 + \gamma_2/2 \right) \sin\varphi_{\mathrm{L}} - \left(m_2 - \gamma_1/2 \right) \cos\varphi_{\mathrm{L}} \right] dL \\
+ \left[m_1^2 \left(4\sin^2\varphi_{\mathrm{L}} - 1 \right) + m_2^2 \left(4\cos^2\varphi_{\mathrm{L}} - 1 \right) \right] R_{\mathrm{L}}(dL)^2 \qquad \text{(D.72)}
\end{aligned}
$$

with $r_{\mathrm{L}} =: \sqrt{R_{\mathrm{L}}} e^{\mathrm{i}\varphi_{\mathrm{L}}}$, we have

$$\frac{dT_{\mathrm{R}}}{T_{\mathrm{R}}} \simeq \left\{ 2\sqrt{R_{\mathrm{L}}} \left[(m_1 + \gamma_2/2) \sin\varphi_{\mathrm{L}} - (m_2 - \gamma_1/2) \cos\varphi_{\mathrm{L}} \right] + \gamma_3 \right\} dL + \left\{ m_1^2 \left[\left(4\sin^2\varphi_{\mathrm{L}} - 1 \right) R_{\mathrm{L}} - 1 \right] + m_2^2 \left[\left(4\cos^2\varphi_{\mathrm{L}} - 1 \right) R_{\mathrm{L}} - 1 \right] \right\} (dL)^2 . \quad \text{(D.73)}$$

This leads to

$$\frac{\langle dT_{\mathrm{R}} \rangle}{dL} = \gamma_3 T_{\mathrm{R}} - \frac{T_{\mathrm{R}} (1 - R_{\mathrm{L}})}{\ell}, \quad \frac{\langle (dT_{\mathrm{R}})^2 \rangle}{dL} = \frac{2T_{\mathrm{R}}^2 R_{\mathrm{L}}}{\ell}, \quad \text{(D.74)}$$

and the higher moments vanish to the first order in dL. Here, the ensemble average is taken for given T_{R} and R_{L} in two steps, first averaging over the attached thin slice m_i and then averaging over the phase φ_{L} of the reflected wave. Since φ_{L} is assumed to be independently and uniformly distributed over $[0, 2\pi]$, the equations

$$\langle \cos\varphi_{\mathrm{L}} \rangle = \langle \sin\varphi_{\mathrm{L}} \rangle = 0, \quad \langle \cos^2\varphi_{\mathrm{L}} \rangle = \langle \sin^2\varphi_{\mathrm{L}} \rangle = 1/2 \quad \text{(D.75)}$$

are used. We have similar scaling equations also for T_{L} by reversing the sign of the non-Hermiticity γ_3. Moreover, using Eq. (D.54), we have

$$\frac{\langle dR_{\mathrm{L}} \rangle}{dL} = \frac{(1 - R_{\mathrm{L}})^2}{\ell}, \quad \frac{\langle (dR_{\mathrm{L}})^2 \rangle}{dL} = \frac{2R_{\mathrm{L}} (1 - R_{\mathrm{L}})^2}{\ell}, \quad \text{(D.76)}$$

and the same scaling equations for R_{R}.

In the obtained scaling equations (D.74) and (D.76), non-Hermiticity appears solely through the γ_3 terms. By contrast, the γ_1 and γ_2 terms just shift the phase of the waves and have no influence on the conductances. Consequently, when we define $\tilde{T}_{\mathrm{R}}$ and $\tilde{T}_{\mathrm{L}}$ by

$$\tilde{T}_{\mathrm{R}} := e^{-\gamma_3 L} T_{\mathrm{R}}, \quad \tilde{T}_{\mathrm{L}} := e^{+\gamma_3 L} T_{\mathrm{L}}, \quad \text{(D.77)}$$

the transfer amplitudes $\tilde{T}_{\mathrm{R}}$ and $\tilde{T}_{\mathrm{L}}$ and the reflection amplitudes R_{L} and R_{R} are described by the conventional Fokker-Planck equation (DMPK equation) for Hermitian systems. In particular, the average conductance $\tilde{G}^{\mathrm{av}}$ and the typical conductance $\tilde{G}^{\mathrm{typ}}$ are given as [Dor82, MPK88, Bee97, Bee15]

$$\frac{\tilde{G}^{\mathrm{av}}}{G_{\mathrm{c}}} := \frac{\langle \tilde{G} \rangle}{G_{\mathrm{c}}} = e^{-L/4\ell} f\left(L/\ell\right) \sim e^{-L/4\ell} \quad (L/\ell \to \infty), \quad \text{(D.78)}$$

$$\frac{\tilde{G}^{\mathrm{typ}}}{G_{\mathrm{c}}} := e^{\langle \log \tilde{G}/G_{\mathrm{c}} \rangle} = e^{-L/\ell}, \quad \text{(D.79)}$$

where G_{c} is the conductance quantum, and f is the following slowly-varying function [Abr81]:

$$f(x) := \frac{2}{\pi} \int_0^\infty t \frac{\tanh t}{\cosh t} e^{-xt^2/\pi^2} dt. \quad \text{(D.80)}$$

Thus, the conductances of the original non-Hermitian system are given as

$$\frac{G_{\mathrm{R}}^{\mathrm{av}}}{G_{\mathrm{c}}} \sim e^{(\gamma_3 - 1/4\ell)L}, \quad \text{(D.81)}$$

$$\frac{G_{\mathrm{R}}^{\mathrm{typ}}}{G_{\mathrm{c}}} = e^{(\gamma_3 - 1/\ell)L}, \quad \text{(D.82)}$$

$$\frac{G_{\mathrm{L}}^{\mathrm{av}}}{G_{\mathrm{c}}} \sim e^{(-\gamma_3 - 1/4\ell)L}, \quad \text{(D.83)}$$

$$\frac{G_{\mathrm{L}}^{\mathrm{typ}}}{G_{\mathrm{c}}} = e^{(-\gamma_3 - 1/\ell)L}. \quad \text{(D.84)}$$

Either G_{R} or G_{L} diverges for sufficiently strong non-Hermiticity as a signature of the unidirectional delocalization. For $\gamma_3 \geq 0$, for example, the transition point at which the typical conductance $G_{\mathrm{R}}^{\mathrm{typ}}$ from the left to the right begins to diverge is given by

$$\gamma_3 = \gamma_{\mathrm{c}} \coloneqq \frac{1}{\ell}. \tag{D.85}$$

Around this transition point, the conductance exhibits the critical behavior

$$\frac{|G_{\mathrm{R}}^{\mathrm{typ}} - G_{\mathrm{c}}|}{G_{\mathrm{c}}} \propto |\gamma_3 - \gamma_{\mathrm{c}}|. \tag{D.86}$$

D.4.2 Classes AI and AI†

Symmetry imposes constraints on systems and can change the universality of localization transitions. Non-Hermitian Hamiltonians in class AI respect time-reversal symmetry. In the presence of time-reversal symmetry defined by

$$\tau_x h^* \tau_x^{-1} = h, \tag{D.87}$$

the non-Hermitian terms $\mathrm{i}\,(\gamma_1/2)\,\tau_x$ and $\mathrm{i}\,(\gamma_2/2)\,\tau_y$ in Eq. (D.55) disappear. Still, the non-Hermitian term $\mathrm{i}\,(\gamma_3/2)\,\tau_z$ is allowed to be present, which leads to the unidirectional delocalization. Thus, the universality of the localization transitions in class AI is the same as that in class A.

On the other hand, when non-Hermitian Hamiltonians belong to class AI† (orthogonal class) and respect reciprocity defined by

$$\tau_x h^T \tau_x^{-1} = h, \tag{D.88}$$

the non-Hermitian term $\mathrm{i}\,(\gamma_3/2)\,\tau_z$ in Eq. (D.55) disappears. Consequently, the unidirectional delocalization is forbidden and the conductances for $L \gg \ell$ are given as

$$\frac{G_{\mathrm{R}}^{\mathrm{av}}}{G_{\mathrm{c}}} = \frac{G_{\mathrm{L}}^{\mathrm{av}}}{G_{\mathrm{c}}} \sim e^{-L/4\ell}, \tag{D.89}$$

$$\frac{G_{\mathrm{R}}^{\mathrm{typ}}}{G_{\mathrm{c}}} = \frac{G_{\mathrm{L}}^{\mathrm{typ}}}{G_{\mathrm{c}}} = e^{-L/\ell}. \tag{D.90}$$

The universality of the non-Hermitian localization in class AI† is the same as the Hermitian counterpart.

D.4.3 Classes AII and AII†

An important feature of class AII (symplectic class) in Hermitian systems is Kramers degeneracy. This Kramers-pair structure survives even in non-Hermitian systems: eigenstates with real eigenenergy form Kramers pairs in class AII [KHG+19], whereas generic eigenstates with complex eigenenergy form Kramers pairs in class AII† [KSUS19]. This difference in the Kramers-pair structure makes a difference in the universality of localization transitions, as described below. It is also notable that the transmission eigenvalues are not generally degenerate in the presence of non-Hermiticity, whereas they form Kramers pairs in Hermitian systems in class AII.

We investigate a non-Hermitian continuum model

$$h = (\mathrm{i}\partial_x + \Delta\sigma_x + \mathrm{i}\gamma_{03}/2)\,\tau_z + m_0(x) + m_1(x)\,\tau_x, \tag{D.91}$$

which respects time-reversal symmetry

$$(\sigma_y\tau_x)\, h^* \,(\sigma_y\tau_x)^{-1} = h \tag{D.92}$$

and hence belongs to class AII. Here, Pauli matrices σ_i's describe the internal degrees of freedom such as spin, while τ_i's describe the valley degrees of freedom. The non-Hermitian terms such as $\mathrm{i}\,(\gamma_{13}/2)\,\sigma_x\tau_z$, $\mathrm{i}\,(\gamma_{23}/2)\,\sigma_y\tau_z$, and $\mathrm{i}\,(\gamma_{33}/2)\,\sigma_z\tau_z$ are forbidden because of time-reversal symmetry. In a similar manner to class A, the reflection and the transmission matrices of a thin slice of the system are given as

$$r_{\mathrm{L}}\,(dL) = r_{\mathrm{R}}\,(dL) = -\mathrm{i}m_1 dL, \tag{D.93}$$

$$t_{\mathrm{R}}\,(dL) = 1 - \mathrm{i}\,(m_0 - E + \Delta\sigma_x + \mathrm{i}\gamma_{03}/2)\,dL - \frac{1}{2}\left(m_0^2 + m_1^2\right)(dL)^2\,, \tag{D.94}$$

$$t_{\mathrm{L}}\,(dL) = 1 - \mathrm{i}\,(m_0 - E - \Delta\sigma_x - \mathrm{i}\gamma_{03}/2)\,dL - \frac{1}{2}\left(m_0^2 + m_1^2\right)(dL)^2\,. \tag{D.95}$$

Thus, we have

$$\frac{1}{2}\left\langle \mathrm{tr}\left[r_{\mathrm{L}}\,(dL)\, r_{\mathrm{L}}^\dagger\,(dL)\right]\right\rangle = \frac{1}{2}\left\langle \mathrm{tr}\left[r_{\mathrm{R}}\,(dL)\, r_{\mathrm{R}}^\dagger\,(dL)\right]\right\rangle = \frac{dL}{\ell}, \tag{D.96}$$

$$\frac{1}{2}\left\langle \mathrm{tr}\left[t_{\mathrm{R}}\,(dL)\, t_{\mathrm{R}}^\dagger\,(dL)\right]\right\rangle = 1 - \left(\frac{1}{\ell} - \gamma_{03}\right)dL, \tag{D.97}$$

$$\frac{1}{2}\left\langle \mathrm{tr}\left[t_{\mathrm{L}}\,(dL)\, t_{\mathrm{L}}^\dagger\,(dL)\right]\right\rangle = 1 - \left(\frac{1}{\ell} + \gamma_{03}\right)dL, \tag{D.98}$$

with the mean free path $\ell \coloneqq 1/2\mu_1$. Similarly to class A, one of $\left\langle \mathrm{tr}\left[t_{\mathrm{R}}\,(dL)\, t_{\mathrm{R}}^\dagger\,(dL)\right]\right\rangle$ and $\left\langle \mathrm{tr}\left[t_{\mathrm{L}}\,(dL)\, t_{\mathrm{L}}^\dagger\,(dL)\right]\right\rangle$ is amplified by non-Hermiticity γ_{03} and the other is attenuated. Hence, the same scaling equations [i.e., Eqs. (D.74) and (D.76)] describe the probability distribution of the conductances, and either of the conductances G_{R} and G_{L} is amplified by non-Hermiticity γ_{03}. Thus, the unidirectional delocalization is realized in the same manner as class A.

By contrast, a different type of non-Hermitian delocalization appears in class AII†. We investigate a non-Hermitian continuum model

$$h = \left(\mathrm{i}\partial_x + \Delta\sigma_x + \mathrm{i}\,(\gamma_{33}/2)\,\sigma_z\right)\tau_z + m_0\,(x) + m_1\,(x)\,\tau_x, \tag{D.99}$$

which respects reciprocity

$$(\sigma_y\tau_x)\, h^T \,(\sigma_y\tau_x)^{-1} = H \tag{D.100}$$

and hence belongs to class AII†. In contrast to class AII, the non-Hermitian term $\mathrm{i}\,(\gamma_{33}/2)\,\sigma_z\tau_z$ is allowed to be present, whereas $\mathrm{i}\,(\gamma_{03}/2)\,\tau_z$ is forbidden. In this case, the reflection and the transmission matrices of a thin slice are given as

$$r_{\mathrm{L}}\,(dL) = r_{\mathrm{R}}\,(dL) = -\mathrm{i}m_1 dL, \tag{D.101}$$

$$t_{\mathrm{R}}\,(dL) = 1 - \mathrm{i}\,(m_0 - E + \Delta\sigma_x + \mathrm{i}\,(\gamma_{33}/2)\,\sigma_z)\,dL - \frac{1}{2}\left(m_0^2 + m_1^2\right)(dL)^2\,, \tag{D.102}$$

$$t_{\mathrm{L}}\,(dL) = 1 - \mathrm{i}\,(m_0 - E - \Delta\sigma_x - \mathrm{i}\,(\gamma_{33}/2)\,\sigma_z)\,dL - \frac{1}{2}\left(m_0^2 + m_1^2\right)(dL)^2\,, \tag{D.103}$$

which lead to

$$\frac{1}{2}\left\langle \mathrm{tr}\left[r_{\mathrm{L}}\,(dL)\, r_{\mathrm{L}}^\dagger\,(dL)\right]\right\rangle = \frac{1}{2}\left\langle \mathrm{tr}\left[r_{\mathrm{R}}\,(dL)\, r_{\mathrm{R}}^\dagger\,(dL)\right]\right\rangle = \frac{dL}{\ell}, \tag{D.104}$$

$$\frac{1}{2}\left\langle \mathrm{tr}\left[t_{\mathrm{R}}\,(dL)\, t_{\mathrm{R}}^\dagger\,(dL)\right]\right\rangle = \frac{1}{2}\left\langle \mathrm{tr}\left[t_{\mathrm{L}}\,(dL)\, t_{\mathrm{L}}^\dagger\,(dL)\right]\right\rangle = 1 - \frac{dL}{\ell}. \tag{D.105}$$

In contrast to classes A and AII, non-Hermiticity γ_{33} disappears in these equations. Nevertheless, it leads to non-Hermitian delocalization with the bidirectional nature instead of the unidirectional one. To see this bidirectional delocalization, we perform the polar decomposition

$$t_{\mathrm{R}} = U_{\mathrm{R}} \begin{pmatrix} \sqrt{T_+} & 0 \\ 0 & \sqrt{T_-} \end{pmatrix} \tag{D.106}$$

with a unitary matrix U_{R}, and consider incremental changes of the transmission eigenvalues T_+ and T_-. Here, because of reciprocity, the other transmission matrix t_{L} is

$$t_{\mathrm{L}} = \sigma_y t_{\mathrm{R}} \sigma_y^{-1} = \left(\sigma_y U_{\mathrm{R}} \sigma_y^{-1}\right) \begin{pmatrix} \sqrt{T_-} & 0 \\ 0 & \sqrt{T_+} \end{pmatrix}, \tag{D.107}$$

and hence the transmission eigenvalues are identical. Then, noticing

$$\begin{aligned} &U_{\mathrm{R}}^\dagger(L) \left[t_{\mathrm{R}}(L+dL)\, t_{\mathrm{R}}^\dagger(L+dL)\right] U_{\mathrm{R}}(L) \\ &\quad = \begin{pmatrix} \sqrt{T_+(L)} & 0 \\ 0 & \sqrt{T_-(L)} \end{pmatrix} \frac{t_{\mathrm{R}}(dL)\, t_{\mathrm{R}}^\dagger(dL)}{\left|1 - r_{\mathrm{R}}(dL)\, r_{\mathrm{L}}(L)\right|^2} \begin{pmatrix} \sqrt{T_+(L)} & 0 \\ 0 & \sqrt{T_-(L)} \end{pmatrix}, \end{aligned} \tag{D.108}$$

we have the scaling equations

$$\frac{dT_\pm}{T_\pm} = \left(2m_1\sqrt{R_{\mathrm{L}}}\sin\varphi_{\mathrm{L}} \pm \gamma_{33}\right) dL + m_1^2 \left[\left(4\sin^2\varphi_{\mathrm{L}} - 1\right) R_{\mathrm{L}} - 1\right] (dL)^2 . \tag{D.109}$$

Therefore, non-Hermiticity γ_{33} amplifies one of the transmission eigenvalues and attenuates the other. For $L \gg \ell$, the conductances are given as

$$\frac{G_{\mathrm{R}}^{\mathrm{av}}}{G_{\mathrm{c}}} = \frac{G_{\mathrm{L}}^{\mathrm{av}}}{G_{\mathrm{c}}} \sim e^{(|\gamma_{33}| - 1/4\ell)L}, \tag{D.110}$$

$$\frac{G_{\mathrm{R}}^{\mathrm{typ}}}{G_{\mathrm{c}}} = \frac{G_{\mathrm{L}}^{\mathrm{typ}}}{G_{\mathrm{c}}} = e^{(|\gamma_{33}| - 1/\ell)L}. \tag{D.111}$$

Consequently, the eigenstates are bidirectionally delocalized for sufficiently strong γ_{33} in contrast to both classes A and AII. This bidirectional delocalization originates from the Kramers-pair structure in class AII†: when one eigenstate of a Kramers pair is delocalized toward one direction, the other is delocalized toward the opposite direction. This is to be contrasted with the Kramers-pair structure in class AII, in which both eigenstates of a Kramers pair are delocalized toward the same direction.

D.4.4 Classes AIII and AIII†

Chiral or sublattice symmetry enables the delocalization of zero modes even in Hermitian systems, accompanied by Dyson's singularity [Dys53]. This delocalization results from the constraint

$$S^\dagger(E) = S(-E) \tag{D.112}$$

on unitary scattering matrices $S(E)$ due to chiral or sublattice symmetry. In fact,

$$S^\dagger(0) = S(0) \tag{D.113}$$

is respected for the zero modes and the reflection matrices become Hermitian, i.e.,

$$r_{\mathrm{L}}^\dagger = r_{\mathrm{L}}, \quad r_{\mathrm{R}}^\dagger = r_{\mathrm{R}}. \tag{D.114}$$

Then, the phases of the reflection matrices are confined to be 0 or π, which contrasts with the standard classes. Consequently, the zero modes are delocalized even in one dimension and the conductances for $L \gg \ell$ are given as [BMSA98, BFGM00]

$$\frac{G^{\mathrm{av}}}{G_{\mathrm{c}}} \sim \sqrt{2\ell/\pi L}, \quad \frac{G^{\mathrm{typ}}}{G_{\mathrm{c}}} \sim e^{-\sqrt{8L/\pi\ell}}. \tag{D.115}$$

In the following, we consider the influence of non-Hermiticity on the delocalization due to chiral or sublattice symmetry.

We investigate a non-Hermitian continuum model

$$h = -\mathrm{i}\tau_z \partial_x + \mathrm{i}\left(\gamma_1/2\right)\tau_x + m_2\left(x\right)\tau_y, \tag{D.116}$$

which respects chiral symmetry

$$\tau_x h^\dagger \tau_x^{-1} = -H. \tag{D.117}$$

Notably, the non-Hermitian term $\mathrm{i}\left(\gamma_3/2\right)\tau_z$ in Eq. (D.55) is not allowed because of chiral symmetry. The nonunitary scattering matrix $S_{dL}\left(E\right)$ of a thin slice of this system is given as

$$\begin{aligned} S_{dL}\left(E\right) &\coloneqq \begin{pmatrix} r_{\mathrm{L}}\left(dL\right) & t_{\mathrm{L}}\left(dL\right) \\ t_{\mathrm{R}}\left(dL\right) & r_{\mathrm{R}}\left(dL\right) \end{pmatrix} \\ &= \begin{pmatrix} \left(m_2 + \gamma_1/2\right) dL & 1 + \mathrm{i}E\, dL - m_2^2 \left(dL\right)^2/2 \\ 1 + \mathrm{i}E\, dL - m_2^2 \left(dL\right)^2/2 & -\left(m_2 - \gamma_1/2\right) dL \end{pmatrix}. \end{aligned} \tag{D.118}$$

Despite $S_{dL}^\dagger\left(E\right) S_{dL}\left(E\right) \neq 1$, this nonunitary scattering matrix becomes Hermitian for zero modes (i.e., $E = 0$). An incremental change of the transmission amplitude T_{R} for these zero modes is

$$\frac{dT_{\mathrm{R}}}{T_{\mathrm{R}}} \simeq -2\left(m_2 - \gamma_1/2\right)\sqrt{R_{\mathrm{L}}}\left(\cos\varphi_{\mathrm{L}}\right) dL + m_2^2\left[\left(4\cos^2\varphi_{\mathrm{L}} - 1\right) R_{\mathrm{L}} - 1\right]\left(dL\right)^2. \tag{D.119}$$

Since the phase φ_{L} of r_{L} is assumed to be independently and uniformly distributed over $\{0, \pi\}$, we have

$$\left\langle \cos\phi_{\mathrm{L}} \right\rangle = \left\langle \sin\phi_{\mathrm{L}} \right\rangle = 0, \quad \left\langle \cos^2\phi_{\mathrm{L}} \right\rangle = \left\langle \sin^2\phi_{\mathrm{L}} \right\rangle = 1, \tag{D.120}$$

and hence

$$\frac{\left\langle dT_{\mathrm{R}} \right\rangle}{dL} = -\frac{T_{\mathrm{R}}\left(1 - 3R_{\mathrm{L}}\right)}{\ell}, \quad \frac{\left\langle \left(dT_{\mathrm{R}}\right)^2 \right\rangle}{dL} = \frac{4T_{\mathrm{R}}^2 R_{\mathrm{L}}}{\ell}. \tag{D.121}$$

Similarly, an incremental change of the moments of the reflection amplitude R_{L} is

$$\frac{\left\langle dR_{\mathrm{L}} \right\rangle}{dL} = \frac{\left(1 - R_{\mathrm{L}}\right)\left(1 - 3R_{\mathrm{L}}\right)}{\ell}, \quad \frac{\left\langle \left(dR_{\mathrm{L}}\right)^2 \right\rangle}{dL} = \frac{4R_{\mathrm{L}}\left(1 - R_{\mathrm{L}}\right)^2}{\ell}. \tag{D.122}$$

In these scaling equations, non-Hermiticity γ_1 is not relevant to the transmission or the reflection amplitude. Thus, the conductances for the zero modes are given by Eq. (D.115), and the universality of non-Hermitian localization in class AIII is the same as the Hermitian counterpart.

On the other hand, non-Hermiticity changes the universality of Anderson localization in class AIII†. We investigate a non-Hermitian continuum model

$$h = \left(-\mathrm{i}\partial_x + \mathrm{i}\gamma_3/2\right)\tau_z + m_2\left(x\right)\tau_y, \tag{D.123}$$

which respects sublattice symmetry

$$\tau_x h \tau_x^{-1} = -H. \tag{D.124}$$

In contrast to chiral symmetry, the non-Hermitian term $\mathrm{i}\,(\gamma_3/2)\,\tau_z$ is allowed even in the presence of sublattice symmetry. Consequently, the unidirectional delocalization is possible in a manner similar to class A, and the conductances are given as

$$\frac{G^{\mathrm{av}}}{G_{\mathrm{c}}} \sim \sqrt{\frac{2\ell}{\pi L}}\, e^{\pm\gamma_3 L}, \quad \frac{G^{\mathrm{typ}}}{G_{\mathrm{c}}} \sim e^{\pm\gamma_3 L - \sqrt{8L/\pi\ell}}. \tag{D.125}$$

D.5 Non-Hermitian localization on lattices

D.5.1 Hatano-Nelson model (class A)

We investigate the Hatano-Nelson model [HN96, HN97, HN98]

$$\hat{H} = \sum_n \left\{ -\frac{1}{2}\left[\left(J + \frac{\gamma}{2}\right) \hat{c}_{n+1}^\dagger \hat{c}_n + \left(J - \frac{\gamma}{2}\right) \hat{c}_n^\dagger \hat{c}_{n+1} \right] + m_n \hat{c}_n^\dagger \hat{c}_n \right\} \tag{D.126}$$

with $J, \gamma, m_n \in \mathbb{R}$. Here, the disordered potential m_n is uniformly distributed over $[-W/2, W/2]$ with $W \geq 0$. The localization lengths as a function of the disorder strength W are shown in Fig. 6.2 (a) in Chap. 6, and those as a function of non-Hermiticity γ are shown in Fig. D.1 (a). For $\gamma \geq 0$, the right localization length ξ_{R} diverges at a critical point $W = W_{\mathrm{c}}$ or $\gamma = \gamma_{\mathrm{c}}$, whereas the left localization length ξ_{L} remains finite. This is a signature of the unidirectional delocalization and is consistent with the two-parameter scaling theory of conductances for continuum models. The phase diagram is shown in Fig. D.1 (b).

The nature of the unidirectional delocalization is understood by the GL (1)-gauge transformation (imaginary-gauge transformation in Ref. [HN96, HN97, HN98]). With the new fermion operators by the GL (1)-gauge transformation

$$\hat{f}_n \coloneqq e^{-n\theta} \hat{c}_n, \quad \hat{f}_n^\dagger \coloneqq e^{n\theta} \hat{c}_n^\dagger \quad (\theta \in \mathbb{C}), \tag{D.127}$$

the Hamiltonian reads

$$\hat{H} = \sum_n \left\{ -\frac{1}{2}\left[\left(J + \frac{\gamma}{2}\right) e^{-\theta} \hat{f}_{n+1}^\dagger \hat{f}_n + \left(J - \frac{\gamma}{2}\right) e^{\theta} \hat{f}_n^\dagger \hat{f}_{n+1} \right] + m_n \hat{f}_n^\dagger \hat{f}_n \right\}. \tag{D.128}$$

Here, choosing θ such that

$$\left(J + \frac{\gamma}{2}\right) e^{-\theta} = \left(J - \frac{\gamma}{2}\right) e^{\theta} = \tilde{J}, \tag{D.129}$$

i.e.,

$$\theta = \frac{1}{2} \log\left(\frac{J + \gamma/2}{J - \gamma/2} \right), \quad \tilde{J} = \sqrt{J^2 - (\gamma/2)^2}, \tag{D.130}$$

we have the Hermitian Anderson model

$$\hat{H} = \sum_n \left[-\frac{\tilde{J}}{2} \left(\hat{f}_{n+1}^\dagger \hat{f}_n + \hat{f}_n^\dagger \hat{f}_{n+1} \right) + m_n \hat{f}_n^\dagger \hat{f}_n \right]. \tag{D.131}$$

Thus, the localization lengths of the Hatano-Nelson model are

$$\xi_{\mathrm{L}} = \left(\xi_0^{-1} + \theta\right)^{-1}, \quad \xi_{\mathrm{R}} = \left(\xi_0^{-1} - \theta\right)^{-1}, \tag{D.132}$$

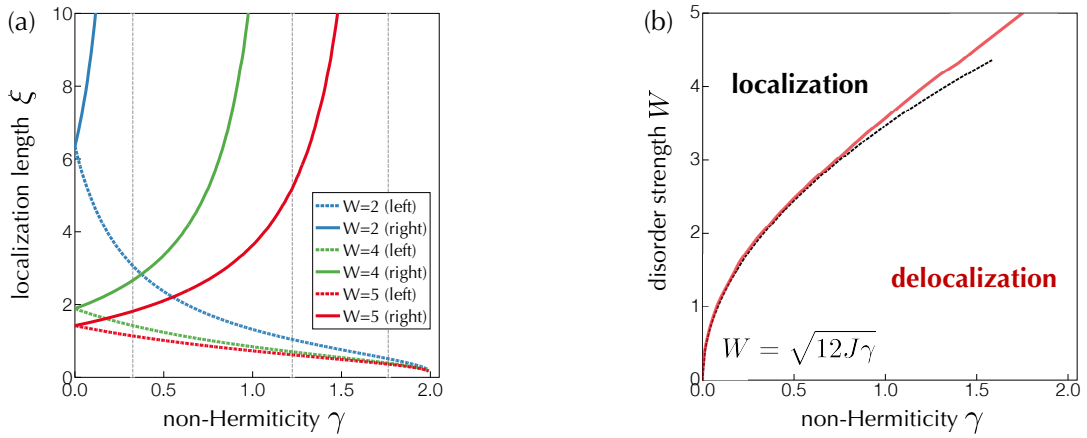

Figure D.1: Localization transition in the Hatano-Nelson model ($L = 5000, J = 1.0, E = 0$). Each datum shows the average over 1000 samples. (a) Localization length. For $\gamma \geq 0$, the right localization length diverges at a transition point $\gamma = \gamma_c$, whereas the left localization length remains finite. The transition points (dotted lines) are $\gamma_c = 0.325$ ($W = 2.0$), $\gamma_c = 1.23$ ($W = 4.0$), and $\gamma_c = 1.77$ ($W = 5.0$). (b) Phase diagram. The red solid curve shows the numerically obtained phase boundary. For sufficiently small γ and W, the phase boundary is given as $W = \sqrt{12J\gamma}$ (black dotted curve). Reproduced from Fig. S1 of Supplemental Material of Ref. [KR21]. Copyright 2021 by the American Physical Society.

where ξ_0 is the localization length of the Hermitian Anderson model in Eq. (D.131). For $\gamma \geq 0$ ($\gamma \leq 0$), the localization length ξ_R (ξ_L) diverges at $\gamma = \gamma_c$ such that $\xi_0^{-1} = |\theta(\gamma_c)|$. Around this critical point, we have

$$\xi \sim \frac{1}{|\theta'(\gamma_c)(\gamma - \gamma_c)|} \propto |\gamma - \gamma_c|^{-1}. \tag{D.133}$$

For sufficiently weak disorder, we have

$$\xi_0^{-1} \simeq \frac{\langle m_n^2 \rangle}{2(\tilde{J}^2 - E^2)}. \tag{D.134}$$

When m_n is uniformly distributed over $[-W/2, W/2]$, we have $\langle m_n^2 \rangle = W^2/12$. Then, the critical point is given as

$$|\gamma_c| \simeq \frac{W^2}{12J} \tag{D.135}$$

for the band center $E = 0$. This is consistent with the results for the continuum model, as well as the numerical result in Fig. D.1 (b).

D.5.2 Non-Hermitian Anderson model with random gain or loss (class AI†)

Non-Hermitian Hamiltonians $\hat{H}$ in class AI† (orthogonal class) respect reciprocity defined by

$$\hat{\mathcal{T}} \hat{H} \hat{\mathcal{T}}^{-1} = \hat{H}^\dagger \tag{D.136}$$

with an antiunitary operator $\hat{\mathcal{T}}$. When $\hat{\mathcal{T}}$ is complex conjugation, reciprocity means

$$J_R^T = J_L, \quad M_n^T = M_n. \tag{D.137}$$

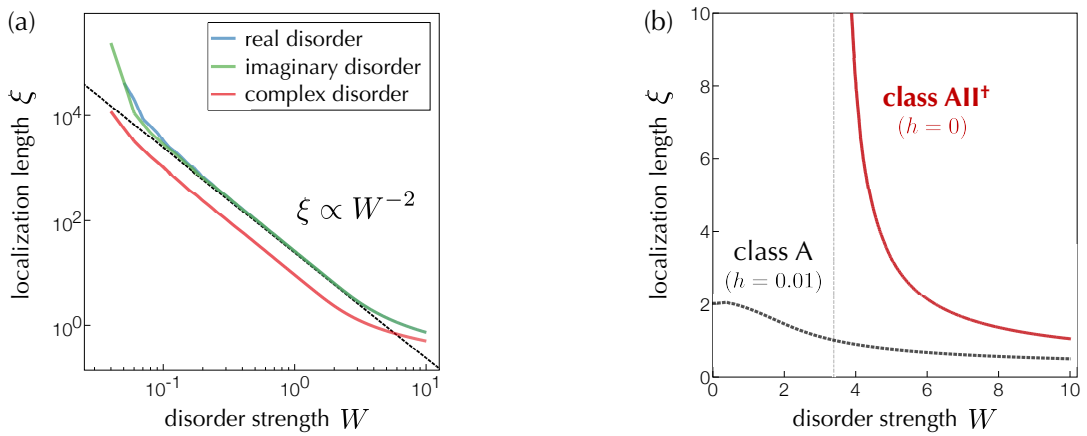

Figure D.2: Localization lengths in non-Hermitian disordered systems on one-dimensional lattices with reciprocity ($L = 5000, J = 1.0, E = 0$). Each datum shows the average over 1000 samples. (a) Non-Hermitian Anderson model with random gain or loss (class AI†). For all the types of Hermitian and non-Hermitian disorder, no transition occurs and the universality class is the same. The dotted line shows $\xi = 24J^2/W^2$. (b) Symplectic Hatano-Nelson model (class AII†; $\gamma = 1.0, \Delta = 0.1$). In contrast to the Hatano-Nelson model without symmetry protection, both right and left localization lengths diverge at a transition point $W_\mathrm{c} = 3.39$ (red solid curve). Because of the reciprocity-protected nature of the delocalization, even a small reciprocity-breaking perturbation $h = 0.01$ destroys the delocalization (black dotted curve). Reproduced from Fig. S2 of Supplemental Material of Ref. [KR21]. Copyright 2021 by the American Physical Society.

Consequently, we have

$$\xi_\mathrm{L} = \xi_\mathrm{R}, \quad |\det M_\mathrm{Ln}| = |\det M_\mathrm{Rn}| = 1, \tag{D.138}$$

which imposes

$$\xi_\mathrm{L} = \xi_\mathrm{R} < \infty \tag{D.139}$$

and forbids delocalization even in the presence of non-Hermiticity.

In particular, we investigate the non-Hermitian Anderson model with random gain or loss

$$\hat{H} = \sum_n \left\{ -\frac{J}{2} \left(\hat{c}_{n+1}^\dagger \hat{c}_n + \hat{c}_n^\dagger \hat{c}_{n+1} \right) + (m_n + \mathrm{i}\gamma_n)\, \hat{c}_n^\dagger \hat{c}_n \right\} \tag{D.140}$$

with $J, m_n, \gamma_n \in \mathbb{R}$. We here consider the following three types of disorder:

- real disorder ($m_n \in [-W/2, W/2]$, $\gamma_n = 0$)
- imaginary disorder ($m_n = 0$, $\gamma_n \in [-W/2, W/2]$)
- complex disorder ($m_n, \gamma_n \in [-W/2, W/2]$)

Figure D.2 (a) shows the localization length ξ as a function of the disorder strength W. For all the types of Hermitian and non-Hermitian disorder, ξ remains finite even for small W, and no delocalization occurs. Moreover, ξ gets smaller in proportion to W^{-2} in the same manner as the Hermitian case. These results are consistent with the scaling theory of conductances for continuum models, which demonstrates that the universality of the non-Hermitian localization transitions in class AI† is the same as the Hermitian counterpart.

D.5.3 Symplectic Hatano-Nelson model (class AII†)

We investigate a symplectic (reciprocal) generalization of the Hatano-Nelson model

$$\hat{H} = \sum_n \left\{ -\frac{1}{2} \left[\hat{c}_{n+1}^\dagger \left(J + \frac{\gamma\sigma_z}{2} - \mathrm{i}\Delta\sigma_x \right) \hat{c}_n + \hat{c}_n^\dagger \left(J - \frac{\gamma\sigma_z}{2} + \mathrm{i}\Delta\sigma_x \right) \hat{c}_{n+1} \right] + \hat{c}_n^\dagger \left(m_n + h\sigma_z \right) \hat{c}_n \right\} \tag{D.141}$$

with $J, \gamma, \Delta, m_n, h \in \mathbb{R}$. For $h = 0$, the Hamiltonian respects reciprocity, i.e.,

$$(\sigma_y \mathcal{K})\, \hat{H}\, (\sigma_y \mathcal{K})^{-1} = \hat{H}^\dagger \tag{D.142}$$

with complex conjugation $\mathcal{K}$, and hence belongs to class AII†. As a result of reciprocity, the left localization length ξ_{L} coincides with the right localization length ξ_{R}. On the other hand, a magnetic field $h \neq 0$ breaks reciprocity. The disordered potential m_n is uniformly distributed over $[-W/2, W/2]$ with $W \geq 0$.

The localization lengths as a function of the non-Hermiticity γ are shown in Fig. 6.2 (b) in Chap. 6, and those as a function of the disorder strength W are shown in Fig. D.2 (b). In contrast to the original Hatano-Nelson model without symmetry protection, both left and right localization lengths diverge at a critical point, which is consistent with the bidirectional delocalization predicted by the scaling theory of conductances for continuum models. As a consequence of the reciprocity-protected nature of the delocalization, even a small reciprocity-breaking perturbation $h \neq 0$ vanishes the delocalization. Although ξ_{L} is different from ξ_{R} in the absence of reciprocity, no appreciable difference can be seen for such a small perturbation as $h = 0.01$ considered in Figs. 6.2 (b) and D.2 (b).

The nature of the bidirectional delocalization is understood by the following SL (2)-gauge transformation

$$\hat{f}_n := \begin{pmatrix} e^{-n\theta} & 0 \\ 0 & e^{n\theta} \end{pmatrix} V^{-1} \hat{c}_n, \quad \hat{f}_n^\dagger := \hat{c}_n^\dagger V \begin{pmatrix} e^{n\theta} & 0 \\ 0 & e^{-n\theta} \end{pmatrix} \quad [\theta \in \mathbb{C},\ V \in \mathrm{SL}\,(2)]\,. \tag{D.143}$$

With the new fermion operators $\hat{f}_n$ and $\hat{f}_n^\dagger$, the Hamiltonian without the magnetic field (i.e., $h = 0$) reads

$$\begin{aligned} \hat{H} = \sum_n \Bigg\{ -\frac{1}{2} \Bigg[& \hat{f}_{n+1}^\dagger \begin{pmatrix} e^{-(n+1)\theta} & 0 \\ 0 & e^{(n+1)\theta} \end{pmatrix} V^{-1} \left(J + \frac{\gamma\sigma_z}{2} - \mathrm{i}\Delta\sigma_x \right) V \begin{pmatrix} e^{n\theta} & 0 \\ 0 & e^{-n\theta} \end{pmatrix} \hat{f}_n \\ & + \hat{f}_n^\dagger \begin{pmatrix} e^{-n\theta} & 0 \\ 0 & e^{n\theta} \end{pmatrix} V^{-1} \left(J - \frac{\gamma\sigma_z}{2} + \mathrm{i}\Delta\sigma_x \right) V \begin{pmatrix} e^{(n+1)\theta} & 0 \\ 0 & e^{-(n+1)\theta} \end{pmatrix} \hat{f}_{n+1} \Bigg] + m_n \hat{f}_n^\dagger \hat{f}_n \Bigg\}\,. \end{aligned} \tag{D.144}$$

Let us choose V such that it diagonalizes $J + \gamma\sigma_z/2 - \mathrm{i}\Delta\sigma_x$, i.e.,

$$V^{-1} \left(J + \frac{\gamma\sigma_z}{2} - \mathrm{i}\Delta\sigma_x \right) V = \begin{pmatrix} J + \sqrt{(\gamma/2)^2 - \Delta^2} & 0 \\ 0 & J - \sqrt{(\gamma/2)^2 - \Delta^2} \end{pmatrix}. \tag{D.145}$$

Then, the Hamiltonian reads

$$\begin{aligned} \hat{H} = \sum_n \Bigg\{ -\frac{1}{2} \Bigg[& \hat{f}_{n+1}^\dagger \begin{pmatrix} e^{-\theta} \left(J + \sqrt{(\gamma/2)^2 - \Delta^2} \right) & 0 \\ 0 & e^{\theta} \left(J - \sqrt{(\gamma/2)^2 - \Delta^2} \right) \end{pmatrix} \hat{f}_n \\ & + \hat{f}_n^\dagger \begin{pmatrix} e^{\theta} \left(J - \sqrt{(\gamma/2)^2 - \Delta^2} \right) & 0 \\ 0 & e^{-\theta} \left(J + \sqrt{(\gamma/2)^2 - \Delta^2} \right) \end{pmatrix} \hat{f}_{n+1} \Bigg] + m_n \hat{f}_n^\dagger \hat{f}_n \Bigg\}\,. \end{aligned} \tag{D.146}$$

Furthermore, let us choose θ such that it satisfies

$$e^{-\theta}\left(J+\sqrt{(\gamma/2)^2-\Delta^2}\right)=e^{\theta}\left(J-\sqrt{(\gamma/2)^2-\Delta^2}\right)=\tilde{J}, \tag{D.147}$$

i.e.,

$$\theta=\frac{1}{2}\log\left(\frac{J+\sqrt{(\gamma/2)^2-\Delta^2}}{J-\sqrt{(\gamma/2)^2-\Delta^2}}\right), \quad \tilde{J}=\sqrt{J^2-(\gamma/2)^2+\Delta^2}. \tag{D.148}$$

Consequently, the Hamiltonian reduces to the Hermitian Anderson model

$$\hat{H}=\sum_n\left\{-\frac{\tilde{J}}{2}\left(\hat{f}_{n+1}^{\dagger}\hat{f}_n+\hat{f}_n^{\dagger}\hat{f}_{n+1}\right)+m_n\hat{f}_n^{\dagger}\hat{f}_n\right\}. \tag{D.149}$$

Thus, the localization length of the reciprocal Hatano-Nelson model is given as

$$\xi_{\mathrm{L}}=\xi_{\mathrm{R}}=\left(\xi_0^{-1}-\left|\mathrm{Re}\left(\theta\right)\right|\right)^{-1}, \tag{D.150}$$

where ξ_0 is the localization length of the Hermitian Anderson model in Eq. (D.149). As can be seen from Eq. (D.148), $\mathrm{Re}\left(\theta\right)$ is zero for $|\gamma|\leq 2\left|\Delta\right|$, which leads to the plateau of the localization length in Fig. 6.2 (b) in Chap. 6. Importantly, the above SL (2)-gauge transformation is inapplicable in the presence of reciprocity-breaking perturbations, which forbids the bidirectional delocalization.

Acknowledgements

I would like to thank my advisor, Prof. Masahito Ueda, for his guidance throughout my graduate course. I would also be grateful to my collaborators, especially Prof. Shinsei Ryu, Prof. Masatoshi Sato, and Prof. Ken Shiozaki, who have deep insights into physics and share common interests with me. I would appreciate the review of this thesis by the committee members, Prof. Kenji Fukushima, Prof. Kensuke Kobayashi, Prof. Shuichi Murakami, Prof. Mio Murao, and Prof. Takashi Oka. The work in my graduate course was supported by KAKENHI Grant No. JP19J21927 from the Japan Society for the Promotion of Science.

Bibliography

[AA80] S. Aubry and G. André, *Analyticity breaking and Anderson localization in incommensurate lattices*, Ann. Israel Phys. Soc. **3** (1980) 133.

[AALR79] E. Abrahams, P. W. Anderson, D. C. Licciardello, and T. V. Ramakrishnan, *Scaling Theory of Localization: Absence of Quantum Diffusion in Two Dimensions*, Phys. Rev. Lett. **42** (1979) 673.

[ABF+14] A. Altland, D. Bagrets, L. Fritz, A. Kamenev, and H. Schmiedt, *Quantum Criticality of Quasi-One-Dimensional Topological Anderson Insulators*, Phys. Rev. Lett. **112** (2014) 206602.

[Abr81] A. A. Abrikosov, *The paradox with the static conductivity of a one-dimensional metal*, Solid State Commun. **37** (1981) 997.

[Abr88] ———, *Fundamentals of the Theory of Metals*, North Holland, Amsterdam, 1988.

[Adl69] S. L. Adler, *Axial-Vector Vertex in Spinor Electrodynamics*, Phys. Rev. **177** (1969) 2426.

[AFU17] Y. Ashida, S. Furukawa, and M. Ueda, *Parity-time-symmetric quantum critical phenomena*, Nat. Commun. **8** (2017) 15791.

[AGD63] A. A. Abrikosov, L. P. Gorkov, and I. E. Dzyaloshinski, *Methods of Quantum Field Theory in Statistical Physic*, Prentice Hall, Englewood Cliffs, New Jersey, 1963.

[AHN16] A. Amir, N. Hatano, and D. R. Nelson, *Non-Hermitian localization in biological networks*, Phys. Rev. E **93** (2016) 042310.

[AKLL80] B. L. Altshuler, D. Khmel'nitzkii, A. I. Larkin, and P. A. Lee, *Magnetoresistance and Hall effect in a disordered two-dimensional electron gas*, Phys. Rev. B **22** (1980) 5142.

[Ali12] J. Alicea, *New directions in the pursuit of Majorana fermions in solid state systems*, Rep. Prog. Phys. **75** (2012) 076501.

[AM76] N. W. Ashcroft and N. D. Mermin, *Solid State Physics*, Saunders College Publishing, New York, 1976.

[AMV18] N. P. Armitage, E. J. Mele, and A. Vishwanath, *Weyl and Dirac semimetals in three-dimensional solids*, Rev. Mod. Phys. **90** (2018) 015001.

[And58] P. W. Anderson, *Absence of Diffusion in Certain Random Lattices*, Phys. Rev. **109** (1958) 1492.

[AOR+11] J. Alicea, Y. Oreg, G. Refael, F. von Oppen, and M. P. A. Fisher, *Non-Abelian statistics and topological quantum information processing in 1D wire networks*, Nat. Phys. **7** (2011) 412.

[AS06] A. Altland and B. Simons, *Condensed Matter Field Theory*, Cambridge University Press, Cambridge, England, 2006.

[ATAF80] P. W. Anderson, D. J. Thouless, E. Abrahams, and D. S. Fisher, *New method for a scaling theory of localization*, Phys. Rev. B **22** (1980) 3519.

[AYF17] S. Assawaworrarit, X. Yu, and S. Fan, *Robust wireless power transfer using a nonlinear parity-time-symmetric circuit*, Nature **546** (2017) 387.

[AZ97] A. Altland and M. R. Zirnbauer, *Nonstandard symmetry classes in mesoscopic normal-superconducting hybrid structures*, Phys. Rev. B **55** (1997) 1142.

[BA13] J. C. Budich and E. Ardonne, *Equivalent topological invariants for one-dimensional Majorana wires in symmetry class D*, Phys. Rev. B **88** (2013) 075419.

[BB98] C. M. Bender and S. Boettcher, *Real Spectra in Non-Hermitian Hamiltonians Having $\mathcal{PT}$ Symmetry*, Phys. Rev. Lett. **80** (1998) 5243.

[BB11] A. A. Burkov and L. Balents, *Weyl Semimetal in a Topological Insulator Multilayer*, Phys. Rev. Lett. **107** (2011) 127205.

[BB19] E. J. Bergholtz and J. C. Budich, *Non-Hermitian Weyl physics in topological insulator ferromagnet junctions*, Phys. Rev. Research **1** (2019) 012003(R).

[BB20] J. C. Budich and E. J. Bergholtz, *Non-Hermitian Topological Sensors*, Phys. Rev. Lett. **125** (2020) 180403.

[BBH17a] W. A. Benalcazar, B. A. Bernevig, and T. L. Hughes, *Quantized electric multipole insulators*, Science **357** (2017) 61.

[BBH17b] W. A. Benalcazar, B. A. Bernevig, and T. L. Hughes, *Electric multipole moments, topological multipole moment pumping, and chiral hinge states in crystalline insulators*, Phys. Rev. B **96** (2017) 245115.

[BBJ02] C. M. Bender, D. C. Brody, and H. F. Jones, *Complex Extension of Quantum Mechanics*, Phys. Rev. Lett. **89** (2002) 270401.

[BBJM07] C. M. Bender, D. C. Brody, H. F. Jones, and B. K. Meister, *Faster than Hermitian Quantum Mechanics*, Phys. Rev. Lett. **98** (2007) 040403.

[BBK21] E. J. Bergholtz, J. C. Budich, and F. K. Kunst, *Exceptional topology of non-Hermitian systems*, Rev. Mod. Phys. **93** (2021) 015005.

[BBPS13] C. M. Bender, B. K. Berntson, D. Parker, and E. Samuel, *Observation of $\mathcal{PT}$ phase transition in a simple mechanical system*, Am. J. Phys. **81** (2013) 173.

[BC96] N. A. Bruce and J. T. Chalker, *Multiple scattering in the presence of absorption: a theoretical treatment for quasi one-dimensional systems*, J. Phys. A **29** (1996) 3761.

[BCKB19] J. C. Budich, J. Carlström, F. K. Kunst, and E. J. Bergholtz, *Symmetry-protected nodal phases in non-Hermitian systems*, Phys. Rev. B **99** (2019) 041406(R).

[BEC+17] B. Bradlyn, L. Elcoro, J. Cano, M. G. Vergniory, Z. Wang, C. Felser, M. I. Aroyo, and B. A. Bernevig, *Topological quantum chemistry*, Nature **547** (2017) 298.

[Bee97] C. W. J. Beenakker, *Random-matrix theory of quantum transport*, Rev. Mod. Phys. **69** (1997) 731.

[Bee15] ———, *Random-matrix theory of Majorana fermions and topological superconductors*, Rev. Mod. Phys. **87** (2015) 1037.

[Ben07] C. M. Bender, *Making sense of non-Hermitian Hamiltonians*, Rep. Prog. Phys. **70** (2007) 947.

[Ber04] M. V. Berry, *Physics of Nonhermitian Degeneracies*, Czech. J. Phys. **54** (2004) 1039.

[BF97] L. Balents and M. P. A. Fisher, *Delocalization transition via supersymmetry in one dimension*, Phys. Rev. B **56** (1997) 12970.

[BFGM00] P. W. Brouwer, A. Furusaki, I. A. Gruzberg, and C. Mudry, *Localization and Delocalization in Dirty Superconducting Wires*, Phys. Rev. Lett. **85** (2000) 1064.

[BFvdBM21] B. A. Bhargava, I. C. Fulga, J. van den Brink, and A. G. Moghaddam, *Non-Hermitian skin effect of dislocations and its topological origin*, Phys. Rev. B **104** (2021) L241402.

[BG05] A. Böttcher and S. M. Grudsky, *Spectral Properties of Banded Toeplitz Matices*, SIAM, Philadelphia, 2005.

[BG12] D. C. Brody and E.-M. Graefe, *Mixed-State Evolution in the Presence of Gain and Loss*, Phys. Rev. Lett. **109** (2012) 230405.

[BHB11] A. A. Burkov, M. D. Hook, and L. Balents, *Topological nodal semimetals*, Phys. Rev. B **84** (2011) 235126.

[BHZ06] B. A. Bernevig, T. L. Hughes, and S.-C. Zhang, *Quantum Spin Hall Effect and Topological Phase Transition in HgTe Quantum Wells*, Science **314** (2006) 1757.

[BJ69] J. S. Bell and R. Jackiw, *A PCAC puzzle:* $\pi^0 \to \gamma\gamma$ *in the* σ*-model*, Nuovo Cimento A **60** (1969) 47.

[BJZ+08] J. Billy, V. Josse, Z. Zuo, A. Bernard, B. Hambrecht, P. Lugan, D. Clément, L. Sanchez-Palencia, P. Bouyer, and A. Aspect, *Direct observation of Anderson localization of matter waves in a controlled disorder*, Nature **453** (2008) 891.

[BKS20] D. S. Borgnia, A. J. Kruchkov, and R.-J. Slager, *Non-Hermitian Boundary Modes and Topology*, Phys. Rev. Lett. **124** (2020) 056802.

[BL02] D. Bernard and A. LeClair, *A Classification of Non-Hermitian Random Matrices*, Springer, Dordrecht, 2002.

[BLH19] W. A. Benalcazar, T. Li, and T. L. Hughes, *Quantization of fractional corner charge in C_n-symmetric higher-order topological crystalline insulators*, Phys. Rev. B **99** (2019) 245151.

[BLLC19] M. Brandenbourger, X. Locsin, E. Lerner, and C. Coulais, *Non-reciprocal robotic metamaterials*, Nat. Commun. **10** (2019) 4608.

[BMSA98] P. W. Brouwer, C. Mudry, B. D. Simons, and A. Altland, *Delocalization in Coupled One-Dimensional Chains*, Phys. Rev. Lett. **81** (1998) 862.

[BNV+17] B. Bahari, A. Ndao, F. Vallini, A. E. Amili, Y. Fainman, and B. Kanté, *Nonreciprocal lasing in topological cavities of arbitrary geometries*, Science **358** (2017) 636.

[BP07] H.-P. Breuer and F. Petruccione, *The Theory of Open Quantum Systems*, Oxford University Press, Oxford, 2007.

[BPB96] C. W. J. Beenakker, J. C. J. Paasschens, and P. W. Brouwer, *Probability of Reflection by a Random Laser*, Phys. Rev. Lett. **76** (1996) 1368.

[Bro14] D. C. Brody, *Biorthogonal quantum mechanics*, J. Phys. A **47** (2014) 035305.

[Bro16] ———, *Consistency of PT-symmetric quantum mechanics*, J. Phys. A **49** (2016) 10LT03.

[BS21] T. Bessho and M. Sato, *Nielsen-Ninomiya Theorem with Bulk Topology: Duality in Floquet and Non-Hermitian Systems*, Phys. Rev. Lett. **127** (2021) 196404.

[BSB97] P. W. Brouwer, P. G. Silvestrov, and C. W. J. Beenakker, *Theory of directed localization in one dimension*, Phys. Rev. B **56** (1997) R4333(R).

[BWH+18] M. A. Bandres, S. Wittek, G. Harari, M. Parto, J. Ren, M. Segev, D. Christodoulides, and M. Khajavikhan, *Topological insulator laser: Experiments*, Science **359** (2018) eaar4005.

[Car93] H. Carmichael, *An Open Systems Approach to Quantum Optics*, Springer, Berlin, 1993.

[Car96] J. Cardy, *Scaling and Renormalization in Statistical Physics*, Cambridge University Press, Cambridge, England, 1996.

[CB18] J. Carlström and E. J. Bergholtz, *Exceptional links and twisted Fermi ribbons in non-Hermitian systems*, Phys. Rev. A **98** (2018) 042114.

[CC20] M. N. Chernodub and A. Cortijo, *Non-Hermitian Chiral Magnetic Effect in Equilibrium*, Symmetry **12** (2020) 761.

[CDS19] N. R. Cooper, J. Dalibard, and I. B. Spielman, *Topological bands for ultracold atoms*, Rev. Mod. Phys. **91** (2019) 015005.

[CGCS10] Y. D. Chong, L. Ge, H. Cao, and A. D. Stone, *Coherent Perfect Absorbers: Time-Reversed Lasers*, Phys. Rev. Lett. **105** (2010) 053901.

[CGS11] Y. D. Chong, L. Ge, and A. D. Stone, *$\mathcal{PT}$-Symmetry Breaking and Laser-Absorber Modes in Optical Scattering Systems*, Phys. Rev. Lett. **106** (2011) 093902.

[CH85] C. G. Callan and J. A. Harvey, *Anomalies and fermion zero modes on strings and domain walls*, Nucl. Phys. B **250** (1985) 427.

[CHC+19] A. Cerjan, S. Huang, K. P. Chen, Y. Chong, and M. C. Rechtsman, *Experimental realization of a Weyl exceptional ring*, Nat. Photon. **13** (2019) 623.

[CNGP+09] A. H. Castro Neto, F. Guinea, N. M. R. Peres, K. S. Novoselov, and A. K. Geim, *The electronic properties of graphene*, Rev. Mod. Phys. **81** (2009) 109.

[COZ+17] W. Chen, S. K. Özdemir, G. Zhao, J. Wiersig, and L. Yang, *Exceptional points enhance sensing in an optical microcavity*, Nature **548** (2017) 192.

[CSBB19] J. Carlström, M. Stålhammar, J. C. Budich, and E. J. Bergholtz, *Knotted non-Hermitian metals*, Phys. Rev. B **99** (2019) 161115(R).

[CTSR16] C.-K. Chiu, J. C. Y. Teo, A. P. Schnyder, and S. Ryu, *Classification of topological quantum matter with symmetries*, Rev. Mod. Phys. **88** (2016) 035005.

[CXYF18] A. Cerjan, M. Xiao, L. Yuan, and S. Fan, *Effects of non-Hermitian perturbations on Weyl Hamiltonians with arbitrary topological charges*, Phys. Rev. B **97** (2018) 075128.

[CYR13] C.-K. Chiu, H. Yao, and S. Ryu, *Classification of topological insulators and superconductors in the presence of reflection symmetry*, Phys. Rev. B **88** (2013) 075142.

[CYWR20] P.-Y. Chang, J.-S. You, X. Wen, and S. Ryu, *Entanglement spectrum and entropy in topological non-Hermitian systems and nonunitary conformal field theory*, Phys. Rev. Research **2** (2020) 033069.

[CZ18] Y. Chen and H. Zhai, *Hall conductance of a non-Hermitian Chern insulator*, Phys. Rev. B **98** (2018) 245130.

[Dal05] A. J. Daley, *Quantum trajectories and open many-body quantum systems*, Adv. Phys. **63** (2005) 77.

[Dat95] S. Datta, *Electronic Transport in Mesoscopic Systems*, Cambridge University Press, Cambridge, England, 1995.

[DCM92] J. Dalibard, Y. Castin, and K. Mølmer, *Wave-function approach to dissipative processes in quantum optics*, Phys. Rev. Lett. **68** (1992) 580.

[DDT01a] P. Dorey, C. Dunning, and R. Tateo, *Spectral equivalences, Bethe ansatz equations, and reality properties in $\mathcal{PT}$-symmetric quantum mechanics*, J. Phys. A **34** (2001) 5679.

[DDT01b] _____, *Supersymmetry and the spontaneous breakdown of $\mathcal{PT}$ symmetry*, J. Phys. A **34** (2001) L391.

[DG91] G. Deleuze and F. Guattari, *Qu'est-ce que la philosophie?*, Les Éditions de Minuit, Paris, 1991.

[DHM19] B. Dóra, M. Heyl, and R. Moessner, *The Kibble-Zurek mechanism at exceptional points*, Nat. Commun. **10** (2019) 2254.

[DMB+16] J. Doppler, A. A. Mailybaev, J. Böhm, U. Kuhl, A. Girschikm, F. Libisch, T. J. Milburn, P. Rabl, N. Moiseyev, and S. Rotter, *Dynamically encircling an exceptional point for asymmetric mode switching*, Nature **537** (2016) 76.

[Dor82] O. N. Dorokhov, *Transmission coefficient and the localization length of an electron in N bound disordered chains*, JETP Lett. **36** (1982) 318.

[DSAHR11] S. Das Sarma, S. Adam, E. H. Hwang, and E. Rossi, *Electronic transport in two-dimensional graphene*, Rev. Mod. Phys. **83** (2011) 407.

[DSS+21] M. M. Denner, A. Skurativska, F. Schindler, M. H. Fischer, R. Thomale, T. Bzdušek, and T. Neupert, *Exceptional topological insulators*, Nat. Commun. **12** (2021) 5681.

[Dys53] F. J. Dyson, *The Dynamics of a Disordered Linear Chain*, Phys. Rev. **92** (1953) 1331.

[Dys62] F. J. Dyson, *The Threefold Way. Algebraic Structure of Symmetry Groups and Ensembles in Quantum Mechanics*, J. Math. Phys. **3** (1962) 1199.

[DZR92] R. Dum, P. Zoller, and H. Ritsch, *Monte Carlo simulation of the atomic master equation for spontaneous emission*, Phys. Rev. A **45** (1992) 4879.

[Efe97a] K. Efetov, *Supersymmetry in Disorder and Chaos*, Cambridge University Press, Cambridge, England, 1997.

[Efe97b] K. B. Efetov, *Directed Quantum Chaos*, Phys. Rev. Lett. **79** (1997) 491.

[EGMCM07] R. El-Ganainy, K. G. Makris, D. N. Christodoulides, and Z. H. Musslimani, *Theory of coupled optical PT-symmetric structures*, Opt. Lett. **32** (2007) 2632.

[EGMK+18] R. El-Ganainy, K. G. Makris, M. Khajavikhan, Z. H. Musslimani, S. Rotter, and D. N. Christodoulides, *Non-Hermitian physics and PT symmetry*, Nat. Phys. **14** (2018) 11.

[EKB19] E. Edvardsson, F. K. Kunst, and E. J. Bergholtz, *Non-Hermitian extensions of higher-order topological phases and their biorthogonal bulk-boundary correspondence*, Phys. Rev. B **99** (2019) 081302(R).

[EM08] F. Evers and A. D. Mirlin, *Anderson transitions*, Rev. Mod. Phys. **80** (2008) 1355.

[EMV09] A. M. Essin, J. E. Moore, and D. Vanderbilt, *Magnetoelectric Polarizability and Axion Electrodynamics in Crystalline Insulators*, Phys. Rev. Lett. **102** (2009) 146805.

[ESHK11] K. Esaki, M. Sato, K. Hasebe, and M. Kohmoto, *Edge states and topological phases in non-Hermitian systems*, Phys. Rev. B **84** (2011) 205128.

[FEGG17] L. Feng, R. El-Ganainy, and L. Ge, *Non-Hermitian photonics based on parity-time symmetry*, Nat. Photon. **11** (2017) 752.

[Fes58] H. Feshbach, *Unified theory of nuclear reactions*, Ann. Phys. **5** (1958) 357.

[Fes62] ———, *A unified theory of nuclear reactions. II*, Ann. Phys. **19** (1962) 287.

[FF19] C. Fang and L. Fu, *New classes of topological crystalline insulators having surface rotation anomaly*, Sci. Adv. **5** (2019) eaat2374.

[FHW21] Y. Fu, J. Hu, and S. Wan, *Non-Hermitian second-order skin and topological modes*, Phys. Rev. B **103** (2021) 045420.

[Fis78] M. E. Fisher, *Yang-Lee Edge Singularity and ϕ^3 Field Theory*, Phys. Rev. Lett. **40** (1978) 1610.

[FK91] J. Fröhlich and T. Kerler, *Universality in quantum Hall systems*, Nucl. Phys. B **354** (1991) 369.

[FK98] T. Fukui and N. Kawakami, *Breakdown of the Mott insulator: Exact solution of an asymmetric Hubbard model*, Phys. Rev. B **58** (1998) 16051.

[FK06] L. Fu and C. L. Kane, *Time reversal polarization and a Z_2 adiabatic spin pump*, Phys. Rev. B **74** (2006) 195312.

[FK07] ———, *Topological insulators with inversion symmetry*, Phys. Rev. B **76** (2007) 045302.

[FK08] ———, *Superconducting Proximity Effect and Majorana Fermions at the Surface of a Topological Insulator*, Phys. Rev. Lett. **100** (2008) 096407.

[FKM07] L. Fu, C. L. Kane, and E. J. Mele, *Topological Insulators in Three Dimensions*, Phys. Rev. Lett. **98** (2007) 106803.

[FKW08] K. Fukushima, D. E. Kharzeev, and H. J. Warringa, *Chiral magnetic effect*, Phys. Rev. D **78** (2008) 074033.

[FPW54] H. Feshbach, C. E. Porter, and V. F. Weisskopf, *Model for Nuclear Reactions with Neutrons*, Phys. Rev. **96** (1954) 448.

[FPY94] V. Freilikher, M. Pustilnik, and I. Yurkevich, *Effect of Absorption on the Wave Transport in the Strong Localization Regime*, Phys. Rev. Lett. **73** (1994) 810.

[FSA15] R. Fleury, D. Sounas, and A. Alù, *An invisible acoustic sensor based on parity-time-symmetry*, Nat. Commun. **6** (2015) 5905.

[Fu11] L. Fu, *Topological Crystalline Insulators*, Phys. Rev. Lett. **106** (2011) 106802.

[FWM+14] L. Feng, Z. J. Wong, R.-M. Ma, Y. Wang, and X. Zhang, *Single-mode laser by parity-time symmetry breaking*, Science **346** (2014) 972.

[FXF+13] L. Feng, Y.-L. Xu, W. S. Fegadolli, M.-H. Lu, J. E. B. Oliveira, V. R. Almeida, Y.-F. Chen, and A. Scherer, *Experimental demonstration of a unidirectional reflectionless parity-time metamaterial at optical frequencies*, Nat. Mater. **12** (2013) 108.

[FZ97] J. Feinberg and A. Zee, *Non-hermitian random matrix theory: Method of hermitian reduction*, Nucl. Phys. B **504** (1997) 579.

[FZ99] J. Feinberg and A. Zee, *Non-Hermitian localization and delocalization*, Phys. Rev. E **59** (1999) 6433.

[Gad93] R. Gade, *Anderson localization for sublattice models*, Nucl. Phys. **398** (1993) 499.

[GAK+18] Z. Gong, Y. Ashida, K. Kawabata, K. Takasan, S. Higashikawa, and M. Ueda, *Topological Phases of Non-Hermitian Systems*, Phys. Rev. X **8** (2018) 031079.

[Gam28] G. Gamow, *Zur Quantentheorie des Atomkernes*, Z. Physik **51** (1928) 204.

[GBvWC20] A. Ghatak, M. Brandenbourger, J. van Wezel, and C. Coulais, *Observation of non-Hermitian topology and its bulk-edge correspondence in an active mechanical metamaterial*, Proc. Natl. Acad. Sci. USA **117** (2020) 29561.

[GBZ16] N. Goldman, J. C. Budich, and P. Zoller, *Topological quantum matter with ultracold gases in optical lattices*, Nat. Phys. **12** (2016) 639.

[GEB+15] T. Gao, E. Estrecho, K. Y. Bliokh, T. C. H. Liew, M. D. Fraser, S. Brodbeck, M. Kemp, C. Schneider, S. Höfling, Y. Yamamoto, F. Nori, Y. S. Kivshar, A. G. Truscott, R. G. Dall, and E. A. Ostrovskaya, *Observation of non-Hermitian degeneracies in a chaotic exciton-polariton billiard*, Nature **526** (2015) 554.

[GGR21] P. Glorioso, A. Gromov, and S. Ryu, *Effective response theory for Floquet topological systems*, Phys. Rev. Research **3** (2021) 013117.

[GK98] I. Y. Goldsheid and B. A. Khoruzhenko, *Distribution of Eigenvalues in Non-Hermitian Anderson Models*, Phys. Rev. Lett. **80** (1998) 2897.

[GKN08] E. M. Graefe, H. J. Korsch, and A. E. Niederle, *Mean-Field Dynamics of a Non-Hermitian Bose-Hubbard Dimer*, Phys. Rev. Lett. **101** (2008) 150408.

[GLK79] L. P. Gor'kov, A. I. Larkin, and D. E. Khmel'nitskii, *Particle conductivity in a two-dimensional random potential*, JETP Lett. **30** (1979) 228.

[Gol92] N. Goldenfeld, *Lectures on Phase Transitions and the Renormalization Group*, Westview Press, Boulder, 1992.

[GS08] U. Günther and B. F. Samsonov, *Naimark-Dilated $\mathcal{PT}$-Symmetric Brachistochrone*, Phys. Rev. Lett. **101** (2008) 230404.

[GSD+09] A. Guo, G. J. Salamo, D. Duchesne, R. Morandotti, M. Volatier-Ravat, V. Aimez, G. A. Siviloglou, and D. N. Christodoulides, *Observation of $\mathcal{PT}$-Symmetry Breaking in Complex Optical Potentials*, Phys. Rev. Lett. **103** (2009) 093902.

[GW91] R. Gade and F. Wegner, *The $n = 0$ replica limit of $\mathrm{U}(n)$ and $\mathrm{U}(n)\,\mathrm{SO}(n)$ models*, Nucl. Phys. **360** (1991) 213.

[GWWK20] C.-X. Guo, X.-R. Wang, C. Wang, and S.-P. Kou, *Non-Hermitian dynamic strings and anomalous topological degeneracy on a non-Hermitian toric-code model with parity-time symmetry*, Phys. Rev. B **101** (2020) 144439.

[Hal88] F. D. M. Haldane, *Model for a Quantum Hall Effect without Landau Levels: Condensed-Matter Realization of the "Parity Anomaly"*, Phys. Rev. Lett. **61** (1988) 2015.

[Ham20] R. Hamazaki, private communication, 2020.

[HBL+18] G. Harari, M. A. Bandres, Y. Lumer, M. C. Rechtsman, Y. D. Chong, M. Khajavikhan, D. N. Christodoulides, and M. Segev, *Topological insulator laser: Theory*, Science **359** (2018) eaar4003.

[HBR19] L. Herviou, J. H. Bardarson, and N. Regnault, *Defining a bulk-edge correspondence for non-Hermitian Hamiltonians via singular-value decomposition*, Phys. Rev. A **99** (2019) 052118.

[Hcv05] P. Hořava, *Stability of Fermi Surfaces and K Theory*, Phys. Rev. Lett. **95** (2005) 016405.

[Hei12] W. D. Heiss, *The physics of exceptional points*, J. Phys. A **45** (2012) 444016.

[HH11] Y. C. Hu and T. L. Hughes, *Absence of topological insulator phases in non-Hermitian PT-symmetric Hamiltonians*, Phys. Rev. B **84** (2011) 153101.

[HHI+20] T. Helbig, T. Hofmann, S. Imhof, M. Abdelghany, T. Kiessling, L. W. Molenkamp, C. H. Lee, A. Szameit, M. Greiter, and R. Thomale, *Generalized bulk-boundary correspondence in non-Hermitian topolectrical circuits*, Nat. Phys. **16** (2020) 747.

[HHS+20] T. Hofmann, T. Helbig, F. Schindler, N. Salgo, M. Brzezińska, M. Greiter, T. Kiessling, D. Wolf, A. Vollhardt, A. Kabaši, C. H. Lee, A. Bilušić, R. Thomale, and T. Neupert, *Reciprocal skin effect and its realization in a topolectrical circuit*, Phys. Rev. Research **2** (2020) 023265.

[HHW+17] H. Hodaei, A. U. Hassan, S. Wittek, H. Garcia-Gracia, R. El-Ganainy, D. N. Christodoulides, and M. Khajavikhan, *Enhanced sensitivity at higher-order exceptional points*, Nature **548** (2017) 187.

[HK10] M. Z. Hasan and C. L. Kane, *Colloquium: Topological insulators*, Rev. Mod. Phys. **82** (2010) 3045.

[HKKU20] R. Hamazaki, K. Kawabata, N. Kura, and M. Ueda, *Universality classes of non-Hermitian random matrices*, Phys. Rev. Research **2** (2020) 023286.

[HKM+19] A. E. Hassan, F. K. Kunst, A. Moritz, G. Andler, E. J. Bergholtz, and M. Bourennane, *Corner states of light in photonic waveguides*, Nat. Photon. **13** (2019) 697.

[HKU19] R. Hamazaki, K. Kawabata, and M. Ueda, *Non-Hermitian Many-Body Localization*, Phys. Rev. Lett. **123** (2019) 090603.

[HLN80] S. Hikami, A. I. Larkin, and Y. Nagaoka, *Spin-Orbit Interaction and Magnetoresistance in the Two Dimensional Random System*, Prog. Theor. Phys. **63** (1980) 707.

[HMH+14] H. Hodaei, M.-A. Miri, M. Heinrich, D. N. Christodoulides, and M. Khajavikhan, *Parity-time-symmetric microring lasers*, Science **346** (2014) 975.

[HN96] N. Hatano and D. R. Nelson, *Localization Transitions in Non-Hermitian Quantum Mechanics*, Phys. Rev. Lett. **77** (1996) 570.

[HN97] ———, *Vortex pinning and non-Hermitian quantum mechanics*, Phys. Rev. B **56** (1997) 8651.

[HN98] ———, *Non-Hermitian delocalization and eigenfunctions*, Phys. Rev. B **58** (1998) 8384.

[HPB11] T. L. Hughes, E. Prodan, and B. A. Bernevig, *Inversion-symmetric topological insulators*, Phys. Rev. B **83** (2011) 245132.

[HPG19] M. R. Hirsbrunner, T. M. Philip, and M. J. Gilbert, *Topology and observables of the non-Hermitian Chern insulator*, Phys. Rev. B **100** (2019) 081104(R).

[HRB19] L. Herviou, N. Regnault, and J. H. Bardarson, *Entanglement spectrum and symmetries in non-Hermitian fermionic non-interacting models*, SciPost Phys. **7** (2019) 069.

[HS20] Y. Huang and B. I. Shklovskii, *Anderson transition in three-dimensional systems with non-Hermitian disorder*, Phys. Rev. B **101** (2020) 014204.

[Huc95] B. Huckestein, *Scaling theory of the integer quantum Hall effect*, Rev. Mod. Phys. **67** (1995) 357.

[HZZ+21] B. Hu, Z. Zhang, H. Zhang, L. Zheng, W. Xiong, Z. Yue, X. Wang, J. Xu, Y. Cheng, X. Liu, and J. Christensen, *Non-Hermitian topological whispering gallery*, Nature **597** (2021) 655.

[IBB+18] S. Imhof, C. Berger, F. Bayer, J. Brehm, L. W. Molenkamp, T. Kiessling, F. Schindler, C. H. Lee, M. Greiter, T. Neupert, and R. Thomale, *Topolectrical-circuit realization of topological corner modes*, Nat. Phys. **14** (2018) 925.

[ID89] C. Itzykson and J.-M. Drouffe, *Statistical Field Theory*, vol. I, Cambridge University Press, Cambridge, England, 1989.

[IM87] K. Ishikawa and T. Matsuyama, *A microscopic theory of the quantum Hall effect*, Nucl. Phys. B **280** (1987) 523.

[Imr97] Y. Imry, *Introduction to Mesoscopic Physics*, Oxford University Press, New York, 1997.

[IT19] K.-I. Imura and Y. Takane, *Generalized bulk-edge correspondence for non-Hermitian topological systems*, Phys. Rev. B **100** (2019) 165430.

[Iva01] D. A. Ivanov, *Non-Abelian Statistics of Half-Quantum Vortices in p-Wave Superconductors*, Phys. Rev. Lett. **86** (2001) 268.

[Jac62] J. D. Jackson, *Classical Electrodynamics*, John Wiley & Sons, New York, 1962.

[JLY+19] H. Jiang, L.-J. Lang, C. Yang, S.-L. Zhu, and S. Chen, *Interplay of non-Hermitian skin effects and Anderson localization in nonreciprocal quasiperiodic lattices*, Phys. Rev. B **100** (2019) 054301.

[JOL+14] H. Jing, S. K. Özdemir, X.-Y. Lü, J. Zhang, L. Yang, and F. Nori, *$\mathcal{PT}$-symmetric phonon laser*, Phys. Rev. Lett. **113** (2014) 053604.

[JS19] L. Jin and Z. Song, *Bulk-boundary correspondence in a non-Hermitian system in one dimension with chiral inversion symmetry*, Phys. Rev. B **99** (2019) 081103.

[KAKU18] K. Kawabata, Y. Ashida, H. Katsura, and M. Ueda, *Parity-time-symmetric topological superconductor*, Phys. Rev. B **98** (2018) 085116.

[Kam11] A. Kamenev, *Field Theory of Non-Equilibrium Systems*, Cambridge University Press, Cambridge, England, 2011.

[Kar78] M. Karoubi, *K-Theory*, Springer, Berlin, 1978.

[Kat66] T. Kato, *Perturbation Theory for Linear Operators*, Springer, Berlin, 1966.

[KAU17] K. Kawabata, Y. Ashida, and M. Ueda, *Information Retrieval and Criticality in Parity-Time-Symmetric Systems*, Phys. Rev. Lett. **119** (2017) 190401.

[KB20] R. Koch and J. C. Budich, *Bulk-boundary correspondence in non-Hermitian systems: stability analysis for generalized boundary conditions*, Eur. Phys. J. D **74** (2020) 70.

[KBS19] K. Kawabata, T. Bessho, and M. Sato, *Classification of Exceptional Points and Non-Hermitian Topological Semimetals*, Phys. Rev. Lett. **123** (2019) 066405.

[KD19] F. K. Kunst and V. Dwivedi, *Non-Hermitian systems and topology: A transfer-matrix perspective*, Phys. Rev. B **99** (2019) 245116.

[KdBvW+17] J. Kruthoff, J. de Boer, J. van Wezel, C. L. Kane, and R.-J. Slager, *Topological Classification of Crystalline Insulators through Band Structure Combinatorics*, Phys. Rev. X **7** (2017) 041069.

[KDP80] K. v. Klitzing, G. Dorda, and M. Pepper, *New Method for High-Accuracy Determination of the Fine-Structure Constant Based on Quantized Hall Resistance*, Phys. Rev. Lett. **45** (1980) 494.

[KEBB18] F. K. Kunst, E. Edvardsson, J. C. Budich, and E. J. Bergholtz, *Biorthogonal Bulk-Boundary Correspondence in Non-Hermitian Systems*, Phys. Rev. Lett. **121** (2018) 026808.

[KFar] V. Kozii and L. Fu, *Non-Hermitian Topological Theory of Finite-Lifetime Quasiparticles: Prediction of Bulk Fermi Arc Due to Exceptional Point*, 2017, arXiv:1708.05841.

[KGM08] S. Klaiman, U. Günther, and N. Moiseyev, *Visualization of Branch Points in $\mathcal{PT}$-Symmetric Waveguides*, Phys. Rev. Lett. **101** (2008) 080402.

[Kha18] E. Khalaf, *Higher-order topological insulators and superconductors protected by inversion symmetry*, Phys. Rev. B **97** (2018) 205136.

[KHG+19] K. Kawabata, S. Higashikawa, Z. Gong, Y. Ashida, and M. Ueda, *Topological unification of time-reversal and particle-hole symmetries in non-Hermitian physics*, Nat. Commun. **10** (2019) 297.

[Kit01] A. Y. Kitaev, *Unpaired Majorana fermions in quantum wires*, Phys.-Usp. **44** (2001) 131.

[Kit09] A. Kitaev, *Periodic table for topological insulators and superconductors*, AIP Conf. Proc. **1134** (2009) 22.

[KM05a] C. L. Kane and E. J. Mele, *Z_2 Topological Order and the Quantum Spin Hall Effect*, Phys. Rev. Lett. **95** (2005) 146802.

[KM05b] ———, *Quantum Spin Hall Effect in Graphene*, Phys. Rev. Lett. **95** (2005) 226801.

[KMOS10] B. Kramer, A. MacKinnon, T. Ohtsuki, and K. Slevin, *Finite Size Scaling Analysis of the Anderson Transition*, Int. J. Mod. Phys. B **24** (2010) 1841.

[Kog79] J. B. Kogut, *An introduction to lattice gauge theory and spin systems*, Rev. Mod. Phys. **51** (1979) 659.

[Koh85] M. Kohmoto, *Topological invariant and the quantization of the Hall conductance*, Ann. Phys. **160** (1985) 343.

[KOK05] B. Kramer, T. Ohtsuki, and S. Kettemann, *Random network models and quantum phase transitions in two dimensions*, Phys. Rep. **417** (2005) 211.

[KOS20] K. Kawabata, N. Okuma, and M. Sato, *Non-Bloch band theory of non-Hermitian Hamiltonians in the symplectic class*, Phys. Rev. B **101** (2020) 195147.

[KP21] K.-M. Kim and M. J. Park, *Disorder-driven phase transition in the second-order non-Hermitian skin effect*, Phys. Rev. B **104** (2021) L121101.

[KPVW18] E. Khalaf, H. C. Po, A. Vishwanath, and H. Watanabe, *Symmetry Indicators and Anomalous Surface States of Topological Crystalline Insulators*, Phys. Rev. X **8** (2018) 031070.

[KR21] K. Kawabata and S. Ryu, *Nonunitary Scaling Theory of Non-Hermitian Localization*, Phys. Rev. Lett. **126** (2021) 166801.

[KS20] K. Kawabata and M. Sato, *Real spectra in non-Hermitian topological insulators*, Phys. Rev. Research **2** (2020) 033391.

[KSR21] K. Kawabata, K. Shiozaki, and S. Ryu, *Topological Field Theory of Non-Hermitian Systems*, Phys. Rev. Lett. **126** (2021) 216405.

[KSS20] K. Kawabata, M. Sato, and K. Shiozaki, *Higher-order non-Hermitian skin effect*, Phys. Rev. B **102** (2020) 205118.

[KSU18] K. Kawabata, K. Shiozaki, and M. Ueda, *Anomalous helical edge states in a non-Hermitian Chern insulator*, Phys. Rev. B **98** (2018) 165148.

[KSUS19] K. Kawabata, K. Shiozaki, M. Ueda, and M. Sato, *Symmetry and Topology in Non-Hermitian Physics*, Phys. Rev. X **9** (2019) 041015.

[KvMB18] F. K. Kunst, G. van Miert, and E. J. Bergholtz, *Lattice models with exactly solvable topological hinge and corner states*, Phys. Rev. B **97** (2018) 241405(R).

[KWB+07] M. König, S. Wiedmann, C. Brüne, A. Roth, H. Buhmann, L. W. Molenkamp, X.-L. Qi, and S.-C. Zhang, *Quantum Spin Hall Insulator State in HgTe Quantum Wells*, Science **318** (2007) 766.

[KYK19] K. Kimura, T. Yoshida, and N. Kawakami, *Chiral-symmetry protected exceptional torus in correlated nodal-line semimetals*, Phys. Rev. B **100** (2019) 115124.

[KYZ16] V. V. Konotop, J. Yang, and D. A. Zezyulin, *Nonlinear waves in $\mathcal{PT}$-symmetric systems*, Rev. Mod. Phys. **88** (2016) 035002.

[LAP+08] Y. Lahini, A. Avidan, F. Pozzi, M. Sorel, R. Morandotti, D. N. Christodoulides, and Y. Silberberg, *Anderson Localization and Nonlinearity in One-Dimensional Disordered Photonic Lattices*, Phys. Rev. Lett. **100** (2008) 013906.

[LAZV19] J. Y. Lee, J. Ahn, H. Zhou, and A. Vishwanath, *Topological Correspondence between Hermitian and Non-Hermitian Systems: Anomalous Dynamics*, Phys. Rev. Lett. **123** (2019) 206404.

[LBH+17] D. Leykam, K. Y. Bliokh, C. Huang, Y. D. Chong, and F. Nori, *Edge Modes, Degeneracies, and Topological Numbers in Non-Hermitian Systems*, Phys. Rev. Lett. **118** (2017) 040401.

[LC14] T. E. Lee and C.-K. Chan, *Heralded Magnetism in Non-Hermitian Atomic Systems*, Phys. Rev. X **4** (2014) 041001.

[LC18] H.-K. Lau and A. A. Clerk, *Fundamental limits and non-reciprocal approaches in non-Hermitian quantum sensing*, Nat. Commun. **9** (2018) 4320.

[Lee16] T. E. Lee, *Anomalous Edge State in a Non-Hermitian Lattice*, Phys. Rev. Lett. **116** (2016) 133903.

[Leiar] M. Lein, *On Choosing a Physically Meaningful Topological Classification for Non-Hermitian Systems and the Issue of Diagonalizability*, 2020, arXiv:2010.09261.

[LF91] A. Lopez and E. Fradkin, *Fractional quantum Hall effect and Chern-Simons gauge theories*, Phys. Rev. B **44** (1991) 5246.

[LGV15] S. Longhi, D. Gatti, and G. D. Valle, *Robust light transport in non-Hermitian photonic lattices*, Sci. Rep. **5** (2015) 13376.

[LH13] S.-D. Liang and G.-Y. Huang, *Topological invariance and global Berry phase in non-Hermitian systems*, Phys. Rev. A **87** (2013) 012118.

[LHL+19] J. Li, A. K. Harter, J. Liu, L. de Melo, Y. N. Joglekar, and L. Luo, *Observation of parity-time symmetry breaking transitions in a dissipative Floquet system of ultracold atoms*, Nat. Commun. **10** (2019) 855.

[LHY+20] T. Liu, J. J. He, T. Yoshida, Z.-L. Xiang, and F. Nori, *Non-Hermitian topological Mott insulators in one-dimensional fermionic superlattices*, Phys. Rev. B **102** (2020) 235151.

[Lie18a] S. Lieu, *Topological phases in the non-Hermitian Su-Schrieffer-Heeger model*, Phys. Rev. B **97** (2018) 045106.

[Lie18b] ———, *Topological symmetry classes for non-Hermitian models and connections to the bosonic Bogoliubov–de Gennes equation*, Phys. Rev. B **98** (2018) 115135.

[LJS14] L. Lu, J. Joannopoulos, and M. Soljačić, *Topological photonics*, Nat. Photon. **8** (2014) 821.

[LL60] L. D. Landau and E. M. Lifshitz, *Mechanics*, Pergamon Press, Oxford, 1960.

[LLG19] C. H. Lee, L. Li, and J. Gong, *Hybrid Higher-Order Skin-Topological Modes in Nonreciprocal Systems*, Phys. Rev. Lett. **123** (2019) 016805.

[LLMG20] L. Li, C. H. Lee, S. Mu, and J. Gong, *Critical non-Hermitian skin effect*, Nat. Commun. **11** (2020) 5491.

[LLY20] E. Lee, H. Lee, and B.-J. Yang, *Many-body approach to non-Hermitian physics in fermionic systems*, Phys. Rev. B **101** (2020) 121109.

[LM21] Z. Li and R. S. K. Mong, *Homotopical characterization of non-Hermitian band structures*, Phys. Rev. B **103** (2021) 155129.

[LMC20] S. Lieu, M. McGinley, and N. R. Cooper, *Tenfold Way for Quadratic Lindbladians*, Phys. Rev. Lett. **124** (2020) 040401.

[LMLG21] L. Li, S. Mu, C. H. Lee, and J. Gong, *Quantized classical response from spectral winding topology*, Nat. Commun. **12** (2021) 5294.

[Lon09] S. Longhi, *Bloch Oscillations in Complex Crystals with $\mathcal{PT}$ Symmetry*, Phys. Rev. Lett. **103** (2009) 123601.

[Lon10] S. Longhi, *$\mathcal{PT}$-symmetric laser absorber*, Phys. Rev. A **82** (2010) 031801(R).

[Lon19a] S. Longhi, *Topological Phase Transition in non-Hermitian Quasicrystals*, Phys. Rev. Lett. **122** (2019) 237601.

[Lon19b] S. Longhi, *Probing non-Hermitian skin effect and non-Bloch phase transitions*, Phys. Rev. Research **1** (2019) 023013.

[Lon19c] ———, *Metal-insulator phase transition in a non-Hermitian Aubry-André-Harper model*, Phys. Rev. B **100** (2019) 125157.

[Lon20] S. Longhi, *Non-Bloch-Band Collapse and Chiral Zener Tunneling*, Phys. Rev. Lett. **124** (2020) 066602.

[LOS21a] X. Luo, T. Ohtsuki, and R. Shindou, *Universality Classes of the Anderson Transitions Driven by Non-Hermitian Disorder*, Phys. Rev. Lett. **126** (2021) 090402.

[LOS21b] ———, *Transfer matrix study of the Anderson transition in non-Hermitian systems*, Phys. Rev. B **104** (2021) 104203.

[LPH+19] Y. Li, Y.-G. Peng, L. Han, M.-A. Miri, W. Li, M. Xiao, X.-F. Zhu, J. Zhao, A. Alù, S. Fan, and C.-W. Qiu, *Anti-parity-time symmetry in diffusive systems*, Science **364** (2019) 170.

[LPT+17] J. Langbehn, Y. Peng, L. Trifunovic, F. von Oppen, and P. W. Brouwer, *Reflection-Symmetric Second-Order Topological Insulators and Superconductors*, Phys. Rev. Lett. **119** (2017) 246401.

[LR85] P. A. Lee and T. V. Ramakrishnan, *Disordered electronic systems*, Rev. Mod. Phys. **57** (1985) 287.

[LRE+11] Z. Lin, H. Ramezani, T. Eichelkraut, T. Kottos, H. Cao, and D. N. Christodoulides, *Unidirectional Invisibility Induced by $\mathcal{PT}$-Symmetric Periodic Structures*, Phys. Rev. Lett. **106** (2011) 213901.

[LRM14] T. E. Lee, F. Reiter, and N. Moiseyev, *Entanglement and Spin Squeezing in Non-Hermitian Phase Transitions*, Phys. Rev. Lett. **113** (2014) 250401.

[LSDS10] R. M. Lutchyn, J. D. Sau, and S. Das Sarma, *Majorana Fermions and a Topological Phase Transition in Semiconductor-Superconductor Heterostructures*, Phys. Rev. Lett. **105** (2010) 077001.

[LSGR21] Y. Liu, H. Shapourian, P. Glorioso, and S. Ryu, *Gauging anomalous unitary operators*, Phys. Rev. B **104** (2021) 155144.

[LT19] C. H. Lee and R. Thomale, *Anatomy of skin modes and topology in non-Hermitian systems*, Phys. Rev. B **99** (2019) 201103(R).

[LVK19] S. Liu, A. Vishwanath, and E. Khalaf, *Shift Insulators: Rotation-Protected Two-Dimensional Topological Crystalline Insulators*, Phys. Rev. X **9** (2019) 031003.

[LWF+15] B. Q. Lv, H. M. Weng, B. B. Fu, X. P. Wang, H. Miao, J. Ma, P. Richard, X. C. Huang, L. X. Zhao, G. F. Chen, Z. Fang, X. Dai, T. Qian, and H. Ding, *Experimental Discovery of Weyl Semimetal TaAs*, Phys. Rev. X **5** (2015) 031013.

[LWY+15] L. Lu, Z. Wang, D. Ye, L. Ran, L. Fu, J. D. Joannopoulos, and M. Soljačić, *Experimental observation of Weyl points*, Science **349** (2015) 622.

[LXKKSar] X. Luo, Z. Xiao, T. O. Kohei Kawabata, and R. Shindou, *Unifying the Anderson Transitions in Hermitian and Non-Hermitian Systems*, 2021, arXiv:2105.02514.

[LY52] T. D. Lee and C. N. Yang, *Statistical Theory of Equations of State and Phase Transitions. II. Lattice Gas and Ising Model*, Phys. Rev. **87** (1952) 410.

[LYRF21] H. Liu, J.-S. You, S. Ryu, and I. C. Fulga, *Supermetal-insulator transition in a non-Hermitian network model*, Phys. Rev. B **104** (2021) 155412.

[LZ19] X.-W. Luo and C. Zhang, *Higher-Order Topological Corner States Induced by Gain and Loss*, Phys. Rev. Lett. **123** (2019) 073601.

[LZA+19] T. Liu, Y.-R. Zhang, Q. Ai, Z. Gong, K. Kawabata, M. Ueda, and F. Nori, *Second-Order Topological Phases in Non-Hermitian Systems*, Phys. Rev. Lett. **122** (2019) 076801.

[LZO+16] Z.-P. Liu, J. Zhang, S. K. Özdemir, B. Peng, H. Jing, X.-Y. Lü, C.-W. Li, L. Yang, F. Nori, and Y.-x. Liu, *Metrology with $\mathcal{PT}$-Symmetric Cavities: Enhanced Sensitivity near the $\mathcal{PT}$-Phase Transition*, Phys. Rev. Lett. **117** (2016) 110802.

[LZYC20] C.-H. Liu, K. Zhang, Z. Yang, and S. Chen, *Helical damping and dynamical critical skin effect in open quantum systems*, Phys. Rev. Research **2** (2020) 043167.

[LZZar] C. Lv, R. Zhang, and Q. Zhou, *Curving the space by non-Hermiticity*, 2021, arXiv:2106.02477.

[MA19] M.-A. Miri and A. Alù, *Exceptional points in optics and photonics*, Science **363** (2019) eaar7709.

[MABVFT18] V. M. Martinez Alvarez, J. E. Barrios Vargas, and L. E. F. Foa Torres, *Non-Hermitian robust edge states in one dimension: Anomalous localization and eigenspace condensation at exceptional points*, Phys. Rev. B **97** (2018) 121401(R).

[Mag08] U. Magnea, *Random matrices beyond the Cartan classification*, J. Phys. A **41** (2008) 045203.

[MB07] J. E. Moore and L. Balents, *Topological invariants of time-reversal-invariant band structures*, Phys. Rev. B **75** (2007) 121306(R).

[MC20] A. McDonald and A. A. Clerk, *Exponentially-enhanced quantum sensing with non-Hermitian lattice dynamics*, Nat. Commun. **11** (2020) 5382.

[MCD93] K. Mølmer, Y. Castin, and J. Dalibard, *Monte Carlo wave-function method in quantum optics*, J. Opt. Soc. Am. B **10** (1993) 524.

[MEGCM08] K. G. Makris, R. El-Ganainy, D. N. Christodoulides, and Z. H. Musslimani, *Beam Dynamics in $\mathcal{PT}$ Symmetric Optical Lattices*, Phys. Rev. Lett. **100** (2008) 103904.

[MF13] T. Morimoto and A. Furusaki, *Topological classification with additional symmetries from Clifford algebras*, Phys. Rev. B **88** (2013) 125129.

[MHar] Y. Ma and T. L. Hughes, *The Quantum Skin Hall Effect*, 2020, arXiv:2008.02284.

[MH17] H. Menke and M. M. Hirschmann, *Topological quantum wires with balanced gain and loss*, Phys. Rev. B **95** (2017) 174506.

[MKA+20] N. Matsumoto, K. Kawabata, Y. Ashida, S. Furukawa, and M. Ueda, *Continuous Phase Transition without Gap Closing in Non-Hermitian Quantum Many-Body Systems*, Phys. Rev. Lett. **125** (2020) 260601.

[MKKO20] K. Mochizuki, D. Kim, N. Kawakami, and H. Obuse, *Bulk-edge correspondence in nonunitary Floquet systems with chiral symmetry*, Phys. Rev. A **102** (2020) 062202.

[MLLG20] S. Mu, C. H. Lee, L. Li, and J. Gong, *Emergent Fermi surface in a many-body non-Hermitian fermionic chain*, Phys. Rev. B **102** (2020) 081115(R).

[MMEGC08] Z. H. Musslimani, K. G. Makris, R. El-Ganainy, and D. N. Christodoulides, *Optical Solitons in $\mathcal{PT}$ Periodic Potentials*, Phys. Rev. Lett. **100** (2008) 030402.

[Moi11] N. Moiseyev, *Non-Hermitian Quantum Mechanics*, Cambridge University Press, Cambridge, England, 2011.

[Mos02a] A. Mostafazadeh, *Pseudo-Hermiticity versus PT symmetry: The necessary condition for the reality of the spectrum of a non-Hermitian Hamiltonian*, J. Math. Phys. **43** (2002) 205.

[Mos02b] ———, *Pseudo-Hermiticity versus PT symmetry II: A complete characterization of non-Hermitian Hamiltonians with a real spectrum*, J. Math. Phys. **43** (2002) 2814.

[Mos02c] ———, *Pseudo-Hermiticity versus PT symmetry III: Equivalence of pseudo-Hermiticity and the presence of antilinear symmetries*, J. Math. Phys. **43** (2002) 3944.

[Mos03] ———, *Exact PT-symmetry is equivalent to Hermiticity*, J. Phys. A **36** (2003) 7081.

[Mos09] A. Mostafazadeh, *Spectral Singularities of Complex Scattering Potentials and Infinite Reflection and Transmission Coefficients at Real Energies*, Phys. Rev. Lett. **102** (2009) 220402.

[MOZ+19] S. Mittal, V. V. Orre, G. Zhu, M. A. Gorlach, A. Poddubny, and M. Hafezi, *Photonic quadrupole topological phases*, Nat. Photon. **13** (2019) 692.

[MP20] Y. Michishita and R. Peters, *Equivalence of Effective Non-Hermitian Hamiltonians in the Context of Open Quantum Systems and Strongly Correlated Electron Systems*, Phys. Rev. Lett. **124** (2020) 196401.

[MPBC18] A. McDonald, T. Pereg-Barnea, and A. A. Clerk, *Phase-Dependent Chiral Transport and Effective Non-Hermitian Dynamics in a Bosonic Kitaev-Majorana Chain*, Phys. Rev. X **8** (2018) 041031.

[MPK88] P. A. Mello, P. Pereyra, and N. Kumar, *Macroscopic approach to multichannel disordered conductors*, Ann. Phys. **181** (1988) 290.

[MPS15] S. Malzard, C. Poli, and H. Schomerus, *Topologically Protected Defect States in Open Photonic Systems with Non-Hermitian Charge-Conjugation and Parity-Time Symmetry*, Phys. Rev. Lett. **115** (2015) 200402.

[MR19] P. A. McClarty and J. G. Rau, *Non-Hermitian topology of spontaneous magnon decay*, Phys. Rev. B **100** (2019) 100405(R).

[MSA98] C. Mudry, B. D. Simons, and A. Altland, *Random Dirac Fermions and Non-Hermitian Quantum Mechanics*, Phys. Rev. Lett. **80** (1998) 4257.

[MSHSP14] I. Mondragon-Shem, T. L. Hughes, J. Song, and E. Prodan, *Topological Criticality in the Chiral-Symmetric AIII Class at Strong Disorder*, Phys. Rev. Lett. **113** (2014) 046802.

[Mur07] S. Murakami, *Phase transition between the quantum spin Hall and insulator phases in 3D: emergence of a topological gapless phase*, New J. Phys. **9** (2007) 356.

[MW18] A. Matsugatani and H. Watanabe, *Connecting higher-order topological insulators to lower-dimensional topological insulators*, Phys. Rev. B **98** (2018) 205129.

[MZS+16] P. Miao, Z. Zhang, J. Sun, W. Walasik, S. Longhi, N. M. Litchinitser, and L. Feng, *Orbital angular momentum microlaser*, Science **353** (2016) 6298.

[NAJM19] M. Naghiloo, N. Abbasi, Y. N. Joglekar, and K. W. Murch, *Quantum state tomography across the exceptional point in a single dissipative qubit*, Nat. Phys. **15** (2019) 1232.

[NBS20] D. Nakamura, T. Bessho, and M. Sato, in preparation, 2020.

[NJL61a] Y. Nambu and G. Jona-Lasinio, *Dynamical Model of Elementary Particles Based on an Analogy with Superconductivity. II*, Phys. Rev. **124** (1961) 246.

[NJL61b] ———, *Dynamical Model of Elementary Particles Based on an Analogy with Superconductivity. I*, Phys. Rev. **122** (1961) 345.

[NKU18] M. Nakagawa, N. Kawakami, and M. Ueda, *Non-Hermitian Kondo Effect in Ultracold Alkaline-Earth Atoms*, Phys. Rev. Lett. **121** (2018) 203001.

[NN83] H. B. Nielsen and M. Ninomiya, *The Adler-Bell-Jackiw anomaly and Weyl fermions in a crystal*, Phys. Lett. B **130** (1983) 389.

[NQI+20] Y. Nagai, Y. Qi, H. Isobe, V. Kozii, and L. Fu, *DMFT Reveals the Non-Hermitian Topology and Fermi Arcs in Heavy-Fermion Systems*, Phys. Rev. Lett. **125** (2020) 227204.

[NS83] A. J. Niemi and G. W. Semenoff, *Axial Anomaly Induced Fermion Fractionization and Effective Gauge Theory Actions in Odd Dimensional Space-Times*, Phys. Rev. Lett. **51** (1983) 2077.

[NS98] D. R. Nelson and N. M. Shnerb, *Non-Hermitian localization and population biology*, Phys. Rev. E **58** (1998) 1383.

[NSS+08] C. Nayak, S. H. Simon, A. Stern, M. Freedman, and S. Das Sarma, *Non-Abelian anyons and topological quantum computation*, Rev. Mod. Phys. **80** (2008) 1083.

[NWAK19] X. Ni, M. Weiner, A. Alù, and A. B. Khanikaev, *Observation of higher-order topological acoustic states protected by generalized chiral symmetry*, Nat. Mater. **18** (2019) 113.

[OA10] T. Oka and H. Aoki, *Dielectric breakdown in a Mott insulator: Many-body Schwinger-Landau-Zener mechanism studied with a generalized Bethe ansatz*, Phys. Rev. B **81** (2010) 033103.

[OKSS20] N. Okuma, K. Kawabata, K. Shiozaki, and M. Sato, *Topological Origin of Non-Hermitian Skin Effects*, Phys. Rev. Lett. **124** (2020) 086801.

[OLH+21] F. E. Öztürk, T. Lappe, G. Hellmann, J. Schmitt, J. Klaers, F. Vewinger, J. Kroha, and M. Weitz, *Observation of a non-Hermitian phase transition in an optical quantum gas*, Science **372** (2021) 88.

[OPA+19] T. Ozawa, H. M. Price, A. Amo, N. Goldman, M. Hafezi, L. Lu, M. C. Rechtsman, D. Schuster, J. Simon, O. Zilberberg, and I. Carusotto, *Topological photonics*, Rev. Mod. Phys. **91** (2019) 015006.

[OPW20] S. Ono, H. C. Po, and H. Watanabe, *Refined symmetry indicators for topological superconductors in all space groups*, Sci. Adv. **6** (2020) eaaz8367.

[ORNY19] S. K. Özdemir, S. Rotter, F. Nori, and L. Yang, *Parity-time symmetry and exceptional points in photonics*, Nat. Mater. **18** (2019) 783.

[ORvO10] Y. Oreg, G. Refael, and F. von Oppen, *Helical Liquids and Majorana Bound States in Quantum Wires*, Phys. Rev. Lett. **105** (2010) 177002.

[OS19] N. Okuma and M. Sato, *Topological Phase Transition Driven by Infinitesimal Instability: Majorana Fermions in Non-Hermitian Spintronics*, Phys. Rev. Lett. **123** (2019) 097701.

[OS21] ———, *Quantum anomaly, non-Hermitian skin effects, and entanglement entropy in open systems*, Phys. Rev. B **103** (2021) 085428.

[OTO+20] Y. Ota, K. Takata, T. Ozawa, A. Amo, Z. Jia, B. Kante, M. Notomi, Y. Arakawa, and S. Iwamoto, *Active topological photonics*, Nanophotonics **9** (2020) 547.

[OTY20] R. Okugawa, R. Takahashi, and K. Yokomizo, *Second-order topological non-Hermitian skin effects*, Phys. Rev. B **102** (2020) 241202(R).

[OTY21] R. Okugawa, R. Takahashi, and K. Yokomizo, *Non-Hermitian band topology with generalized inversion symmetry*, Phys. Rev. B **103** (2021) 205205.

[OY19] R. Okugawa and T. Yokoyama, *Topological exceptional surfaces in non-Hermitian systems with parity-time and parity-particle-hole symmetries*, Phys. Rev. B **99** (2019) 041202(R).

[PBHB18] C. W. Peterson, W. A. Benalcazar, T. L. Hughes, and G. Bahl, *A quantized microwave quadrupole insulator with topologically protected corner states*, Nature **555** (2018) 346.

[PBK+15] C. Poli, M. Bellec, U. Kuhl, F. Mortessagne, and H. Schomerus, *Selective enhancement of topologically induced interface states in a dielectric resonator chain*, Nat. Commun. **6** (2015) 6710.

[PCS+16] P. Peng, W. Cao, C. Shen, W. Qu, J. Wen, L. Jiang, and Y. Xiao, *Anti-parity-time symmetry with flying atoms*, Nat. Phys. **12** (2016) 1139.

[PG87] R. E. Prange and S. M. Girvin (eds.), *The Quantum Hall Effect*, Springer, New York, 1987.

[PHG18] T. M. Philip, M. R. Hirsbrunner, and M. J. Gilbert, *Loss of Hall conductivity quantization in a non-Hermitian quantum anomalous Hall insulator*, Phys. Rev. B **98** (2018) 155430.

[PIF19] M. Papaj, H. Isobe, and L. Fu, *Nodal arc of disordered Dirac fermions and non-Hermitian band theory*, Phys. Rev. B **99** (2019) 201107(R).

[PK98] M. B. Plenio and P. L. Knight, *The quantum-jump approach to dissipative dynamics in quantum optics*, Rev. Mod. Phys. **70** (1998) 101.

[PLB+20] C. W. Peterson, T. Li, W. A. Benalcazar, T. L. Hughes, and G. Bahl, *A fractional corner anomaly reveals higher-order topology*, Science **368** (2020) 1114.

[PMB96] J. C. J. Paasschens, T. S. Misirpashaev, and C. W. J. Beenakker, *Localization of light: Dual symmetry between absorption and amplification*, Phys. Rev. B **54** (1996) 11887.

[PMRar] A. Panigrahi, R. Moessner, and B. Roy, *Non-Hermitian dislocation modes: Stability and melting across exceptional points*, 2021, arXiv:2105.05244.

[PN13] D. I. Pikulin and Y. V. Nazarov, *Two types of topological transitions in finite Majorana wires*, Phys. Rev. B **87** (2013) 235421.

[POL+14] B. Peng, S. K. Özdemir, F. Lei, F. Monifi, M. Gianfreda, G. L. Long, S. Fan, F. Nori, C. M. Bender, and L. Yang, *Parity-time-symmetric whispering-gallery microcavities*, Nat. Phys. **10** (2014) 394.

[POL+16] B. Peng, S. K. Özdemir, M. Liertzer, W. Chen, J. Kramer, H. Yılmaz, J. Wiersig, S. Rotter, and L. Yang, *Chiral modes and directional lasing at exceptional points*, Proc. Natl. Acad. Sci. U.S.A. **113** (2016) 6845.

[POR+14] B. Peng, S. K. Özdemir, S. Rotter, H. Yilmaz, M. Liertzer, F. Monifi, C. M. Bender, F. Nori, and L. Yang, *Loss-induced suppression and revival of lasing*, Science **346** (2014) 328.

[PS95] M. E. Peskin and D. V. Schroeder, *An Introduction to Quantum Field Theory*, Westview Press, Boulder, 1995.

[PTG+20] L. S. Palacios, S. Tchoumakov, M. Guix, I. P. S. Sánchez, and A. G. Grushin, *Guided accumulation of active particles by topological design of a second-order skin effect*, Nat. Commun. **12** (2020) 4691.

[PVW17] H. C. Po, A. Vishwanath, and H. Watanabe, *Symmetry-based indicators of band topology in the 230 space groups*, Nat. Commun. **8** (2017) 50.

[PWH+18] M. Parto, S. Wittek, H. Hodaei, G. Harari, M. A. Bandres, J. Ren, M. C. Rechtsman, M. Segev, D. N. Christodoulides, and M. Khajavikhan, *Edge-Mode Lasing in 1D Topological Active Arrays*, Phys. Rev. Lett. **120** (2018) 113901.

[PWV18] H. C. Po, H. Watanabe, and A. Vishwanath, *Fragile Topology and Wannier Obstructions*, Phys. Rev. Lett. **121** (2018) 126402.

[QHRZ09] X.-L. Qi, T. L. Hughes, S. Raghu, and S.-C. Zhang, *Time-Reversal-Invariant Topological Superconductors and Superfluids in Two and Three Dimensions*, Phys. Rev. Lett. **102** (2009) 187001.

[QHZ08] X.-L. Qi, T. L. Hughes, and S.-C. Zhang, *Topological field theory of time-reversal invariant insulators*, Phys. Rev. B **78** (2008) 195424.

[QHZ10] X.-L. Qi, T. L. Hughes, and S.-C. Zhang, *Topological invariants for the Fermi surface of a time-reversal-invariant superconductor*, Phys. Rev. B **81** (2010) 134508.

[QNO+18] F. Quijandría, U. Naether, S. K. Özdemir, F. Nori, and D. Zueco, *$\mathcal{PT}$-symmetric circuit QED*, Phys. Rev. A **97** (2018) 053846.

[QZ11] X.-L. Qi and S.-C. Zhang, *Topological insulators and superconductors*, Rev. Mod. Phys. **83** (2011) 1057.

[RBM+12] A. Regensburger, C. Bersch, M.-A. Miri, G. Onishchukov, D. N. Christodoulides, and U. Peschel, *Parity-time synthetic photonic lattices*, Nature **488** (2012) 167.

[RDF+08] G. Roati, C. D'Errico, L. Fallani, M. Fattori, C. Fort, M. Zaccanti, G. Modugno, M. Modugno, and M. Inguscio, *Anderson localization of a non-interacting Bose-Einstein condensate*, Nature **453** (2008) 895.

[Red84] A. N. Redlich, *Parity violation and gauge noninvariance of the effective gauge field action in three dimensions*, Phys. Rev. D **29** (1984) 2366.

[RG00] N. Read and D. Green, *Paired states of fermions in two dimensions with breaking of parity and time-reversal symmetries and the fractional quantum Hall effect*, Phys. Rev. B **61** (2000) 10267.

[RH17] R. Roy and F. Harper, *Periodic table for Floquet topological insulators*, Phys. Rev. B **96** (2017) 155118.

[RHS19] W. B. Rui, M. M. Hirschmann, and A. P. Schnyder, *$\mathcal{PT}$-symmetric non-Hermitian Dirac semimetals*, Phys. Rev. B **100** (2019) 245116.

[RL09] M. S. Rudner and L. S. Levitov, *Topological Transition in a Non-Hermitian Quantum Walk*, Phys. Rev. Lett. **102** (2009) 065703.

[RLLar] M. S. Rudner, M. Levin, and L. S. Levitov, *Survival, decay, and topological protection in non-Hermitian quantum transport*, 2016, arXiv:1605.07652.

[RMEG+10] C. E. Rüter, K. G. Makris, R. El-Ganainy, D. N. Christodoulides, M. Segev, and D. Kip, *Observation of parity-time symmetry in optics*, Nat. Phys. **6** (2010) 192.

[Rot09] I. Rotter, *A non-Hermitian Hamilton operator and the physics of open quantum systems*, J. Phys. A **42** (2009) 153001.

[Roy09] R. Roy, *Topological phases and the quantum spin Hall effect in three dimensions*, Phys. Rev. B **79** (2009) 195322.

[RSFL10] S. Ryu, A. P. Schnyder, A. Furusaki, and A. W. W. Ludwig, *Topological insulators and superconductors: tenfold way and dimensional hierarchy*, New J. Phys. **12** (2010) 065010.

[RZS19] W. B. Rui, Y. X. Zhao, and A. P. Schnyder, *Topology and exceptional points of massive Dirac models with generic non-Hermitian perturbations*, Phys. Rev. B **99** (2019) 241110(R).

[SA17] M. Sato and Y. Ando, *Topological superconductors: a review*, Rep. Prog. Phys. **80** (2017) 076501.

[Sat06] M. Sato, *Nodal structure of superconductors with time-reversal invariance and Z_2 topological number*, Phys. Rev. B **73** (2006) 214502.

[SBD16] L. M. Sieberer, M. Buchhold, and S. Diehl, *Keldysh field theory for driven open quantum systems*, Rep. Prog. Phys. **79** (2016) 096001.

[SBFS07] T. Schwartz, G. Bartal, S. Fishman, and M. Segev, *Transport and Anderson localization in disordered two-dimensional photonic lattices*, Nature **446** (2007) 52.

[SBGI20] N. Silberstein, J. Behrends, M. Goldstein, and R. Ilan, *Berry connection induced anomalous wave-packet dynamics in non-Hermitian systems*, Phys. Rev. B **102** (2020) 245147.

[Sch44] E. Schrödinger, *What is Life?*, Cambridge University Press, Cambridge, England, 1944.

[Sch13] H. Schomerus, *Topologically protected midgap states in complex photonic lattices*, Opt. Lett. **38** (2013) 1912.

[Sch20] ———, *Nonreciprocal response theory of non-Hermitian mechanical metamaterials: Response phase transition from the skin effect of zero modes*, Phys. Rev. Research **2** (2020) 013058.

[SCV+18] F. Schindler, A. M. Cook, M. G. Vergniory, Z. Wang, S. S. P. Parkin, B. A. Bernevig, and T. Neupert, *Higher-order topological insulators*, Sci. Adv. **4** (2018) eaat0346.

[SF18] H. Shen and L. Fu, *Quantum Oscillation from In-Gap States and a Non-Hermitian Landau Level Problem*, Phys. Rev. Lett. **121** (2018) 026403.

[SFF17] Z. Song, Z. Fang, and C. Fang, *$(d-2)$-Dimensional Edge States of Rotation Symmetry Protected Topological States*, Phys. Rev. Lett. **119** (2017) 246402.

[SGPS+18] M. Serra-Garcia, V. Peri, R. Süsstrunk, O. R. Bilal, T. Larsen, L. G. Villanueva, and S. D. Huber, *Observation of a phononic quadrupole topological insulator*, Nature **555** (2018) 342.

[SHEK12] M. Sato, K. Hasebe, K. Esaki, and M. Kohmoto, *Time-Reversal Symmetry in Non-Hermitian Systems*, Prog. Theor. Phys. **127** (2012) 937.

[Shi19] K. Shiozaki, in preparation, 2019.

[SIV20] C. Scheibner, W. T. M. Irvine, and V. Vitelli, *Non-Hermitian Band Topology and Skin Modes in Active Elastic Media*, Phys. Rev. Lett. **125** (2020) 118001.

[SJ81] A. D. Stone and J. D. Joannopoulos, *Probability distribution and new scaling law for the resistance of a one-dimensional Anderson model*, Phys. Rev. B **24** (1981) 3592.

[SJCPA16] P. San-Jose, J. Cayao, E. Prada, and R. Aguado, *Majorana bound states from exceptional points in non-topological superconductors*, Sci. Rep. **6** (2016) 21427.

[SJGG+17] P. St-Jean, V. Goblot, E. Galopin, A. Lemaître, T. Ozawa, L. L. Gratiet, I. Sagnes, J. Bloch, and A. Amo, *Lasing in topological edge states of a one-dimensional lattice*, Nat. Photon. **11** (2017) 651.

[SLTDS10] J. D. Sau, R. M. Lutchyn, S. Tewari, and S. Das Sarma, *Generic New Platform for Topological Quantum Computation Using Semiconductor Heterostructures*, Phys. Rev. Lett. **104** (2010) 040502.

[SLZ+11] J. Schindler, A. Li, M. C. Zheng, F. M. Ellis, and T. Kottos, *Experimental study of active LRC circuits with $\mathcal{PT}$ symmetries*, Phys. Rev. A **84** (2011) 040101(R).

[SMJZ13] R.-J. Slager, A. Mesaros, V. Juriŭić, and J. Zaanen, *The space group classification of topological band-insulators*, Nat. Phys. **9** (2013) 98.

[SN98] N. M. Shnerb and D. R. Nelson, *Winding Numbers, Complex Currents, and Non-Hermitian Localization*, Phys. Rev. Lett. **80** (1998) 5172.

[SO21] K. Shiozaki and S. Ono, *Symmetry indicator in non-Hermitian systems*, Phys. Rev. B **104** (2021) 035424.

[SP21] F. Schindler and A. Prem, *Dislocation non-Hermitian skin effect*, Phys. Rev. B **104** (2021) L161106.

[SR11] A. P. Schnyder and S. Ryu, *Topological phases and surface flat bands in superconductors without inversion symmetry*, Phys. Rev. B **84** (2011) 060504(R).

[SRFL08] A. P. Schnyder, S. Ryu, A. Furusaki, and A. W. W. Ludwig, *Classification of topological insulators and superconductors in three spatial dimensions*, Phys. Rev. B **78** (2008) 195125.

[SRP20] L. Sá, P. Ribeiro, and T. c. v. Prosen, *Complex Spacing Ratios: A Signature of Dissipative Quantum Chaos*, Phys. Rev. X **10** (2020) 021019.

[SS14] K. Shiozaki and M. Sato, *Topology of crystalline insulators and superconductors*, Phys. Rev. B **90** (2014) 165114.

[SS20] H. Shackleton and M. S. Scheurer, *Protection of parity-time symmetry in topological many-body systems: Non-Hermitian toric code and fracton models*, Phys. Rev. Research **2** (2020) 033022.

[SSC13] M. Segev, Y. Silberberg, and D. N. Christodoulides, *Anderson localization of light*, Nat. Photon. **7** (2013) 197.

[SSG16] K. Shiozaki, M. Sato, and K. Gomi, *Topology of nonsymmorphic crystalline insulators and superconductors*, Phys. Rev. B **93** (2016) 195413.

[SSH79] W. P. Su, J. R. Schrieffer, and A. J. Heeger, *Solitons in Polyacetylene*, Phys. Rev. Lett. **42** (1979) 1698.

[STF09] M. Sato, Y. Takahashi, and S. Fujimoto, *Non-Abelian Topological Order in s-Wave Superfluids of Ultracold Fermionic Atoms*, Phys. Rev. Lett. **103** (2009) 020401.

[Suz76] M. Suzuki, *Relationship between d-Dimensional Quantal Spin Systems and $(d+1)$-Dimensional Ising Systems: Equivalence, Critical Exponents and Systematic Approximants of the Partition Function and Spin Correlations*, Prog. Theor. Phys. **56** (1976) 1454.

[SWV+18] F. Schindler, Z. Wang, M. G. Vergniory, A. M. Cook, A. Murani, S. Sengupta, A. Y. Kasumov, R. Deblock, S. Jeon, I. Drozdov, H. Bouchiat, S. Guéron, A. Yazdani, B. A. Bernevig, and T. Neupert, *Higher-order topology in bismuth*, Nat. Phys. **14** (2018) 918.

[SYW19a] F. Song, S. Yao, and Z. Wang, *Non-Hermitian Skin Effect and Chiral Damping in Open Quantum Systems*, Phys. Rev. Lett. **123** (2019) 170401.

[SYW19b] F. Song, S. Yao, and Z. Wang, *Non-Hermitian Topological Invariants in Real Space*, Phys. Rev. Lett. **123** (2019) 246801.

[SZF18] H. Shen, B. Zhen, and L. Fu, *Topological Band Theory for Non-Hermitian Hamiltonians*, Phys. Rev. Lett. **120** (2018) 146402.

[SZH21] X.-Q. Sun, P. Zhu, and T. L. Hughes, *Geometric Response and Disclination-Induced Skin Effects in Non-Hermitian Systems*, Phys. Rev. Lett. **127** (2021) 066401.

[TB19] L. Trifunovic and P. W. Brouwer, *Higher-Order Bulk-Boundary Correspondence for Topological Crystalline Phases*, Phys. Rev. X **9** (2019) 011012.

[TE05] L. N. Trefethen and M. Embree, *Spectra and Pseudospectra*, Princeton University Press, Princeton, 2005.

[Tho74] D. J. Thouless, *Electrons in disordered systems and the theory of localization*, Phys. Rep. **13** (1974) 93.

[TJWar] A. Tiwari, A. Jahin, and Y. Wang, *Chiral Dirac Superconductors: Second-order and Boundary-obstructed Topology*, 2020, arXiv:2005.12291.

[TK10] J. C. Y. Teo and C. L. Kane, *Topological defects and gapless modes in insulators and superconductors*, Phys. Rev. B **82** (2010) 115120.

[TK20] F. Terrier and F. K. Kunst, *Dissipative analog of four-dimensional quantum Hall physics*, Phys. Rev. Research **2** (2020) 023364.

[TKNdN82] D. J. Thouless, M. Kohmoto, M. P. Nightingale, and M. den Nijs, *Quantized Hall Conductance in a Two-Dimensional Periodic Potential*, Phys. Rev. Lett. **49** (1982) 405.

[TME20] A. F. Tzortzakakis, K. G. Makris, and E. N. Economou, *Non-Hermitian disorder in two-dimensional optical lattices*, Phys. Rev. B **101** (2020) 014202.

[TN18] K. Takata and M. Notomi, *Photonic Topological Insulating Phase Induced Solely by Gain and Loss*, Phys. Rev. Lett. **121** (2018) 213902.

[TPVW19] F. Tang, H. C. Po, A. Vishwanath, and X. Wan, *Comprehensive search for topological materials using symmetry indicators*, Nature **566** (2019) 486.

[Van18] D. Vanderbilt, *Berry Phases in Electronic Structure Theory: Electric Polarization, Orbital Magnetization and Topological Insulators*, Cambridge University Press, Cambridge, England, 2018.

[VDNS21] P. M. Vecsei, M. M. Denner, T. Neupert, and F. Schindler, *Symmetry indicators for inversion-symmetric non-hermitian topological band structures*, Phys. Rev. B **103** (2021) L201114.

[VEF+19] M. G. Vergniory, L. Elcoro, C. Felser, N. Regnault, B. A. Bernevig, and Z. Wang, *A complete catalogue of high-quality topological materials*, Nature **566** (2019) 480.

[Vol03] G. E. Volovik, *The Universe in a Helium Droplet*, Oxford University Press, Oxford, 2003.

[WACB16] Z. Wang, A. Alexandradinata, R. J. Cava, and B. A. Bernevig, *Hourglass fermions*, Nature **532** (2016) 189.

[WBN20] C. C. Wanjura, M. Brunelli, and A. Nunnenkamp, *Topological framework for directional amplification in driven-dissipative cavity arrays*, Nat. Commun. **11** (2020) 3149.

[WDWF21] K. Wang, A. Dutt, C. C. Wojcik, and S. Fan, *Topological complex-energy braiding of non-Hermitian bands*, Nature **598** (2021) 59.

[WDY+21] K. Wang, A. Dutt, K. Y. Yang, C. C. Wojcik, J. Vučković, and S. Fan, *Generating arbitrary topological windings of a non-Hermitian band*, Science **371** (2021) 1240.

[Wei95] S. Weinberg, *The Quantum Theory of Fields*, Cambridge University Press, Cambridge, England, 1995.

[WGK20] X.-R. Wang, C.-X. Guo, and S.-P. Kou, *Defective edge states and number-anomalous bulk-boundary correspondence in non-Hermitian topological systems*, Phys. Rev. B **101** (2020) 121116(R).

[Wie08] D. S. Wiersma, *The physics and applications of random lasers*, Nat. Phys. **4** (2008) 359.

[Wie13] ———, *Disordered photonics*, Nat. Photon. **7** (2013) 188.

[Wie14] J. Wiersig, *Enhancing the Sensitivity of Frequency and Energy Splitting Detection by Using Exceptional Points: Application to Microcavity Sensors for Single-Particle Detection*, Phys. Rev. Lett. **112** (2014) 203901.

[Wig59] E. P. Wigner, *Group Theory and its Application to the Quantum Mechanics of Atomic Spectra*, Academic Press, New York, 1959.

[WKH+20] S. Weidemann, M. Kremer, T. Helbig, T. Hofmann, A. Stegmaier, M. Greiter, R. Thomale, and A. Szameit, *Topological funneling of light*, Science **368** (2020) 311.

[WKLS21] S. Weidemann, M. Kremer, S. Longhi, and A. Szameit, *Coexistence of dynamical delocalization and spectral localization through stochastic dissipation*, Nat. Photon. **15** (2021) 576.

[WKP+17] S. Weimann, M. Kremer, Y. Plotnik, Y. Lumer, S. Nolte, K. G. Makris, M. Segev, M. C. Rechtsman, and A. Szameit, *Topologically protected bound states in photonic parity-time-symmetric crystals*, Nat. Mater. **16** (2017) 433.

[WLG+19] Y. Wu, W. Liu, J. Geng, X. Song, X. Ye, C.-K. Duan, X. Rong, and J. Du, *Observation of parity-time symmetry breaking in a single-spin system*, Science **364** (2019) 878.

[WPV18] H. Watanabe, H. C. Po, and A. Vishwanath, *Structure and topology of band structures in the 1651 magnetic space groups*, Sci. Adv. **4** (2018) eaat8685.

[WRZ19] H. Wang, J. Ruan, and H. Zhang, *Non-Hermitian nodal-line semimetals with an anomalous bulk-boundary correspondence*, Phys. Rev. B **99** (2019) 075130.

[WSBcvF20] C. C. Wojcik, X.-Q. Sun, T. Bzdušek, and S. Fan, *Homotopy characterization of non-Hermitian Hamiltonians*, Phys. Rev. B **101** (2020) 205417.

[WTVS11] X. Wan, A. M. Turner, A. Vishwanath, and S. Y. Savrasov, *Topological semimetal and Fermi-arc surface states in the electronic structure of pyrochlore iridates*, Phys. Rev. B **83** (2011) 205101.

[WZ71] J. Wess and B. Zumino, *Consequences of anomalous ward identities*, Phys. Lett. B **37** (1971) 95.

[WZ92a] X. G. Wen and A. Zee, *Classification of Abelian quantum Hall states and matrix formulation of topological fluids*, Phys. Rev. B **46** (1992) 2290.

[WZ92b] X. G. Wen and A. Zee, *Shift and spin vector: New topological quantum numbers for the Hall fluids*, Phys. Rev. Lett. **69** (1992) 953.

[XBA+15] S.-Y. Xu, I. Belopolski, N. Alidoust, M. Neupane, G. Bian, C. Zhang, R. Sankar, G. Chang, Z. Yuan, C.-C. Lee, S.-M. Huang, H. Zheng, J. Ma, D. S. Sanchez, B. Wang, A. Bansil, F. Chou, P. P. Shibayev, H. Lin, S. Jia, and M. Z. Hasan, *Discovery of a Weyl fermion semimetal and topological Fermi arcs*, Science **349** (2015) 613.

[XDW+20] L. Xiao, T. Deng, K. Wang, G. Zhu, Z. Wang, W. Yi, and P. Xue, *Non-Hermitian bulk-boundary correspondence in quantum dynamics*, Nat. Phys. **16** (2020) 761.

[Xio18] Y. Xiong, *Why does bulk boundary correspondence fail in some non-hermitian topological models*, J. Phys. Commun. **2** (2018) 035043.

[XLH+21] W.-T. Xue, M.-R. Li, Y.-M. Hu, F. Song, and Z. Wang, *Simple formulas of directional amplification from non-Bloch band theory*, Phys. Rev. B **103** (2021) L241408.

[XMJH16] H. Xu, D. Mason, L. Jiang, and J. G. E. Harris, *Topological energy transfer in an optomechanical system with exceptional points*, Nature **537** (2016) 80.

[XWD17] Y. Xu, S.-T. Wang, and L.-M. Duan, *Weyl Exceptional Rings in a Three-Dimensional Dissipative Cold Atomic Gas*, Phys. Rev. Lett. **118** (2017) 045701.

[XWZ+19] L. Xiao, K. Wang, X. Zhan, Z. Bian, K. Kawabata, M. Ueda, W. Yi, and P. Xue, *Observation of Critical Phenomena in Parity-Time-Symmetric Quantum Dynamics*, Phys. Rev. Lett. **123** (2019) 230401.

[XYG+19] H. Xue, Y. Yang, F. Gao, Y. Chong, and B. Zhang, *Acoustic higher-order topological insulator on a kagome lattice*, Nat. Mater. **18** (2019) 108.

[XZB+17] L. Xiao, X. Zhan, Z. H. Bian, K. K. Wang, X. Zhang, X. P. Wang, J. Li, K. Mochizuki, D. Kim, N. Kawakami, W. Yi, H. Obuse, B. C. Sanders, and P. Xue, *Observation of topological edge states in parity-time-symmetric quantum walks*, Nat. Phys. **13** (2017) 1117.

[XZGC21] W. Xi, Z.-H. Zhang, Z.-C. Gu, and W.-Q. Chen, *Classification of topological phases in one dimensional interacting non-Hermitian systems and emergent unitarity*, Sci. Bull. **66** (2021) 1731.

[YH19] Z. Yang and J. Hu, *Non-Hermitian Hopf-link exceptional line semimetals*, Phys. Rev. B **99** (2019) 081102(R).

[YH21] T. Yoshida and Y. Hatsugai, *Correlation effects on non-Hermitian point-gap topology in zero dimension: Reduction of topological classification*, Phys. Rev. B **104** (2021) 075106.

[YHU+ar] L. Yamauchi, T. Hayata, M. Uwamichi, T. Ozawa, and K. Kawaguchi, *Chirality-driven edge flow and non-Hermitian topology in active nematic cells*, 2020, arXiv:2008.10852.

[YJL+18] C. Yin, H. Jiang, L. Li, R. Lü, and S. Chen, *Geometrical meaning of winding number and its characterization of topological phases in one-dimensional chiral non-Hermitian systems*, Phys. Rev. A **97** (2018) 052115.

[YJS21] Y. Yu, M. Jung, and G. Shvets, *Zero-energy corner states in a non-Hermitian quadrupole insulator*, Phys. Rev. B **103** (2021) L041102.

[YKH19] T. Yoshida, K. Kudo, and Y. Hatsugai, *Non-Hermitian fractional quantum Hall states*, Sci. Rep. **9** (2019) 16895.

[YL52] C. N. Yang and T. D. Lee, *Statistical Theory of Equations of State and Phase Transitions. I. Theory of Condensation*, Phys. Rev. **87** (1952) 404.

[YL99] I. V. Yurkevich and I. V. Lerner, *Delocalization in an Open One-Dimensional Chain in an Imaginary Vector Potential*, Phys. Rev. Lett. **82** (1999) 5080.

[YM19] K. Yokomizo and S. Murakami, *Non-Bloch Band Theory of Non-Hermitian Systems*, Phys. Rev. Lett. **123** (2019) 066404.

[YM20] ———, *Topological semimetal phase with exceptional points in one-dimensional non-Hermitian systems*, Phys. Rev. Research **2** (2020) 043045.

[YM21] ———, *Non-Bloch band theory in bosonic Bogoliubov–de Gennes systems*, Phys. Rev. B **103** (2021) 165123.

[YMB21] K. Yang, S. C. Morampudi, and E. J. Bergholtz, *Exceptional Spin Liquids from Couplings to the Environment*, Phys. Rev. Lett. **126** (2021) 077201.

[YMH20] T. Yoshida, T. Mizoguchi, and Y. Hatsugai, *Mirror skin effect and its electric circuit simulation*, Phys. Rev. Research **2** (2020) 022062.

[YNA+19] K. Yamamoto, M. Nakagawa, K. Adachi, K. Takasan, M. Ueda, and N. Kawakami, *Theory of Non-Hermitian Fermionic Superfluidity with a Complex-Valued Interaction*, Phys. Rev. Lett. **123** (2019) 123601.

[YPK18] T. Yoshida, R. Peters, and N. Kawakami, *Non-Hermitian perspective of the band structure in heavy-fermion systems*, Phys. Rev. B **98** (2018) 035141.

[YPKH19] T. Yoshida, R. Peters, N. Kawakami, and Y. Hatsugai, *Symmetry-protected exceptional rings in two-dimensional correlated systems with chiral symmetry*, Phys. Rev. B **99** (2019) 121101(R).

[YSHC21] Z. Yang, A. P. Schnyder, J. Hu, and C.-K. Chiu, *Fermion Doubling Theorems in Two-Dimensional Non-Hermitian Systems for Fermi Points and Exceptional Points*, Phys. Rev. Lett. **126** (2021) 086401.

[YSW18a] Z. Yan, F. Song, and Z. Wang, *Majorana Corner Modes in a High-Temperature Platform*, Phys. Rev. Lett. **121** (2018) 096803.

[YSW18b] S. Yao, F. Song, and Z. Wang, *Non-Hermitian Chern Bands*, Phys. Rev. Lett. **121** (2018) 136802.

[YW18] S. Yao and Z. Wang, *Edge States and Topological Invariants of Non-Hermitian Systems*, Phys. Rev. Lett. **121** (2018) 086803.

[YY20] Y. Yi and Z. Yang, *Non-Hermitian Skin Modes Induced by On-Site Dissipations and Chiral Tunneling Effect*, Phys. Rev. Lett. **125** (2020) 186802.

[YZFH20] Z. Yang, K. Zhang, C. Fang, and J. Hu, *Non-Hermitian Bulk-Boundary Correspondence and Auxiliary Generalized Brillouin Zone Theory*, Phys. Rev. Lett. **125** (2020) 226402.

[YZT+12] S. M. Young, S. Zaheer, J. C. Y. Teo, C. L. Kane, E. J. Mele, and A. M. Rappe, *Dirac Semimetal in Three Dimensions*, Phys. Rev. Lett. **108** (2012) 140405.

[ZF20] X.-X. Zhang and M. Franz, *Non-Hermitian Exceptional Landau Quantization in Electric Circuits*, Phys. Rev. Lett. **124** (2020) 046401.

[ZHI+15] B. Zhen, C. W. Hsu, Y. Igarashi, L. Lu, I. Kaminer, A. Pick, S.-L. Chua, J. D. Joannopoulos, and M. Soljačić, *Spawning rings of exceptional points out of Dirac cones*, Nature **525** (2015) 354.

[ZHK89] S. C. Zhang, T. H. Hansson, and S. Kivelson, *Effective-Field-Theory Model for the Fractional Quantum Hall Effect*, Phys. Rev. Lett. **62** (1989) 82.

[ZJS+19] T. Zhang, Y. Jiang, Z. Song, H. Huang, Y. He, Z. Fang, H. Weng, and C. Fang, *Catalogue of topological electronic materials*, Nature **566** (2019) 475.

[ZL19] H. Zhou and J. Y. Lee, *Periodic table for topological bands with non-Hermitian symmetries*, Phys. Rev. B **99** (2019) 235112.

[ZLLZ19] H. Zhou, J. Y. Lee, S. Liu, and B. Zhen, *Exceptional surfaces in PT-symmetric non-Hermitian photonic systems*, Optica **6** (2019) 190.

[ZMT+18] H. Zhao, P. Miao, M. H. Teimourpour, S. Malzard, R. El-Ganainy, H. Schomerus, and L. Feng, *Topological hybrid silicon microlasers*, Nat. Commun. **9** (2018) 981.

[ZOH+21] W. Zhang, X. Ouyang, X. Huang, X. Wang, H. Zhang, Y. Yu, X. Chang, Y. Liu, D.-L. Deng, and L.-M. Duan, *Observation of Non-Hermitian Topology with Nonunitary Dynamics of Solid-State Spins*, Phys. Rev. Lett. **127** (2021) 090501.

[ZPY+18] H. Zhou, C. Peng, Y. Yoon, C. W. Hsu, K. A. Nelson, L. Fu, J. D. Joannopoulos, M. Soljačić, and B. Zhen, *Observation of bulk Fermi arc and polarization half charge from paired exceptional points*, Science **359** (2018) 1009.

[ZQW+19] H. Zhao, X. Qiao, T. Wu, B. Midya, S. Longhi, and L. Feng, *Non-Hermitian topological light steering*, Science **365** (2019) 1163.

[ZR21] H.-G. Zirnstein and B. Rosenow, *Exponentially growing bulk Green functions as signature of nontrivial non-Hermitian winding number in one dimension*, Phys. Rev. B **103** (2021) 195157.

[ZRLC+19] Z. Zhang, M. Rosendo López, Y. Cheng, X. Liu, and J. Christensen, *Non-Hermitian Sonic Second-Order Topological Insulator*, Phys. Rev. Lett. **122** (2019) 195501.

[ZRP+15] J. M. Zeuner, M. C. Rechtsman, Y. Plotnik, Y. Lumer, S. Nolte, M. S. Rudner, M. Segev, and A. Szameit, *Observation of a Topological Transition in the Bulk of a Non-Hermitian System*, Phys. Rev. Lett. **115** (2015) 040402.

[ZRR21] H.-G. Zirnstein, G. Refael, and B. Rosenow, *Bulk-Boundary Correspondence for Non-Hermitian Hamiltonians via Green Functions*, Phys. Rev. Lett. **126** (2021) 216407.

[ZRS+14] X. Zhu, H. Ramezani, C. Shi, J. Zhu, and X. Zhang, *$\mathcal{PT}$-Symmetric Acoustics*, Phys. Rev. X **4** (2014) 031042.

[ZSH+19] M. Zhang, W. Sweeney, C. W. Hsu, L. Yang, A. D. Stone, and L. Jiang, *Quantum Noise Theory of Exceptional Point Amplifying Sensors*, Phys. Rev. Lett. **123** (2019) 180501.

[ZTJ+21] X. Zhang, Y. Tian, J.-H. Jiang, M.-H. Lu, and Y.-F. Chen, *Observation of higher-order non-Hermitian skin effect*, Nat. Commun. **12** (2021) 5377.

[ZYFar] K. Zhang, Z. Yang, and C. Fang, *Universal non-Hermitian skin effect in two and higher dimensions*, 2021, arXiv:2102.05059.

[ZYF20] K. Zhang, Z. Yang, and C. Fang, *Correspondence between Winding Numbers and Skin Modes in Non-Hermitian Systems*, Phys. Rev. Lett. **125** (2020) 126402.

[ZYX20] Q.-B. Zeng, Y.-B. Yang, and Y. Xu, *Topological phases in non-Hermitian Aubry-André-Harper models*, Phys. Rev. B **101** (2020) 020201(R).

[ZZ18] A. A. Zyuzin and A. Y. Zyuzin, *Flat band in disorder-driven non-Hermitian Weyl semimetals*, Phys. Rev. B **97** (2018) 041203(R).

[ZZS+16] Z. Zhang, Y. Zhang, J. Sheng, L. Yang, M.-A. Miri, D. N. Christodoulides, B. He, Y. Zhang, and M. Xiao, *Observation of Parity-Time Symmetry in Optically Induced Atomic Lattices*, Phys. Rev. Lett. **117** (2016) 123601.